METAMORPHISM OF THE JUMPING BROOK METAMORPHIC SUITE, WESTERN CAPE BRETON HIGHLANDS, NOVA SCOTIA: MICROSTRUCTURE, P-T-t PATHS, AND TECTONIC IMPLICATIONS

BY

HEATHER ELIZABETH PLINT

Submitted in partial fulfillment of the requirements
for the degree of Master of Science
at
Dalhousie University,
Halifax, Nova Scotia, Canada
April, 1987

DALHOUSIE UNIVERSITY

DEPARTMENT OF GEOLOGY

The undersigned hereby certify that they have read and recommended to the Faculty of Graduate Studies for acceptance a thesis entitled "Metamorphism of the Jumping Brook Metamorphic Suite Western Cape Breton Highlands, Nova Scotia: Microstructure, P-T-t Paths, and Tectonic Implications."

by Heather Elizabeth Plint

in partial fulfillment of the requirements for the degree of Master of Science.

Dated April 1, 1987

External Examiner

Research Supervisor

Examining Committee

DALHOUSIE UNIVERSITY

Date April 1, 1987

Author Heather Elizabeth Plint

Title "Metamorphism of the Jumping Brook Metamorphic Suite Western Cape Breton Highlands, Nova Scotia: Microstructure, P-T-t Paths, and Tectonic Implications"

Department or School: Department of Geology

Degree: M.Sc. Convocation May Year 1987

Permission is herewith granted to Dalhousie University to circulate and to have copied for non-commercial purposes, at its discretion, the above title upon the request of individuals or institutions.

Signature of Author

TABLE OF CONTENTS

LIST OF MAPS

LIST OF FIGURES

LIST OF TABLES

ABSTRACT

Detailed mapping and sampling for petrography and ^{40}Ar-^{39}Ar dating were carried out in the Cheticamp area of the Cape Breton Highlands in order to document the P-T and deformation history of the Jumping Brook metamorphic suite. This volcanic-sedimentary sequence shows evidence of Barrovian, prograde, regional metamorphism to amphibolite facies conditions. Metamorphic grade increases east-northeastwards through biotite, garnet, staurolite-kyanite, and kyanite zones. Peak conditions based on geothermometry and geobarometry are 709° to 715°C and 7.5 to 8.0 kb. These temperatures are consistent with zonation elimination in high-grade garnets and with inferred mineral reactions. Nearly identical ^{40}Ar-^{39}Ar cooling ages on biotite (390 Ma $\pm$ 4 Ma) and hornblende (383 Ma $\pm$ 4 Ma to 389 Ma $\pm$ 4 Ma) indicate rapid Devonian cooling.

Inclusion trail geometry, internal-external fabric relations, and relict matrix crenulations support the interpretation of syn- to post-tectonic porphyroblast growth. Porphyroblast overgrowth of different stages of crenulation cleavage, and other microstructures, allow determination of a consistent relative growth sequence for the medium- to high-grade rocks: chlorite^1, chloritoid, garnet^1, staurolite, oligoclase and kyanite, garnet^2, and chlorite^2.

These crenulations (F_4) are interpreted to be part of a continuous deformation sequence beginning with early, tight to isoclinal, macroscopic to microscopic folding about north-northeasterly trending axes (F_1) and transposition of these folds along axial planar S_1. The crenulations are related to northerly extension. Differential uplift along northerly trending high strain zones can account for the observed metamorphic progression.

The metamorphic P-T-(relative)t path is characteristic of crustal thickening. Comparison of the path with theoretical P-T-t paths generated by a one-dimensional, conductive model for overthrusting indicates that peak metamorphic conditions can be reproduced for a thrust slab of 20 km and high heat flow and that exponential erosion alone does not account for the observed cooling ages. Modelling results, the available isotopic data, and the geological P-T-t path suggest the Jumping Brook metamorphic suite was deposited no earlier than the Ordovician, buried while geologically young (<100 Ma) at about 430 Ma, reaching peak metamorphic conditions at approximately 400 Ma, and tectonically exhumed and rapidly cooled in the early Devonian.

ACKNOWLEDGEMENTS

I thank Dr. R. A. Jamieson for suggesting this research topic, for her guidance and useful discussions throughout the course of this work, and particularly for showing me the "Joy of Brooks" and how to put my finger up the fold axis. I am grateful to Dr. R.P. Raeside for critical review of the rough draft and many useful suggestions for its clarification and improvement, and to Dr. P. Reynolds for guidance and assistance in the ^{40}Ar-^{39}Ar dating. Special thanks are due to Dr. S.M. Barr and Dr. R.P. Raeside for the use of the helicopter and to K.A. Connors, S. Dudka, and J.A. Marcotte for the field assistance. The co-operation of Parks Canada in permitting sample collection in the Cape Breton Highlands National Park and the financial support of the Geological Survey of Canada is greatly appreciated. Thanks are also due to G. Brown, K. Maxwell, R. McKay, K. Taylor, and A. Grist for technical help and to F. Stefani for assistance with photography. Last, but not least, I would like to thank L.R. Richard for all her help with the "computer stuff", use of her computer and programs, many interesting geological discussions, the moral support, and "always looking on the bright side of life", D.R. Issler for his patience, moral support and help in

countless ways, but especially for all the help with the thermal modelling and plotting, and A.M. Ryan for all those bits of advice, many useful discussions, and the encouragement.

CHAPTER 1

INTRODUCTION AND GEOLOGICAL SETTING

1.1 INTRODUCTION

Interpretation of porphyroblast-matrix relations in deformed metamorphic rocks is an essential tool for determining equilibrium mineral assemblages, phase equilibria, and ultimately P-T-t histories. Recent models proposed by Bell (1985) and Bell et al. (1986) for porphyroblast growth in crenulated rocks provides a means of deciphering an unambiguous relative sequence of porphyroblast growth. Bell (1985) interprets sigmoidal trails as crenulations overgrown by porphyroblasts in contrast to traditional interpretations of porphyroblast rotation (eg. Spry, 1969). Thus, application of this nonrotational model, particularily in high-grade rocks where the early stages of deformation may be erased by progressive metamorphism and deformation and by recrystallization of the matrix, also provides insight into fabric development.

Comparison of P-T-t paths generated by quantitative thermal models (eg. England and Thompson, 1984; Roydon and Hodges, 1984) with petrologic P-T-t paths and

radiometric metamorphic cooling ages can provide important information for understanding of the tectonothermal history of an orogenic region, and in particular, can provide insight into thermal parameters such as mantle heat flow and crustal radiogenic heat production, physical parameters such as depth of burial at the initiation of metamorphism, and subsequent uplift rates.

This work defines the field relations, macroscopic structures, porphyroblast-matrix relations, metamorphic reactions, and P-T conditions, in a sequence of low- to high-grade metamorphosed volcanic and sedimentary rocks, in the western highlands of Cape Breton Island, Nova Scotia. A P-T-(relative)time path for the high-grade rocks is constructed from these results on the basis of the sequence of microstructural events determined from porphyroblast-matrix relations. This P-T-t path and ^{40}Ar-^{39}Ar cooling ages on hornblende and biotite are compared to a simple, one-dimensional, computer, thermal model for overthrusting. This provides constraint on the timing of metamorphism and uplift in the region and hence, has some important implications for regional tectonics.

1.2 REGIONAL SETTING

Until recently, most of the metamorphic rocks of the Cape Breton Highlands were described as "undivided gneiss" or tenuously correlated with southeastern Cape Breton Island (eg. Milligan, 1970; Keppie, 1979) and all of Cape Breton Island was considered to be part of the Avalon Zone (eg. Williams, 1979). Since 1978, virtually all of the Highlands has been mapped at 1:50,000 or larger (Barr et al., 1987a) and four tectonostratigraphic subdivisions have been proposed (Barr and Raeside, 1986) (Figure 1.1). These are the: Southeastern, Bras d'Or, Highlands, and Northwestern Highlands zones. The Southeastern zone includes the Fourchu Group (Weeks, 1954) and dioritic to granitic intrusions overlain by Cambrian to Ordovician sedimentary rocks. The Bras d'Or zone is characterized by gneissic basement overlain by the Precambrian George River Series (Milligan, 1970) and early to late Paleozoic sedimentary and volcanic sequences. The Highlands zone consists of ortho- and para-gneisses flanked by lower grade metavolcanic and metasedimentary rocks and intruded by diverse and abundant Precambrian to Carboniferous plutons. The Northwestern zone comprises Grenvillian basement

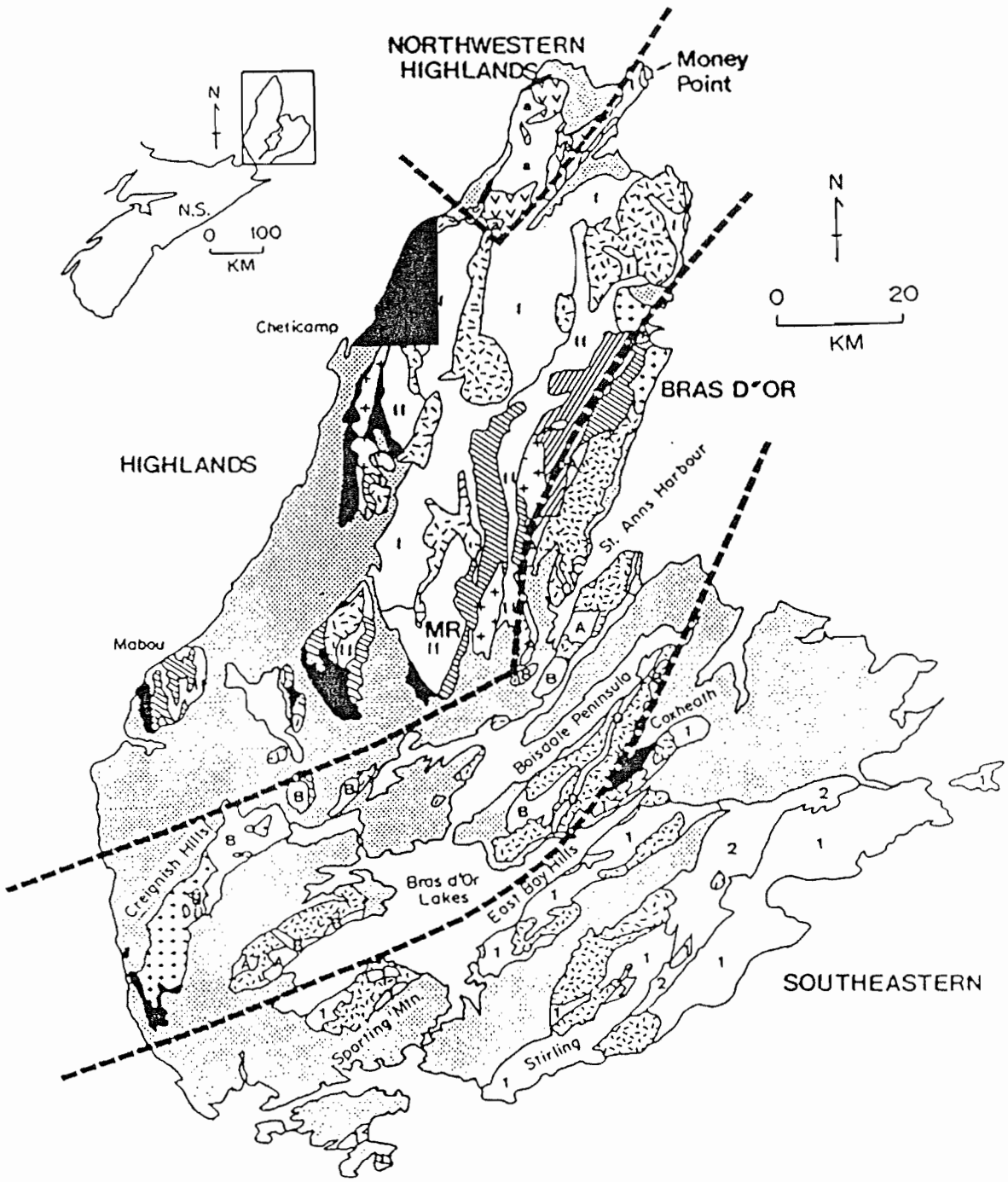

Figure 1.1. Generalized geology and tectonostratigraphic subdivisions of Cape Breton Island from Barr and Raeside (1986). The study area (shaded) is located in the Highlands zone. MR denotes Middle River area.

Figure 1.1. LEGEND

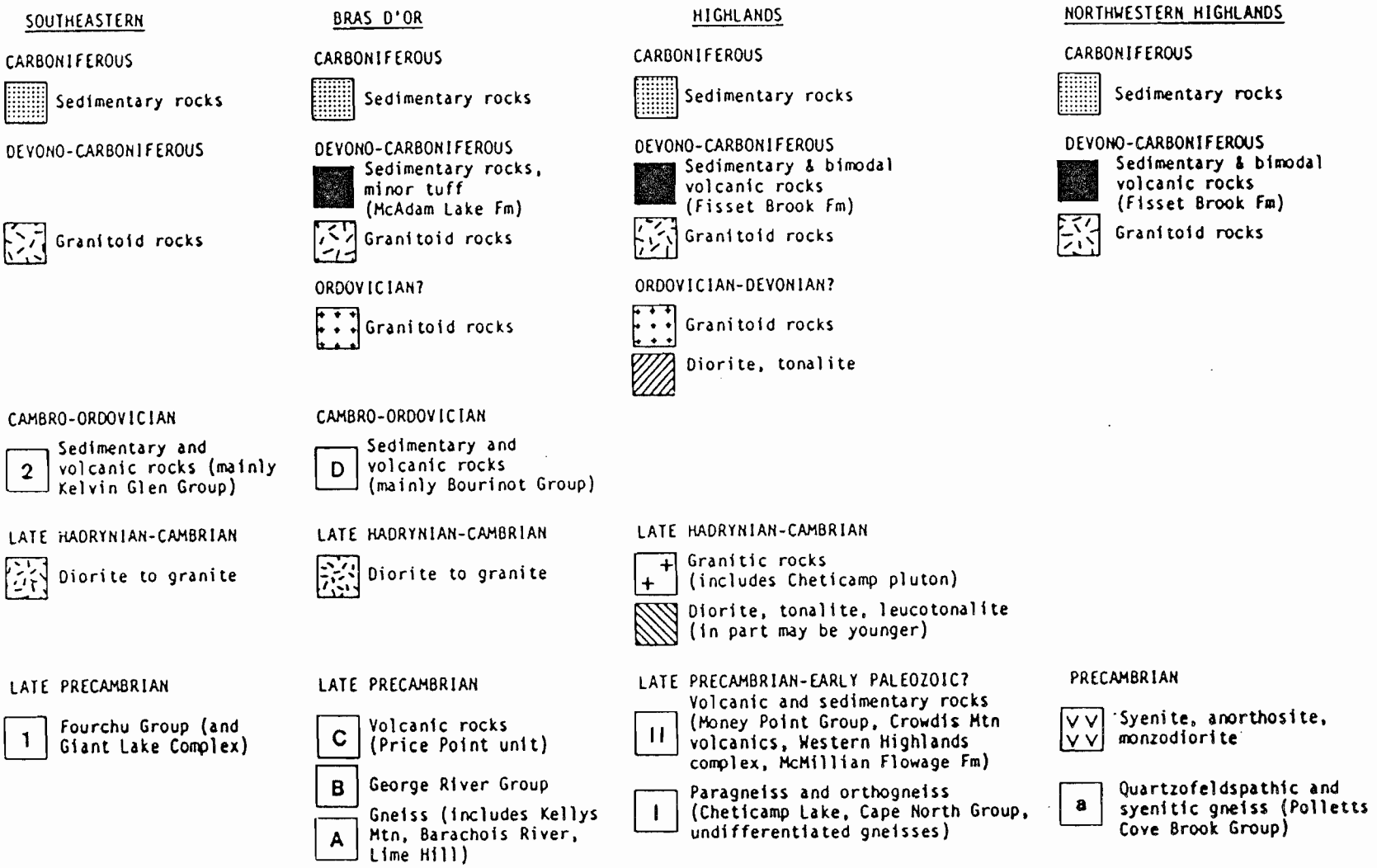

including felsic to mafic gneisses, monzogranite, anorthosite, and syenite. The boundary between the Highlands and Northeastern Highlands zones is a mylonitic fault zone and that between the Southeastern and Bras d'Or zones is inferred to be a fault (Barr and Raeside, 1986). The nature of the boundary between the Bras d'Or and the Highlands zones is unknown. Only the Southeastern and Bras d'Or zones are considered to be Avalon Zone equivalents whereas the regional correlations of the Highlands and Northwestern Highlands zones are still uncertain (Barr and Raeside, 1986).

The study area is included in the Highlands zone (Figure 1.1), and is underlain by the largest correlatable sequence in the highlands known as the western Highlands volcanic-sedimentary belt (Jamieson et al., 1987). This area is important for several reasons:
(1) it contains well exposed sections in the central part of the the western Highlands volcanic-sedimenatry belt about which controversy exists regarding the depositional age, the relative timing of metamorphism and deformation, and the presence or absence of basement.
(2) it has potential correlations with the Gander Zone in Newfoundland (cf. Barr and Raeside, 1986) which, in turn has implications for regional tectonics, mineralization,

and interpretation of recently acquired aeromagnetic and seismic data in the Gulf of the St. Lawrence and the Cabot Strait.

Therefore, there is need to consider the geology of this area in detail, particularily the lithological sequence, the structural and metamorphic relations, and the time of deposition and of metamorphism.

1.3 LOCATION AND ACCESS

The study area occupies an area of approximately 150 square kilometres within the Cape Breton Highlands National Park, between Cheticamp and Pleasant Bay in the western Cape Breton Highlands (Figure 1.2). To the north, the study area is bounded by the Cabot Trail and to the south, by the Cheticamp River. The Gulf of St. Lawrence forms the western boundary. The eastern boundary trends parallel to Benjies Lake Brook, approximately one kilometre east of the Cabot Trail. Access is restricted to the Cabot Trail, a few hiking trails, and two gravel roads used for park maintenance and fire control. Some access to the interior of the map area was obtained by helicopter.

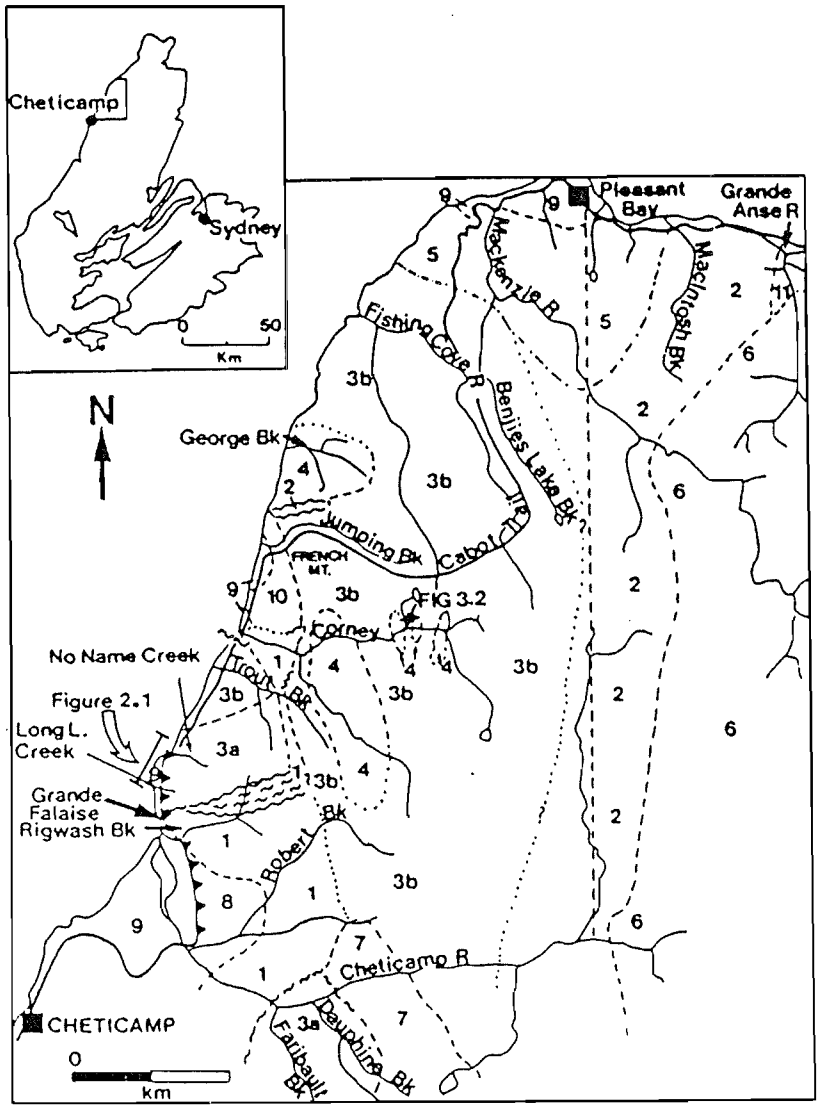

Figure 1.2. General geology of the study area and Pleasant Bay Gneiss Complex to the east. Inset map gives regional location. Heavy dashed line marks the eastern boundary of the study area. Geology modified after Barr et al. (1985) on the basis of this work. Thrust fault after Currie (1977). Shear zones along Cheticamp River after Craw (1984) and Jamieson et al. (1987). Geology of the French Mountain-Cabot Trail-Jumping Brook area after Conrod (1984). Geographical locations referred to in text, location of lithological section of Figure 2.2, and area of data collection for Figure 3.2 are shown. The location of the area shown in Figure 2.4 is east of the eastern boundary (heavy dashed line) of the study area shown here.

Figure 1.2. **LEGEND**

Unknown Age

11. Pink foliated granitoid

10. Foliated muscovite granitoid

Carboniferous

9. Carboniferous sedimentary rocks of the Horton and Windsor Groups

Devonian - Carboniferous

8. Fisset Brook Formation, mainly bimodal volcanics

7. Salmon Pool pluton, syenogranite

6. Margaree pluton, granodiorite

5. Predominantly biotite granodiorite

Silurian or older

4. George Brook amphibolite

3. Jumping Brook metamorphic suite
   (b) metasedimentary rocks
   (a) metavolcanic rocks

2. Pleasant Bay Gneiss Complex

Cambrian

1. Cheticamp pluton


geological contacts: assumed, approximate, arbitrary, observed


Ductile shear zone

Shear (<2 metres wide)

High angle fault


Thrust fault

1.4 PREVIOUS WORK

Early workers showed that the metamorphic rocks of the study area consist of low- to medium-grade metavolcanic and metasedimentary schists bounded to the east by high-grade ortho- and para-gneisses (McLaren, 1955; Neale, 1963). Milligan (1970) and Chatterjee (1980) examined mineralization in the low- to medium-grade metavolcanic-metasedimentary sequence exposed in the Faribault Brook area just south of the study area (Figure 1.2). Neale (1963), Milligan (1970), and Chatterjee (1980) correlated the metavolcanic-metasedimentary sequence with the Precambrian George River Series.

Currie (1982, 1987) defined the Pleasant Bay Gneiss Complex, consisting predominantly of the high-grade ortho- and para-gneisses, which he interpreted to be basement unconformably overlain by the Jumping Brook Complex, consisting of the low- to medium-grade metavolcanic and sedimentary rocks reported by Mclaren (1955). Currie et al. (1982) interpreted the Jumping Brook Complex to be Ordovician-Silurian based on a U-Pb age of 439 $\pm$ 7 Ma for zircons in a rhyolite dyke which they interpreted to feed the Complex.

Currie (1987) recognized three periods of prograde metamorphism and deformation in the study area relative to the the intrusion of a Cambrian granodiorite (referred to in this study as the Cheticamp pluton and as the Corney Brook Complex by Currie, 1975, 1982). He divided the metamorphic episodes into two "pre-Corney Brook" metamorphisms and a "post-Corney Brook" metamorphism plus a late, pervasive retrograde metamorphism. According to Currie (1987), the intrusion of the Cheticamp pluton marked the culmination of the second phase of deformation and metamorphism in the Pleasant Bay Complex. Currie (1987) estimated peak P-T conditions for this second metamorphism at 620^{o}C and 7 kb. The associated deformation produced a pervasive foliation locally axial planar to rootless, isoclinal folds. Currie (1987) was unable to determine the details of the first metamorphism and deformation affecting the Pleasant Bay Complex except that migmatites and a pervasive foliation were formed.

In the Jumping Brook Complex, early deformation, prior to significant metamorphism caused overturned and recumbent, eastward-verging, macroscopic folding not observed in the Pleasant Bay Complex (Currie, 1987). Currie (1987) suggested a thin-skinned deformation style, the Pleasant Bay Complex forming a basement to the

recumbently folded Jumping Brook Complex. Significant "post-Corney Brook" metamorphism was primarily associated with late, upright, northerly plunging folds in the Jumping Brook Complex (Currie, 1987). This metamorphism is interpreted to have occurred during the Devonian Acadian Orogeny with peak conditions of 650°C and 3 to 4 kb. Currie did not describe the retrograde metamorphism in detail but presumably it is associated with the waning stages of the "post-Corney Brook" metamorphism.

Craw (1984) and Conrod (1984) found no evidence of the stratigraphic unconformity between the Jumping Brook Complex and Pleasant Bay Gneiss Complex reported by Currie (1987). In a detailed study of the Jumping Brook Complex exposed along the Cheticamp River, Craw (1984) recognized three northerly trending belts increasing in metamorphic grade from west to east, which he interpreted to represent different structural levels of an originally continuous sequence, juxtaposed by westerly directed thrusting. Craw (1984) found no evidence for the involvement of basement in the thrusting.

Craw (1984) defined three major phases of deformation in the Jumping Brook Complex. The first deformation involved tight to isoclinal, macroscopic to microscopic folding of bedding and the development of an

axial planar foliation in the low-grade belt. The second deformation resulted in folding of an earlier foliation and development of an axial planar foliation in the medium- to high-grade belts. Craw (1984) suggested the folded foliation may be equivalent to the pervasive foliation of the low-grade belt although he found no unequivocal evidence to support this possibility. Craw (1984) proposed that metamorphism and deformation were continuous during the first and second deformation phases. Peak metamorphic conditions of 600° to 650°C and about 4 kb were reached in the latter stages of the second deformation phase and juxtaposition of the medium- and high-grade belts was initiated possibly as early as the second deformation phase (Craw, 1984). As metamorphism waned, juxtaposition was completed, resulting in the third deformation phase characterized by shear zones and upright, open to tight, northerly plunging folds in the high-grade belt (Craw, 1984). He recognized an open, upright, northerly plunging antiform as the only macroscopic, post-metamorphic structure in the Cheticamp River area.

1.5 RECENT WORK

Plint et al. (1986) and Connors (1986) examined the geology of the Jumping Brook Complex and confirmed Craw's structural interpretations. Connors (1986) determined that metamorphism was syn- to post-tectonic with respect to the prevasive foliation and locally postdated crenulations which deform this foliation. Based on whole-rock chemistry, Connors (1986) suggested that the metavolcanic rocks may have been island arc tholeiites.

Jamieson et al. (1986) reported U-Pb ages on zircons for plutonic rocks in the Cape Breton Highlands. They dated the apparently syntectonic Belle Cote Road orthogneiss at 433 $\pm$ 20 Ma thus constraining the timing of the latest amphibolite facies metamorphism to late Ordovician or early Devonian and restricting the host gneisses to middle Ordovician - late Silurian.

Jamieson et al. (1987) documented the lithologies of the low- to medium-grade metavolcanic-metasedimentary sequence and the high-grade gneisses south of the study area, and suggested that the Jumping Brook Complex may be lower Paleozoic based on a boulder conglomerate containing granite boulders which compositionally resemble the Cambrian Cheticamp pluton. Jamieson et al.

(1987) found problems with Currie's (1982, 1987) terminology of the metamorphic rocks of the western Highlands and proposed a nomenclature, consistent with the North American Stratigraphic Code (1983). This nomenclature, although not yet formalized since detailed mapping in the Highlands zone is still in progress, is used here. Hence, the rocks of the study area are placed in the Jumping Brook metamorphic suite including some rock types previously included in the Pleasant Bay Gneiss Complex (Currie, 1982, 1987) and all of Currie's (1982, 1987) Jumping Brook Complex. The term Pleasant Bay Gneiss Complex (Currie, 1982, 1987) is retained here for the quartzo-feldspathic schists, orthogneisses, and intrusive rocks east of Benjies Lake Brook (Figures 1.1 and 1.2). Jamieson et al. (1987) further subdivided the Jumping Brook metamorphic suite into a number of lithologic units: Faribault Brook metavolcanics, Dauphinee Brook schist, Rocky Brook schist, and Corney Brook schist. The Faribault Brook metavolcanics are equivalent to Craw's (1984) low-grade belt, whereas the Dauphinee Brook schist spans the low- to medium-grade belts. The Corney Brook schist includes part of Craw's (1984) medium-grade belt. An additional unit, the Fishing Cove River schist, defined in this work (Chapter 2), is equivalent to the

high-grade belt of Craw (1984). Table 1.1 summarizes the nomenclature development for the Jumping Brook metamorphic suite.

1.6 SUMMARY

Three major problems requiring field investigation exist in the Cheticamp area. (1) The low- to high-grade rock relations (that is, continuous sequence versus stratigraphic unconformity) and the presence or absence of basement are under debate and require detailed examination of the stratigraphy of the Jumping Brook metamorphic suite. (2) The depositional age of the Jumping Brook metamorphic suite, traditionally considered to be late Precambrian (eg. Milligan, 1970), is unknown and may be Ordovician-Silurian (Currie et al., 1982; Jamieson et al., 1986). Thus, the relative age of the Jumping Brook metamorphic suite to surrounding rocks such as the Cambrian Cheticamp pluton is important for settling age disputes. (3) The deformational and metamorphic histories of the Jumping Brook metamorphic suite as defined by Craw (1984) and Currie (1982, 1987) are sufficiently different in the number of deformation and metamorphic events, the style of deformation, and the

Table 1.1. Nomenclature development of the Jumping Brook metamorphic suite.

PRE - 1975	1975 - 1986	1986 - 1987
McLaren (1955) Neale (1963) Milligan (1970) (see also Chatterjee, 1980)	Currie (1975, 1982, 1987) Jamieson and Craw (1983) Craw (1984) Conrod (1984) Barr et al. (1985) Connors (1986) Plint et al. (1986) Jamieson et al. (1986)	Jamieson et al. (1987)
GEORGE RIVER GROUP AND FORCHU GROUP	Part of the western Highlands volcanic-sedimentary complex JUMPING BROOK COMPLEX PLEASANT BAY GNEISS COMPLEX	Part of the western Highlands volcanic-sedimentary belt JUMPING BROOK METAMORPHIC SUITE PLEASANT BAY GNEISS COMPLEX

relative timing of metamorphism and deformation that their interpretations require modification.

1.7 OBJECTIVES AND APPROACH

During the 1985 field season and several weeks in 1986, detailed mapping (1:10,000 scale) of the metamorphic rocks within and outside the study area was carried out in order to meet the following objectives:

(1) To determine the stratigraphy and structure of the Jumping Brook metamorphic suite and the geological relations of the suite to the Pleasant Bay Gneiss Complex.

(2) To determine the age of the Jumping Brook metamorphic suite relative to the Cambrian Cheticamp pluton and the relative timing of deformation and metamorphism in the suite.

(3) To derive a P-T-t path for all or part of the Jumping Brook metamorphic suite using petrography, microstructure, mineral chemistry, phase equilibria, and ^{40}Ar-^{39}Ar isotopic dating.

(4) To calculate theoretical P-T-t paths using a one-dimensional, thermal model, and to compare the results to

the geological P-T-t path in order to constrain the tectonothermal environment of metamorphism.

(5) To compare the lithologies and structures of the Jumping Brook metamorphic suite to other exposures of the western Highlands volcanic-sedimentary belt at Money Point and in the Middle River area to confirm the correlation of these units made by Barr et al. (1985).

Mapping was mainly restricted to coastal, road, and stream exposures as the mountain tops, with the exception of the Pleasant Bay area, are devoid of outcrop. The final geological map was reduced to a 1:25,000 scale (back pocket, Map 1).

Samples were collected for petrological examination and microprobe analysis of the dominant lithologies and various mineral phases, whole rock geochemistry, and ^{40}Ar-^{39}Ar isotopic dating of suitable lithologies. Sample selection for thin sectioning was based on lithologic representation, and applicability of mineralogy to geobarometry, geothermometry, and isotopic dating. All sample locations are shown on Map 2.

CHAPTER 2

LITHOLOGIES, FIELD RELATIONS, AND GEOCHEMISTRY

2.1 INTRODUCTION

The rock types of the study area include (1) the Jumping Brook metamorphic suite (Jamieson et al., 1987) and (2) later intrusive and extrusive rocks. Quartzo-feldspathic schists to ortho(?)gneisses and megacrystic granodioritic orthogneisses, exposed in the northern part and east of, the study area are described below and form part of the Pleasant Bay Gneiss Complex (Currie, 1982, 1987). However, they were not investigated further in this work. The volcanic and sedimentary rocks of the Upper Devonian Fisset Brook Formation and the sedimentary rocks of the Carboniferous Horton and Windsor Groups are exposed locally in the study area. These rocks were not examined in detail and therefore, their distribution on Map 1 (back pocket) is based partly on this study but mainly on work by McLaren (1955), Neale (1963), Currie (1982, 1987), Blanchard (1982), Blanchard et al. (1984), and Barr et al. (1985).

2.2 JUMPING BROOK METAMORPHIC SUITE

All units of the Jumping Brook metamorphic suite defined by Jamieson et al. (1987), excluding the Rocky Brook schist, are exposed as mappable units in the study area. Possible Rocky Brook schist equivalents occur as metre-scale layers in the Dauphinee Brook and Corney Brook schists but are not mappable units in the study area. An additional unit, the Fishing Cove River schist, is defined here and consists of high-grade schists and paragneisses grouped with the Corney Brook schist by Jamieson et al. (1987). The Faribault Brook metavolcanics and Dauphinee Brook schist are locally interlayered but deformation precludes determination of a depositional stratigraphy for the Jumping Brook metamorphic suite (section 3.2). Therefore, the lithologic units of the Jumping Brook metamorphic suite are described in order of first exposure in an approximately east to west, well exposed transect along Corney Brook (Figure 1.2 and Map 1), beginning at the structural base. This succession is referred to here as a "lithological stratigraphy", indicating it is based strictly on lithology, and does <u>not</u> imply a depositional stratigraphy.

Rocks of the Jumping Brook metamorphic suite are generally well foliated, fine-grained, and

compositionally layered and commonly exhibit northerly trending, moderately- to shallowly-plunging crenulation and mineral-stretching lineations (Chapter 3).

2.2.1 Faribault Brook Metavolcanics

The Faribault Brook metavolcanics are exposed along the Cabot Trail, a private service road just north of Grande Falaise, Trout Brook, No Name Creek, and Long Lake Creek (Figure 1.2). On the basis of field and petrographic data the following sub-units have been distinguished:

(i) metabasites

(ii) chlorite schists

(iii) felsic phyllites and schists

(see Figure 2.1, Table 2.1)

The chlorite schists are the dominant sub-unit of the Faribault Brook metavolcanics in the study area and are most abundant along Trout Brook. The metabasites and the felsic phyllites and schists occur interlayered with the chlorite schists and are more abundant near the structural base, in exposures along the Cabot Trail (Figure 2.1). Contacts between the sub-units are concordant and sharp.

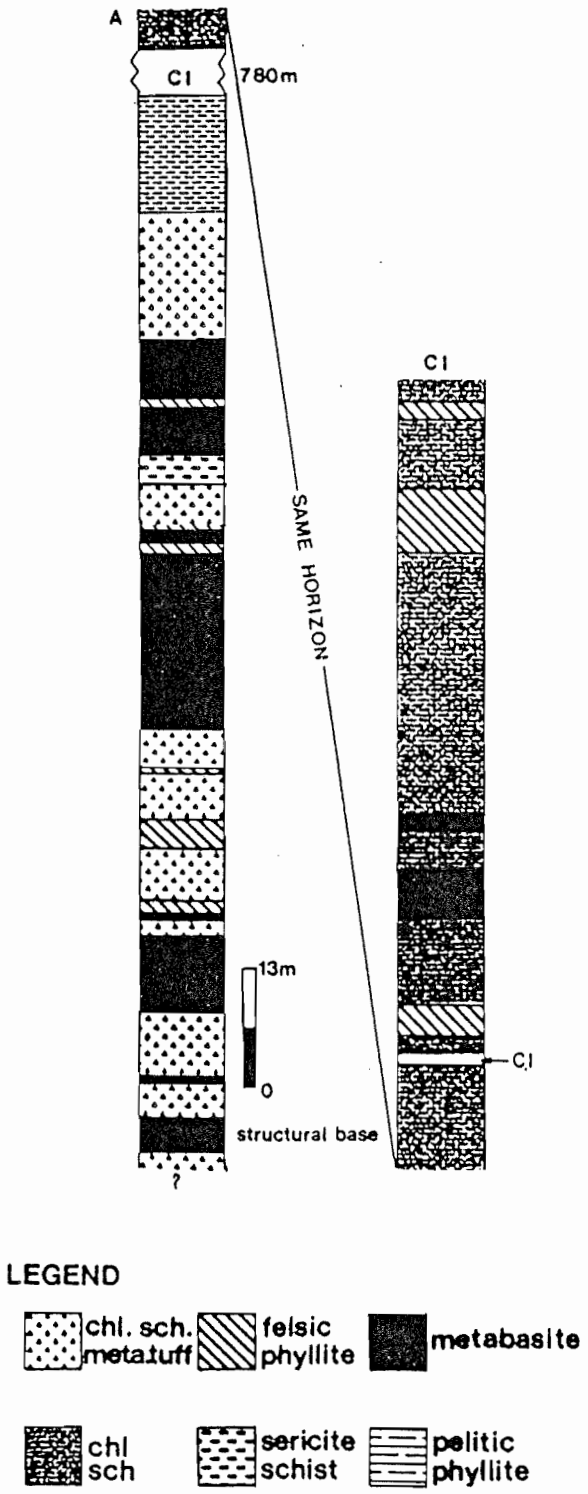

Figure 2.1. Lithological section through the Faribault Brook metavolcanics as exposed along the Cabot Trail modified after Plint et al., 1986. Thicknesses of units are visual estimates from stuctural dip. All data from this work. CI = covered interval (not to scale). Rock units are described in the text.

Table 2.1. Summary of field and petrographic criteria for distinction of the metavolcanic units and possible potoliths. Legend for abbreviations used is given in Appendix 1, Table A1.1.

LITHOLOGY	FIELD CRITERIA	PETROGRAPHIC CRITERIA	PROTOLITH
Banded, pink to grey phyllite	Compositional layering, colour	prismatic terminations in qtz, euhedral relict pl phenocrysts	flow banded rhyolite /silicic tuff[1]
Buff phyllite to schist	Compositional layering absent, colour	as above	silicic tuff[1]
Chlorite schist	Paucity of relict pheno-, crysts, rare. comp. layering, well foliated	rare ep pseudomorphs after pyroxene, relict pl phenocrysts	? strongly deformed flow or tuff[1]
	Abundant green-white relict pl phenocrysts, comp.layering	ep pseudomorphs after pyroxene, locally act-bearing	crsytal tuff[1] or phyric flow
Metabasite	Massive w.r.t. schist and phyllite, rare banding & relict pl phenocrysts	locally act-bearing, rare relict pl phenocrysts & micro-ophitic textures	basic to inter-mediate intrus-ion or flow

1. lithified or coherent pyroclastic deposit (Self, 1982)

(i) Metabasites

The metabasites are green, nondescript rocks, moderately foliated but massive compared to the chlorite schists and felsic phyllites. The latter feature presumably reflects the greater competency of the metabasites. The metabasite layers are 0.2 to 20 metres thick and locally contain ellipsoidal, epidote-rich pods elongated parallel to the foliation.

(ii) Chlorite Schists

The chlorite schists form layers 0.3 to 23 metres thick. They are slightly calcareous, contain abundant relict plagioclase crystals, and characteristically exhibit compositional layering defined by variation in relative abundances of quartz and feldspar to epidote and chlorite.

(iii) Felsic Phyllites and Schists

The felsic phyllites and schists form 1 centimetre to 15 metre thick layers and contain minor, but locally abundant, relict feldspar and quartz crystals. This sub-unit is further subdivided into (1) pink to grey, compositionally-laminated phyllitic metafelsites and (2) buff to pale yellow, locally garnet-bearing and compositionally laminated, quartz-sericite schists.

Compositional laminations are defined by alternating muscovite-rich and quartz-rich layers. The felsic phyllites and schists are locally interlayered with the low-grade pelitic phyllites of the Dauphinee Brook schist. The quartz-sericite schists have been recently correlated with the Rocky Brook schist (cf. Jamieson et al., 1987).

(iv) Protoliths

Possible relict pillow structures reported in the Faribault Brook area (Connors, 1986) and petrographic evidence (Connors, 1986; Plint et al., 1986) confirm a volcanic origin for the Faribault Brook metavolcanics. However, protolith determination is hindered by strong deformation and obliteration of macroscopic primary structures.

The banding and general paucity of porphyroclasts in the banded, phyllitic metafelsites suggests they are metarhyolites, but since this banding is tectonically modified (section 3.2) a volcaniclastic origin cannot be precluded. The buff to yellow quartz-sericite schists have been interpreted as silicic tuffs (Connors, 1986; Plint et al., 1986) but may have been flows. Where relict plagioclase crystals are abundant, the chlorite schists are interpreted to have been crystal tuffs but may have

been porphyritic flows. Where these relicts are rare or absent, a protolith is indeterminate. Concordant and sharp contacts with the chlorite and felsic schists suggest the metabasites are extrusive although these contacts are likely modified by deformation. Rare relict ophitic textures in some of the metabasites may represent the centres of thick flows or indicate that some of the metabasites were intrusive. Protolith interpretations are summarized in Table 2.1.

2.2.2 Dauphinee Brook Schist

The Dauphinee Brook schist is exposed along the Cabot Trail, south of Trout Brook and along Trout Brook. It consists of intimately interlayered pelitic to semipelitic phyllites to schists, and psammitic schist interpreted to be metamorphosed equivalents of shales, siltstones, and arkoses.

The pelitic phyllites are greenish grey to black, fissile rocks characterized by a well developed, phyllitic sheen. Fine- grain size precludes determination of mineralogy in hand specimen. The semipelitic phyllites are distinguished from the pelitic phyllites as those which contain at least 35% quartz and locally, contain small (1-3 cm) quartz porphyroclasts. Dark grey, pelitic lenses are observed locally in the semipelitic phyllites.

The psammitic schist is massive relative to the pelitic and semipelitic phyllites and is characterized by abundant, blue quartz porphyroclasts. Rarely, it contains metre-scale layers with abundant, pink feldspar porphyroclasts and layers of metaconglomerate with quartz, feldspar, and siltstone clasts (averaging 5 by 2 mm) in a chlorite-rich matrix. As feldspar and chlorite are generally minor phases in the psammitic schist, these layers may be volcaniclastic in origin or may simply indicate a poorly sorted protolith.

Eastwards, the Dauphinee Brook schist increases slightly in grain size and contains abundant biotite and locally garnet porphyroblasts. Locally, these mica(-garnet) schists contain fine-grained, arenaceous, calcareous layers and en echelon lenses 1 to 5 cm thick. These layers are folded, with axial planes parallel to the pervasive foliation, suggesting the en echelon lenses are remnants of transposed tight to isoclinal folds (Figure 2.2).

Quartz and quartz-feldspar veinlets (0.2 to 1.0 mm wide) trend parallel to and cut the foliation in the Dauphinee Brook schist, and many are boudinaged or isoclinally folded with axial planes parallel to the foliation.

Figure 2.2. (a) Field photo of en echelon quartz-carbonate lenses in the mica(-garnet) schists of the Dauphinee Brook schist interpreted to be remnants of transposed, tight to isoclinal folds. Lens cap diameter is 4.5 cm. (b) Boulder sample of the same rock type showing tight folds of the quartz-carbonate layers.

The mica(-garnet) schists locally grade into siliceous muscovite schists on the scale of an outcrop. These muscovite schists, and rare concordant layers of pink, fine-grained quartz-feldspar-muscovite(-garnet) schists locally exposed in the mica(-garnet) schists, are interpreted on a compositional basis to be metarhyolites or felsic tuffs. Concordant, unmetamorphosed, feldspar-porphyritic basaltic dykes have intruded the mica(-garnet) schists in the Robert Brook area and are probably related to the volcanic rocks of the Upper Devonian Fisset Brook Formation.

The mica(-garnet) schists are transitional between the lowest grade exposures of the Dauphinee Brook schist exposed along the Cabot Trail, and the Corney Brook schist exposed in the eastern parts of Corney Brook and Robert Brook. However, they are grouped with the Dauphinee Brook schist on the basis of well developed compositional layering and the overall finer grain size (of matrix and porphyroblasts) relative to the Corney Brook schist.

Locally interlayered with mica(-garnet) schists are white to grey, granular, commonly massive and well jointed quartzites. The quartzites contain minor relict, euhedral to subhedral, plagioclase and quartz crystals suggesting they are metamorphosed silicic tuffs. Near the

structural top of the Dauphinee Brook schist along Corney Brook, white to pale green, impure marbles interlayered with quartzites are exposed in a zone approximately 30 metres wide (normal to the foliation). The marbles are fine- to medium- grained, locally containing porphyroblasts of garnet, ?wollastonite, and diopside. The associated quartzites locally contain hornblende porphyroblasts.

Interlayered with the quartzites, marbles, and mica-(garnet) schists are rare metre-scale layers of a very fine- grained, pelitic, dark grey feldspar schist spotted with abundant, small (1-2 mm), rounded white plagioclase and microcline porphyroblasts (section 4.3). A well developed schistosity wraps around the porphyroblasts.

2.2.3 Corney Brook Schist

The Corney Brook schist consists of pelitic, staurolite-garnet schists, and interlayered semipelitic schists, locally with psammitic schists, exposed along the Cheticamp River, Corney Brook, and the northernmost ends of Jumping Brook and Robert Brook. The transition between the Dauphinee Brook and Corney Brook schists is gradational but it is defined here on the first appearance of staurolite.

The staurolite-garnet schists are well foliated, commonly crenulated, and characterized by abundant large porphyroblasts of staurolite and garnet in a phyllitic matrix (Figure 2.3). Prismatic staurolite, up to 6 cm in length, commonly shows cruciform twinning and is randomly oriented on foliation surfaces. Small biotite, kyanite, and plagioclase porphyroblasts are also developed although kyanite and plagioclase are rarely evident in hand specimen. The interlayered semipelitic schists consist of quartz, feldspar, biotite, garnet, and locally staurolite and kyanite. Minor, 1 to 5 metre layers of biotite-muscovite(-garnet) schist are locally exposed within the staurolite-garnet schist and probably reflect compositional variation within the original sediments.

Minor, metre-scale zones of fine-grained, hornblende-rich amphibolites and hornblendites (Appendix 1, Table A1.3), locally cross-cut by George Brook amphibolite (section 2.4.1), are interlayered with the Corney Brook schist in exposures along Corney Brook. The hornblende-rich amphibolites and hornblendites consist of acicular hornblende (randomly oriented on the foliation plane), feldspar, minor quartz, and locally epidote. On the basis of grain size and lack of igneous textures, the hornblende-rich amphibolites and hornblendites are interpreted to be mafic flows or high level intrusions.

a

b

Figure 2.3. (a) Field photo of the staurolite-garnet schists. Note random orientation of staurolite on the foliation surface and cross twins. Lens cap diameter is 4.5 cm. (b) Slabbed sample of staurolite-garnet schists.

Concordant, 1 to 7 metre layers of quartzite like those in the Dauphinee Brook schist are locally exposed in the Corney Brook schist.

2.2.4 Fishing Cove River Schist

This unit consists predominantly of biotite schists and paragneisses and is locally exposed as schlieren in the Pleasant Bay Gneiss Complex. The Fishing Cove River schist was previously considered to be a part of the Pleasant Bay Gneiss Complex (Currie, 1982, 1987; Plint et al., 1986). As no field evidence is found to support an original discontinuity between this unit and those already described, the Fishing Cove River schist is placed in the Jumping Brook metamorphic suite (section 2.5). The abundance of quartz-feldspar schists and orthogneisses in the Pleasant Bay Gneiss Complex is used to distinguish the complex from the Jumping Brook metamorphic suite.

The biotite schists and paragneisses are composed primarily of fine- to medium-grained, grey, pelitic to semipelitic, metasedimentary rocks, locally containing plagioclase porphyroclasts or hornblende, staurolite, garnet, and kyanite porphyroblasts. Pelitic lithologies are most common along Fishing Cove River and Benjies Lake Brook and in the easterly reaches of Corney Brook.

Locally, concordant layers of hornblende-rich amphibolites and hornblendites similar to those exposed in the Corney Brook schist, are exposed in the Fishing Cove River schist. Rare, nonfoliated, fine-grained, diabasic dykes and rhyolite of unknown affinity intrude the biotite schists and paragneisses.

Gneissic layering is defined by variation in the relative proportion of biotite to quartz and feldspar, but it is emphasized by the intrusion of sills of biotite granodiorite, fine-grained mafic rocks (now metamorphosed to biotite-hornblende schist and amphibolite), medium-grained granitoid rocks, undeformed to strongly sheared, granite pegmatites, and veins of quartz or quartz and feldspar. Pegmatites and amphibolites also commonly truncate the layering. The amphibolites are probably equivalent to the George Brook amphibolite (section 2.4.1) although not mappable as a separate unit as a separate unit in the Fishing Cove River schist at a 1:10,000 scale. They are commonly garnet-bearing and are referred to as garnet amphibolites in subsequent discussions. A sedimentary protolith for the Fishing Cove River schist is suggested by its aluminous composition and by pelitic to semipelitic, ?relict, compositional layering.

A one metre wide, concordant layer of pebble metaconglomerate is exposed in the Fishing Cove River schist near the headwaters of Robert Brook. Clasts (averaging 1 to 5 mm wide and 1 to 6 cm long) of quartz, feldspar, sandstone, and granite are elongate parallel to the mineral lineation with axial ratios up to 6:1. The metaconglomerate consists of 35 to 40 % clasts set in a fine-grained semipelitic, garnet-bearing matrix. Contacts with surrounding schists are sharp. The metaconglomerate, although a very minor component of the Corney Brook schist, may be equivalent to the conglomerate sub-unit of the Rocky Brook schist exposed further south (cf. Jamieson et al., 1987).

Exposed within the biotite schists and paragneisses in the easterly reaches of Corney Brook and along the northern part of Fishing Cove River is a fine-grained, strongly foliated, granitic, muscovite(-garnet) orthogneiss, locally intruded by pegmatite. This granite forms a very minor component of, and is therefore is grouped with, the Fishing Cove River schist.

2.3 PLEASANT BAY GNEISS COMPLEX

The Pleasant Bay Gneiss Complex (Currie, 1982, 1987) includes tonalitic to granodioritic orthogneiss, amphibolite, pelitic gneiss, and foliated granitoid rocks (Jamieson et al., 1987). On the basis of this work, the Pleasant Bay Gneiss Complex east of the study area is subdivided into (1) MacIntosh Brook quartzo-feldspathic gneiss, (2) MacKenzies Mountain megacrystic orthogneiss, (3) Grande Anse River biotite schists, and (4) miscellaneous foliated intrusive rocks. The relative ages of these units are unclear and therefore, they are described in order of decreasing abundance (cf. Figure 2.4). The distribution of these units is shown in Figure 2.4 (see also Figure 1.2 and Map 1).

2.3.1 MacIntosh Brook quartzo-feldspathic gneiss

The gneiss is granodioritic, composed of plagioclase, quartz, K-feldspar, biotite, and muscovite. It exhibits a well developed gneissic banding of alternating quartzo-feldspathic and biotite-rich, centimetre-scale layers and locally contains concordant layers of (garnet-)amphibolite. The MacIntosh Brook gneiss also occurs as concordant zones in the MacKenzies Mountain orthogneiss. It is unclear whether the MacIntosh

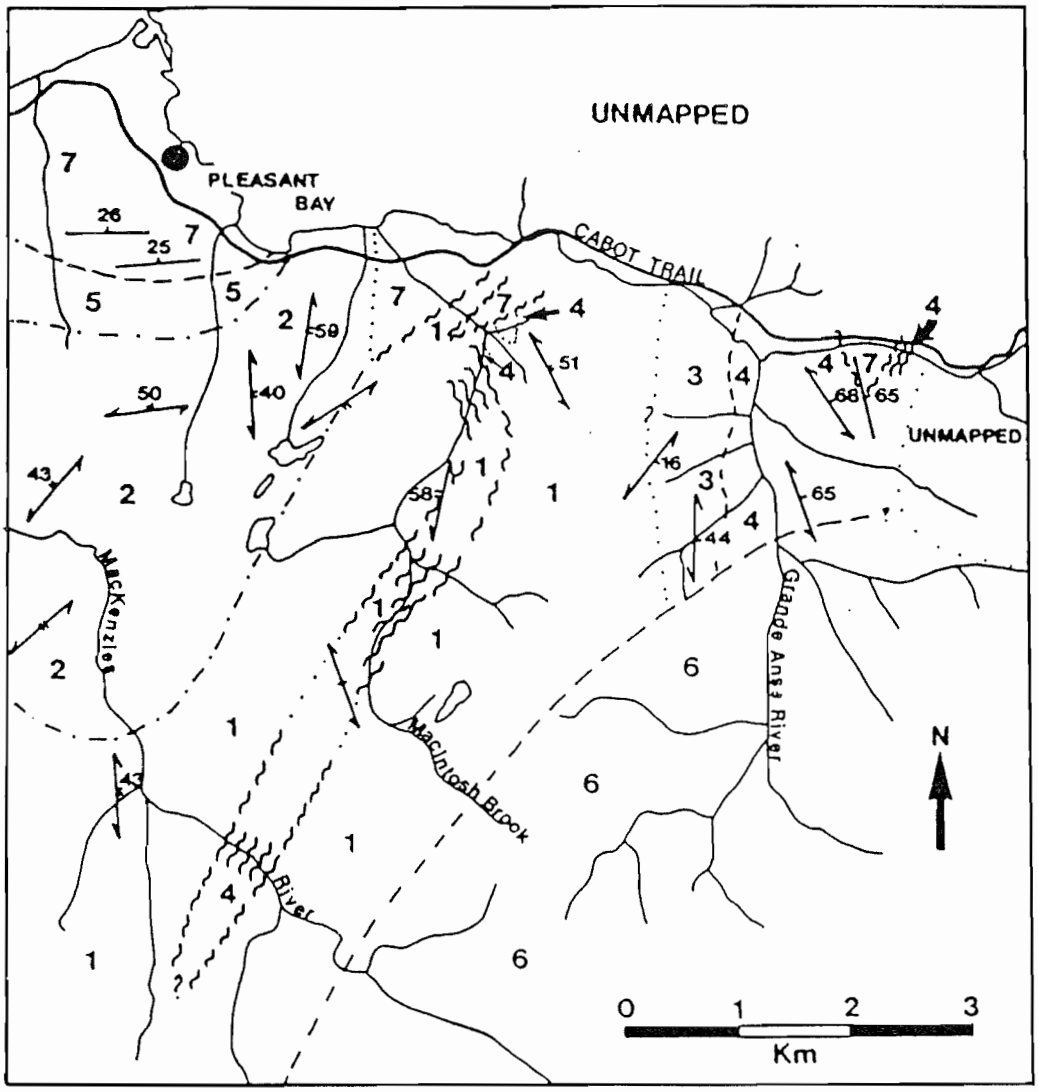

Figure 2.4. Geology of the Pleasant Bay Gneiss Complex (terminology after Currie, 1982, 1987) based on mapping done in this work. Regional location indicated in Figure 1.2. Regional structural trends are shown. Rock units are described in text. Areas indicated as "unmapped" were not mapped by the author.

Figure 2.4. **LEGEND**

Carboniferous

7. Horton Group clastic sedimentary rocks

Devonian

6. Margaree pluton, granodiorite

5. Predominantly biotite granodiorite

Silurian or older

4. Miscellaneous granitoid intrusions

3. Grande Anse biotite schists and amphibolite, minor marble

2. Predominantly Mackensies Mountain megacrystic orthogneiss

1. MacIntosh quartzo-feldspathic gneiss

SYMBOLS


Contact, asssumed, approximate, arbitrary, observed

Foliation, strike and dip


Ductile to brittle shear zone

Shear (< 2 metres wide)

Fault

Brook gneiss had an igneous or sedimentary protolith, but gradations into apparently granitic gneisses near the headwaters of MacIntosh Brook suggest an igneous protolith. Therfore, it may be equivalent to the Belle Cote Road orthogneiss described by Jamieson et al. (1986, 1987).

2.3.2 MacKenzies Mountain megacrystic orthogneiss

Granodioritic, megacrystic orthogneiss, locally garnet- or magnetite-bearing varies from a K-feldspar megacrystic gneiss (up to approximately 30% megacrysts) to a coarse-grained, foliated gneiss. Megacrysts are strung out along the foliation. Locally, the orthogneiss contains schlieren of the Fishing Cove River schist which in places are interlayered with garnet amphibolites or quartzo-feldspathic gneisses. The megacrystic gneiss is intruded by biotite granodiorite and granite pegmatite dykes and sills.

2.3.3 Grande Anse River biotite schists

This unit is composed of fine- to medium-grained biotite schist, calcareous amphibolite, and rare marble. Quartz-feldspar-muscovite veins, displaying pinch and swell structure, trend parallel to the foliation, and where abundant, give the rock a migmatitic appearance.

These rocks are interpreted to have a sedimentary protolith due to their calcareous nature and the presence of marble. However, the geological affinities of this unit are unknown due to poor exposure and it is placed in the Pleasant Bay Gneiss Complex for the purposes of this discussion.

2.3.4 Miscellaneous intrusive rocks

This division includes the pink foliated granite exposed along the Grande Anse River and described by Plint et al. (1986), a tonalitic, foliated granitoid rock intruded by aplitic dykes and exposed along an eastern tributary of MacIntosh Brook, and variably foliated, K-feldspar-megacrystic granitoid rocks exposed along the main branch of MacIntosh Brook and along an eastern tributary to the Grande Anse River. In the latter exposure, the granitoid rocks are strongly sheared. Regional correlations for these intrusive rocks are unknown.

2.4 PLUTONIC ROCKS

Barr et al. (1985) and Plint et al. (1986) have described the intrusive rocks of the Jumping Brook

metamorphic suite and thus, only those examined in detail and relevant to later discussions are described below.

2.4.1 George Brook Amphibolite

Medium- to fine-grained, foliated amphibolite commonly with a relict dioritic texture, and composed of hornblende, plagioclase, quartz, and minor biotite is exposed along George Brook and along Corney Brook (Figure 1.2 and Map 1) and informally referred to here as the George Brook amphibolite. The George Brook amphibolite is exposed in the Dauphinee Brook schist, Corney Brook schist, and occupies the transition between the Corney Brook and Fishing Cove River schists in exposures along Corney Brook. Rare centimetre-scale protomylonite zones trend parallel to the foliation. Contacts between the George Brook amphibolite and metasedimentary schists are concordant, and the pervasive foliation in the diorite is parallel to that in the surrounding lithologies. These observations suggest that the metasedimentary rocks and the George Brook amphibolite have shared at least one period of deformation. The amphibolite locally grades into biotite-hornblende-feldspar-quartz(-garnet) schist, commonly near contacts with the the metasedimentary rocks, which suggests that these contacts are sheared.

In exposures along the south branch of Corney Brook

and George Brook, pink aplitic to medium-grained granitic dykes (feldspar+quartz+biotite±muscovite), biotite granodiorite and unmetamorphosed pink, porphyritic rhyolite (probably part of the Fisset Brook Formation) intrude the George Brook amphibolite. Medium-grained, granitic dykes are locally tightly folded with axial planes parallel to the foliation. Concordant and discordant epidote-rich veins are common and medium-grained, hornblende-rich enclaves (cf. Conrod, 1984) are present in the George Brook amphibolite.

As in the Fishing Cove River schist, metre-scale layers of medium- to coarse-grained amphibolite are interlayered concordantly with the Dauphinee Brook and Corney Brook schists. In contrast to the George Brook amphibolite, these amphibolites contain no relict dioritic textures and are only approximately 1 to 3 metres thick. However, as these amphibolites are not individually mappable units they are grouped with the George Brook amphibolite.

Table 2.2 lists the whole rock chemistry for two samples of George Brook amphibolite showing relict dioritic texture and four samples of correlated amphibolite lacking relict igneous textures and exposed as metre-scale layers in the Corney Brook and Fishing

Table 2.2. Whole rock geochemistry of the George Brook aphibolite and correlated rocks. Samples 85-621d and 85-631g have relict dioritic textures. Major element whole rock chemistry for average gabbro (gb) and average diorite (dio) after Best (1982) are also shown. * indicates major or trace elements are an average of two analyses.

	85-706b	85-708b	85-245	85-345	85-621d	85-631g	Avg gb	Avg dio
SiO_2	46.96	48.11	53.91	50.51	45.85*	47.71	50.14	57.48
TiO_2	1.89	3.16	0.52	0.52	0.74	0.75	1.12	0.95
Al_2O_3	18.35	14.53	15.51	16.15	12.33	12.62	15.48	16.67
FeO	11.61	14.62	12.11	10.42	11.81	9.27	10.33	7.17
MnO	0.26	0.36	0.33	0.20	0.15	0.17	0.12	0.12
MgO	6.61	5.38	4.80	7.67	17.31	14.87	7.59	3.71
CaO	9.33	7.94	7.68	10.91	5.82	7.02	9.58	6.58
Na_2O	3.24	2.85	2.06	1.47	0.84	1.94	2.39	3.54
K_2O	0.30	0.91	1.50	0.97	0.56	0.17	0.93	1.76
P_2O_5	0.20	0.32	0.03	0.03	0.13	0.15	0.24	0.29
H_2O^+	0.54	0.89	1.07	0.87	5.20	4.00	0.75	0.21
TOTAL	99.29	99.07	99.52	99.72	100.74	98.67	98.67	99.88
Ba	50	260	385	216*	200	41		
Rb	3	29	61	42	20	4		
Sr	490	231	108	90	38	93		
Y	35	32	36	10	17	21		
Zr	169	151	37	14	85	89		
Nb	8	7	3	2	6	5		
Th	0	0	0	0	3	8		
Pb	16	5	36	3	8	14		
Ga	27	27	17	18	12	11		
Zn	176	124	239	91	100	103		
Cu	27	43	24	5	15	0		
Ni	47	19	16	26	369	260		
V	340	602	462	363	170	158		
Cr	188	7	15	130	1634	1154		

Cove River schists. Average major whole rock chemistry of gabbro and diorite are also shown in Table 2.2.

The two samples with relict igneous textures are extremely high in Mg, possibly reflecting Mg-enrichment during metamorphism. The SiO_2-contents of all the samples range from 46.96 to 53.91 weight percent, suggesting a gabbroic protolith, although major element chemistry has likely been modified by mobilization related to metamorphism. In addition, estimated relative percentages of Fe-Mg minerals (i.e. biotite and hornblende) to silicates, carbonates, and oxides range between 45 and 60%, in the range given by the IUGS classification for gabbros. Therefore, it is probable that the George Brook amphibolite and correlative rocks are metagabbros.

2.4.2 Cheticamp pluton

The Cheticamp pluton crops out in a narrow belt along the western margin of the Cape Breton Highlands from Corney Brook to the Northeast Margaree River south of the map area (Currie, 1975, 1982, 1987; Jamieson and Craw, 1983; Barr et al., 1985; Barr et al., 1987b). Its contacts with surrounding rocks of the map area are sheared or faulted (Figures 1.2 and 2.5). In exposures along Corney Brook, the Cheticamp pluton is cut by small faults and is unconformably overlain by, and in fault

Figure 2.5. Faulted contact between the Cheticamp pluton and the chloritoid-bearing phyllites of the Dauphinee Brook schist, exposed approximately 100 m south of the Corney Brook along the Cabot Trail. Fault surface orientation is 167°/88° NE. Arrow indicates layer of unmetamorphosed ?Horton Group arkose described in the text.

contact with, coarse-grained Horton Group arkose and conglomerate. Along the coast near Corney Brook, several easterly trending,, approximately 1 meter wide shear zones cut the pluton. Cataclastic deformation in the pluton results from small scale faults and from thrust faulting which has brought the pluton westward over the Fisset Brook Formation in the southern part of the study area (Currie, 1977, 1982, 1987; Barr et al., 1985).

In the map area the pluton is a medium- to coarse-grained, red, biotite(-muscovite) granodiorite intruded by fine-grained rhyolitic and plagioclase-porphyritic basaltic dykes (Barr et al., 1987b). Chloritized hornblende, reported by Currie (1982, 1987) in the northern exposures of the Cheticamp pluton, was not observed in this study. Fine- to medium-grained, nonfoliated to well foliated gabbroic to ?dioritic intrusive rocks are common near the Cheticamp pluton. Contacts between the Cheticamp pluton and these gabbroic rocks are visible near the mouth of Corney Brook and in nearby coastal sections but it is unclear which unit is younger. The affinities of the nonfoliated gabbroic rocks to the George Brook amphibolite, if any, are unknown. However, the foliated gabbroic rocks are relatively fine-grained and biotite-rich, as is the George Brook

amphibolite at possibly sheared contacts and therefore, they may be strongly deformed George Brook amphibolite.

The age of the Cheticamp pluton has been determined by Rb-Sr geochronology to be 530 ± 44 Ma (Cormier, 1972, recalculated by Keppie and Smith, 1978). This date has been confirmed by a U-Pb age of 550 ± 8 Ma (Jamieson et al., 1986) and a Rb-Sr age of 525 ± 40 Ma (Barr et al., 1987b).

2.4.3 Biotite Granodiorite

The Pleasant Bay Gneiss Complex and Fishing Cove River schist are intruded by sills and dykes of a commonly massive, locally weakly foliated, equigranular biotite(-muscovite) granodiorite and locally by rare monzogranite and tonalite which are probably related to the same magmatic event as the the granodiorite (Appendix 1, Figure A1.1, Table A1.2). The granodiorite contains enclaves of the MacKenzies Mountain megacrystic gneiss and is locally intruded by pegmatites and fine-grained granitic and diabasic dykes. Fairbairn et al. (1960) report a Rb-Sr whole-rock isochron age of 398 Ma for the granodiorite.

2.5 SUMMARY AND DISCUSSION

In the map area, the lithological stratigraphy of the Jumping Brook metamorphic suite consists of low- to medium-grade, metamorphosed, mafic to felsic, volcaniclastic rocks and flows overlain by medium- to high-grade, metamorphosed, pelitic to psammitic sedimentary rocks with minor volcaniclastic rocks, mafic flows, and carbonate rocks. Gabbroic intrusive rocks have been deformed with the Jumping Brook metamorphic suite. Metamorphic grade increases towards the east-northeast and is reflected by the appearance of staurolite and kyanite in the Corney Brook and Fishing Cove River schists. The transition between the Dauphinee Brook and Corney Brook schists is gradational. Although the transition between the Corney Brook and Fishing Cove River schists is obscured by George River amphibolite, no lithological, metamorphic, or structural evidence was found in the field to support a primary or tectonic discontinuity between these units as suggested by Currie (1987) (see section 4.3).

The nature of the boundary between the Jumping Brook metamorphic suite and Pleasant Bay Gneiss Complex defined here on the basis of the appearance of abundant quartz-feldspar schist and orthogneiss is unclear. No breccias

or mylonites are observed in the transition zone. Based on the presence of Fishing Cove River schist enclaves in the orthogneisses of the Pleasant Bay Gneiss Complex, the original boundary may have been partly intrusive or subsequently obscured by younger intrusions.

Sheared and faulted contacts between the Cheticamp pluton and the Jumping Brook metamorphic suite precludes determination of the relative ages of these units.

CHAPTER 3

STRUCTURE

3.1 INTRODUCTION

Deformation in the study area is polyphase (Currie, 1982, 1987; Craw, 1984; Conrod, 1984; Connors, 1986, Plint et al., 1986) and pre-, syn-, and post-metamorphic structures are observed. Field and petrographic observations indicate at least five, possibly six, deformation events in the Jumping Brook metamorphic suite. These structures are described in order from earliest to latest and are summarized in Table 3.1. Details of the microstructures are given in Chapter 4.

3.2 PRIMARY STRUCTURES

A common assumption in polydeformed regions is that compositional layering in metasedimentary rocks is bedding. This is not always valid (Hobbs et al., 1976; Davis, 1984). If fold transposition is extensive, the result is a compositional layering similar in appearance to bedding. The only clues that the bedding is

Table 3.1: Summary of deformation phases and related structures in the Jumping Brook metamorphic suite.

Deformation	Fabric	Lineation	Folds
	S_o		
D_1	S_1 axial planar cleavage	L_1 northerly trending intersection (S_o-S_1), mineral alignment, defm relict clasts	F_1 tight to isoclinal, rootless, intrafolial
D_2	S_2 schistosity, locally a crenulation cleavage	L_2 northerly trending, mineral align., defm relict clasts	F_2 crenulation (observed only in thin section)
D_3	S_3 mylonitic banding	L_3?	F_3 tight to isoclinal
D_4	S_4 incipient crenulation cleavage	L_4 fine, northerly trending crenulation axes	F_4 macro- to microscopic, upright, open to close folds
D_5	S_5 incipient axial planar and crenulation cleavage	L_5 large low A, easterly trending crenulation axes	F_5 kink folds & crenulations
D_6	S_6 fault surfaces	L_6 slickensides	------

tectonically modified are discontinuities in the compositional layering and relict fold hinges.

Compositional layering in the metasedimentary rocks of the Jumping Brook metamorphic suite superficially appears to be undisturbed bedding (Figure 3.1), but the presence of transposed isoclinal folds, local discontinuities, and strong variation in the compositional layering indicates it has been tectonically modified. Microstructures suggest that most of the compositional layering in the low-grade rocks is modified bedding whereas that in the medium- to high-grade rocks may be either tectonically modified bedding or partly metamorphic in origin (section 4.3). Thus, compositional layering is referred to as S_o^* in all subsequent discussions to indicate that it is a strongly modified primary layering.

3.3 ISOCLINAL FOLDS, CRENULATIONS, AND RELATED FABRICS (D_1 and D_2)

Parallel foliation and compositional layering and local intersection angles of 10° to 20° observed in exposures along Corney Brook and Robert Brook, and up to 30° to 45° reported in the Faribault Brook area (Craw, 1984; Connors, 1986), indicate the presence of

Figure 3.1: Tectonically modified bedding (S_o^*) in the Dauphinee Brook schist, exposed approximately 300 m south of Trout Brook along the Cabot Trail. Massive layers are psammitic schists; schistose layers are pelitic phyllites. Hammer is 25 cm long.

macroscopic, tight to isoclinal folds of compositional layering in the study area. These intersections and corresponding intersection lineations suggest antiformal north-northeasterly trending folds with closures towards the west and easterly dipping axial planes.

Mesoscopic and microscopic, tight to isoclinal, rootless, intrafolial folds of compositional layering, to which the pervasive foliation is axial planar, are best preserved in the low- to medium-grade metasedimentary rocks. Gently to moderately plunging fold axes trend north-northeasterly and north-northwesterly (Figure 3.2) and are interpreted to be related to the macroscopic folds. The wide variation in orientation is partly due to difficulty in obtaining reliable measurements from commonly poorly exposed intrafolial fold axes. Transposition of the small scale folds along the pervasive foliation is locally observed in outcrop and thin section. Locally in the Dauphinee Brook and Corney Brook schists and in the Faribault Brook metavolcanics, quartz, quartz-feldspar, and quartz-carbonate veins and veinlets cut the foliation but are folded and transposed in the same orientation as the folds of compositional layering. Felsic metavolcanic and quartzite layers in the

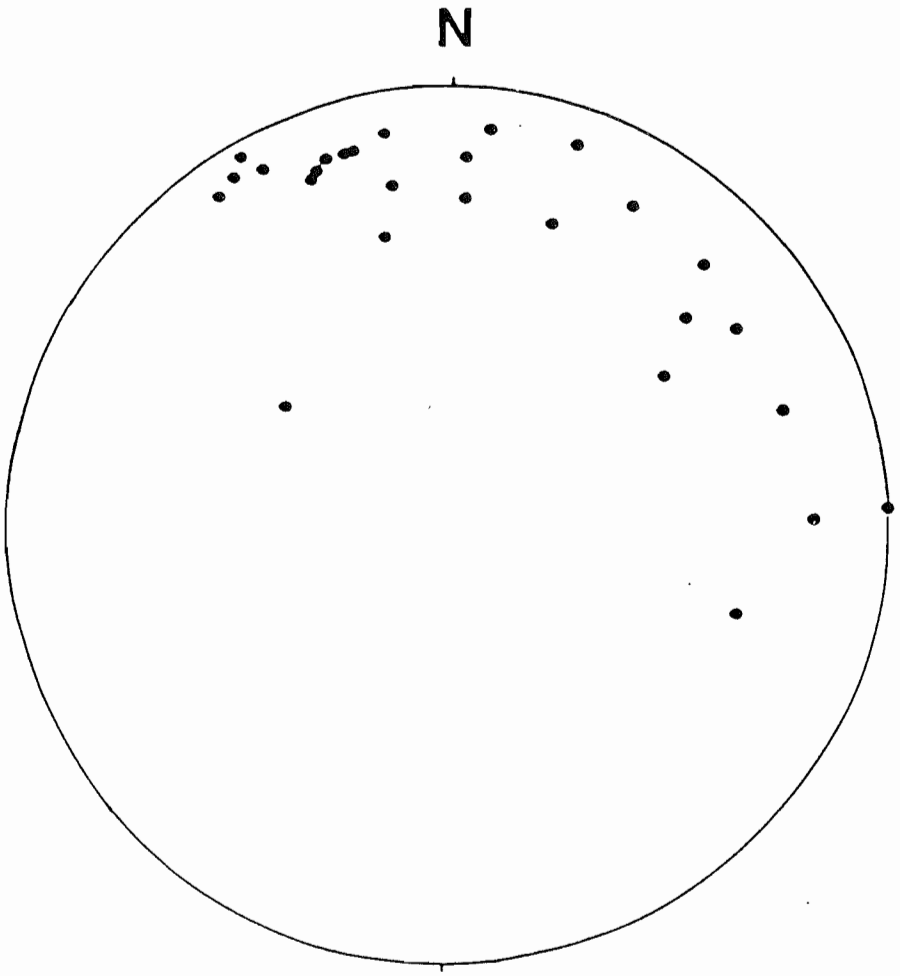

Figure 3.2: Equal area plot of axes of rootless, intrafolial, tight to isoclinal folds (F_1) in S_0*. Measurements were taken mainly of a well exposed 50 metre section along Corney Brook indicated in Figure 1.2. Total 28 points.

Jumping Brook metamorphic suite are locally necked and boudinaged.

Pervasive foliation in the metavolcanic and metasedimentary rocks is defined mainly by chlorite and by micas and chlorite, respectively. Slaty cleavage is well developed in the pelitic and semipelitic phyllites and in the felsic metavolcanic phyllites. The chlorite schists and metatuffs are schistose, possibly reflecting an original grain size difference relative to the phyllites. The metabasites and psammites are only moderately foliated reflecting the high competencies of these lithologies. Schistosity is pronounced in the medium- to high-grade pelites and semipelites, and locally an earlier foliation, defined by phyllosilicates at approximately 20^{o} to the pervasive schistosity, is evident in hand specimen. Craw (1984) also noted relicts of early foliations in the medium- to high-grade rocks. Microstructural interpretations (section 4.3) indicate that S_o^*, S_1, and S_2 result from a continuous deformation event, that S_2 formed by crenulation of S_1, and that S_1 and S_2 are the dominant fabric in the low-grade rocks and medium- to high-grade rocks, respectively. However, the orientation of S_2 in the low-grade rocks has only been identified in thin section.

Mutually parallel mineral and stretching lineations are widespread in the Jumping Brook metamorphic suite although they are most common in the medium- to high-grade rocks. Mineral lineations are defined by aligned chlorite in the metavolcanic rocks, by aligned chlorite or biotite in the metasedimentary rocks, and by aligned hornblende in the amphibolites. Stretching lineations are defined by elongated clasts in the metasedimentary rocks and locally, by elongated garnet porphyroblasts in the Fishing Cove River schist, and by elongated plagioclase in the amphibolites. These lineations have northerly trends and shallow to moderate plunges (Figure 3.3). In the medium- to high-grade rocks, the stretching lineations are interpreted to have developed during D_2 and suggest extension in a northerly direction. Whether the lineations in the low-grade rocks formed contemporaneously with those in the medium- to high-grade rocks is unclear as D_2 has apparently affected the former only slightly. Thus, the lineations in the low-grade rocks may have formed pre-D_2 and are grouped with L_1 in Table 3.1.

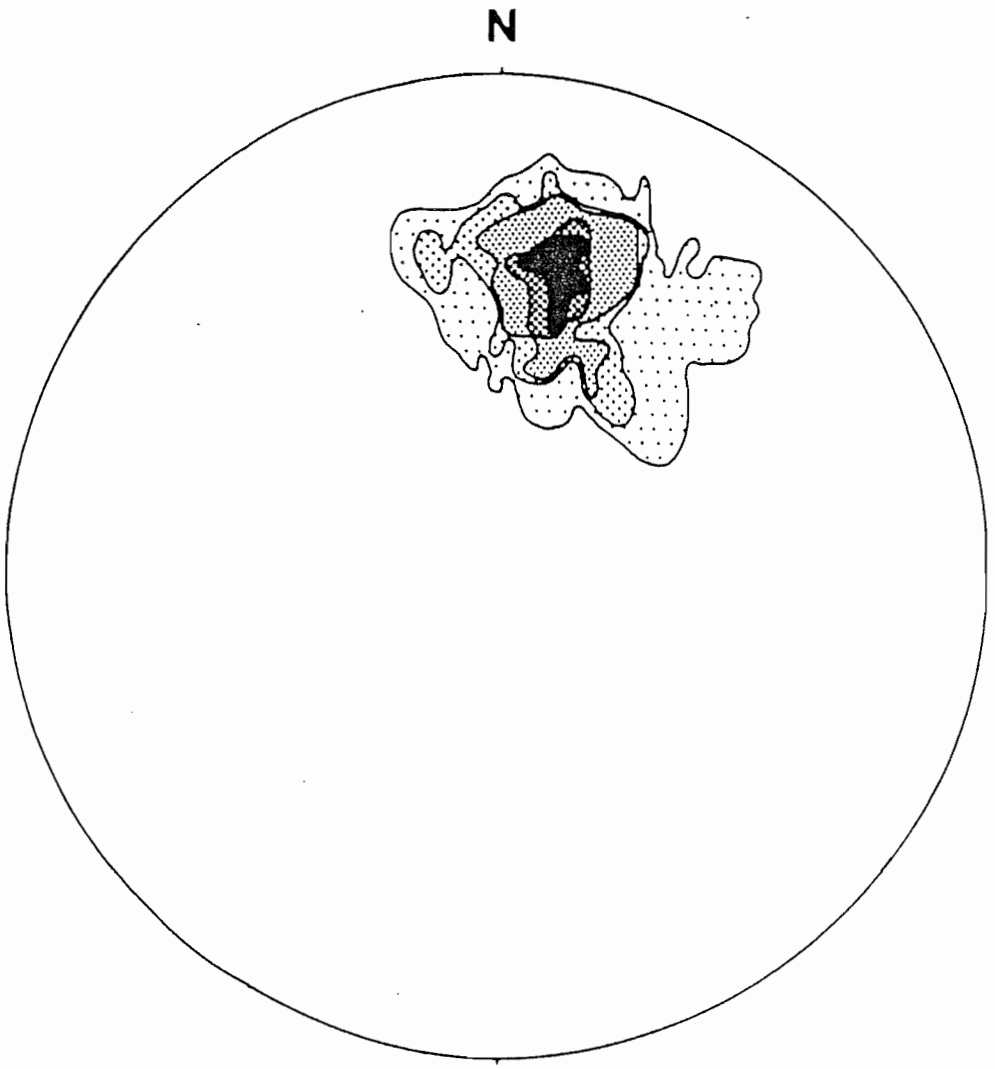

Figure 3.3: Contoured equal area plot of L_1 and L_2 lineation orientations in the Jumping Brook metamorphic suite. Contour intervals at 3, 7, 9, and 15 % of 1% of the area. Total 73 points. Stipple density increases with increasing density of points.

3.4 SHEARING (D3)

Protomylonite to mylonite zones, a few metres to 1.3 kilometres in apparent width, are developed along contacts between the Cheticamp pluton and surrounding rocks. Rare, near-vertical, open folds with northwestly-trending axial planes and northwest-plunging axes (eg. $310^{o}/80^{o}$) in the mylonite zone exposed just east of the Cabot Trail near Grande Falaise, suggest shearing occurred along an approximately vertical plane, although sense of shear could not be determined. The foliation in the sheared contact west of the south branch of Corney Brook has an easterly trend and dips approximately 50^{o} to the north. Foliation is well developed and intensified in the metasedimentary schists along the sheared contact exposed west of the south branch of Corney Brook. In the Cabot Trail exposures near Corney Brook, the contact between the Cheticamp pluton and Dauphinee Brook schist is faulted (Figure 2.5). Biotite in the pluton is strongly chloritized and the pervasive foliation in the low-grade pelites is highly contorted. A slice of nonmetamorphosed, coarse-grained arkose (probably of the Horton Group) is incorporated into the pelitic phyllite indicating that movement along this contact was initiated

or re-activated during Carboniferous faulting (D_6 - see below).

Craw (1984) reported several post-peak metamorphic shear zones in the Cheticamp River transect of the Jumping Brook metamorphic suite (section 1.4). An approximately 10 metre wide, northerly trending shear zone in the George Brook amphibolite (Figure 3.4) exposed on the south branch of Corney Brook may be the northerly extension of the most westerly ductile shear zone mapped by Craw (1984). Axial planes of tight to isoclinal folds of epidote(-hornblende) and quartz-feldspar veins within the shear zone are parallel to the mylonitic foliation, which trends 170° and dips approximately 60° to the east. Exposure is insufficient for determination of shear sense. Near the western margin of the shear zone, sheared George Brook amphibolite anastomoses around relatively less deformed pods of foliated amphibolite. Strongly foliated, possibly sheared, George Brook amphibolite, exposed along the main branch of Corney Brook, is probably a northward continuation of this zone.

It is clear that the shearing, both along the Cheticamp pluton contacts and in the George Brook amphibolite, postdates S_1/S_2 development in the Jumping Brook metamorphic suite. The northerly trending shear

Figure 3.4: Northerly trending shear zone approximately 10 metres wide (normal to the foliation) in the George Brook amphibolite, exposed along the south branch of Corney Brook. Hammer is 25 cm long.

zones according to Craw (1984), are related to westerly directed ductile thrusting of the major antiformal packages and hence postdates D_1/D_2 and predates the upright folding (D_4). The relative timing of the shearing along the boundaries of Cheticamp pluton is unclear. It is at least post-D_1/D_2 as it affects S_1/S_2 foliation in the pelites, and it pre-dates the Carboniferous faulting (D_6) that cuts the shear zones (Barr et al., 1985). Therefore, this shearing may have occurred during the uplift associated with the upright folding (D_4).

3.5 UPRIGHT FOLDING AND RELATED STRUCTURES (D_4)

The most obvious structure in the study area is a post-metamorphic, open, gently northerly-plunging, north-northeasterly trending antiform reflected in the girdle pattern shown by the contoured S-pole plot for pervasive foliation (S_1 and S_2) in Figure 3.5. Co-axial, mesoscopic, gentle to close folds of similar orientation and fine crenulations are observed throughout the metasedimentary and metavolcanic rocks. The D_1/D_2 lineations are almost everywhere parallel to the fine crenulations, although locally they are at a slight angle to one another and the crenulation lineation deforms the

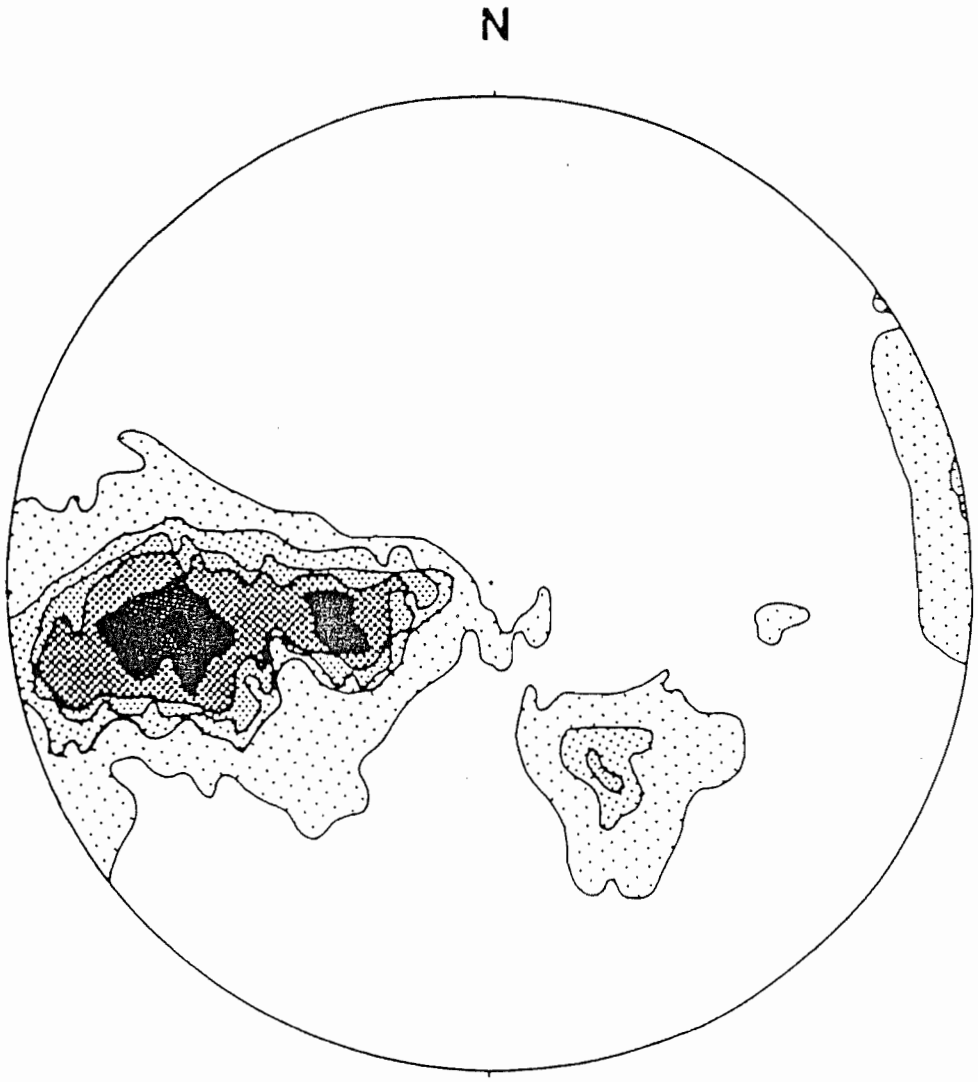

Figure 3.5: Contoured S-pole equal area plot of poles to the pervasive foliation (S_1/S_2) in the Jumping Brook metamorphic suite defining an open, gently northerly plunging, north-northeasterly trending fold. Contour intervals at 1, 3, 4, 5, 7, and 20% of 1% of the area. Total of 457 points. Stipple density increases with increasing density of points.

lineations. However, on the regional scale, the lineations are apparently unaffected by the late upright macroscopic fold suggesting that on the macroscopic scale, extension during D_1/D_2 and D_4 was co-axial and oriented north-northeast. The contoured equal area plots of axial orientations of the mineral and stretching lineations (see Figure 3.3) and of the mesoscopic, gentle to close, upright, symmetrical folds and fine crenulations (Figure 3.6) show these structures are approximately co-axial with the macroscopic fold.

Crenulations are best developed in pelites, chlorite schist, and felsic metavolcanic rocks where phyllosilicates are abundant. Wavelengths of the mesoscopic folds vary widely on outcrop scale from a few centimetres to approximately 10 metres; amplitudes vary from a few centimetres to 1 metre. Extensional fractures filled with fine-grained clay minerals and hematite have developed normal to the crenulations and locally form well developed, planar, easterly trending, moderately to steeply southerly dipping joints. Similar easterly trending, vertical or southerly dipping joints are common in all rocks types of the study area (Figure 3.7), and therefore are interpreted to result from

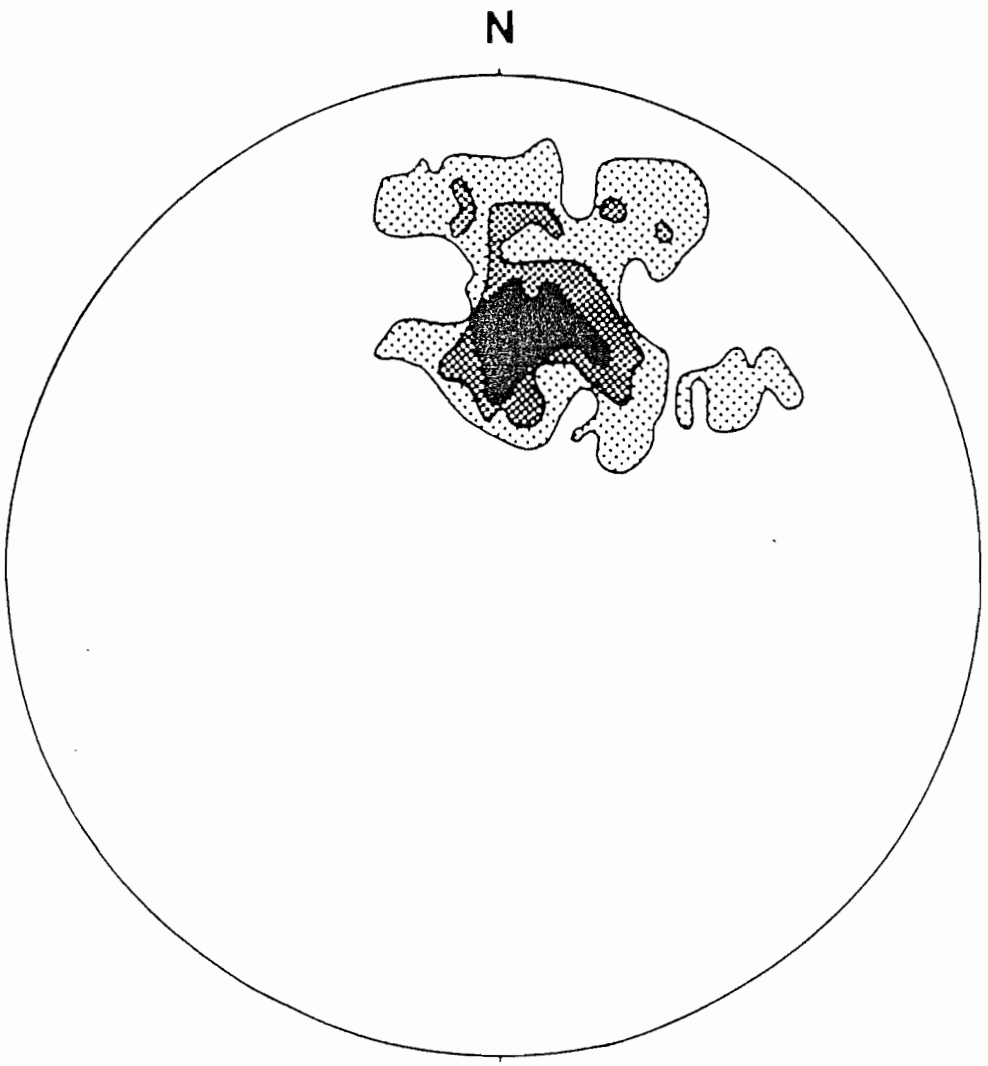

Figure 3.6: Contoured equal area plot of mesoscopic, gentle to close, upright, symmetrical folds (F_4) and fine crenulation axes (L_4) in the Jumping Brook metamorphic suite. Contour intervals at 3, 7, and 13% of 1% of the area. Total of 53 points. Stipple density increases with increasing density of points.

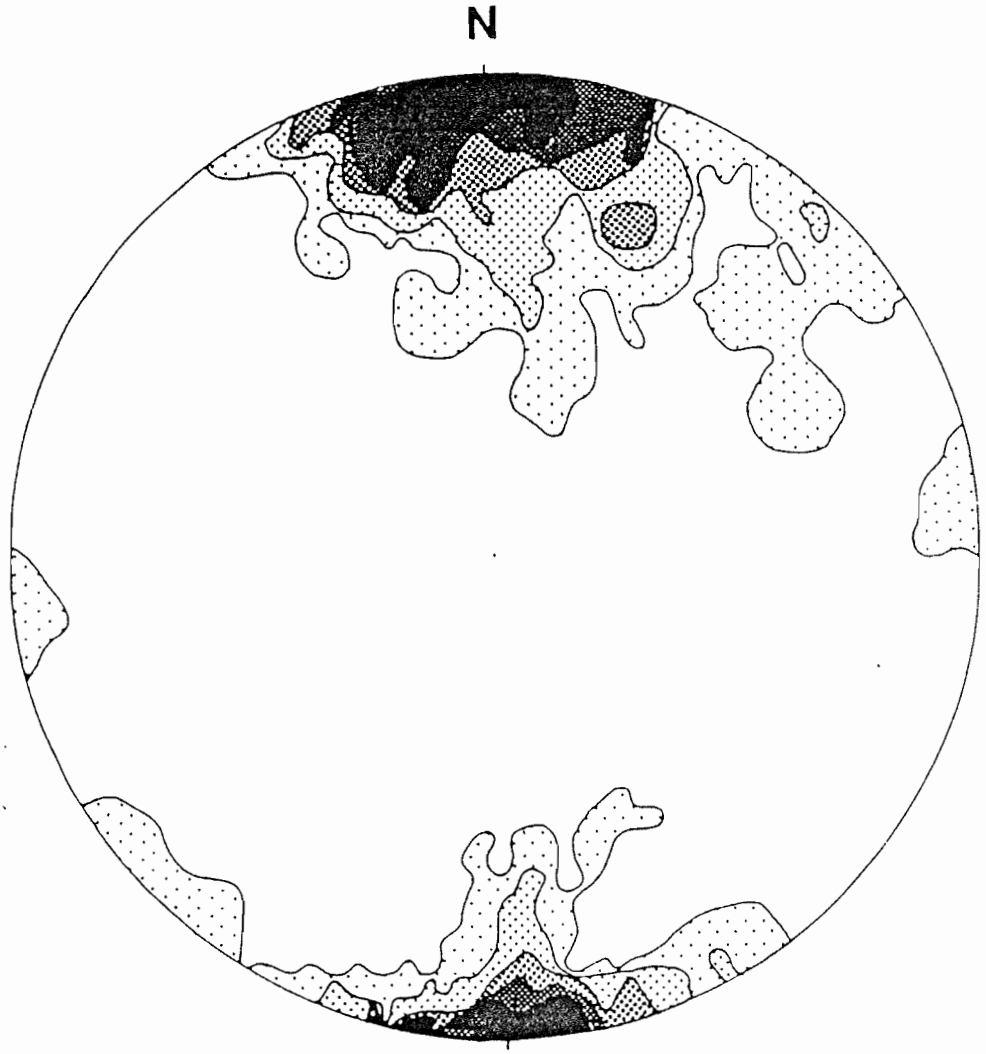

Figure 3.7: Contoured equal area S-pole plot of poles to joint surfaces in the Jumping Brook metamorphic suite. Contours at 2, 4, 6, 8, and 10% of 1% of the area. Total of 99 points. Stipple density increases with increasing density of points.

northerly extension, parallel to the macroscopic fold axis (D_4).

3.6 KINKING AND LATE CRENULATIONS (D_5)

Mesoscopic kink folds and low amplitude (0.1 to 0.3 mm), large wavelength (1 cm) crenulations are common in pelitic phyllites exposed along and near the coast. The D_5 kink folds are generally non-penetrative and exhibit chevron forms whereas the D_5 crenulations are generally penetrative and have rounded forms. Crenulation axes trend approximately east-west, plunge gently westward and deform S_1/S_2 and fine (D_4) crenulations. Kink axes show a bimodal distribution (Figure 3.8). Conjugate kink sets are observed in outcrop and the bimodal distribution in Figure 3.8 may reflect this. Conversely, there may be more than one generation of kinks although no conclusive evidence is found in outcrop for this possibility. Centimetre- to metre-scale fractures and faults are common along kink axial planes.

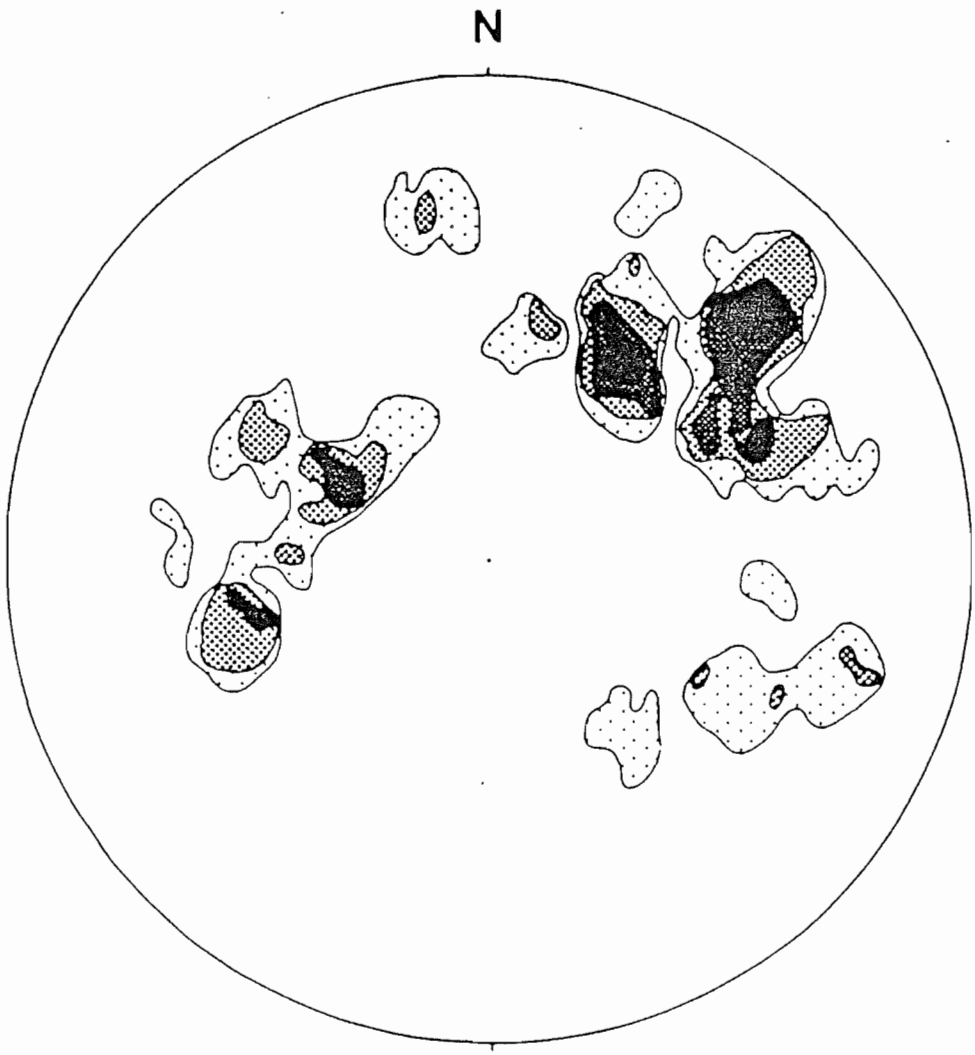

Figure 3.8: Contoured equal area plot of kink fold axes (F_5) in the Jumping Brook metamorphic suite showing a bimodal distribution of orientations. Contours at 2, 4, 5, 7, and 8% of 1% of the area. Total of 67 points. Stipple density increases with increasing density of points.

3.7 FAULTING AND CATACLASIS (D_6)

Extensive Carboniferous faulting and thrusting have occurred along the western coast of the Cape Breton Highlands (Currie, 1977, 1987; Barr et al., 1985). At Grande Falaise, thrust faults bring the Cambrian Cheticamp pluton over the Devonian Fisset Brook Formation which in turn is thrust over Horton Group arkoses (Currie, 1977; Barr et al., 1985). Late mesoscopic faults abound in low-grade metavolcanic and metasedimentary phyllites and schists exposed along the coast, and are present locally in the medium- to high-grade rocks. Coastal morphology is strongly fault-controlled. Breccias, gouge, slickensides, and hematite are common on fault surfaces, and veins of carbonate, and locally gypsum, are abundant in the vicinity of the faults. Minor foliation-parallel faults are observed in the low-grade rocks.

Determination of offset sense of the faults is hindered by the absence of marker horizons, although dip slip movement is indicated by local juxtaposition of felsic and mafic metavolcanic rocks. A detailed investigation of Carboniferous deformation is beyond the scope of this study. However, Figure 3.9 indicates a

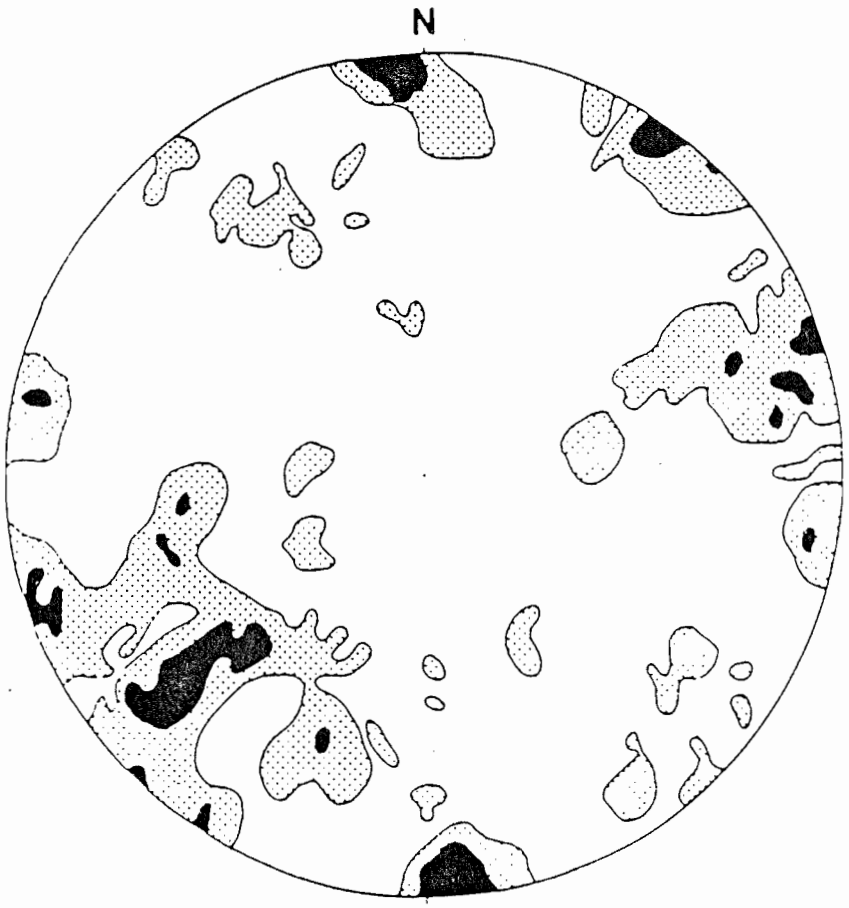

Figure 3.9: Contoured equal area S-pole plot of poles to fault surfaces in the Jumping Brook metamorphic suite showing a large range of orientations. Contours at 2, 4, and 6% of 1% of the area. Total of 146 points. Stipple density increases with increasing density of points.

large range in fault orientations, and a major northwesterly trend with an average dip of approximately 63° to the northeast or southwest. This faulting has been interpreted to be due to rifting during the formation of the Magdalen basin (Bradley, 1982).

3.8 DISCUSSION

Since the interpretation of the structures in the Jumping Brook metamorphic suite requires information gained from microstructures, a structural oveview is given in section 4.5. However, several important points are evident from the macroscopic structures.

Rocks of all grades have experienced the same early deformation (D_1) and later upright folding (D_4). Macroscopic structures observed support Craw's (1984) interpretation that the pervasive foliation in the low-grade rocks is axial planar to recumbent, macroscopic to microscopic, isoclinal folds of the compositional layering (S_o*), and that the foliation in the medium- to high-grade rocks is second generation.

Evidence in Corney Brook exposures for westward-directed thrusting along steep, northerly trending shear zones, as documented by Craw (1984) in the Cheticamp

River area, is found only in a 10 metre northerly trending shear zone in the George Brook amphibolite. This apparent lack of shear zones in the Corney Brook section is probably a function of exposure as the mylonite zones exposed along the Cheticamp River are only a few metres wide and the more easterly zones, if traced northwards, should intersect the inner reaches of Corney Brook where exposure is poor.

Intensity of deformation is partly lithologically controlled. Foliation is best developed in the pelitic and semipelitic phyllites, schists, paragneisses, and metavolcanic chlorite schists. More competent lithologies such as psammites and quartzites are weakly foliated and locally necked or boudinaged.

CHAPTER 4

PETROGRAPHY AND MICROSTRUCTURE

4.1 INTRODUCTION

Porphyroblast-matrix relationships are essential to deciphering structural and metamorphic histories in deformed metamorphic rocks (eg. Rosenfeld, 1968; Zwart, 1962; Spry, 1969). Recent models for the origin of inclusion trails in crenulated rocks (Bell and Rubenach, 1983; Bell, 1985) allow precise determination of the relative timing of porphyroblast growth and crenulation development. Bell's model allows determination of a reliable, relative time sequence of porphyroblast growth which can be used as the basis of petrological determination of P-T-t paths (eg. Bell and Brothers, 1985; Selverstone, 1985; Jamieson and Vernon, 1987).

However, application of these new ideas requires well developed porphyroblast inclusion trails. Conrod (1984), Craw (1984), and Connors (1986) showed that porphyroblasts in the metasedimentary rocks of the Jumping Brook metamorphic suite contain spectacular inclusion trails. As Corney Brook provides an almost complete sequence from the low- to high-grade rocks, a

detailed investigation of the microstructures was done on a suite of rocks from this area in order to:

(1) test the applicability of Bell's (1985) model (section 4.3.1)
(2) determine a sequence of metamorphic mineral growth and fabric-forming events
(3) establish, on a metamorphic and microstructural basis, whether a break exists between the Corney Brook and Fishing Cove River schists
(4) establish a basis for defining a P-T-t path for the Jumping Brook metamorphic suite.

4.2 GENERAL PETROGRAPHIC FEATURES

To facilitate discussion of porphyroblast-matrix relationships (section 4.3), the general petrographic features of the major rock types are described first, and are summarized along with the mineral assemblages in Table A1.1. Modal analyses of thin sections were conducted where required to assess rock types or protoliths. Visual estimates of relative mineral proportions are given in the supplementary individual sample descriptions, Appendix 1. A key for mineral

abbreviations used in the text and tables is listed in Table A1.1.

Polydeformation in the Jumping Brook metamorphic suite creates problems in the application of the terms porphyroclast and porphyroblast because early-formed porphyroblasts may become porphyroclasts with continued or subsequent deformation. Therefore, the term porphyroclast is used here to refer to large mineral grains in a finer grained matrix which represent deformed relicts of the pre-metamorphic and pre-deformational assemblage, such as phenocrysts or detrital grains. Foliation always wraps around porphyroclasts and they show evidence of grain size reduction resulting from cataclasis and recrystallization. In some rocks, the majority of porphyroclasts show little evidence of deformation and preserve original grain shapes indicating they were originally phenocrysts and are therefore is not strictly porphyroclasts following the above definition. In these cases, the porphyroclasts are referred to as relict phenocrysts. "Porphyroblast" is used for any large metamorphic mineral in a finer-grained matrix, even where it has been subsequently deformed and therefore is a porphyroclast by some definitions.

4.2.1 Primary Features and Mineral Assemblages

Relict primary features are common only in the low- to medium-grade rocks and consist of pseudomorphs, porphyroclasts of detrital fragments and igneous minerals, relict phenocrysts, and tectonically modified sedimentary layering. Muscovite, chlorite, or biotite are commonly concentrated in folia around porphyroclasts, relict phenocrysts, and porphyroblasts. Associated strain shadows are ocuppied by quartz, (chlorite, and carbonate).

Xenoblastic, randomly oriented epidote aggregates with hexagonal or rectangular outlines are locally observed in the mafic Faribault Brook metavolcanics (Figure 4.1). The shapes of these aggregates suggest they are pseudomorphs after clinopyroxene. Rare relict clinopyroxene has been reported in the Faribault Brook area by Craw (1984). Relict, euhedral to subhedral, quartz and plagioclase phenocrysts and porphyroclasts are common in all the Faribault Brook metavolcanics. In the metabasites and chlorite schists these plagioclase relicts are commonly replaced by albite, epidote, and white mica whereas in the felsic phyllites and schists, plagioclase is sericitzed. Locally, garnet has nucleated on quartz in the quartz-sericite schists.

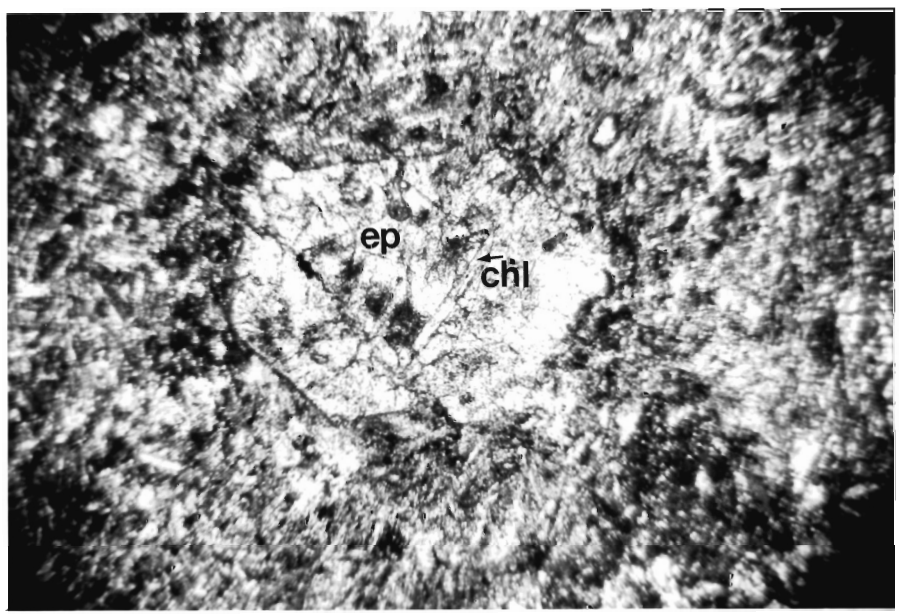

Figure 4.1. Hexagonal-shaped aggregate of epidote (ep) and minor chlorite (chl) in a chlorite schist of the Faribault Brook metavolcanics, interpreted as a pseudomorph after clinopyroxene. Field of view = 2.25 mm.

The metasedimentary phyllites and schists locally contain xenoblastic to subidioblastic quartz, and less commonly plagioclase porphyroclasts. Quartz and plagioclase relict phenocrysts and porphyroclasts are present in the quartzites, and quartz locally preserves prismatic terminations. Muscovite and/or garnet have nucleated on the plagioclase relicts and porphyroclasts in the quartzites. Similarily, garnet in the low- and medium-grade schists locally has nucleated on quartz porphyroclasts and relict phenocrysts. Partially recrystallized quartz inclusions observed in garnet porphyroblasts in some of the medium- to high-grade schists are probably relicts of quartz porphyroclasts.

Porphyroclasts and pseudomorphs indicate that the mafic metavolcanic rocks originally contained calcic plagioclase and clinopyroxene phenocrysts. Porphyroclasts and relict phenocrysts in the felsic metavolcanic phyllites and schists indicate a primary mineral assemblage that included plagioclase and quartz phenocrysts. Based on relict phases, the detrital mineral assemblages in the metasedimentary phyllites and schists included feldspar, quartz, carbonate, apatite, zircon, and probably opaque minerals. Tourmaline may also have been a detrital phase as it is common even in the lowest grade metasedimentary rocks.

Compositional layering in the metavolcanic rocks is defined by the variation in relative proportions of chlorite and epidote to quartz and feldspar, and in the metasedimentary rocks by the variation in the ratio of micas and/or chlorite to quartz and feldspar. In the low-grade rocks, compositional layering is also defined by significant grain size variation, and the coarser layers preserve clastic textures. Thus, in these rocks, compositional layering is interpreted as tectonically modified bedding. In the medium- to high-grade rocks, compositional layering on a centimetre- to metre-scale may also be relict bedding. However, evidence for crenulation cleavage development in these rocks (section 4.3) suggests that some may be the result of metamorphic differentiation.

4.2.2 Foliations and Matrix Textures

All major lithologies are foliated to varying degrees, with the exception of later plutonic rocks. Foliations are generally defined by phyllosilicates and elongate quartz and feldspar. Quartz and feldspar matrix grains and porphyroclasts are variably recrystallized in all rock types.

Foliation in the felsic rocks of the Faribault Brook metavolcanics and in the low-grade metasedimentary rocks

is defined by muscovite and chlorite. At higher grades, foliation in the latter is defined by biotite and muscovite. Chlorite, and locally actinolite or actinolitic hornblende, define the foliation in the mafic rocks of the Faribault Brook metavolcanics, whereas in the George Brook amphibolite and related rocks, hornblende and locally elongated plagioclase define the foliation. Muscovite and elongated polygonal quartz and feldspar grains define the foliation in the muscovite-garnet orthogneiss in the Fishing Cove River schist.

In all rock types, the foliation always wraps around relict phenocrysts, porphyroclasts, and commonly porphyroblasts. Where these are abundant, the foliation anastomoses. All rock types exhibit a schistose to granoblastic-elongate texture (Collerson, 1974) depending on the phyllosilicate content, excluding the quartzites and marbles, which have a subgranoblastic to granoblastic texture.

4.2.3 Porphyroblasts

Porphyroblasts, including chlorite, chloritoid, garnet, biotite, muscovite, plagioclase, microcline, staurolite, kyanite, and amphibole, are developed in most rock types. Porphyroblasts in the metasedimentary rocks are commonly subidioblastic and contain well developed

inclusion trails. Porphyroblast development is strongly compositionally controlled and is most common in phyllosilicate-rich layers. Biotite has grown preferentially in graphitic pelitic lenses in semipelitic phyllites of the Dauphinee Brook schist whereas chloritoid is developed in the surrounding phyllite (Figure 4.2). Kyanite is almost completely restricted to muscovite-rich cleavage domains in the Corney Brook and Fishing Cove River schists. Hornblende porphyroblasts are locally developed in some of the medium-grade psammitic schists, in the quartzites where interlayered with marbles, and are commonly randomly developed on foliation surfaces in the medium- to high-grade amphibolites and hornblende-biotite schists. The latter hornblende porphyroblasts, therefore, are interpreted to be post-tectonic relative to the pervasive foliation. Detailed description of porphyroblasts in the metasedimentary rocks is given in section 4.3.

Rare porphyroblasts of actinolite (locally rimmed by blue-green amphibole) and garnet are present in the mafic and felsic Faribault Brook metavolcanics, respectively. Amphibole, biotite, and garnet porphyroblasts are developed in the George Brook amphibolite and correlated amphibolites. Xenoblastic to idioblastic, locally poikiloblastic, amphibole porphyroblasts in the lowest

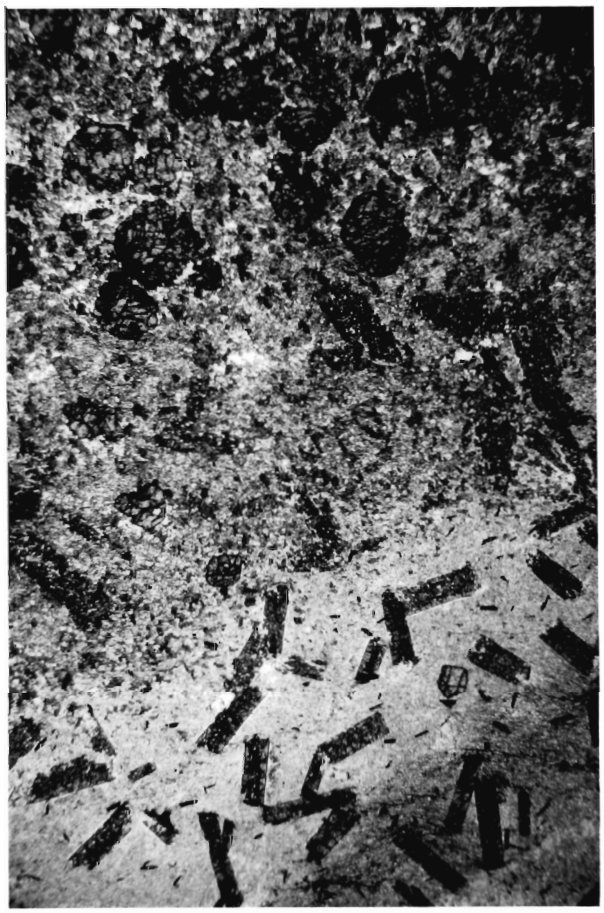

Figure 4.2. An example of compositional control on porphyroblast development in the Jumping Brook metamorphic suite. Upper part of photo is a carbonaceous, pelitic lens in a low-grade semipelitic phyllite of the Dauphinee Brook schist. Garnet and biotite are developed in the pelitic lens, whereas chloritoid is abundant in the surrounding semipelitic schist. Biotite and chloritoid co-exist near the margins of the pelitic lens. Field of view = 10 mm.

grade George Brook amphibolite consist of actinolitic cores with hornblende rims. This zoning disappears towards the east-northeast supporting the interpreted east-northeastward increase in metamorphic grade. In the medium- to high-grade amphibolites, hornblende is commonly subidio- to idio-blastic, poikiloblastic, and randomly oriented on the foliation surface. Biotite is generally subidioblastic, contains zircon and quartz inclusions, and is locally replaced by K-feldspar and chlorite. Garnet is present only in the high-grade amphibolites. It is subidioblastic, contains rare fine-grained quartz and opaque inclusions, and locally shows minor retrogression to chlorite.

4.2.4 Retrogression

Low-grade metamorphism of volcanic rocks involves retrogression of high temperature igneous assemblages and thus distinction between prograde and retrograde metamorphic effects is difficult. For the purposes of this discussion, any replacement of igneous minerals is regarded as prograde metamorphism. Replacement of metamorphic minerals by a later, lower grade metamorphic assemblage is regarded as retrograde metamorphism.

Rare muscovite pseudomorphs after large kyanite blades, commonly containing relict kyanite, are present

in the Fishing Cove River schist (Figure 4.3). These muscovite pseudomorphs are interpreted to be retrograde as grain boundaries between the relict kyanite and the surrounding muscovite are ragged and co-existing phases are strongly retrograded (cf. Guidotti, 1968).

Retrograde alteration is common, but not pervasive, in the metasedimentary rocks. Plagioclase is sericitized, garnet and staurolite are partially replaced by chlorite and iron oxide along fractures and grain boundaries, biotite is replaced by chlorite, iron oxide, and potassium feldspar, and kyanite is replaced along cleavages and grain boundaries by muscovite, chlorite, or submicroscopic intergrowths of clay minerals and phyllosilicates, possibly including chlorite, white mica, and hematite. Chloritoid, and locally staurolite, are retrograded to similar intergrowths along partings and grain boundaries.

Retrogression in the George Brook amphibolite and correlated amphibolites is minor and consists of chloritization of hornblende and biotite and sericitization of plagioclase.

Locally, late prehnite-bearing, epidote-rich veins cut the foliation in the George Brook amphibolite. These veins are interpreted to be retrograde since they cut the foliation and contain a greenschist facies mineralogy

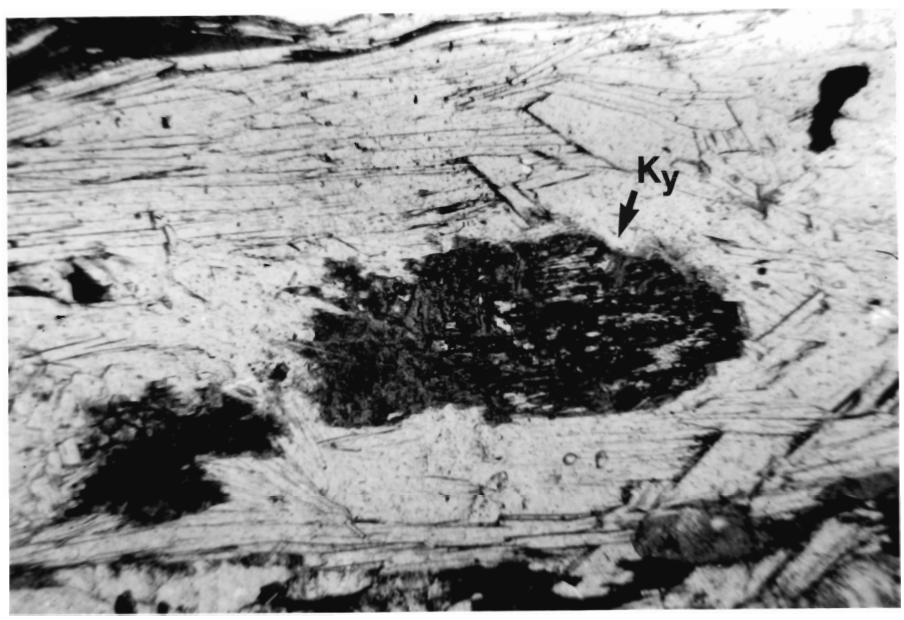

Figure 4.3. Retrograde muscovite pseudomorph after bladed kyanite porphyroblast in a pelitic schist of the Fishing Cove River schist. Note kyanite relict (Ky) in centre of pseudomorph. Field of view = 4.5 mm.

whereas the host rock mineralogy is characteristic of the epidote-amphibolite facies conditions (Chapter 6, section 6.2).

4.3 PORPHYROBLAST-MATRIX RELATIONS

4.3.1 Nonrotational Porphyroblast Model

Recent studies have shown that sigmoidal inclusion trails, traditionally interpreted to reflect porphyroblast rotation (eg. Spry, 1969; Schoneveld, 1977; Lister and Williams, 1983), can result from deformation partitioning and progressive crenulation cleavage development (eg. Bell and Rubenach, 1983; Bell, 1985, 1986; Bell et al., 1986). This "nonrotational model" holds that primary heterogeneities (eg. ductility contrasts between grains, rock types, sedimentary beds) and secondary heterogeneities (eg. early fold hinges, porphyroblasts, porphyroclasts, cleavage domains) in competency take up different components of strain during bulk inhomogeneous flattening or shearing (Bell, 1985). Strain is partitioned into two major components: (1) progressive shearing and (2) progressive flattening. Phyllosilicates easily accommodate shearing along the (001) plane but many common porphyroblast phases and oxides lack this layered structure. They cannot

accommodate the shearing component and hence act as rigid bodies taking up the progressive flattening component. Consequently, dislocation density gradients and therefore, chemical potential gradients, form across the shear zones at the rims of these rigid bodies causing them to dissolve. The net result is rotation or inhomogeneous simple shearing of the matrix around the porphyroblasts, accompanied by porphyroblast dissolution normal to the main foliation, and growth parallel to the foliation (Figure 4.4).

Re-orientation of the matrix foliation, or re-activation of an earlier fabric preserved in the matrix by continued or subsequent deformation, may cause truncation of an inclusion trail fabric by the matrix foliation (Bell, 1985; Bell, 1986). Consequently, in a single thin section, the internal fabric may be continuous with the matrix in one porphyroblast and truncated by the matrix in another porphyroblast of the same mineral. Using traditional criteria (eg. Spry, 1969; Zwart, 1962), one would conclude that growth of the porphyroblast both predated and postdated the development of the matrix foliation in a single section. Bell's nonrotational model is clearly simpler (Figure 4.5).

According to the nonrotational model, porphyroblasts are preferentially dissolved at zones of high strain (eg.

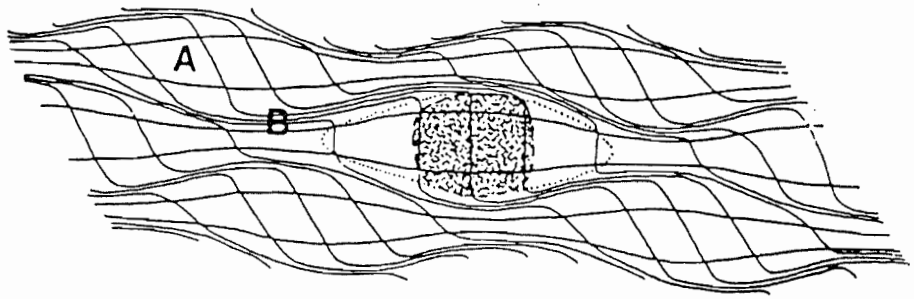

Figure 4.4. Sketch of a strain field around a porphyroblast (shaded) resulting from partitioning of progressive bulk inhomogeneous shortening into (A) dominantly flattening component and (B) dominantly shearing component (after Bell, 1985, Figure 1b). The porphyroblast is a zone of no strain. This diagram illustrates why the porphyroblast does not rotate, provided it does not deform. The shearing component of deformation is taken up in the matrix, whereas the rigid porphyroblast protects an ellipsoidal area of the matrix from the effects of progressive shearing.

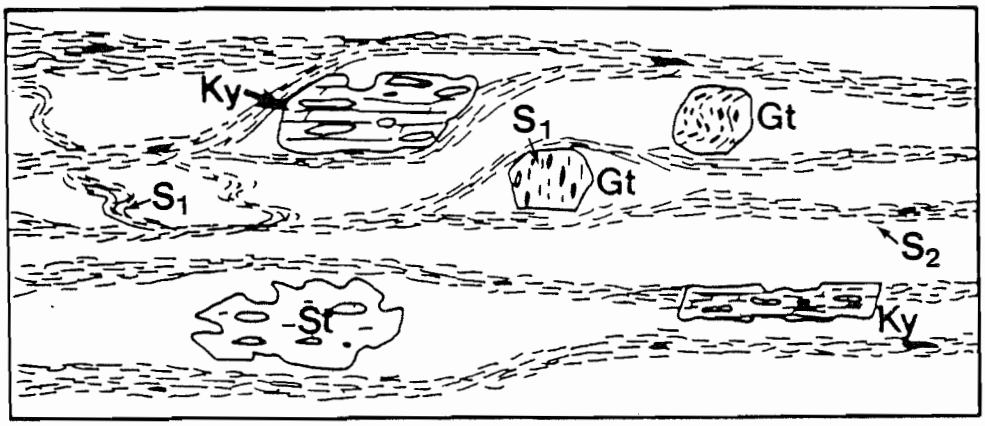

Figure 4.5. Cartoon illustrating traditional versus new interpretations of porphyroblast-matrix relationships. Dashed lines represent micas, blank zones represent areas of dominantly quartz and feldspar. Using traditional criteria (eg. Spry, 1969; Zwart, 1962), the microstructural sequence is pre-tectonic kyanite (Ky) and garnet (Gt) growth, crenulation of S_1 to form S_2 with syntectonic garnet growth and rotation, post-S_2 staurolite (St) and kyanite growth. Using the non-rotational model, the sequence is crenulation of S_1 to form S_2, pre- to early syn-crenulation garnet growth (stage 1 and 2), post-S_2 staurolite and kyanite growth, followed by localized re-orientation of foliation around garnet and kyanite. Note that S_i in kyanite is continuous with S_2 in the porphyroblast in the lower right and truncated by S_2 in porphyroblast in the upper left.

fold limbs), and re-precipitated in sites of low strain (eg. strain shadows or fold hinges), provided the porphyroblasts are stable at the ambient P-T conditions. This is consistent with the common observation that crenulation fold limbs, and ultimately crenulation cleavage domains, are sites of high strain and hence dissolution whereas fold hinges are sites of precipitation (eg. Marlow and Etheridge, 1977). According to Bell (1985) and Bell et al. (1986), fold hinges provide ideal sites for porphyroblast nucleation as (1) they are low strain sites, (2) they contain a large amount of stored strain energy relative to fold limbs in which strain energy is decreased by dissolution of silicates and oxides and recrystallization of phyllosilicates, and (3) they contain extensional microfractures that provide convenient interdiffusion pathways of ions required for porphyroblast growth. Thus, commonly observed sigmoidal inclusion trails may represent crenulations as opposed to porphyroblast rotation.

The subsequent sections describe the microstructure of the pelitic and semipelitic rocks of the Jumping Brook metamorphic suite which contain abundant porphyroblasts exhibiting spectacular inclusion trails. Fabric development in the Jumping Brook metamorphic suite is a

continuous and heterogeneous process. Early fabrics and microstructures are best preserved in the lowest grade rocks of the Dauphinee Brook schist. Later fabrics and microstructures are best developed in the medium-grade mica(-garnet) schists of the Dauphinee Brook schist, in the medium-grade staurolite-garnet schists of the Corney Brook schist, and in the Fishing Cove River schist. Descriptions of the microstructures are thus divided into low-, medium-, and high- grade rocks although the sequence of microstructures overlaps between each division. The terms low-, medium-, and high-grade are used in a relative sense only (both here and in subsequent discussions) since epidote-amphibolite facies is the lowest grade in the study area (section 6.2). The inclusion trails preserve different stages of a crenulation cleavage now observed as the pervasive matrix foliation in the medium- to high-grade rocks. Early stages of this crenulation are locally preserved in the matrix. All six stages of crenulation cleavage formation defined by Bell and Rubenach (1983) are recognized (Table 4.1 and 4.2). The stage preserved in a certain porphyroblastic mineral may vary from sample to sample, but the sequence of growth between porphyroblasts of different minerals is consistent (cf. Bell and Rubenach, 1983).

Table 4.1. Stages of crenulation development after Bell and Rubenach (1983) and corresponding descriptive terms used in text.

STAGE	No.	PROCESSES	DESCRIPTIVE TERMS
	1	original foliation (S1)	straight to weakly sigmoidal, non-crenulated
	2	crenulation of S1	weakly crenulated, weakly sigmoidal
	3	crenulation solution and metamorphic differentiation	strongly sigmoidal, moderately crenulated
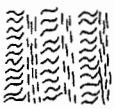	4	new mica growth parallel to S2	strongly sigmoidal, strongly crenulated
	5	destruction of relict crenulation in quartz domains	straight, differentiated crenulation cleavage
	6	homogenized S2 foliation	straight, homogeneous cleavage/schistosity

Table 4.2. Summary of fabric development and porphyroblast growth in the Jumping Brook metamorphic suite. Black bars indicate stage of crenulation cleavage development preserved as inclusion trails in the porphyroblasts. Bar width decreases in order of commonly observed, locally observed, and rarely observed crenulation stages in specific porphyroblasts. Stages after Bell and Rubenach (1983) as shown in Table 4.1. S_2' refers to re-orientated S_2.

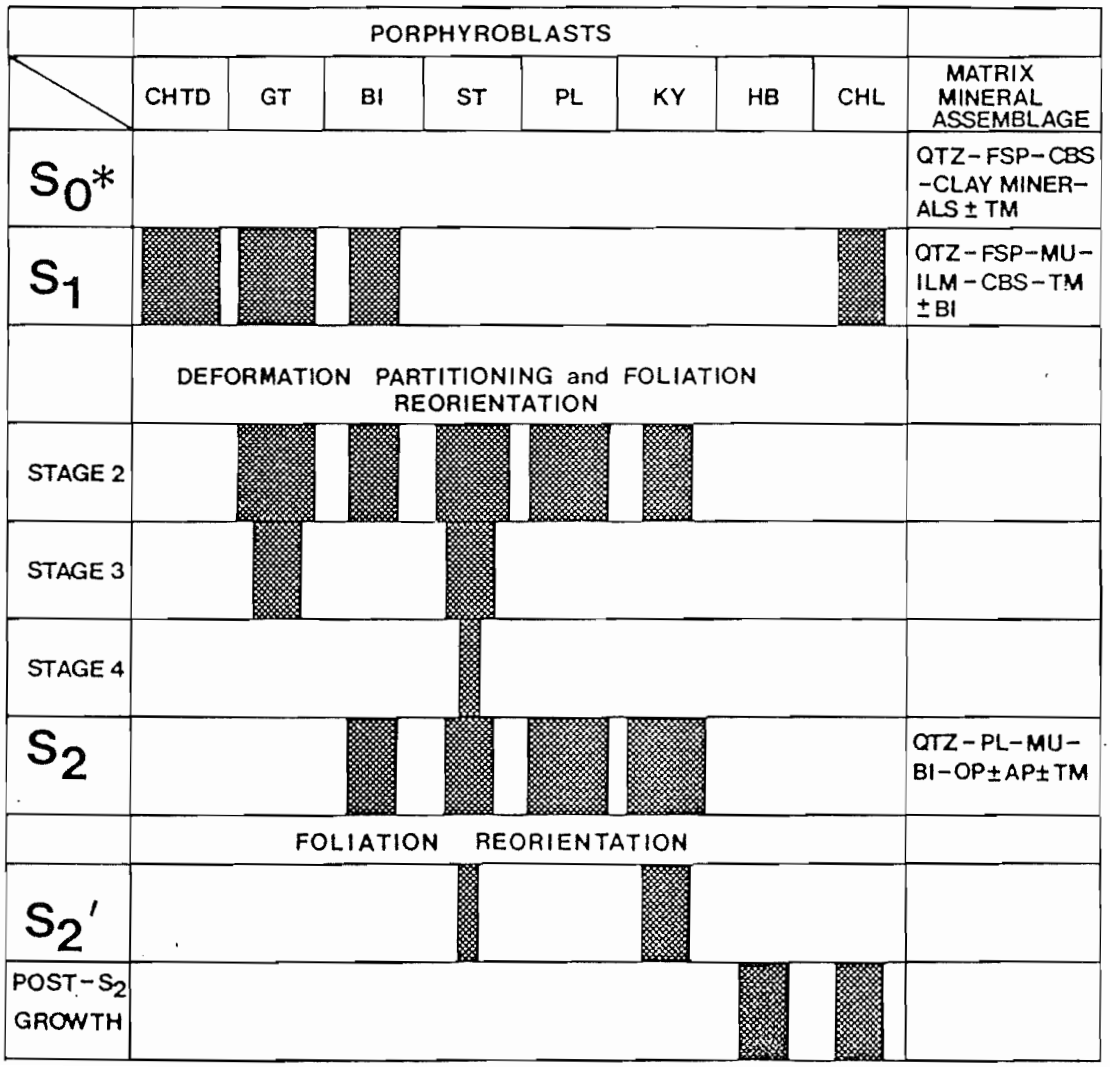

4.3.2 Notation, Terminology, and Garnet Datum

Heterogeneity in fabric development complicates application of standard S_o, S_1, S_2 notation to microstructures in the Jumping Brook metamorphic suite. Generally, the matrix foliation can be shown to be S_2, however in some cases, particularly in the low-grade rocks, the dominant matrix foliation is S_1. Thus, S_1 is used to refer to a fabric (either in the matrix or as inclusion trails) demonstrated to be the earliest foliation. Similarily, S_2 is used for a fabric demonstrated to be a second foliation. S_o^* is used to refer to any compositional layering which is not a differentiated crenulation cleavage. S_o^*, S_1, and S_2 are equivalent to those discussed with reference to the macroscopic structure. S_i (internal foliation) and S_e (external foliation) notation is used for general reference to inclusion trails and matrix fabrics, respectively. Bell and Rubenach's (1983) terminology for crenulation cleavage development is used for description of inclusion trail geometry (Table 4.1). The terms P-section and N-section (after Bell and Rubenach, 1983) are used in photomicrograph captions for sections cut normal to the foliation and parallel to the lineation and for

sections cut normal to both the foliation and the lineation, respectively.

To determine the relative foliation ages where only one foliation is developed, a datum for comparison is required. Since garnet is present at all grades, it is selected as a datum to which fabric generation is compared (Figure 4.6 and section 4.3.4).

4.3.3 Low-Grade Rocks

The earliest microstructures preserved in the low-grade rocks are tight to isoclinal folds of compositional laminations. These folds are transposed along an axial planar S_1.

S_1 in the pelitic phyllites is a slaty, homogeneous, planar cleavage (Table 4.1), commonly deformed by late crenulations and kinks (D_4 and D_5). The semipelitic and psammitic phyllites display an anastomosing cleavage with discrete cleavage domains. The greater the abundance of porphyroclasts, the more strongly ananstomosing is S_1.

Garnet, chloritoid, biotite, and chlorite porphyroblasts are developed in the low-grade rocks. Quartz, plus variable amounts of ilmenite, sericitized feldspar, muscovite, and chlorite, define inclusion trails. Inclusion trails in garnet, chloritoid, and biotite are straight or weakly sigmoidal and continuous

(a)

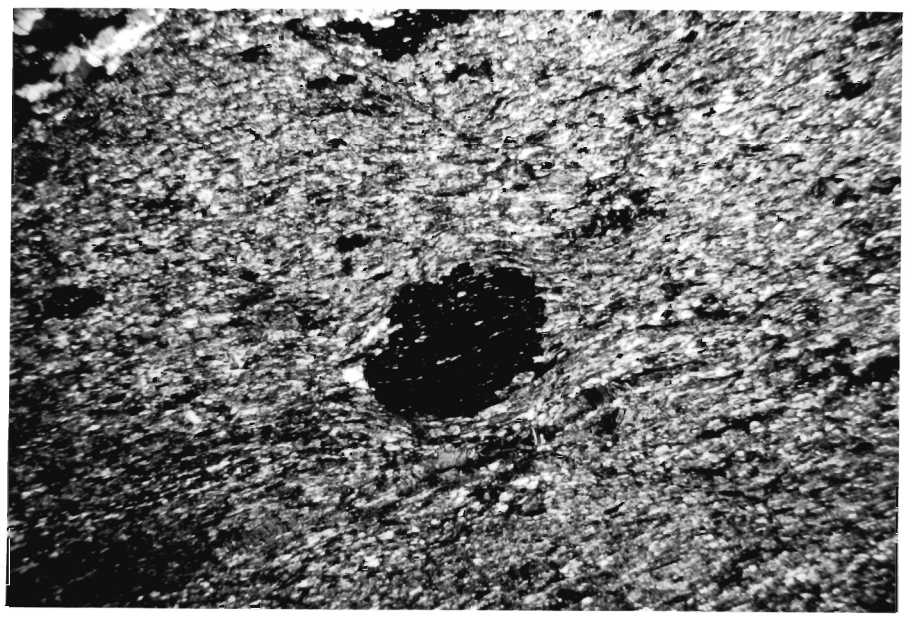

Figure 4.6. The "garnet datum" used to correlate microstructures in this study. (a) Low-grade garnet has overgrown the matrix foliation (S_1) which has subsequently been flattened around the garnet. These garnets locally overgrow a crenulation of S_1 (see Figure 4.11). (b) Medium-grade garnet, with straight inclusion trails oriented at a high angle to the matrix foliation (S_2), is included in staurolite which has overgrown S_2. Inclusion trails in the low-grade garnet are interpreted to be equivalent to those in the medium-grade garnet, thus providing a means of determining the temporal relations of the pervasive foliation in the low-grade rocks and that in the medium- to high-grade rocks. Field of view in (a) and (b) is 10 mm.

(b)

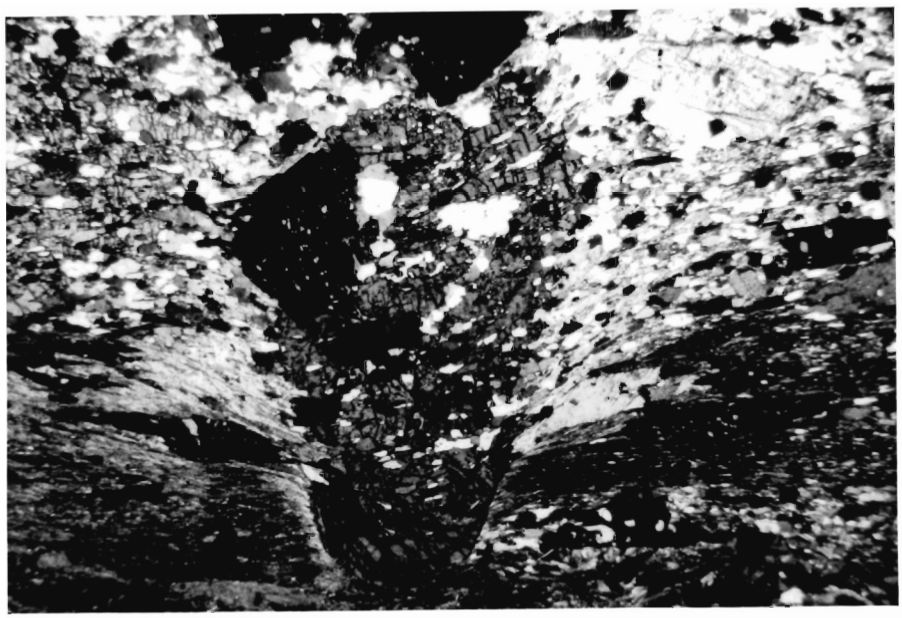

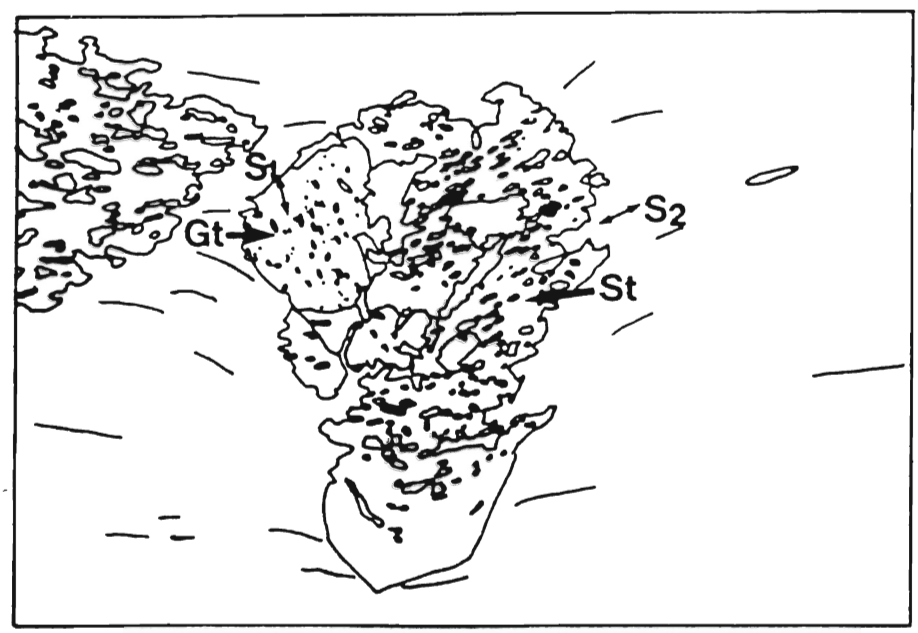

Figure 4.6. (Continued)

with S_e, indicating porphyroblast growth after development of the matrix foliation. Locally, quartz-feldspar veinlets cut S_1, but are tightly folded with axial surfaces parallel to S_1 (Figure 4.7). Biotite has grown parallel to S_1 and cuts through these veinlets, indicating that the veinlets are syn-tectonic and the biotite is post-tectonic. The veinlets presumably formed during the deformation which formed the early tight to isoclinal folds and axial planar cleavage. Similarly, fold limbs of tightly to isoclinally folded veinlets of polygonal quartz in the felsic metavolcanic phyllites and schists are truncated and weakly transposed along discrete cleavage domains (S_1) (Figure 4.8).

There are two generations of chlorite porphyroblasts in the low-grade rocks. Early chlorite porphyroblasts, developed only in the low-grade pelites, lack Si and are wrapped around by the matrix foliation. These porphyroblasts are interpreted to be pre- to syn-tectonic with respect to S_1. The second generation of chlorite porphyroblasts is present at all grades. They are twinned, overgrow the matrix foliation, commonly nucleate on biotite (Figure 4.9a), and in some samples they are aligned with their long axes parallel to S_4 crenulation fold axes (Figure 4.9b).

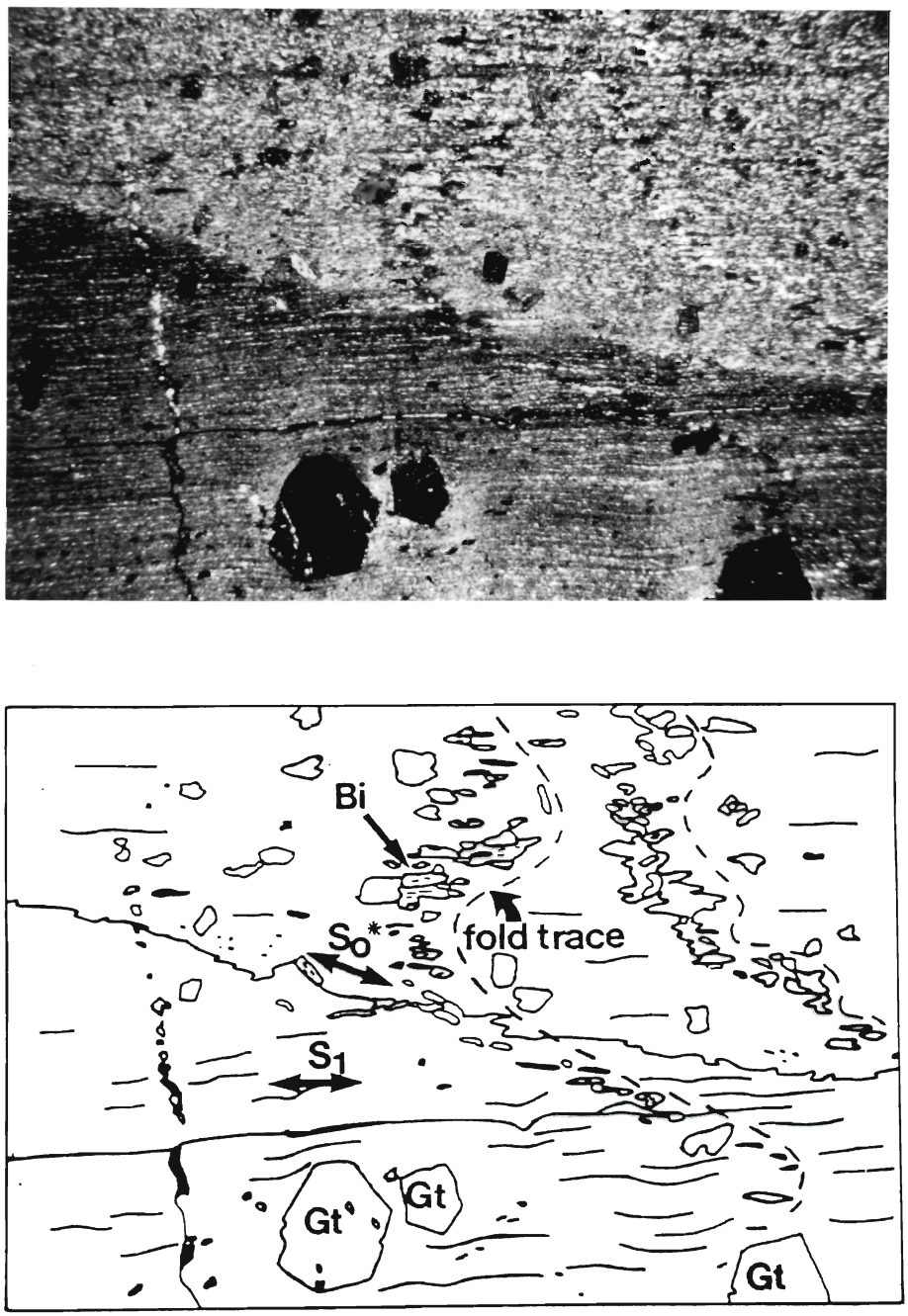

Figure 4.7. Photo and line drawing of tightly folded quartz-feldspar veinlet weakly transposed along axial planar S_1. Post-S_1 biotite has grown parallel to S_1 and cuts the veinlet. S_1 and S_o^* (pelitic-dark, semipelitic-light) intersect at an angle of approximately 10^o. Field of view is 10 mm.

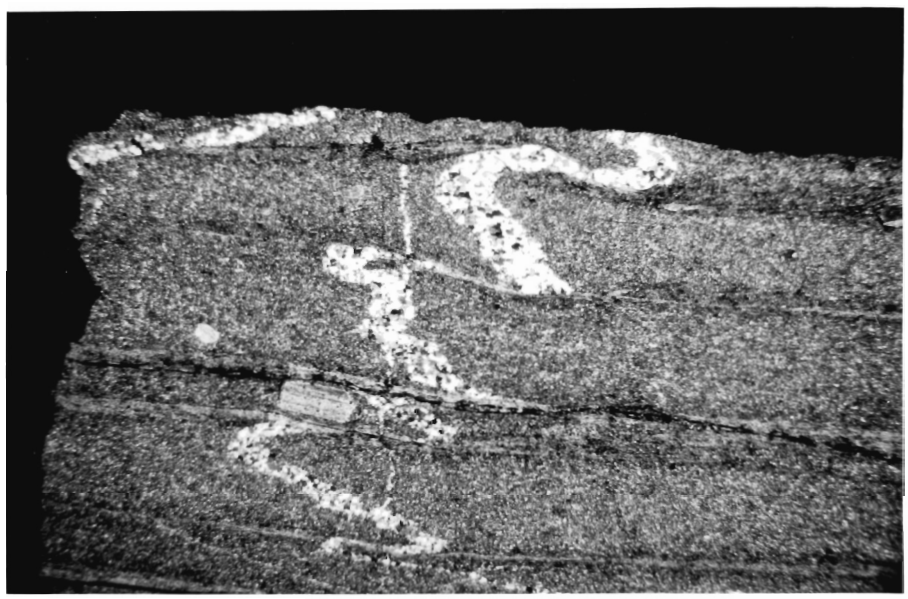

Figure 4.8. Tightly folded veinlet of polygonal quartz, weakly transposed along axial planar S_1, in a felsic metavolcanic phyllite of the Faribault Brook metavolcanics exposed along the Cabot Trail. Field of view is 10 mm.

a

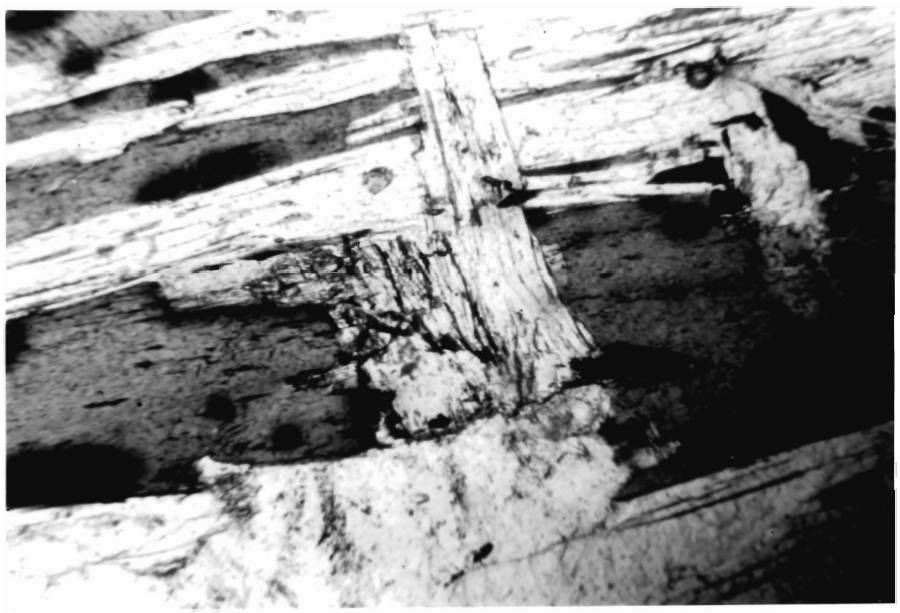

b

Figure 4.9. Post-S_2 chlorite porphyroblasts in medium-grade semipelitic schist (a) has nucleated on biotite which defines S_1, and (b) is aligned with long axis parallel to S_4 crenulation axes. Fields of view: (a) 10 mm, (b) 2.25 mm.

The matrix foliation is commonly bowed around garnet and chloritoid porphyroblasts even though their inclusion trails are continuous with the matrix foliation (see Figure 4.6a), thus indicating flattening subsequent to porphyroblast growth. This is further supported by conjugate microkink bands and basal slip in biotite (Figure 4.10), and microfractures normal to the matrix foliation in garnet. Locally, garnet has overgrown crenulations affecting S_1 (Figure 4.11).

Evidence for late foliation re-orientation is found in the garnet-chloritoid pelitic phyllites. Foliation is continuous between chloritoid porphyroblasts and the matrix. Prismatic ilmenite, aligned parallel to the foliation, in the matrix, and included in chloritoid, conveniently documents relative porphyroblast-matrix movement. Ilmenite prisms are straight where contained completely within the matrix or chloritoid but where they pass from porphyroblast to matrix they are symmetrically bent in opposite directions on either side of the porphyroblast (Figure 4.12). Such symmetry is indicative of simple shear (Bell, 1981). Retrogression of the idioblastic chloritoid to fine- grained clay minerals and chlorite where it is in contact with the matrix foliation indicates that simple shear took place in the matrix at the porphyroblast margins (cf. Figure 4.4). Therefore,

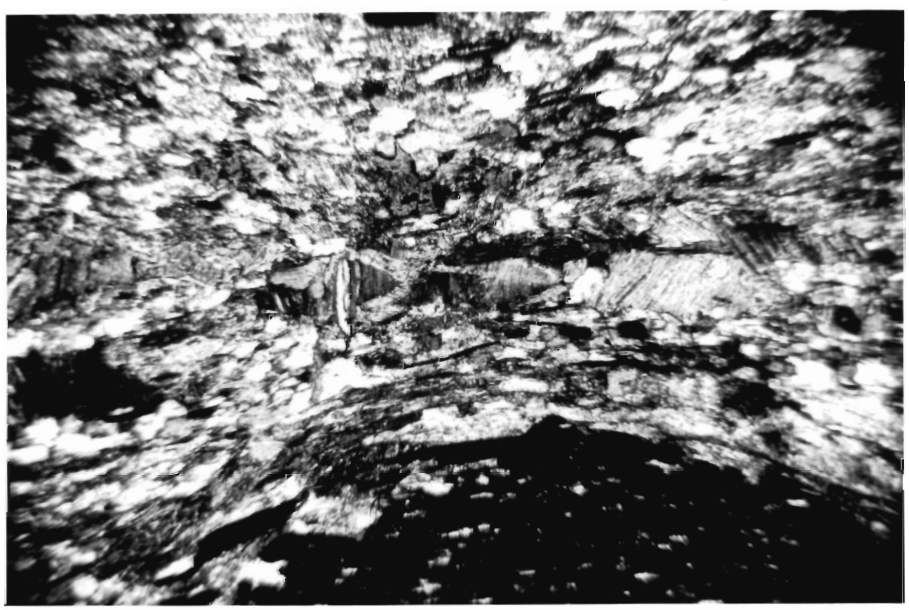

Figure 4.10. Conjugate kinks in a biotite porphyroblast with (001) at a high angle to S_1 in a low-grade semipelitic schist. S_1 bends around garnet porphyroblast which contains fractures perpendicular to S_1. These microstructures indicate flattening normal to S_1 subsequent to porphyroblast growth. Field of view = 2.25 mm.

Figure 4.11. Low-grade garnets have overgrown incipient S_2 crenulation cleavage (arrowed). Note that mica-rich crenulation cleavage domains in the matrix correspond to relatively solid zones in the porphyoblast. Field of view = 10 mm.

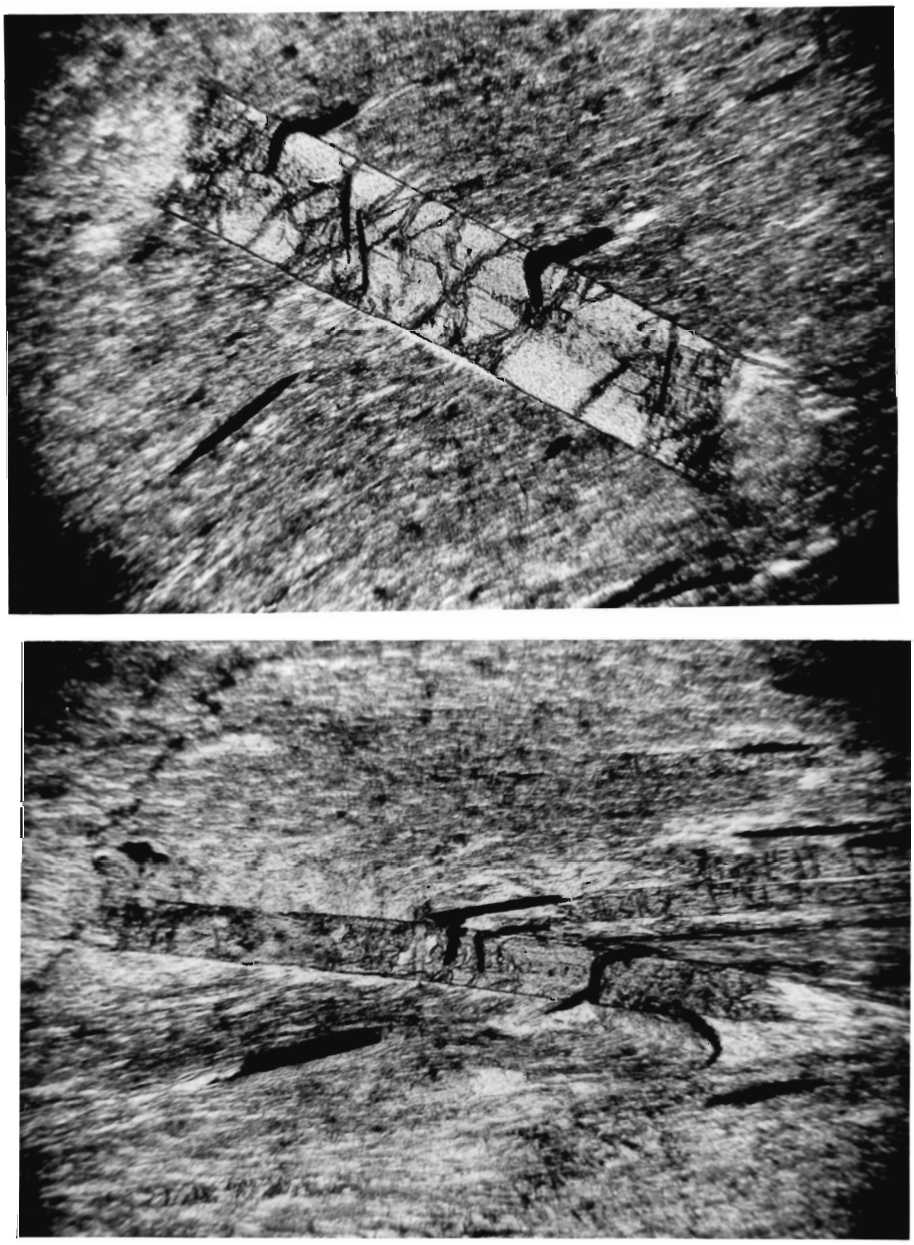

Figure 4.12. Prismatic chloritoids in low-grade pelitic phyllite containing inclusions of prismatic ilmenite. Where the ilmenites pass from porphyroblast to matrix they are bent in opposite directions on either side of chloritoid, indicating relative simple shear between the matrix and the porphyroblast. Chloritoid is retrograded along porphyroblast-matrix boundary perpendicular to the, foliaton suggesting shearing has occurred in the matrix. Fields of view = 2.25 mm.

rotation of the matrix as opposed to the chloritoid porphyroblasts is inferred. The rotation of the matrix around porphyroblasts in some cases appears to be related to the late crenulation (D_4) but in other cases, its origin is unclear. As deformation is a continuous process, it is probable that some of the matrix re-orientation is part of the deformation continuum responsible for the formation of S_1.

Therefore, the microstructural sequence in the low-grade rocks consisted of (1) tight to isoclinal folding of compositional layering, (2) development of an axial planar cleavage and some quartz-feldspar veining, (3) porphyroblast growth and locally, crenulation of S_1 which is overgrown by garnet, (4) tightening of the foliation around porphyroblasts, (5) re-orientation of the matrix around porphyroblasts, and (6) fine crenulation associated with D_4 upright folding (Figure 4.13). The relative timing of (3) and (4) is unclear because they are not observed together in the same sample. Considering the overall heterogeneity of deformation in the Jumping Brook metamorphic suite (see below) they may have occurred contemporaneously.

Figure 4.13. Microstructural sequence of events for the low-grade rocks. 1: (1) Tight to isoclinal folding of compositional layering and transposition of folds along axial planar S_1. (2) Syn-S_1 growth of chlorite[1], and ?growth of ilmenite, and quartz-feldspar veining. (3) Significant porphyroblast growth : (a) Garnet $\pm$ biotite pelitic phyllites: post-S_1 biotite overprints S_1 and quartz-feldspar veinlets and garnet overgrows S_1. (b)Garnet-chloritoid-bearing phyllites: garnet and chloritoid overgrow S_1. Ilmenite may have continued to grow generally along the foliation surface. (4) Flattening perpendicular to S_1. S_1 wraps around garnet, biotite, and chloritoid. Biotite undergoes basal slip and kinking, garnet fractures perpendicular to S_1. Deformation partitioning of S_1 around porphyroblasts and minor retrogression (R) at porphyroblast-matrix contacts. (5) Locally, garnet overgrows D_2 crenulations of S_1. Note that the relative timing of (4) and (5) is unclear although locally (4) is associated with D_4 crenulation suggesting it is later than (5) in some cases. Mineral abbreviations as in Table 4.1.

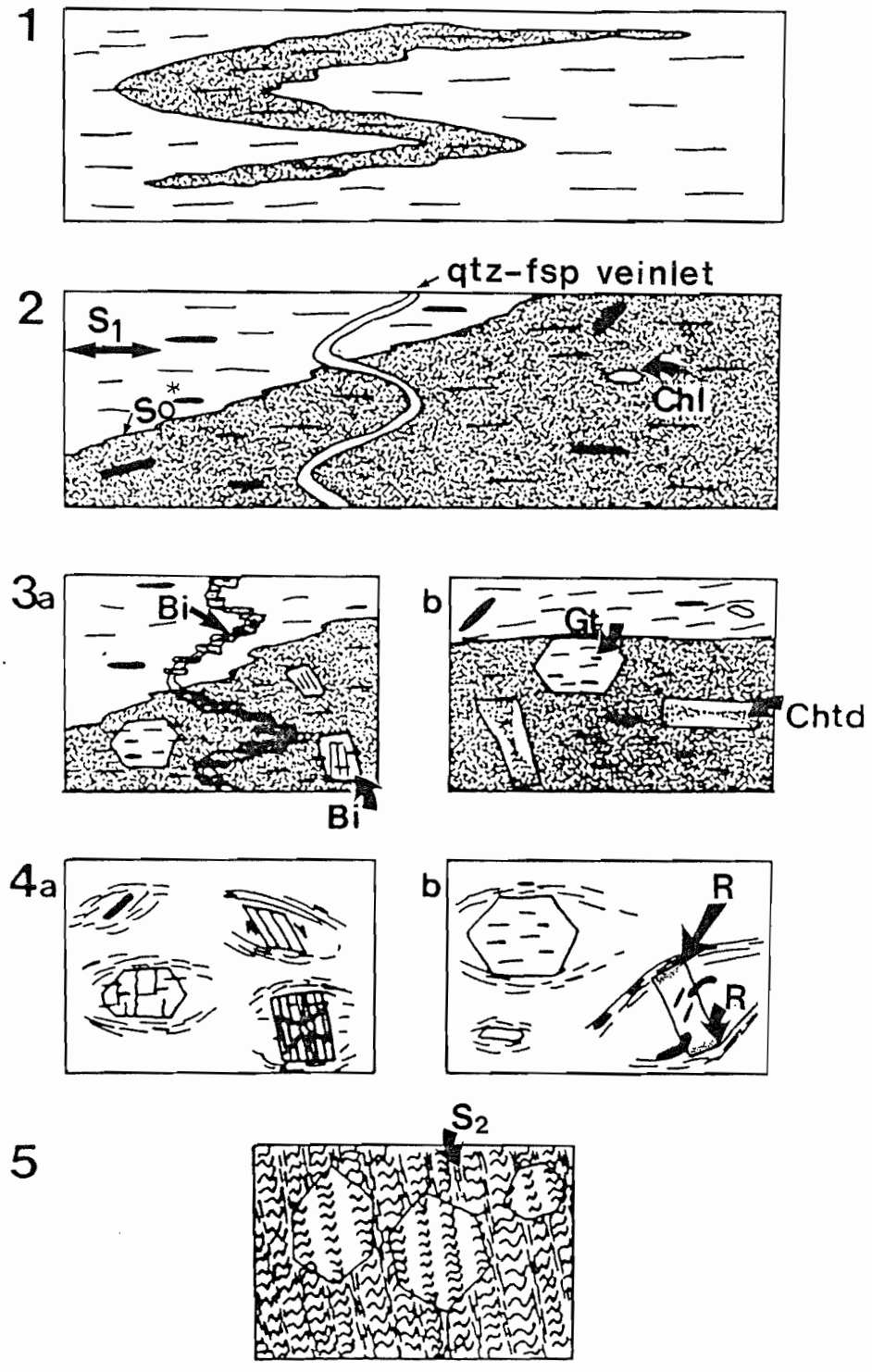

Figure 4.13.

4.3.4 Medium-Grade Rocks

Porphyroblasts of garnet, biotite, staurolite, oligoclase, microcline, and kyanite are developed in the medium-grade rocks. Inclusion trails are mainly defined by quartz and opaque minerals, and minor sericitized feldspar, muscovite, and chlorite. Schistosity in the medium- to high-grade Corney Brook and Fishing Cove River schists varies from planar to anastomosing and is generally developed to stage 5-6 (Tables A1.1 and 4.1).

The earliest preserved microstructure in the medium-grade rocks is the crenulation of pre-existing fabric to form the pervasive foliation in these rocks. Various stages of this crenulation cleavage are preserved as porphyroblast inclusion trails, and locally as crenulations in the matrix, to which the pervasive matrix foliation is axial planar. The matrix crenulations are commonly asymmetrical and show an equivalent or more advanced stage of development relative to the inclusion trails in co-existing porphyroblasts. In the latter case, the associated crenulation cleavage cuts through the porphyroblasts (Figure 4.14).

The age of these fabrics relative to that in the low-grade rocks is determined using the "garnet datum". Since garnet growth in the low- to medium-grade rocks is continuous (see Chapter 6), the rare crenulations

Figure 4.14. Stage 1-2 crenulations preserved in a staurolite porphyroblast of the staurolite-garnet schists, which is cut by S_2 crenulation cleavage associated with stage 2-3 crenulations preserved in the matrix. This confirms the interpretation that the sigmoidal inclusion trails are crenulations and indicates that, in this sample, substantial staurolite growth occurred early in the crenulation cleavage development. Field of view = 10 mm.

overgrown by garnet in the low-grade rocks (see Figure 4.11) are interpreted to be equivalent to those preserved as inclusion trails in garnet in the medium-grade rocks. Thus, S_1 in the low-grade rocks is equivalent to S_i in the medium- (and high-) grade rocks and consequently S_e in the latter is S_2.

Idioblastic to subidioblastic garnet commonly preserves stages 1, 2, and 3 microfolds and contains the lowest grade mineral assemblage as inclusions. Stage 1 inclusion trails in garnet are commonly normal to the matrix foliation. Garnet is typically included in idioblastic to subidioblastic staurolite, which itself shows either stage 2 to 4 inclusion trails, or overgrows the matrix foliation (see Figure 4.6). Locally garnet is boudinaged and quartz and chlorite have filled the fractures (Figure 4.15). Kyanite in the medium-grade rocks is idioblastic to subidioblastic and oligoclase is idioblastic to xenoblastic. Although they rarely preserve stage 2-3 S_i, their inclusion trails are commonly straight and continuous with, or at an acute angle to, the matrix foliation (Figure 4.16). Thus, crenulation stages preserved by staurolite, oligoclase, and kyanite overlap in some sections, but staurolite characteristically shows earlier stages than kyanite or oligoclase (Figure 4.17). Microcline and plagioclase

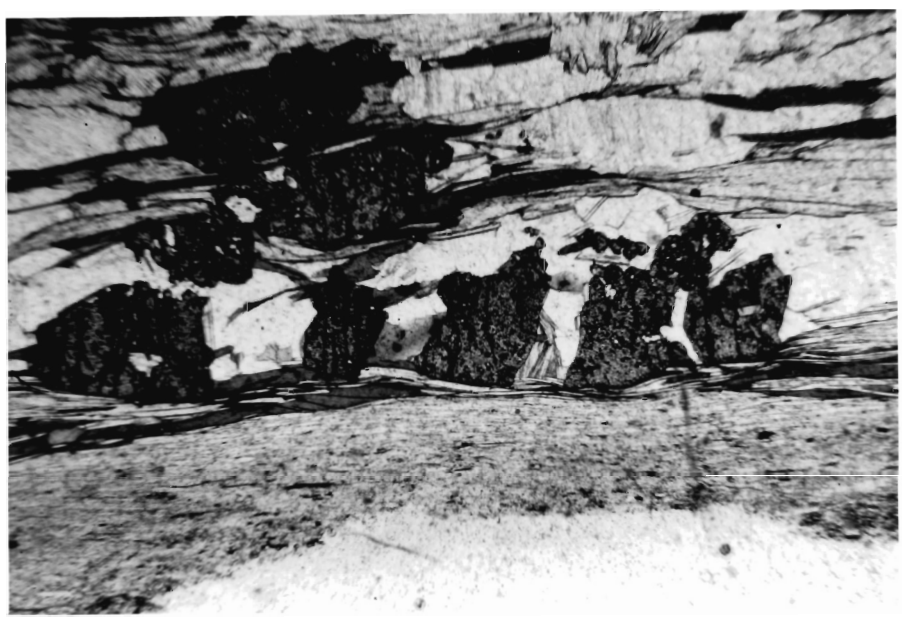

Figure 4.15. P-section of staurolite-garnet schist showing microboudinaged garnet. Quartz and chlorite have filled the fractures. Field of view = 10 mm.

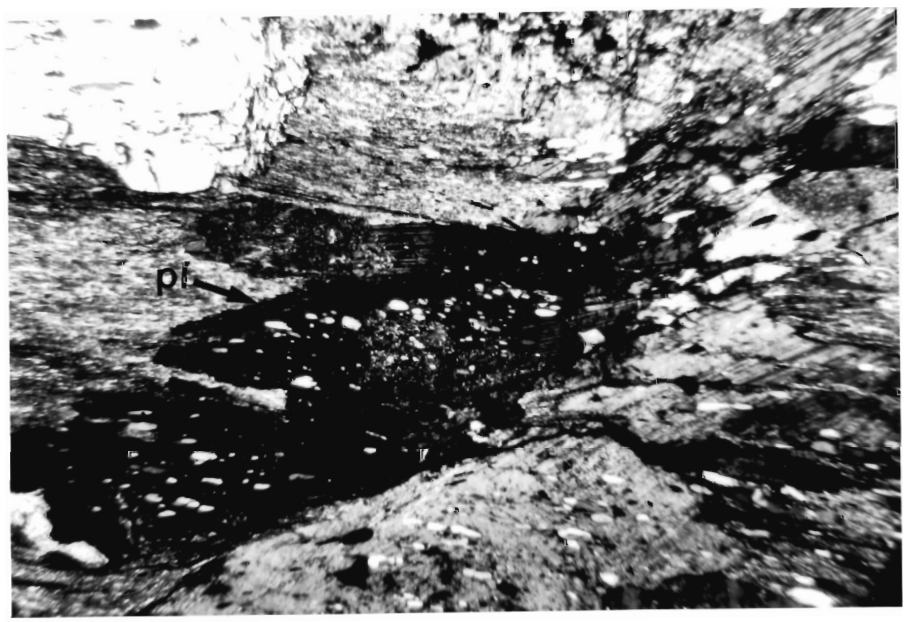

Figure 4.16. Subidioblastic oligoclase porphyroblasts have overgrown S_2. Inclusion trails are defined by quartz. Field of view = 5 mm.

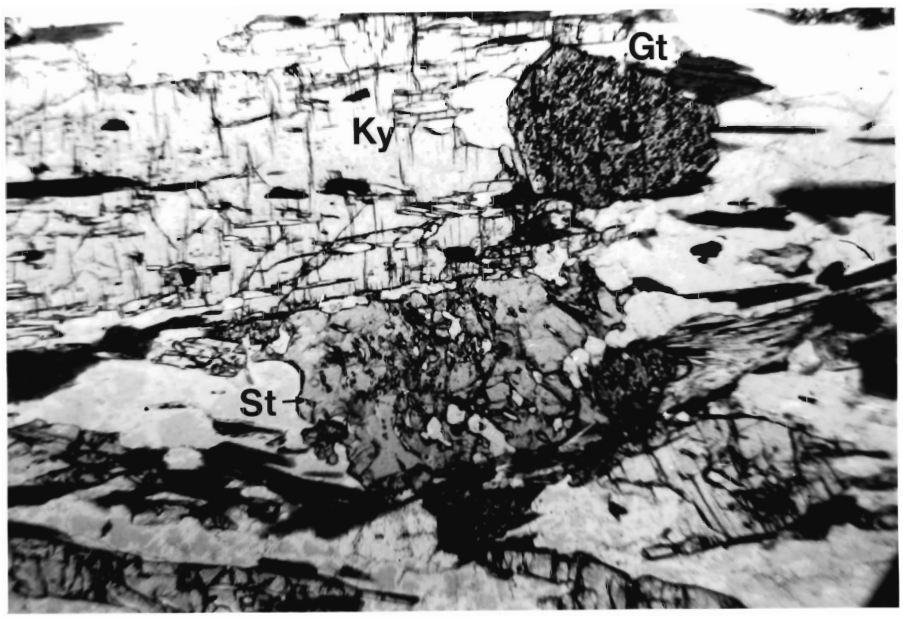

Figure 4.17. Sequence of porphyroblast growth in the staurolite-garnet schists from a P-section (crossed polars). Early garnet (Gt) growth over stage 1 S_1 is visible in garnet at the top right corner of the photo. Inclusion trails in garnet are straight in this sample but vary in orientation relative to S_2. Staurolite (St) has overgrown a stage 2 crenulation whereas kyanite (Ky) has overgrown a stage 5-6 S_2. Inclusions in all the porphyroblasts are mainly quartz and opaque minerals. Note that inclusions are finer grained than the matrix grains of the same minerals indicating porphyroblast growth prior to extensive matrix recrystallization. (Dark lines are ink from preparation for microprobe analysis). Field of view = 10 mm.

porphyroblasts in the feldspar schists preserve stage 2 microfolds. Biotite is subidioblastic and commonly lacks inclusion trails. It grows parallel to both S_1 and S_2, and where inclusion trails are developed they indicate biotite has overgrown S_2.

Garnet and staurolite inclusion trails locally define a differentiated crenulation cleavage (stage 3 to 5), consisting of straight zones of solid porphyroblast and opaque minerals alternating with zones of sigmoidal to straight inclusion trails defined mainly by quartz. Where crenulations of S_1 are peserved in the matrix, the solid porphyroblast zones are continuous with the matrix crenulation cleavage domains (see Figure 4.11). Therefore, the inclusion-free zones are interpreted to have been mica-rich crenulation cleavages, completely replaced by the porphyroblast after the foliation became inactive, and the inclusion-rich zones are interpreted to have been the associated microlithons (cf. Bell and Rubenach, 1983; Bell et al., 1986; Jamieson and Vernon, 1987). This is more common in the medium-grade rocks than in lower grade rocks.

In a few sections, staurolite contains tabular zones of relatively solid staurolite containing fewer inclusions than the rest of the porphyroblast (Figure 4.18). The sharp contacts of these zones truncate the

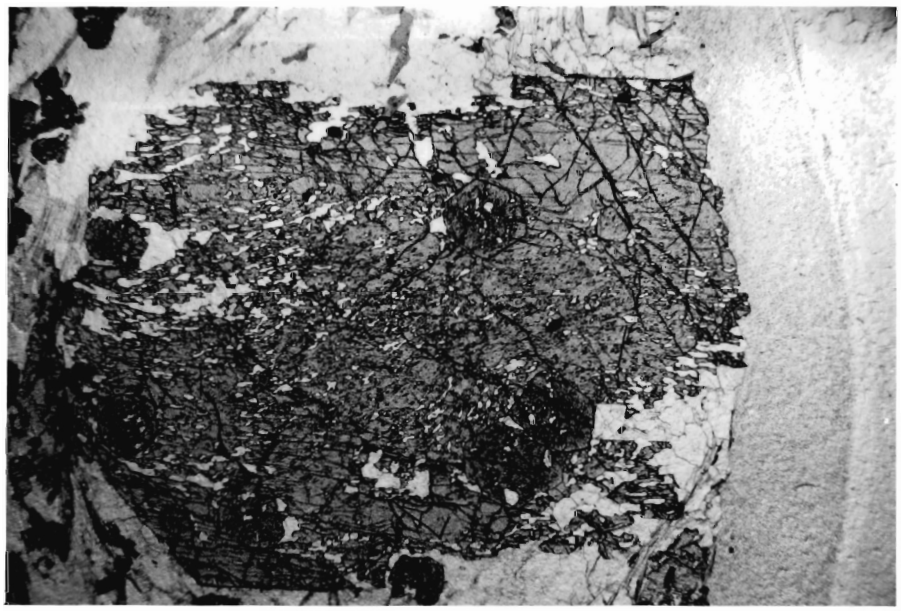

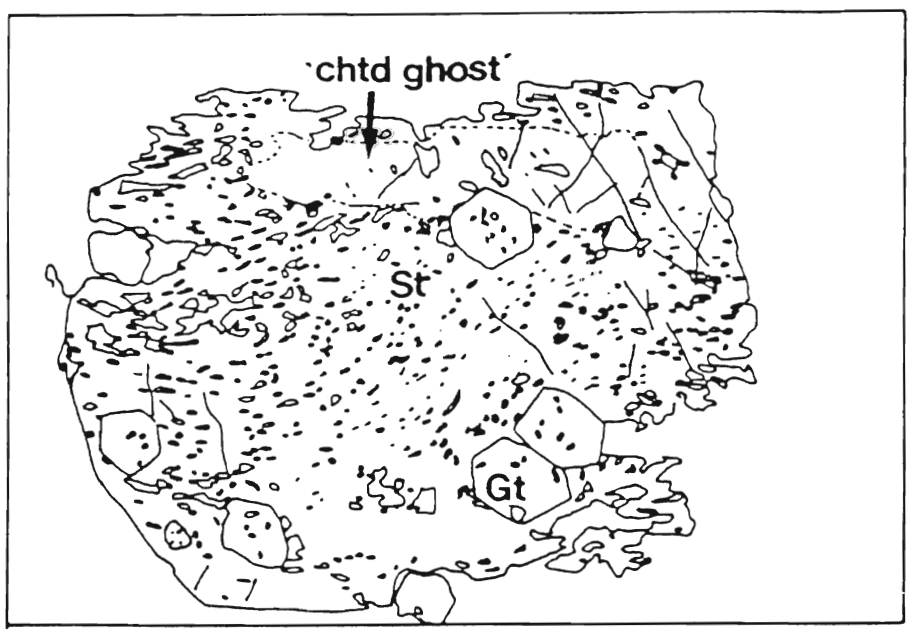

Figure 4.18. Photomicrograph and line drawing of possible chloritoid "ghost" in staurolite, consisting of a roughly prismatic zone of relatively solid staurolite containing possible stage 1 inclusion trails. The rest of the porphyroblast contains abundant inclusions defining a stage 2 crenulation. Field of view 5 mm.

stage 2 inclusion trails in staurolite and contain weakly developed, quartz-defined, stage 1 inclusion trails at a slight angle to those in the surrounding staurolite. On the basis of shape and inclusion trail geometry, these zones are interpreted as chloritoid "ghosts" now completely replaced by staurolite. Details of possible reactions are given in Chapter 6.

Minerals defining S_i are commonly finer-grained than the same minerals in the matrix. The grain size difference is most extreme in porphyroblasts where inclusion trails preserve an early stage of crenulation cleavage development (i.e. stage 1, 2, or 3), suggesting that porphyroblast growth began, and probably ceased, prior to extensive recrystallization and grain growth in the matrix.

Evidence for porphyroblast dissolution along crenulation cleavage domains (S_2) is found in the staurolite-garnet schist. Garnet is idioblastic where included in staurolite but truncated where it is in contact with matrix S_2 (cf. Bell and Rubenach, 1983). In some cases, it is not clear if this dissolution occurred during crenulation cleavage formation or during subsequent foliation re-orientation (Figure 4.19). The cause for this foliation re-orientation, as in the low-grade rocks, is not always clear. It is probably due to

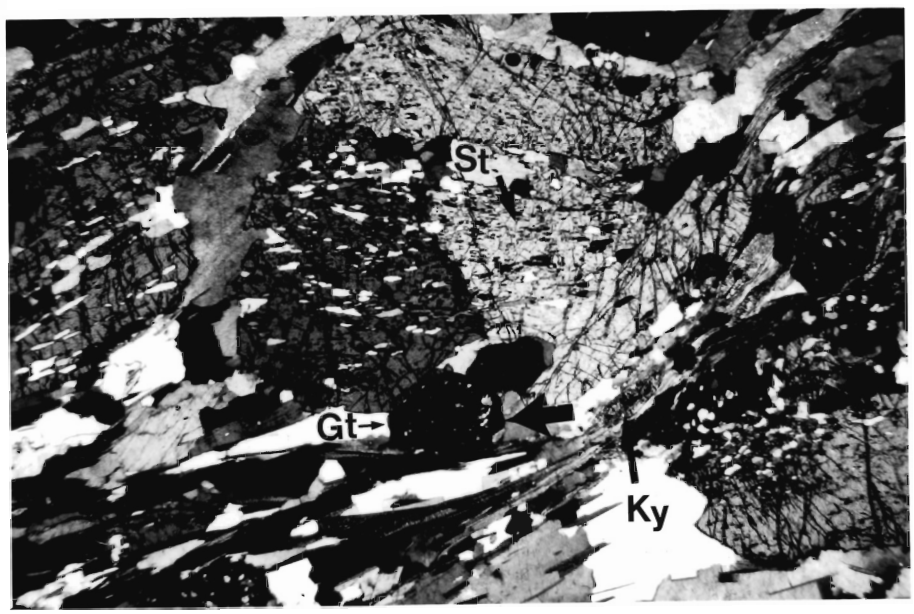

Figure 4.19. Re-orientation of S_2 in the staurolite-garnet schists. St=staurolite, Gt= garnet, Ky=kyanite. Garnet grew early in the deformation evident from stage 1 inclusion trails (not obvious in the photograph). Staurolite overgrowth of a stage 5-6 S_2 and partial inclusion of garnet was followed by matrix S_2 re-orientation around staurolite and consequent truncation of S_i by S_e. Garnet truncation against S_2 (arrowed) may have occurred during S_2 crenulation cleavage development or during S_2 re-orientation. Kyanite and staurolite have subsequently overgrown the re-oriented S_2. Minor subgrain development is evident in staurolite. Field of view = 10 mm.

continued deformation after porphyroblast growth in which the deformation, in order to remain planar on a bulk scale, must anastomose on a small scale. In some sections, staurolite and kyanite have overgrown the re-oriented S_2 (Figure 4.19). This suggests that deformation associated with foliation re-orientation is part of a continuous deformation which formed S_2, rather than a separate later event. Locally however, microshears approximately parallel to S_2 intersect and offset porphyroblasts. Porphyroblasts are strongly retrograded in these zones (Figure 4.20). Therefore, these microshears are interpreted to be retrograde although their relationship to macroscopic deformation is unknown. Porphyroblasts also show minor development of large subgrains suggesting some late recrystallization (eg. Figure 4.19).

The relative timing of biotite growth to other porphyroblasts is difficult to ascertain because it generally lacks inclusion trails. It grows parallel to S_1 and S_2 and probably nucleated and recrystallized throughout the crenulation of S_1 and overgrew S_2. Therefore, the sequence of microstructural events in the medium-grade rocks is: (1) the formation of S_1 and its overgrowth by garnet, biotite, and chloritoid as in the low-grade rocks, followed by (2) syn-crenulation growth

Figure 4.20. Idioblastic staurolite retrograded to chlorite along late microshears. Field of view = 10 mm.

of garnet, staurolite, oligoclase, and kyanite, (3) post-S_2 staurolite, oligoclase, and kyanite growth, (4) local re-orientation of S_2 about porphyroblasts, (5) overgrowth of the re-oriented matrix by staurolite and kyanite, and (6) post-S_2 growth of retrograde chlorite porphyroblasts and locally late microshearing. Biotite continued to nucleate and recrystallize throughout the entire sequence of crenulation cleavage development. There is some overlap between staurolite, kyanite, and oligoclase growth, but staurolite clearly nucleated before kyanite and oligoclase, and the growth of the kyanite and oligoclase generally outlasted that of staurolite. Porphyroblast dissolution occurred during crenulation cleavage formation and foliation re-orientation. Minor formation of large, equidimensional subgrains in porphyroblasts suggests some late-stage recrystallization. This sequence of microstructural events is summarized in Table 4.2.

4.3.5 High-Grade Rocks

The high-grade rocks contain the same porphyroblasts as the medium-grade rocks although staurolite is less abundant in comparison to the staurolite-garnet schists, and is locally absent. Inclusion trails are not as well developed as in the medium-grade rocks, but where present

define the same sequence of porphyroblast growth, with one important exception. In the highest grade (kyanite zone) schists, inclusion-rich garnet cores containing a stage 1 foliation are mantled by relatively inclusion-free rims (Figure 4.21). Inclusions in the cores are fine-grained whereas the few inclusions in the rims are equal in grain size to matrix. These textures are interpreted to reflect early garnet growth approximately contemporaneous with garnet in the staurolite-garnet schists, succeeded by post-S_2 growth. This interpretation is supported by staurolite inclusions in garnet in some samples suggesting post-staurolite garnet growth (Figure 4.22), and by garnet chemistry and zonation profiles (chapter 5, section 5.4). Foliation re-orientation, and subsequent minor porphyroblast recrystallization and shearing are observed in the high-grade rocks.

Fibrolite, randomly oriented in muscovite, is locally present in the high-grade rocks (Figure 4.23). It is interpreted to be post-S_2 based on its random orientation and the improbability that these crystals could survive much deformation.

4.3.6 Flattening versus Shearing

The mechanism of crenulation cleavage development and hence its orientation with respect to the strain

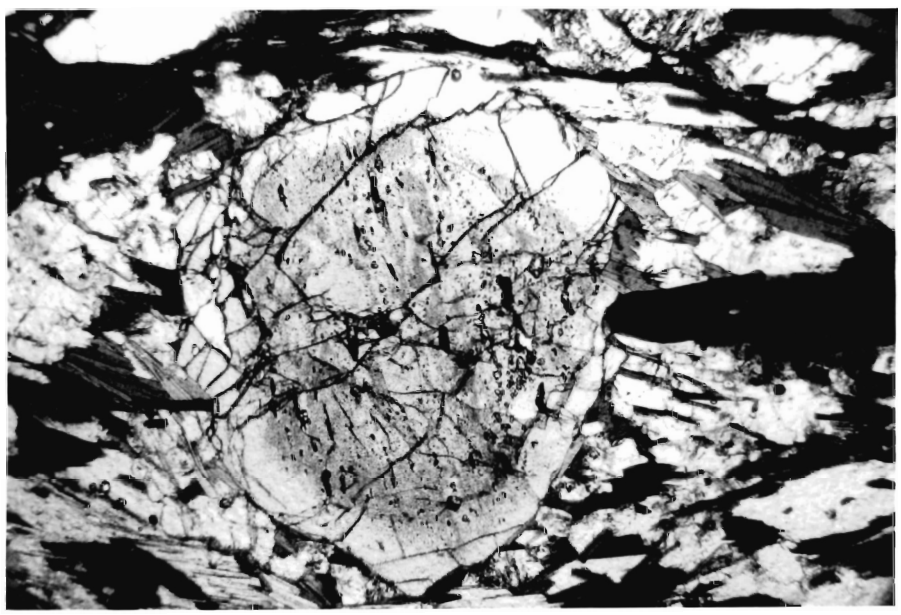

Figure 4.21. Subidioblastic garnet porphyroblast in a high-grade biotite schist (Fishing Cove River schist). Straight inclusion trails in the inclusion-rich core are mantled by a relatively inclusion-free rim interpreted to represent prograde, post-S_2 garnet growth associated with staurolite breakdown. Field of view = 10 mm.

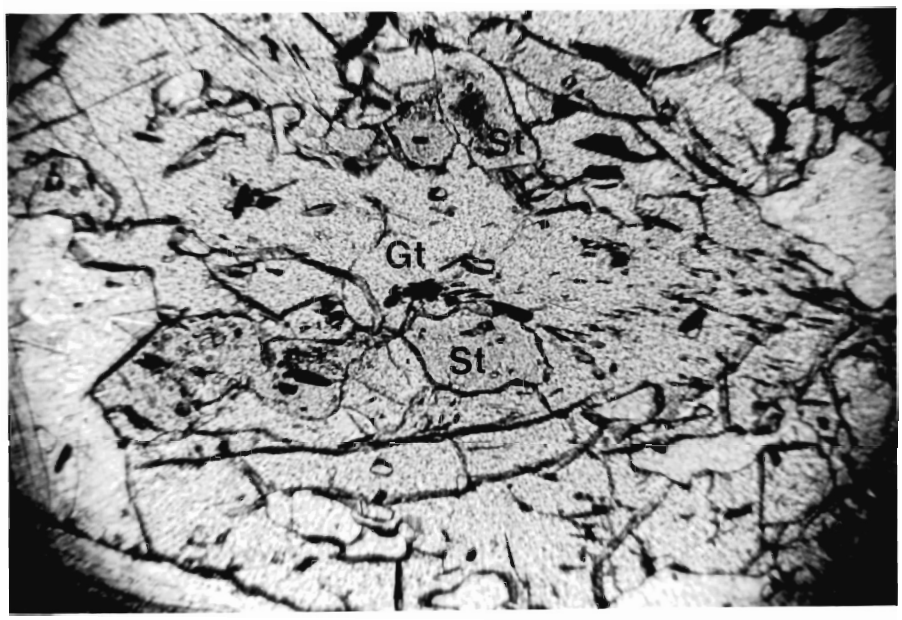

Figure 4.22. Staurolite inclusions in garnet in a staurolite-bearing, high-grade biotite schist (Fishing Cove River schist). Field of view = 10 mm.

Figure 4.23. Randomly oriented fibrolite in muscovite in high-grade biotite-garnet(-kyanite) schist, interpreted to be post-S_2 on the basis of its random orientation and the probability that these crystals would not survive much deformation. Field of view = 2.25 mm.

ellipsoid is a controversial subject. Some researchers consider crenulation cleavage to be a plane of flattening along which dissolution occurs (eg. Cosgrove, 1976; Gray, 1979a; Bell and Rubenach, 1983) whereas others argue it is a plane of shearing (eg. Williams, 1976). The main argument for the latter view is the offset of marker horizons across the cleavage, although this may result from volume reduction by pressure solution (eg. Gray, 1979a). It is probable that both flattening and shearing are involved in crenulation cleavage formation and that one process may dominate over the other in specific cases (eg. Bell and Rubenach, 1983).

Bell (1981) suggested that this controversy could be reconciled by deformation partitioning which causes the crenulation cleavages to anastomose. Consequently, in a non-coaxial situation, the XY plane of the bulk strain ellipsoid will lie at some angle to the cleavage planes, and components of shear will develop along them. Therefore, depending on the scale of observation and the degree of non-coaxiality, the foliation can be subparallel to the local XY plane of the strain ellipsoid and also be a plane of shear. However, deformation partitioning can occur during both progressive bulk inhomogeneous flattening and progressive, inhomogeneous, simple shear (Bell et al., 1986).

Bell (1981) proposed geometric criteria for distinguishing shear and flattening-dominated deformation. Identical asymmetry of kink planes to (001) in micas deformed against porphyroblasts and porphyroclasts indicate progressive inhomogeneous simple shear whereas opposite asymmetry of kink axial planes to (001) in micas and "millipede structures" (Bell and Rubenach, 1980) indicate bulk inhomogenous flattening (Bell, 1981).

Crenulations of S_1 in the Jumping Brook metamorphic suite are apparent only in sections cut parallel to the lineation and perpendicular to the foliation (P-sections). They are commonly asymmetric although locally they are symmetric. Crenulations and apparent shear bands of S_1 are present locally in the same thin section. "Millipede structures" (Bell and Rubenach, 1980) and kinks in micas around poprhyroblasts and porphyroclasts are absent. However, micas commonly bend around porphyroblasts in the medium-to high-grade rocks and at all grades, (001) planes of mica and late chlorite porphyroblasts are kinked where oriented at approximately 60^{o} or more to S_2. Conjugate kinks are developed where (001) planes and S_2 are mutually perpendicular.

The consistent relationship between crenulations in S_1 and L_2 suggests that they formed contemporaneously

during north-northeasterly extension. Assuming that the foliation surface approximates the XY plane of the local strain ellipsoid, the observed relationship between crenulation axes and mineral lineations is predicted by the deformation partitioning model for bulk inhomogeneous flattening (Bell, 1981; Figure 4.4).

The asymmetrical crenulations can form by (1) simultaneous layer-parallel shearing and shortening or (2) layer-parallel shortening followed by shear (Gray, 1979b), and hence their presence in the Jumping Brook metamorphic suite suggests that D_2 contained a shearing and a flattening component. The kinks in micas and chlorite porphyroblasts indicate that post-S_2 deformation was predominantly by flattening but late microshears are also present. Apparent shear bands of S_1 (Figure 4.24) suggest that shearing-dominated deformation on the microscopic scale was locally important.

In conclusion, deformation in the Jumping Brook metamorphic suite is macroscopically to microscopically heterogeneous. If the crenulations result from simple shear, they may be possible kinematic indicators but further detailed work on carefully oriented thin sections is required to fully assess this possibility.

Figure 4.24. Staurolite has overgrown apparent S-planes in a staurolite-garnet schist. Field of view = 2.25 mm.

4.3.7 Discussion

Inclusion trail geometry and early crenulations locally preserved in the matrix of medium- to high-grade pelitic schists indicate S_2 formed by progressive crenulation of S_1. The low-grade rocks are only locally affected by this crenulation, and the pervasive foliation in these rocks is generally S_1 in contrast to the medium- to high-grade rocks where S_2 is the dominant foliation. Porphyroblast inclusion trails are best interpreted as the result of overgrowth of various stages of progressive crenulation cleavage development, not rotation. This interpretation implies that the relative sequence of porphyroblast growth was: chlorite^1, chloritoid and garnet^1, staurolite, oligoclase and kyanite, garnet^2, and chlorite^2. Fibrolite grew post-S_2. Foliation re-orientation has resulted in truncation of S_i by the matrix foliation. In the low-grade pelitic phyllites, deformed ilmenite inclusions document the deformation of the matrix around chloritoid. Kyanite, and locally staurolite, overgrew the re-oriented S_2, indicating that metamorphism outlasted the main phase of ductile deformation. Preservation of several crenulation stages in porphyroblasts of the same mineral in a single thin section indicates syndeformational porphyroblast growth was rapid relative to strain rate. The general lack of

stage 3-4 crenulation inclusion trails in porphyroblasts probably reflects their inability to overgrow active zones of shearing and dissolution (i.e. cleavage domains). Crenulation cleavages that are overgrown by porphyroblasts were probably inactive at the time of porphyroblast growth (cf. Bell et al., 1986). Post-crenulation porphyroblast deformation is localized and consists of microboudinage, minor recrystallization, and microshearing.

Microstructures indicate that the Corney Brook schist and Fishing Cove River schist have experienced the same metamorphic and structural history, supporting the interpretation based on field relations (Chapter 2) that these units represent a single protolithic package. Table 4.2 summarizes the sequence of porphyroblast growth and foliation development in the Jumping Brook metamorphic suite.

4.4 STRUCTURAL OVERVIEW

Figure 4.25 summarizes the macroscopic-microscopic structural relations in the low-grade and medium- to high-grade rocks of the Jumping Brook metamorphic suite.

Craw (1984) proposed that the pervasive foliation in the low-grade rocks is a first phase whereas that in the

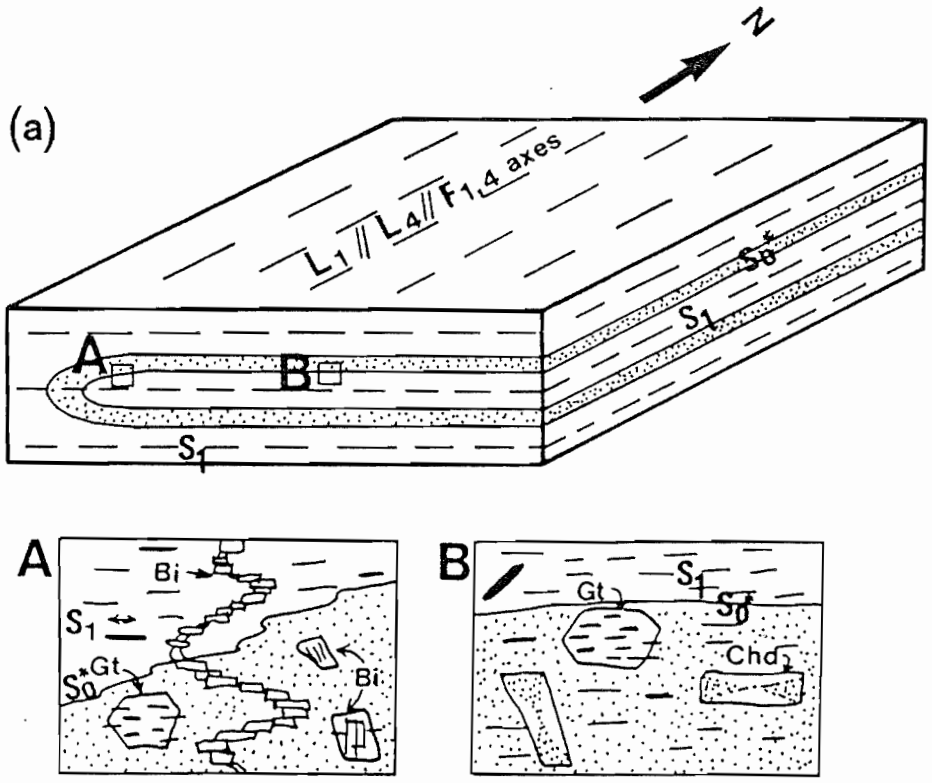

Figure 4.25. Cartoon summarizing macroscopic and microscopic structural relations in the (a) low-grade rocks and (b) medium-to high-grade rocks of the Jumping Brook metamorphic suite. (a) Low-grade rocks: Early tight to isoclinal macroscopic to microscopic folding (F_1) of compositional layering (S_o^*) results in development of axial planar S_1. Syn-S_1 quartz-feldspar veining may be due to dewatering. Porphyroblasts overgrow S_1 and veins. L_1, L_4, and F_4 axes are essentially parallel. Orientation of incipient S_2 observed in thin section is unknown. (b) Medium- to high-grade rocks: Same early history as the low-grade rocks followed by crenulation (F_2) of S_1 to form S_2. F_2 crenulations are only observed in thin section. F_1 folds are observed locally. L_2 and L_4 are essentially parallel.

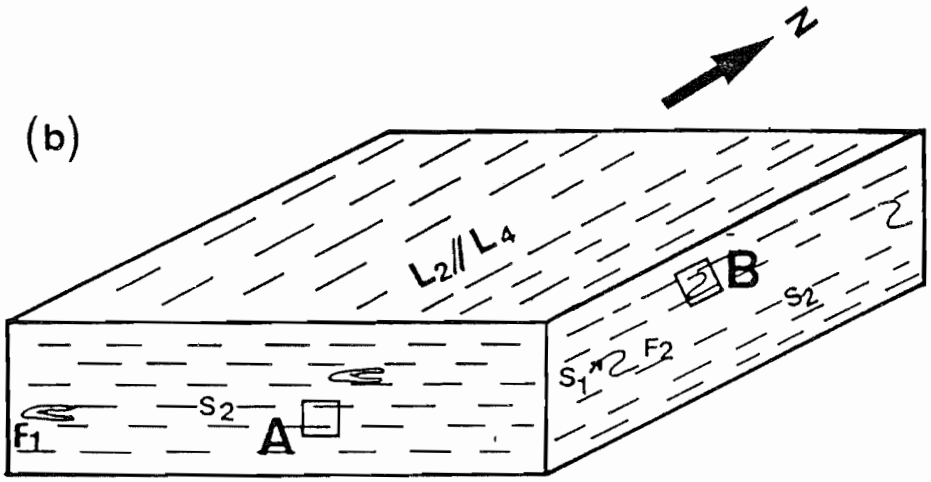

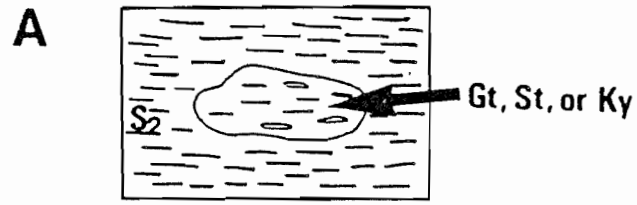

B MEDIUM GRADE rocks

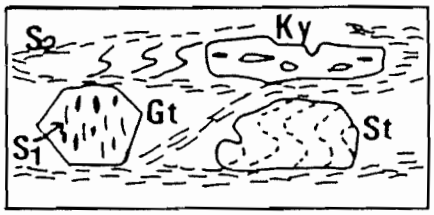

HIGH GRADE rocks

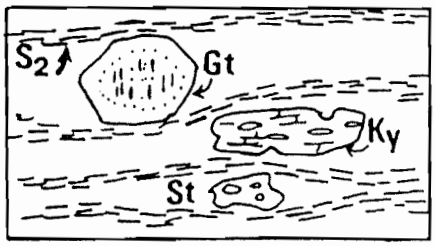

Figure 4.25 (Continued)

medium- to high-grade rocks is a second phase. Microstructural interpretation from this study generally supports this interpretation although microstructures suggest that locally, S_2 is incipiently developed in the low-grade rocks. Therefore, the low-grade rocks have apparently experienced D_2, but to a lesser degree than the medium- to high-grade rocks.

To account for structural differences betwen the low- and medium- to high-grade rocks, Craw (1984) suggested they were farther removed from one another during metamophism and brought closer together or juxtaposed during D_1 in the low-grade rocks and during D_2 in the medium- to high-grade rocks. However, observations discussed in section 4.3 suggest that D_2 crenulations formed during deformation characterized by north-northeasterly extension. This conclusion conflicts with Craw's interpretation of secondary foliation development during westerly directed thrusting which eventually juxtaposed the low-, medium-, and high-grade rocks.

Based on the following points, a means of reconciling this apparent conflict in structural interpretations is suggested:

1. F_1 axes plunge shallowly to the north-northeast.

2. Early crenulation axes (F_2) are observed only in P-sections indicating their axes trend approximately east-west with unknown plunge.
3. Mineral stretching lineations trend north-northeast with a shallow to moderate plunge.
4. Metamorphic grade in the study area increases towards the east-northeast.
5. Foliation is essentially horizontal if the effects of D_4 are removed.
6. Craw's (1984) most westerly high-strain zone (D_3) cuts the George Brook amphibolite, which separates the low-grade rocks from the medium- to high-grade rocks in the study area.
7. Metamorphism is interpreted to have resulted from crustal thickening, possibly due to overthrusting (Chapter 6).

The following structural model attempts to incorporate all these points. Early, tight to isoclinal folding of compositional layering and development of an axial planar S_1 occurred throughout the Jumping Brook metamorphic suite. The mechanism by which these folds formed is unclear from results of this study, but Craw (1984) suggested the folds formed during westward-directed thrusting along steep shear planes. This was

followed by northerly trending extension (D_2) during which L_2, S_2, and F_2 (crenulations) developed in the medium- to high-grade rocks and metamorphism progressed. Since metamorphism is interpreted to have resulted from burial due to crustal thickening, this extension may be related to overthrusting, although no discrete pre-Carboniferous thrust faults have been observed. Differential uplift along late, synmetamorphic, northerly trending, steeply dipping ductile thrusts exposed different structural levels exposed as the medium- to high-grade belt along Corney Brook (cf. Craw, 1984). This sequence is summarized in Figure 4.25.

The reason for northerly extension following early, westerly directed deformation in the sequence is unclear. Further investigation of (1) the kinematics of the early (F_1) folds, (2) the kinematic significance of the F_2 crenulations and the L_2 lineations in the medium- to high-grade rocks, (3) the affects of D_2 on F_1, and (4) the relationship of L_2 to the mineral and stretching lineations in the low-grade rocks is required to clarify the structural history of the Jumping Brook metamorphic suite.

CHAPTER 5

MINERAL CHEMISTRY

5.1 INTRODUCTION

Once a sequence of porphyroblast growth is established, the next step in deciphering a P-T history is to determine the P-T conditions using mineral equilibria and reactions. This requires the chemical compositions of co-existing phases. Therefore, electron microprobe analyses of the major mineral phases in the Dauphinee Brook, Corney Brook, and Fishing Cove River schists and in the George Brook amphibolite (Table 5.1) were carried out to assess variations in mineral chemistry and the degree of chemical equilibration, and for use in geothermometry and geobarometry. Results and interpretations of the mineral chemistry and equilibration are presented in this chapter. Goethermometry and geobarometry are discussed in Chapter 6. Average mineral compositions and standard deviations are given in Tables 5.2-5.3 and 5.5-5.10 and the entire database is listed in Appendix 3. Hand sample and petrographic descriptions of analysed samples are given in Appendix 1. A legend for mineral abbreviations used in the text is listed in Appendix 1, Table A1.1.

Table 5.1. Summary of mineral phases analysed. pe and spe = pelite and semipelite. Legend for abbreviations is given in Appendix 1, Table A1.1. Detailed descriptions of rock types are also presented in Appendix 1.

ZONE	SAMPLE	PHASES ANALYSED							ROCK TYPE
		Chl	Mu	Bi	Gt	Pl	Amp	St	
Ch	850643a						X		late ep vein
Bi	85-107	X	X		X				chtd pe phyllite
	85-K45		X		X				chtd pe phyllite
Gt	85-698c			X	X				hb-gt spe schist
St-Ky	85-659b	X	X	X	X	X		X	gt-spe schist
	85-700b		X	X	X	X		X	st-ky schist
	85-707			X					bi-gt pe schist
	85-708b						X		amphibolite
	85-716a		X		X				gt-bi spe schist
	85-722		X	X	X	X		X	st-gt spe schist
	85-723b	X	X	X	X	X		X	st-gt pe schist
	85-732		X	X		X		X	bi-gt spe schist
Ky	85-441		X	X	X	X			bi pe schist
	85 445				X				bi pe schist
	85-446	X	X	X	X	X			bi pe schist
	85-535		X	X		X			bi spe schist
	85-565			X		X			hb-bi schist
	85-245				X	X	X		gt amphibolite
	85-280				X	X	X		gt amphibolite
	85-343a				X	X	X		gt amphibolite

5.2 CHLORITE

Early (pre-S_1) chlorite porphyroblasts in the lowest grade rocks, post-S_2 chlorite porphyroblasts, and chlorite included in garnet porphyroblasts in the medium-grade rocks were analysed. All are ripidolite excluding a single brunsvigite included in garnet in the Fishing Cove River schist (nomenclature after Hey, 1954; Table 5.2). The post-S_2 chlorite porphyroblasts are significantly more magnesian than either those in the low-grade rocks or those included in garnet, which probably reflects a higher formation temperature for the late porphyroblasts. Locally these porphyroblasts have nucleated on biotite (Figure 4.9).

5.3 MUSCOVITE

Muscovite composition can vary by two major substitutions: Tschermak substitution $(Mg,Fe^{2+})^{vi}$, $Si^{iv} = Al^{vi}$, Al^{iv} to form celadonitic muscovite and substitution of Na^{+} for K^{+} to form paragonite. Metamorphic muscovites are solid-solutions of ideal muscovite and celadonite and tend approach ideal muscovite with increasing metamorphic grade (Miyashiro, 1975).

Table 5.2. Average compositions (MEAN) and standard deviations (S.D.) for microprobe analyses of chlorite. Host phases of chlorite inclusions given in brackets. (E) and (L) indicate early and late porphyroblasts, respectively. H_2O calculated on the basis of listed OH values. All Fe as Fe^{2+}. n = number of analyses.

SAMPLE ANALYSIS	85 - 107 porphyroblasts (E)		85 - 659 porphyroblasts (L)		85-723B inclusions (gt)		85 - 446 inclusion
	Mean	S.D.	Mean	S.D.	Mean	S.D.	
SiO_2	22.82	0.23	24.85	0.04	23.78	0.14	26.55
TiO_2	0.16	0.17	0.10	0.00	0.05	0.04	0.07
Al_2O_3	22.60	0.16	23.03	0.08	22.41	0.30	18.31
FeO	31.51	0.17	22.42	0.02	28.46	0.81	29.98
MnO	0.42	0.04	0.07	0.00	0.15	0.03	1.15
MgO	8.26	0.11	15.83	0.11	11.84	0.25	10.40
CaO	0.00	0.00	0.00	0.00	0.06	0.00	0.01
Na_2O	0.03	0.00	0.50	0.00	0.00	0.00	0.03
K_2O	0.00	0.00	0.00	0.00	0.00	0.00	0.17
H_2O	10.69	0.08	11.38	0.02	11.03	0.04	10.89
Total	96.49		98.18		97.78		97.56
n	5		2		3		1
Si	5.116	0.027	5.233	0.001	5.167	0.011	5.841
Al^{iv}	2.884	0.028	2.767	0.029	2.259	0.068	2.159
Al^{vi}	3.090		2.952		3.482		2.590
Ti	0.028	0.028	0.016	0.000	0.008	0.006	0.012
Fe	5.910	0.021	3.950	0.010	5.171	0.138	5.516
Mn	0.080	0.007	0.013	0.013	0.028	0.005	0.214
Mg	2.760	0.001	4.971	0.027	3.835	0.096	3.410
Ca	0.000	0.000	0.000	0.000	0.014	0.000	0.002
Na	0.013	0.000	0.020	0.020	0.008	0.000	0.013
K	0.000	0.000	0.000	0.000	0.000	0.000	0.048
O	36		36		36		36
OH	16		16		16		16
Fe/Fe+Mg	0.682		0.443		0.574		0.618

Guidotti (1973) and Guidotti and Sassi (1976) reported that muscovite composition is affected by the extensive variable bulk composition (that is, mineral assemblage) and the intensive variables: pressure (P), temperature (T) and activity of water (a_{H2O}). Phase rule considerations (F=C-P+3, where F=variance, C= number of components, and P=number of phases) show that in a three component system (Al-K-Na), a three phase or limiting assemblage is required to eliminate bulk compositional effects on muscovite composition. In limiting assemblages (C=P), a change in mineral composition occurs only by a change in the intensive variables. Guidotti (1973) therefore cautioned that assessment of muscovite compositional variations with metamorphic grade must be done in "specific limiting assemblages".

Guidotti and Sassi (1976) noted that the anorthite content of co-existing plagioclase affects muscovite composition in limiting assemblages, such that X_{Na} in both phases decreases. The addition of Ca, provided it does not form a new phase, increases the variance from 3 to 4 and bulk composition can affect muscovite composition. Since the relationship between co-existing muscovite and plagioclase compositions defined by Guidotti and Sassi (1976) is qualitative, they recommended comparison of $(X_{Na})^{Mu}$ in samples where the

anorthite An content of co-existing plagioclase varies in magnitude by 6 to 8 %. This restriction is met by the samples analysed in this study where the maximum plagioclase compositional variation is 8% An in a given sample (eg. An_{25}-An_{30}).

The commonly cited compositional variations in muscovite composition with increasing metamorphic grade are: an increase in $(Mg+Fe^{2+})$, Ti^{4+}, Al^{iv} and a decrease in $Na/(Na+K)$, Al^{vi} and Si. There is an overall, but not continuous, decrease in Al^{vi} and increase in Ti^{4+} with increasing metamorphic grade in the analysed samples, but no Si decrease or consistent pattern in Fe+Mg variations.

In all samples, matrix white mica and porphyroblasts approach ideal muscovite ($K_2Al_4(Si_6Al_2O_2)OH_4$), with small variations in Tschermak substitution. White mica in late microveinlets in a low-grade pelitic phyllite (85-107) is margarite-rich relative to co-existing white mica in the matrix in the matrix (Figure 5.1, Table 5.3).

All medium- to high-grade samples of the staurolite-garnet and biotite schists in which muscovite was analysed (excluding samples 85-732 and 85-535), contain the limiting assemblage muscovite-plagioclase-kyanite. Consequently, bulk composition should not affect muscovite composition in the medium- to high- grade schists.

Table 5.3. Average compositions (Mean) and standard deviations (S.D.) for microprobe analyses of muscovite. Host phases of muscovite inclusions given in brackets. H_2O calculated on the basis of listed OH values. All Fe as Fe^{2+}. n = number of analyses.

SAMPLE	85 - 107		85 - 107		85 - K45		85 - 659b		85 - 700b		85 - 700b		85 - 722		85 - 723b	
ANALYSIS	matrix		veinlet		matrix		core & rim		core & rim		inclusion (gt)		core & rim		core & rim	
	Mean	S.D.	Mean	S.D.	Mean	S.D.	Mean	S.D.	Mean	S.D.	Mean	S.D.	Mean	S.D.	Mean	S.D.
SiO_2	46.17	0.28	47.20	0.20	45.97	1.47	46.28	0.47	46.90	0.52	46.80	0.28	46.50	0.40	47.06	0.01
TiO_2	0.16	0.03	0.12	0.04	0.16	0.06	0.48	0.07	0.38	0.10	0.45	0.01	0.50	0.05	0.57	0.06
Al_2O_3	35.72	0.41	37.05	1.13	35.69	0.71	36.00	0.46	35.97	0.51	35.88	0.32	35.69	0.63	35.80	0.51
FeO	1.26	0.15	0.95	0.18	1.29	0.08	0.98	0.13	0.84	0.05	0.93	0.06	1.16	0.24	0.86	0.08
MnO	0.08	0.03	0.07	0.02	0.06	0.05	0.07	0.04	0.09	0.01	0.05	0.01	0.06	0.03	0.05	0.03
MgO	0.36	0.06	0.24	0.08	0.44	0.03	0.55	0.05	0.54	0.07	0.56	0.04	0.62	0.05	0.69	0.11
CaO	0.01	0.00	0.21	0.00	0.01	0.00	0.03	0.00	0.03	0.03	0.01	0.00	0.08	0.07	0.04	0.00
Na_2O	1.66	0.07	2.75	1.52	1.51	0.05	1.44	0.04	1.60	0.16	1.64	0.04	1.53	0.05	1.20	0.09
K_2O	8.46	0.23	7.23	3.22	8.57	0.18	8.94	0.34	8.62	0.12	9.00	0.06	8.76	0.27	8.72	0.19
H_2O	4.48	0.03	4.59	0.03	4.46	0.12	4.51	0.04	4.54	0.04	4.54	0.00	4.52	0.05	4.54	0.02
Total	98.36		100.41		98.16		99.28		99.51		99.86		99.42		98.53	
n	3		3		3		8		6		2		6		3	
Si	6.178	0.025	6.157	0.049	6.166	0.044	6.143	0.012	6.192	0.033	6.176	0.033	6.166	0.031	6.206	0.019
Al^{iv}	1.822	0.050	1.843	0.129	1.834	0.045	1.857	0.037	1.808	0.050	2.418	0.054	1.834	0.052	1.794	0.063
Al^{vi}	3.813		3.853		3.811		3.777		3.792		3.164		3.745		3.772	
Ti	0.016	0.003	0.012	0.004	0.016	0.006	0.048	0.007	0.038	0.010	0.001	0.045	0.050	0.004	0.057	0.006
Fe	0.140	0.017	0.103	0.020	0.144	0.005	0.109	0.015	0.092	0.006	0.102	0.007	0.129	0.028	0.095	0.009
Mn	0.010	0.003	0.008	0.002	0.006	0.005	0.008	0.004	0.010	0.001	0.006	0.002	0.007	0.003	0.005	0.003
Mg	0.072	0.013	0.047	0.015	0.087	0.004	0.109	0.009	0.106	0.014	0.110	0.008	0.122	0.011	0.136	0.022
Ca	0.001	0.000	0.029	0.000	0.001	0.000	0.004	0.000	0.004	0.005	0.001	0.000	0.012	0.011	0.006	0.000
Na	0.430	0.018	0.693	0.377	0.392	0.005	0.371	0.012	0.410	0.039	0.418	0.009	0.394	0.011	0.308	0.023
K	1.445	0.046	1.207	0.543	1.468	0.069	1.514	0.058	1.453	0.029	1.514	0.009	1.481	0.032	1.468	0.036
O	24		24		24		24		24		24		24		24	
OH	4		4		4		4		4		4		4		4	
Fe+Mg	0.229		0.150		0.231		0.218		0.198		0.212		0.251		0.231	
Na/Na+K	0.212		0.365		0.211		0.197		0.220		0.216		0.210		0.173	
MARG	0		2		0		1		0		0		1		1	
PARA	23		36		21		19		22		22		21		17	
MUSC	77		62		79		80		78		78		78		82	

Table 5.3. (Continued)

SAMPLE ANALYSIS	85 - 732 core & rim		85 - 441 core & rim		85 - 446 core & rim		85 - 535 core & rim	
	Mean	S.D.	Mean	S.D.	Mean	S.D.	Mean	S.D.
SiO_2	46.61	0.34	46.53	0.41	46.80	0.77	46.83	0.40
TiO_2	0.62	0.10	0.78	0.20	0.59	0.14	0.75	0.09
Al_2O_3	34.98	0.39	35.18	0.40	34.78	0.76	35.15	0.32
FeO	1.48	0.07	1.05	0.13	0.85	0.05	1.04	0.12
MnO	0.08	0.03	0.07	0.03	0.07	0.01	0.09	0.02
MgO	0.72	0.05	0.70	0.11	0.74	0.10	0.85	0.13
CaO	0.02	0.02	0.03	0.01	0.00	0.00	0.03	0.01
Na_2O	1.33	0.07	1.25	0.19	1.00	0.061	1.20	0.04
K_2O	8.98	0.20	8.85	0.79	10.18	0.322	9.47	0.25
H_2O	4.50	0.03	4.50	0.03	4.50	0.061	4.53	0.03
Total	99.32		98.94		99.51		99.94	
n	7		5		5		5	
Si	6.198	0.028	6.193	0.058	6.228	0.051	6.193	0.025
Al^{iv}	1.802	0.049	1.807	0.036	1.772	0.103	1.807	0.049
Al^{vi}	3.683		3.713		3.685		3.672	
Ti	0.063	0.010	0.078	0.020	0.059	0.014	0.075	0.008
Fe	0.165	0.008	0.117	0.014	0.095	0.005	0.116	0.013
Mn	0.009	0.003	0.007	0.003	0.008	0.001	0.010	0.002
Mg	0.143	0.010	0.139	0.023	0.146	0.020	0.167	0.026
Ca	0.003	0.003	0.004	0.002	0.000	0.000	0.004	0.001
Na	0.342	0.019	0.322	0.049	0.259	0.018	0.307	0.009
K	1.523	0.031	1.503	0.131	1.729	0.050	1.598	0.044
O	24		24		24		24	
OH	4		4		4		4	
Fe+Mg	0.308		0.256		0.241		0.283	
Na/Na+K	0.183		0.176		0.130		0.161	
MARG	0		0		0		0	
PARA	18		18		13		16	
MUSC	82		82		87		84	

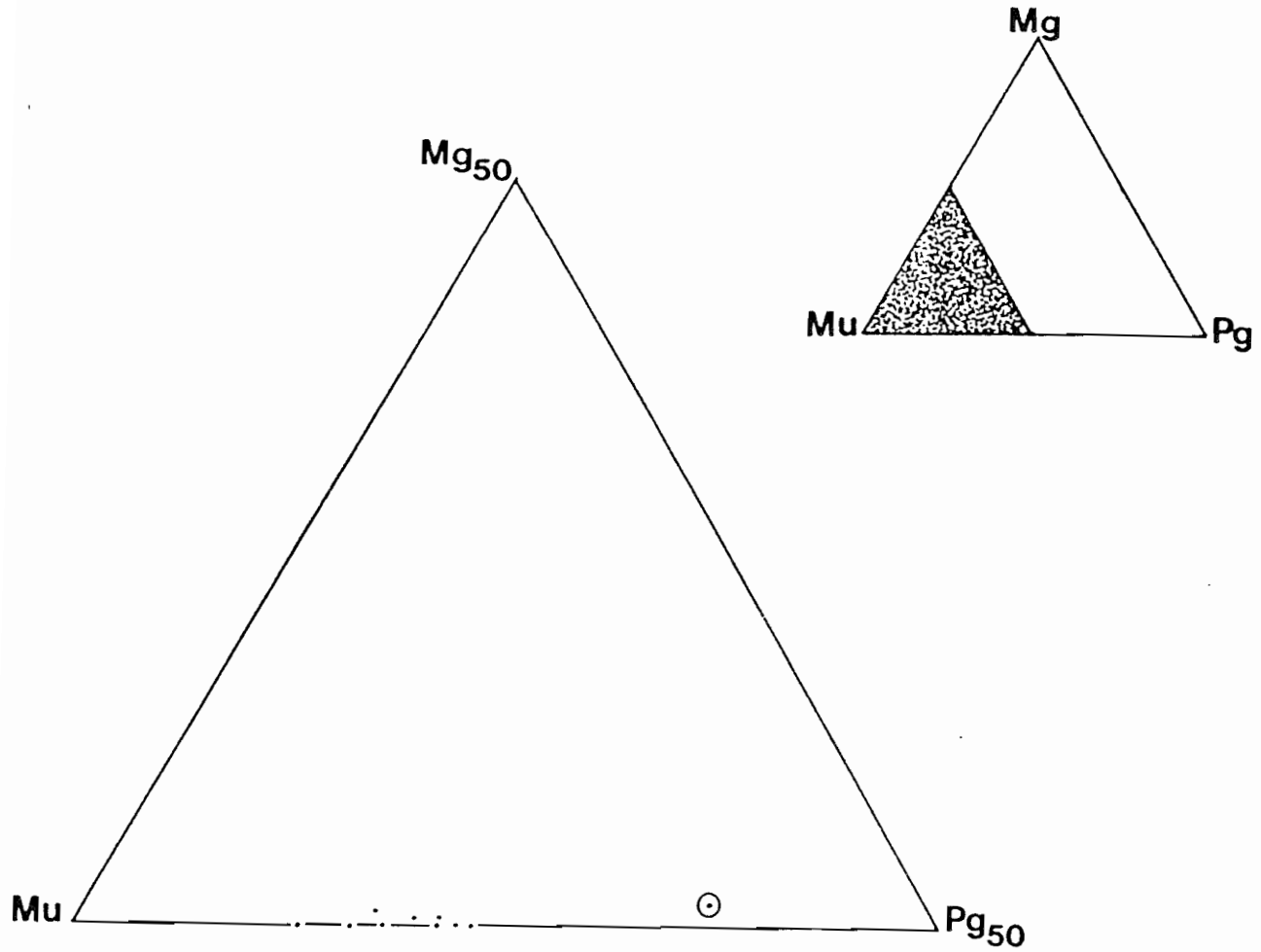

Figure 5.1.Muscovite chemistry as a function of muscovite (Mu), paragonite (Pg), and margarite (Mg) end-members. Inset gives location of figure in the Mu-Pg-Mg ternary system. Circled data point is the composition of muscovite in veinlet, sample 85-107.

Figure 5.2 and Table 5.4 show little relationship between $(X_{Na})^{Mu}$ and $(X_{Na})^{Pl}$ but do show a general increase in X_{Na} muscovite with increasing metamorphic grade. The lower $(X_{Na})^{Mu}$ in sample 85-446 relative to 85-441 (Table 5.4) is in keeping with the interpreted retrograde origin of muscovite in the former. The lack of any relation between $(X_{Na})^{Mu}$ and $(X_{Na})^{Pl}$ plagioclase is probably due to the limited inter-sample range (An_{22}-An_{30}) in plagioclase rims co-existing with muscovite.

Since $(X_{Na})^{Mu}$ is partly controlled by a_{H2O}, it should provide a qualitative indication of a_{H2O} (cf. Guidotti and Sassi, 1976). The range observed in $(X_{Na})^{Mu}$ in closely spaced samples of the same metamorphic grade (eg. 85-722 and 85-723b) suggests local variations in a_{H2O}, consistent with local replacement of kyanite by muscovite. However, plagioclase composition effects on $(X_{Na})^{Mu}$, undetected due to the small database, may be responsible for these variations and further data are required to assess the relations, if any, of $(X_{Na})^{Mu}$ in muscovite to a_{H2O}.

5.4 GARNET

Garnet is a common metamorphic mineral which generally shows compositional zonation and has therefore

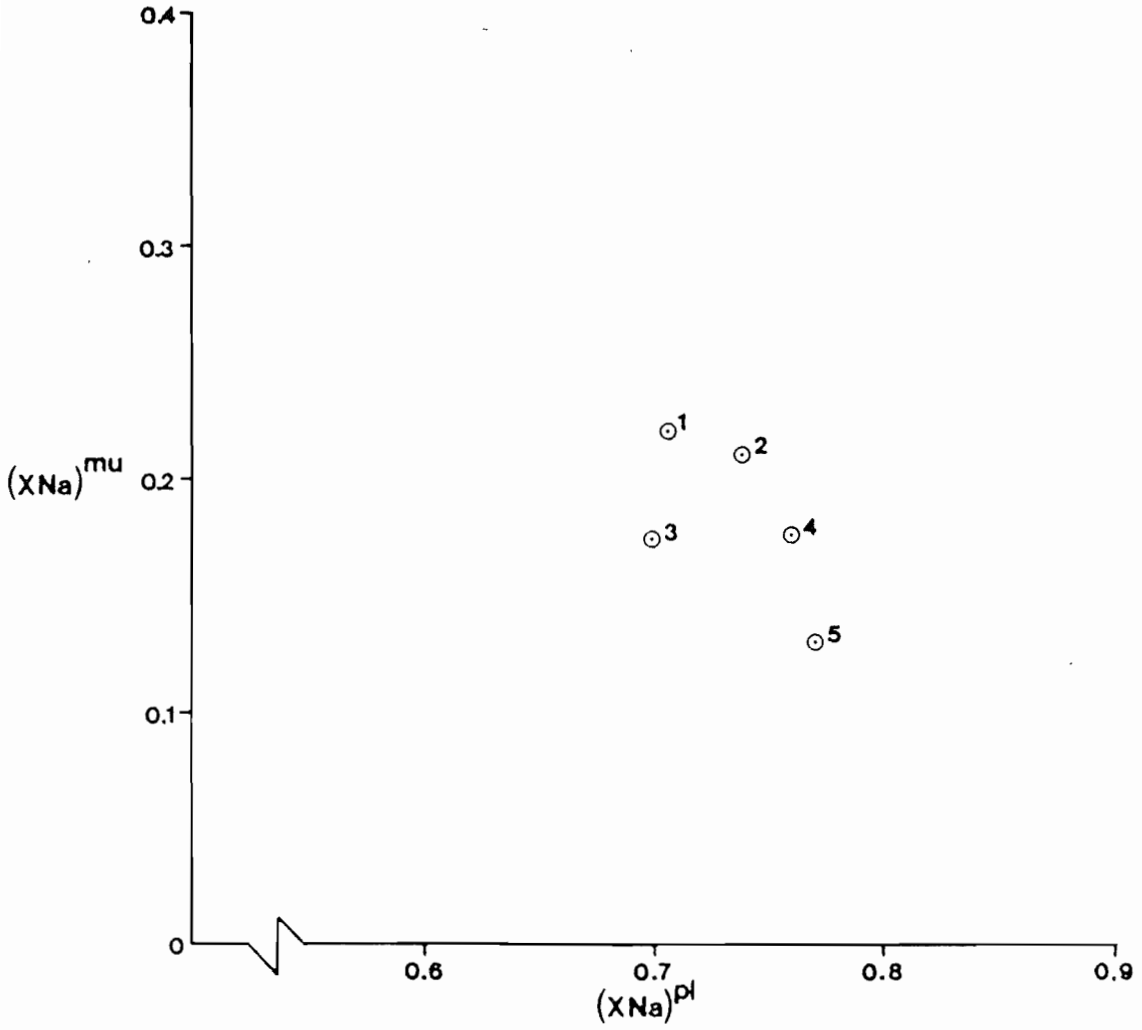

Figure 5.2. Plot of $(X_{Na})^{Mu}$ versus $(X_{Na})^{Pl}$ for samples with the limiting assemblage muscovite-plagioclase-kyanite showing lack of correlation between $(X_{Na})^{Mu}$ and $(X_{Na})^{Pl}$.

Table 5.4. Summary of $(X_{Na})^{Mu}$ versus $(X_{Na})^{Pl}$ values in samples with the limiting assemblage muscovite-plagioclase-kyanite.

# in Fig. 5.3	Sample	$(X_{Na})^{Mu}$	$(X_{Na})^{Pl}$ core	$(X_{Na})^{Pl}$ rim
1	85-700b	0.220	0.696	0.763
2	85-722	0.210	0.744	0.698
3	85-723b	0.173	0.729	0.698
4	85-441	0.176	0.763	0.760
5	85-446	0.130	0.772	0.770

been subject of numerous studies. The most common zonation, referred to as normal, is a decrease in Ca and Mn and increase in Fe and Mg from core to rim. Reverse zonations are those which differ from normal zonations. Two major theories exist on the origin of compositional zonation in garnet: (1) the growth or fractionation-depletion hypothesis and (2) the diffusion hypothesis. In the former, zoning develops by preferential incorporation of Mn into the growing garnet and a continuous or discontinuous change in the composition of the material from which the garnet crystallizes (eg. Hollister, 1966). The result is a bell-shaped growth zonation profile. This theory requires slow volume diffusion. The latter theory involves zonation development by diffusion after growth in a garnet that may or may not have been homogeneous (eg. Miyashiro and Shido, 1973). Diffusion zonation commonly results from cation exchange between garnet and co-wxisting Fe-Mg phases (Tracy, 1982).

Compositional unconformities, with or without associated textural unconformities, have been reported by numerous authors and attributed to prograde-retrograde-prograde sequences of crystal growth (eg. Tracy, 1982) and/or to fluctuation between garnet-producing and garnet-consuming reactions during prograde metamorphism (eg. Thompson et al., 1977; Foster, 1986).

Garnet composition is important to determining P-T histories. Its use in garnet-biotite and garnet-hornblende geothermometry and in garnet-plagioclase-Al_2SiO_5-quartz geobarometry (Ghent, 1976) provides quantitative estimates of metamorphic temperatures and pressures. Spear and Selverstone (1983) applied garnet zonation to P-T-t path determination by deriving petrogenetic (P-T-X) grids for common pelitic assemblages. This technique requires that the garnet rim is always in equilibrium with the matrix assemblage (Spear et al., 1985) and that little or no volume diffusion takes place. Since garnet composition is partly a function of bulk composition, the method also requires comparison between garnets from the same bulk compositions.

All garnets in the study area consist dominantly of almandine (Figure 5.3, Table 5.5). $(X_{Mn})^{Gt}$ is higher in the low-grade rocks than in the medium- and high-grade schists reflecting the lower temperature of spessartine stability relative to almandine (Hsu, 1968).

5.4.1 Metasedimentary Phyllites and Schists

Garnets in the low-grade pelitic phyllites and in most of the medium-grade schists exhibit a bell-shaped, zonation profile with high Ca, Mn cores and high Fe, Mg

Table 5.5. Average compositions (Mean) and standard deviations (S.D.) for microprobe analyses of garnet. "Rim" and "X rim" analyses refer to those where garnet is in contact with biotite, and isolated from biotite, respectively. Analyses of garnet in the matrix and included in kyanite in sample 85 - 441 are distinguished by (matrix) and (ky), respectively. Rim analyses -1 and -2 for 85 - 659b are those used in geothermometry calculations. All Fe as Fe^{2+}. n = number of analyses.

SAMPLE	85 - 107		85 - K45		85 - K45	85 - 698c		85 - 698c		85-698c	85-659b		85-659b	
ANALYSIS	Core		rim		core	core		rim		X rim	core		middle	
	Mean	S.D.	Mean	S.D.		Mean	S.D.	Mean	S.D.		Mean	S.D.	Mean	S.D.
SiO_2	35.90	0.23	36.33	0.22	36.24	37.27	0.29	37.41	0.25	37.32	36.47	0.33	36.57	0.15
TiO_2	0.05	0.01	0.02	0.01		0.09	0.08	0.03	0.00	0.18	0.12	0.04	0.07	0.04
Al_2O_3	20.52	0.25	20.23	0.38	0.70	21.20	0.17	20.78	0.79	21.54	20.83	0.16	20.97	0.19
Cr_2O_3	0.12	0.07	0.07	0.09	0.15	0.08	0.00	0.02	0.00	0.00	0.14	0.04	0.14	0.05
FeO	29.75	0.47	30.62	0.47	28.01	30.14	0.66	31.29	0.11	31.85	32.28	1.48	33.67	1.09
MnO	8.95	0.32	6.55	0.43	9.57	1.92	1.28	0.89	0.06	0.89	3.21	1.70	1.27	1.48
MgO	0.82	0.04	0.87	0.04	0.72	3.09	0.54	3.39	0.04	3.42	1.82	0.27	2.25	0.36
CaO	2.13	0.18	3.39	0.29	3.55	5.94	0.74	5.60	0.11	5.63	5.24	0.16	4.99	0.32
Total	98.24		98.08		98.94	99.73		99.41		100.83	100.11		99.93	
n	7		3		1	2		2		1			8	
Si	5.967	0.040	6.024	0.032	5.962	5.961	0.020	6.002	0.035	5.911	5.899	0.009	5.905	0.020
Al^{iv}	0.033	0.046	0.000	0.053	0.038	0.039	0.013	0.000	0.100	0.089	0.101	0.010	0.095	0.030
Al^{vi}	3.986		3.955		3.977	3.959		3.930		3.933	3.872		3.896	
Ti	0.006	0.002	0.003	0.002	0.000	0.011	0.009	0.004	0.000	0.021	0.014	0.005	0.009	0.005
Cr	4.019	0.046	0.019	0.026	0.044	0.022	0.000	0.006	0.000	0.000	0.040	0.011	0.040	0.014
Fe	4.134	0.062	4.247	0.037	3.854	4.033	0.133	4.199	0.038	4.219	4.367	0.177	4.546	0.144
Mn	1.259	0.042	0.920	0.066	1.334	0.258	0.170	0.121	0.009	0.119	0.440	0.234	0.174	0.202
Mg	0.204	0.009	0.215	0.007	0.177	0.736	0.138	0.811	0.000	0.807	0.437	0.062	0.542	0.864
Ca	0.380	0.032	0.602	0.055	0.626	1.017	0.116	0.962	0.030	0.956	0.908	0.030	0.086	0.054
O	24		24		24	24		24		24	24		24	
Fe/Fe+Mg								0.838		0.839	0.909		0.893	
ALMD	69		71		64	67		69		69	71		85	
GROSS	6		10		11	17		16		16	15		2	
PYROP	4		4		3	12		13		13	7		10	
SPESS	21		15		22	4		2		2	7		3	

Table 5.5. (Continued)

SAMPLE	85-659b		85 - 659b		85 - 659b		85 - 700b		85 - 700b		85 - 700b	85 - 700b	
ANALYSIS	rim -1		rim - 2		X rim		core		middle		rim	X rim	
	Mean	S.D.	Mean	S.D.	Mean	S.D.	Mean	S.D.	Mean	S.D.		Mean	S.D.
SiO_2	36.64	0.21	36.78	0.27	36.85	0.29	36.33	0.26	37.71	0.05	36.83	37.04	0.22
TiO_2	0.05	0.06	0.06	0.04	0.03	0.01	0.08	0.04	0.07	0.07	0.12	0.08	0.04
Al_2O_3	21.13	0.16	21.14	0.24	21.21	0.18	20.54	0.26	21.02	0.09	21.00	21.00	0.27
Cr_2O_3	0.12	0.05	0.16	0.01	0.14	0.02	0.01	0.03	0.16	0.01	0.14	0.16	0.02
FeO	35.05	0.83	34.18	1.18	34.09	0.24	29.90	0.29	31.76	1.87	31.34	32.06	1.08
MnO	0.20	0.04	0.15	0.14	0.17	0.11	4.68	0.69	2.57	1.92	3.36	1.35	1.93
MgO	3.53	0.11	3.34	0.12	3.56	0.14	1.52	0.06	1.75	0.27	1.98	2.76	0.95
CaO	3.16	0.26	3.83	0.70	4.01	0.31	5.86	0.59	5.37	0.57	5.33	4.76	1.09
Total	98.88		99.64		100.06		98.92		100.41		100.10	99.21	
n	2		2		3		2		2		1	3	
Si	5.896	0.059	5.915	0.043	5.901	0.042	5.932	0.019	5.945	0.025	5.930	5.969	0.017
Al^{iv}	0.1040	0.013	0.085	0.046	0.099	0.032	0.068	0.065	0.055	0.006	0.070	0.031	0.054
Al^{vi}	3.904		3.923		3.906		3.887		3.957		3.916	3.958	
Ti	0.006	0.007	0.007	0.004	0.003	0.001	0.009	0.004	0.009	0.009	0.015	0.010	0.005
Cr	0.033	0.014	0.044	0.001	0.041	0.004	0.041	0.008	0.044	0.002	0.040	0.046	0.006
Fe	4.717	0.092	4.597	0.159	4.565	0.019	4.083	0.023	4.302	0.265	4.220	4.321	0.157
Mn	0.027	0.006	0.021	0.019	0.023	0.015	0.647	0.098	0.352	0.263	0.458	0.184	0.263
Mg	0.846	0.023	0.799	0.029	0.850	0.031	0.369	0.014	0.422	0.066	0.475	0.664	0.227
Ca	0.545	0.047	0.659	0.121	0.689	0.054	1.024	0.098	0.931	0.096	0.920	0.822	0.187
O	24		24		24		24		24		24	24	
Fe/Fe+Mg	0.848		0.852		0.843		0.917		0.911		0.899	0.867	
ALMD	77		75		74		67		72		70	72	
GROSS	9		11		11		17		15		15	14	
PYROP	14		13		14		6		7		8	11	
SPESS	0		1		1		10		6		7	3	

Table 5.5. (Continued)

SAMPLE	85 - 716a	85 - 716a		85 - 716a		85 - 716a	85 - 722		85 - 722		85 - 722		85 - 722	
ANALYSIS	core	middle		rim		X rim	core		middle		rim		X rim	
		Mean	S.D.	Mean	S.D.		Mean	S.D.	Mean	S.D.	Mean	S.D.	Mean	S.D.
SiO_2	36.39	36.79	0.51	37.14	0.30	37.19	36.96	0.19	36.77	0.30	36.80	0.36	36.73	0.20
TiO_2	0.09	0.10	0.10	0.07	0.00	0.07	0.03	0.01	0.02	0.01	0.08	0.06	0.03	0.02
Al_2O_3	20.57	20.61	0.16	20.92	0.29	21.01	20.50	0.26	20.42	0.19	20.26	0.13	20.37	0.18
Cr_2O_3	0.14	0.19	0.01	0.19	0.02	0.18	0.06	0.02	0.03	0.01	0.04	0.02	0.06	0.03
FeO	28.37	28.87	1.22	30.92	0.52	33.20	33.69	0.46	33.55	0.21	34.29	0.87	33.30	0.45
MnO	5.55	5.41	1.37	1.00	0.01	0.65	1.17	0.11	1.23	0.07	1.56	0.35	1.22	0.16
MgO	1.52	1.46	0.13	2.89	0.09	2.24	3.65	0.30	3.67	0.15	2.90	0.59	3.56	0.23
CaO	6.14	6.02	0.14	5.70	0.18	5.32	2.87	0.19	2.71	0.25	2.73	0.37	2.96	0.35
Total	98.77	99.45		98.83		99.86	98.93		98.40		98.66		98.23	
n	1	2		2		1	6		11		3		10	
Si	5.944	5.966	0.028	5.985	0.080	5.971	5.995	0.035	5.995	0.022	6.014	0.029	5.999	0.024
Al^{iv}	0.056	0.034	0.005	0.015	0.034	0.029	0.008	0.038	0.005	0.025	0.000	0.035	0.001	0.028
Al^{vi}	3.905	3.905		3.959		3.948	3.912		3.920		3.904		3.921	
Ti	0.011	0.013	0.012	0.008	0.000	0.008	0.003	0.002	0.002	0.001	0.009	0.007	0.004	0.003
Cr	0.040	0.053	0.003	0.053	0.006	0.051	0.017	0.005	0.007	0.003	0.010	0.006	0.016	0.008
Fe	3.875	3.914	0.131	4.166	0.047	4.458	4.570	0.069	4.575	0.041	4.687	0.134	4.548	0.071
Mn	0.768	0.744	0.195	0.136	0.001	0.088	0.161	0.015	0.170	0.011	0.216	0.049	0.168	0.023
Mg	0.370	0.349	0.030	0.694	0.017	0.536	0.882	0.070	0.892	0.033	0.706	0.141	0.866	0.054
Ca	1.075	1.046	0.034	0.984	0.026	0.915	0.498	0.032	0.473	0.043	0.478	0.062	0.518	0.060
O	24	24		24		24	24		24		24		24	
Fe/Fe+Mg	0.913	0.918		0.857		0.893	0.838		0.837		0.869		0.840	
ALMD	64	65		70		74	75		75		77		75	
GROSS	18	17		16		15	8		8		8		8	
PYROP	6	6		12		9	14		14		12		14	
SPESS	13	12		2		2	3		3		3		3	

Table 5.5. (Continued)

SAMPLE ANALYSIS	85 - 723b core		85 - 723b middle		85 - 723b rim	85 - 723b X rim		85 - 441 core (ky)		85 - 441 X rim (Matrix)		85 - 446 Core	
	Mean	S.D.	Mean	S.D.		Mean	S.D.	Mean	S.D.	Mean	S.D.	Mean	S.D.
SiO_2	36.65	0.25	36.95	0.08	36.80	36.99	0.22	37.15	0.03	37.15	0.61	37.37	0.09
TiO_2	0.01	0.00	0.04	0.04	0.07	0.05	0.02	0.04	0.04	0.01	0.00	0.00	0.00
Al_2O_3	20.91	0.04	21.11	0.19	21.01	20.88	0.36	21.20	0.03	21.05	0.21	21.46	0.39
Cr_2O_3	0.18	0.00	0.18	0.05	0.21	0.16	0.03	0.17	0.00	0.20	0.00	0.14	0.02
FeO	33.51	0.25	33.31	0.62	33.39	33.00	0.33	31.50	0.13	31.89	0.26	32.33	0.02
MnO	1.68	0.03	1.58	0.04	1.46	1.63	0.07	1.32	0.06	1.63	0.37	1.75	0.03
MgO	3.42	0.32	3.52	0.13	3.53	3.52	0.06	5.56	0.08	5.19	0.26	5.56	0.21
CaO	3.32	0.22	3.15	0.25	3.34	3.28	0.33	1.93	0.01	1.94	0.01	1.78	0.09
Total	99.68		99.84		99.81	99.51		98.87		99.06		100.38	
n	2		2		1	4		2		2		2	
Si	5.909	0.042	5.929	0.018	5.911	5.954	0.039	5.940	0.004	5.947	0.041	5.911	0.030
Aliv	0.091	0.005	0.071	0.016	0.089	0.046	0.056	0.060	0.001	0.053	0.002	0.089	0.042
Alvi	3.975		3.922		3.890	3.915		3.937		3.920		3.912	
Ti	0.001	0.000	0.005	0.005	0.008	0.005	0.003	0.004	0.004	0.001	0.000	0.000	0.000
Cr	0.051	0.000	0.050	0.014	0.060	0.044	0.008	0.048	0.000	0.057	0.001	0.038	0.006
Fe	4.518	0.035	4.470	0.060	4.485	4.441	0.032	4.211	0.012	4.269	0.074	4.277	0.035
Mn	0.229	0.004	0.214	0.005	0.199	0.222	0.009	0.178	0.008	0.221	0.052	0.234	0.002
Mg	0.821	0.076	0.841	0.026	0.845	0.844	0.017	1.324	0.016	1.238	0.049	1.309	0.039
Ca	0.572	0.037	0.541	0.045	0.575	0.566	0.057	0.331	0.003	0.333	0.006	0.301	0.018
O	24		24		24	24		24		24		24	
Fe/Fe+Mg	0.846		0.842		0.842	0.840		0.761		0.775		0.766	
ALMD	74		74		74	73		70		70		70	
GROSS	9		9		9	9		5		6		5	
PYROP	13		14		14	14		22		20		21	
SPRESS	4		3		3	4		3		4		4	

Table 5.5. (Continued)

SAMPLE	85 - 441		85 - 441		85 - 441 core	85 - 441 middle		85 - 441 rim	
ANALYSIS	rim (ky)		X rim (ky)		(matrix)	(matrix)		(matrix)	
	Mean	S.D.	Mean	S.D.		Mean	S.D.	Mean	S.D.
SiO_2	37.01	0.33	37.04	0.19	37.07	37.42	0.24	36.74	0.03
TiO_2	0.03	0.00	0.03	0.03	0.05	0.04	0.00	0.03	0.02
Al_2O_3	2.94	0.02	21.04	0.04	21.32	21.04	0.22	21.01	0.06
Cr_2O_3	0.18	0.00	0.17	0.01	0.18	0.20	0.02	0.18	0.05
FeO	32.39	1.43	32.01	0.37	31.69	31.95	0.05	32.76	0.52
MnO	2.68	0.64	2.44	0.21	1.27	1.32	0.12	3.33	0.53
MgO	4.42	0.42	4.60	0.01	5.57	5.55	0.05	3.75	0.04
CaO	1.76	0.23	1.79	0.18	1.95	2.01	0.01	1.79	0.10
Total	100.41		99.12		99.10	99.53		99.59	
n	2		2		1	2		3	
Si_{iv}	5.956	0.048	5.951	0.000	5.917	5.954	0.013	5.929	0.016
Al_{vi}	0.044	0.007	0.049	0.014	0.083	0.046	0.024	0.071	0.010
Al	3.928		3.936		3.929	3.900		3.926	
Ti	0.004	0.000	0.004	0.004	0.006	0.005	0.000	0.004	0.003
Cr	0.051	0.000	0.047	0.001	0.051	0.054	0.006	0.050	0.014
Fe	4.360	0.196	4.301	0.028	4.23	4.251	0.011	4.422	0.068
Mn	0.364	0.088	0.333	0.030	0.172	0.177	0.017	0.455	0.072
Mg	1.060	0.100	1.202	0.002	1.325	1.315	0.017	0.902	0.095
Ca	0.303	0.039	0.307	0.029	0.334	0.343	0.001	0.309	0.017
O	24		24		24	24		24	
Fe/Fe+Mg	0.804		0.796		0.762	0.764		0.831	
ALMD	72		71		70	70		72	
GROSS	5		5		5	5		5	
PYROP	17		18		22	22		15	
SPESS	6		6		3	3		8	

Table 5.5. (Continued)

SAMPLE	85 - 446		85 - 446	85 - 245	85 - 245		85 - 280		85 - 280		85 - 343a		85 - 343a	
ANALYSIS	rim		X rim	core	rim		core		rim		core		rim	
	Mean	S.D.			Mean	S.D.	Mean	S.D.	Mean	S.D.	Mean	S.D.	Mean	S.D.
SiO_2	37.10	0.12	37.16	37.09	36.99	0.41	37.31	0.07	37.45	0.24	37.56	0.30	37.65	0.26
TiO_2	0.40	0.00	0.07	0.15	0.08	0.06	0.12	0.00	0.08	0.04	0.05	0.00	0.09	0.04
Al_2O_3	21.07	0.10	21.16	19.75	19.93	0.45	20.97	0.06	20.93	0.27	20.89	0.22	21.13	0.07
Cr_2O_3	0.06	0.01	0.18	0.00	0.02	0.00	0.18	0.01	0.17	0.01	0.16	0.01	0.19	0.01
FeO	31.22	0.50	30.32	27.40	26.91	0.60	27.70	0.02	27.56	0.64	27.36	0.68	27.46	0.80
MnO	4.38	0.01	5.47	3.18	3.44	1.74	2.69	0.52	2.36	0.44	2.39	0.75	2.81	0.86
MgO	4.16	0.14	3.88	2.95	3.22	0.53	3.31	0.33	3.40	0.30	3.13	0.44	3.02	0.34
CaO	1.75	0.18	1.39	8.89	7.74	0.60	7.98	0.31	7.99	0.18	8.29	0.11	7.69	0.75
Total	100.14		99.63	99.41	98.33		100.26		99.94		99.83		100.04	
n	2		1	1	3		2		4		2		3	
Si	5.954	0.004	5.962	5.980	6.003	0.013	5.923	0.011	5.946	0.010	5.971	0.021	5.969	0.031
Al^{iv}	0.046	0.035	0.038	0.020	0.000	0.000	0.077	0.026	0.054	0.002	0.029	0.004	0.031	0.032
Al^{vi}	3.941		3.964	3.734	3.813	0.046	3.848		3.863		3.886		3.919	
Ti	0.005	0.000	0.008	0.018	0.009	0.007	0.014	0.000	0.009	0.005	0.006	0.000	0.010	0.005
Cr	0.017	0.004	0.051	0.000	0.06	0.000	0.051	0.004	0.049	0.003	0.043	0.002	0.052	0.002
Fe	4.190	0.051	4.068	3.694	3.654	0.119	3.677	0.017	3.660	0.073	3.638	0.048	3.641	0.102
Mn	0.595	0.001	0.743	0.434	0.473	0.238	0.362	0.072	0.318	0.062	0.322	0.105	0.378	0.118
Mg	0.995	0.030	0.928	0.709	0.780	0.132	0.781	0.076	0.803	0.068	0.741	0.095	0.713	0.076
Ca	0.300	0.032	0.239	1.536	1.345	0.095	1.357	0.048	1.360	0.02	1.412	0.003	1.306	0.122
O	24		24	24	24		24		24		24		24	
Fe/Fe+Mg	0.808		0.814	0.839	0.824		0.825		0.820		0.831		0.836	
ALMD	69		68	58	59		59		60		60		60	
GROSS	5		4	24	21		22		22		23		22	
PYROP	16		16	11	12		13		13		12		12	
SPESS	10		12	7	8		6		5		5		6	

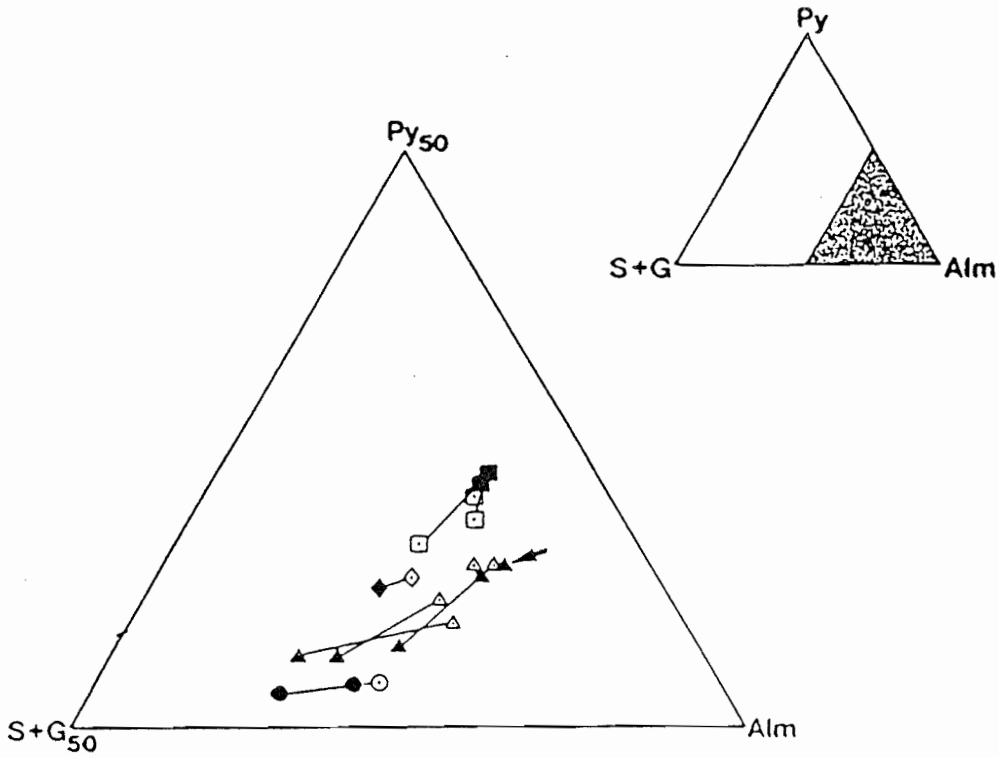

Figure 5.3. Garnet chemistry in the metasedimentary rocks as a function of pyrope (Py), spessartine and grossular (S + G), and almandine (Alm) end-members. Closed and open symbols are core and rim compositions respectively. ●○,▲△,■□ = low-, medium-, and high-grade rocks respectively. Arrowed analysis is the homogeneous garnet of 85-722. Note increase in spessartine component towards rims in the high-grade garnets. Rim compositions shown exclude those modified by retrograde cation exchange with biotite.

rims, indicating normal growth zonation (Figure 5.4) (Hollister, 1966; Tracy, 1982). In contrast, garnets in two staurolite-garnet schist samples (85-722 and 85-723b) near the structural top of the Corney Brook schist show no zonation (Figure 5.5). Matrix garnets in two high-grade biotite schists (85-441 and 85-446) have relatively homogeneous cores, but show an increase in Mn and decrease in Mg near their rims coincident with a change in inclusion pattern (Figure 5.6 a, b, c). The inclusion-rich core of a garnet included in kyanite appears to be relatively homogeneous (Figure 5.6a). The homogeneity of these garnets, in contrast to those in lower grade rocks, likely reflects zonation elimination by volume diffusion, which occurs in the temperature range of approximately 600° to 700°C (Woodsworth, 1977; Yardley, 1977). This interpretation is supported by temperatures of 700° $\pm$ 50°C calculated for a biotite-garnet pair enclosed in kyanite in the highest grade rocks (Chapter 6, Table 6.4, sample 85-441).

Although Mn-rich rims in high-grade garnets are commonly attributed to retrogression (Tracy, 1982), garnet included in kyanite also shows Mn-rich, Mg-poor rims indicating that this zonation was present prior to kyanite growth.

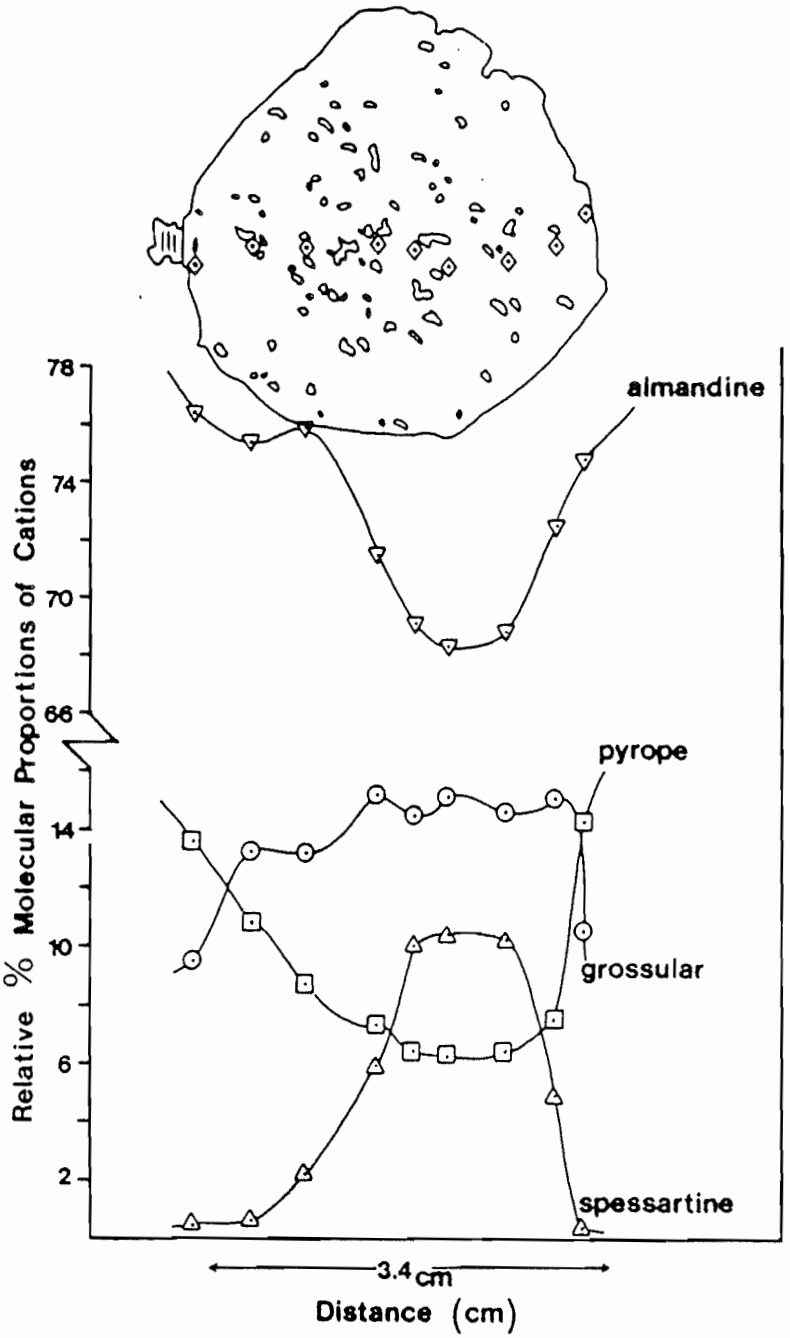

Figure 5.4. Bell-shaped growth zonation profile in medium-grade garnet from sample 85-659b. Diamonds indicate analysed points.

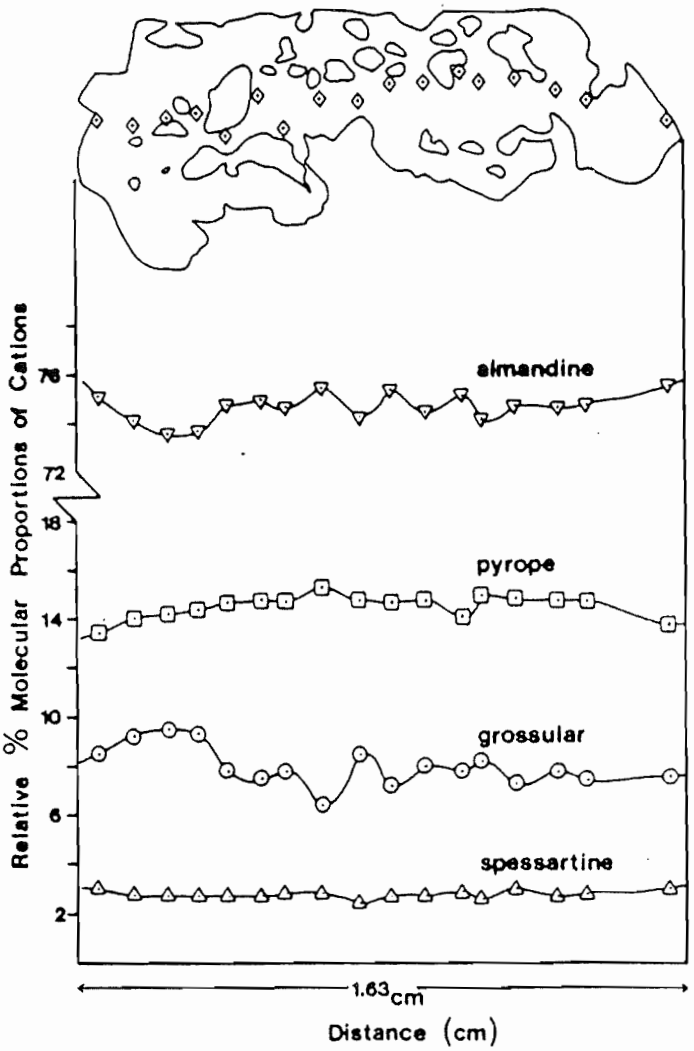

Figure 5.5. Garnet zonation profile for a high-grade garnet porphyroblast in sample 85-722. Homogeneous composition is attributed to zonation elimination by volume diffusion (see text). Diamonds indicate analysed points.

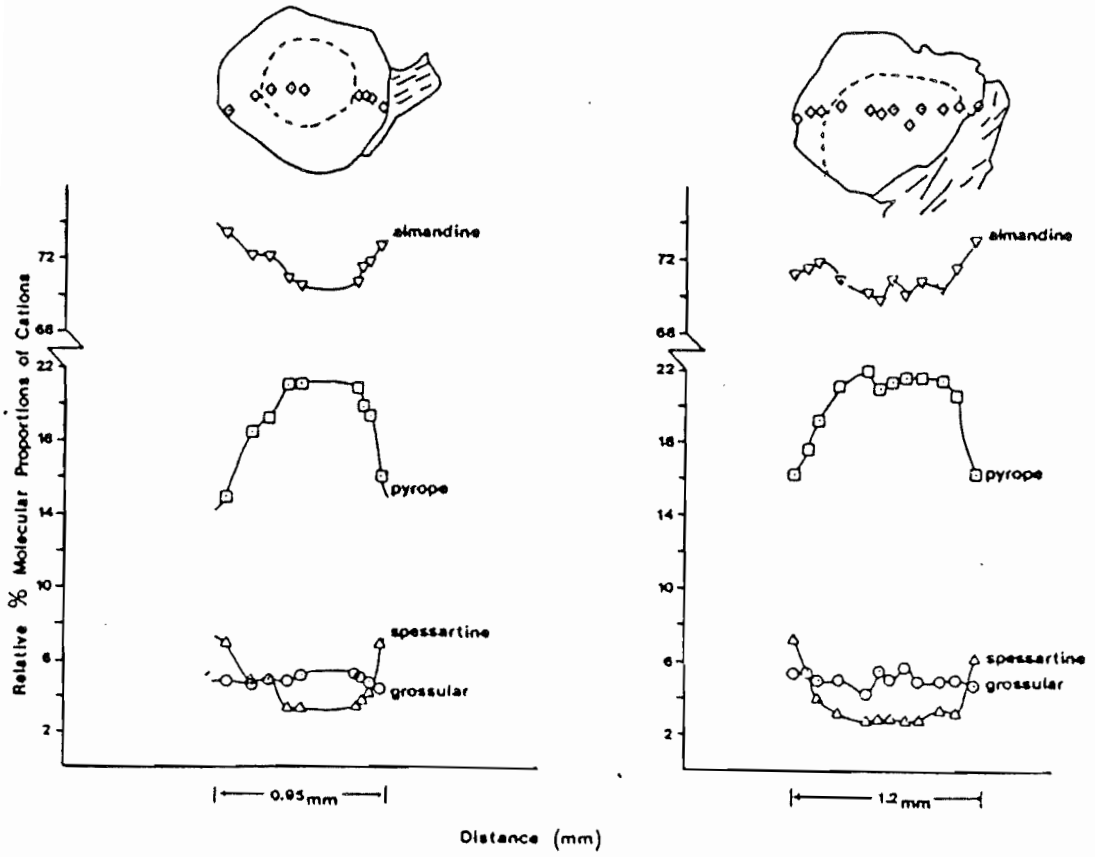

Figure 5.6. (a) Zonation profile for garnet in contact with biotite and enclosed in kyanite. Note increase in spessartine and decrease in pyrope at garnet rims and increase in almandine where in contact with biotite (Bi). (b) Zonation profile for matrix garnet in contact with biotite. Note homogeneous cores, high spessartine-low pyrope rims, and significant increase in almandine and spessartine and decrease in pyrope where in contact with biotite. Dashed lines in (a) and (b) denote core-rim transition defined by the relative abundance of inclusions. (c) Photomicrographs of garnets for which zonation profiles are shown in (a) and (b). Field of view in both photomicrographs is 6 mm.

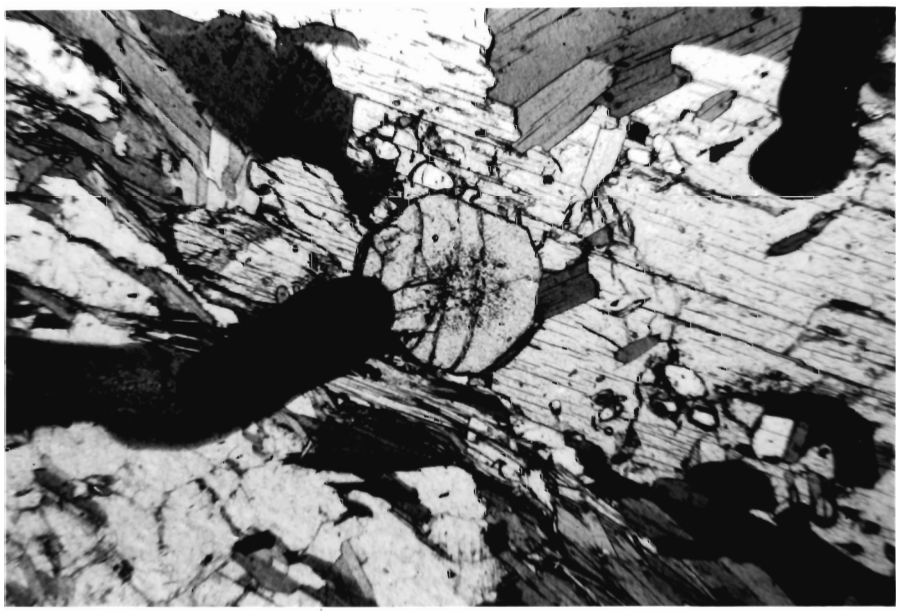

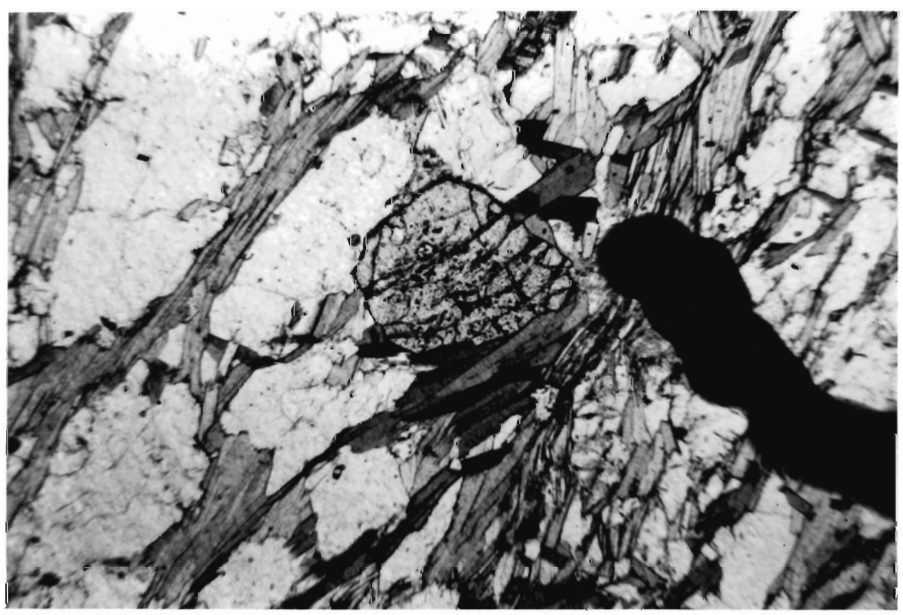

Figure 5.6c.

Inclusion-free rims could represent renewed growth on an earlier, metastable garnet (cf. Foster, 1986), or a decrease in garnet growth rate (Rast and Sturt, 1957), or a combination of the two, for example by a change in garnet-producing reaction that produces a change in growth rate. In the Jumping Brook metamorphic suite, inclusion-free garnet rims are nearly ubiquitous in the highest grade pelitic and semipelitic schists, and the rare inclusions in garnet rims are similar in grain size to the matrix. This suggests that garnet overgrew a recrystallized and coarsened matrix.

Theoretically, different episodes of garnet growth should be reflected in a zoning profile by a compositional "unconformity" unless this is eliminated by subsequent volume diffusion or retrogression. Tracy (1982) suggested that a decrease in $(X_{Mg})^{Gt}$ at rims may result from either garnet growth by a new reaction in which material supplied to garnet is depleted in Mg or from a minor amount of retrograde re-equilibration, although he favoured the first hypothesis. Foster (1986) attributed inclusion-free garnet rims in sillimanite-staurolite schists to renewed garnet growth due to staurolite breakdown, but did not discuss garnet zonation. The hypothesis of late-stage garnet growth due to a new reaction is favoured in the biotite schists of

the Fishing Cove River schist because (1) the high-grade garnets show no retrogression to micas and/or chlorite, (2) garnet included in kyanite exhibits a core/rim structure and coincident compositional change suggesting that these features developed prior to kyanite growth, and therefore prior to peak metamorphism (3) texturally, the inclusion-free rims appear to be a second-stage garnet growth, and (4) in some sections garnet has overgrown and included staurolite (Figure 4.22) suggesting its growth postdated staurolite and was therefore later in the microstructural development sequence than in the staurolite-garnet schists.

The Mg-decrease, Mn-increase, coincident with the core/rim boundary observed in the high-grade garnets supports this interpretation (Figure 5.6). However, a large garnet with a well developed core/rim texture (85-445; Figure 4.21) shows a moderate, normal growth zonation (Figure 5.7). Either garnet in this sample equilibrated with the matrix during growth or more probably, volume diffusion did not completely eliminate zonation in the core due to the large size of the garnet (cf. Yardley, 1977). Therefore, garnet chemistry, although somewhat equivocal, generally supports textural evidence for two stage garnet growth.

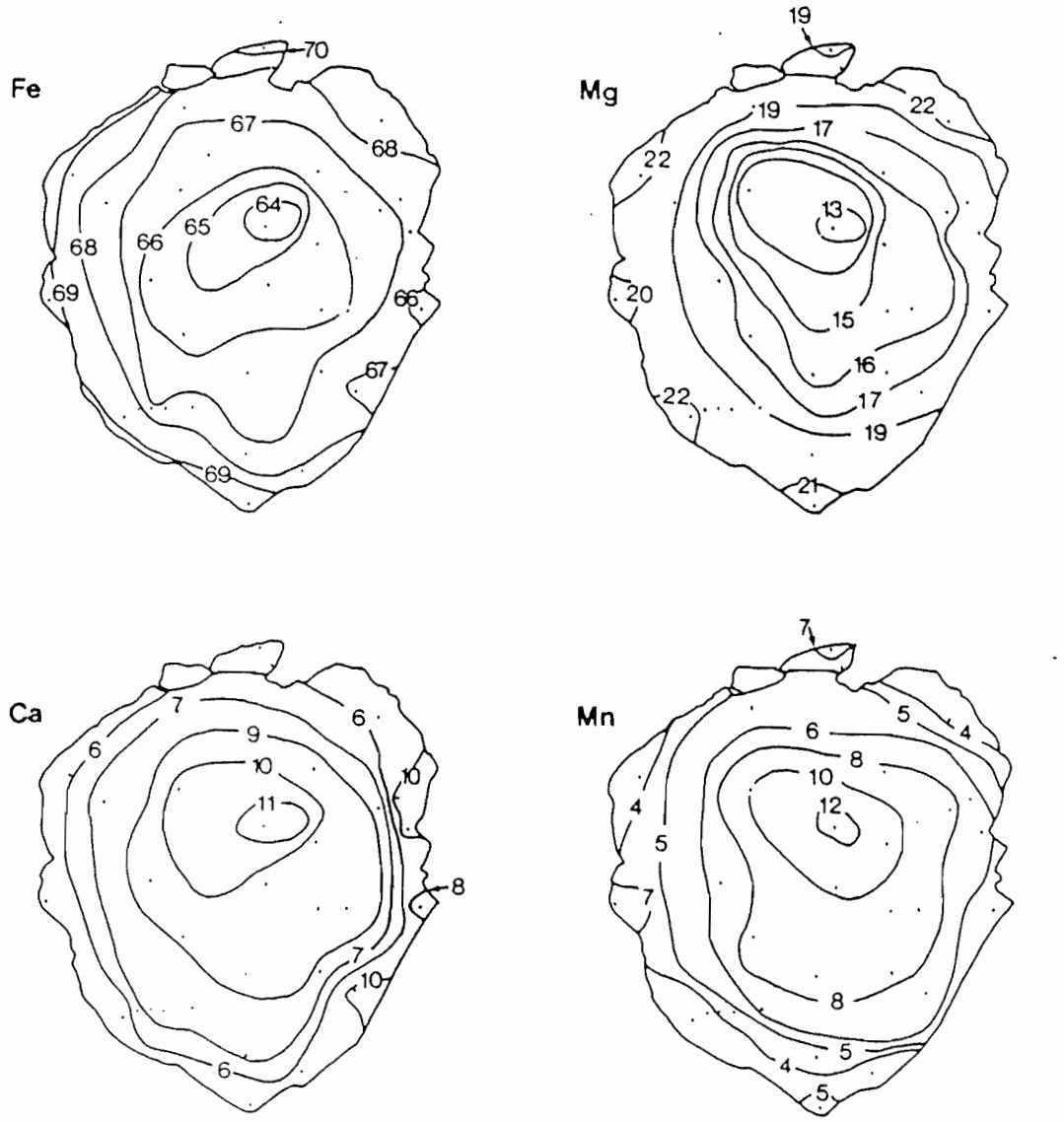

Figure 5.7. Compositional map of a high-grade garnet porphyroblast showing well developed core-rim texture. Map is contoured for relative percentage of molecular proportions of the cations: Fe, Mg, Ca, and Mn. Note moderate, normal growth zonation.

The reason for renewed garnet growth is found in examination of mineral assemblages. The apparent "reverse" zonation exists only in garnets in samples where staurolite is absent, present as relicts, or partially replaced by garnet. Garnet production from staurolite may occur by the reactions:

(1) St + Qtz = Al_2SiO_5 + Gt + H2O

(2) St + Mu + Qtz = Al_2SiO_5 + Gt + Bi + H2O

(Hoschek, 1969). Staurolite in the staurolite-garnet schists (see Table 5.8) contains trace amounts of Mn which, if released during staurolite breakdown, would probably be consumed by the growing garnet which has a strong affinity for Mn. In reaction 2, biotite forming with garnet would probably consume the Mg released by staurolite breakdown. Possible reactions are discussed in detail in Chapter 6.

Where in contact with biotite, garnets in samples 85-722, 85-723b, 85-441, 85-446 show a sharp increase in Fe and Mn and decrease in Mg (Figure 5.6a) in addition to the variations discussed above. Garnet in contact with biotite, both enclosed in kyanite (sample 85-441), shows no compositional variation adjacent to biotite (Figure 5.6b). This suggests that compositional changes in garnet next to biotite postdate kyanite growth and, therefore, result from retrograde cation exchange between biotite

and garnet (cf. Yardley, 1977; Dempster, 1985; Indares and Martignole, 1984). Evidence for retrograde cation exchange between garnet and biotite is found in all samples containing homogeneous garnets, indicating that temperatures were high enough for garnet and biotite to exchange Fe and Mg during cooling.

The effects of retrograde exchange with biotite differ from the effects of late stage growth of inclusion-free rims in several ways: (1) compositional changes are restricted to within a few microns of the garnet edge in contact with the biotite, whereas in the latter case they coincide with the core/rim boundary, (2) Fe increase due to retrograde exchange is more significant than that due to growth of the inclusion-free rims, and (3) retrograde exchange is also observed in staurolite-garnet schists containing homogeneous garnets that lack inclusion-free rims.

Preservation of these compositional differences indicates rapid cooling to, or crystallization below, the closure temperature for volume diffusion in garnet (Woodsworth, 1977; Yardley, 1977; Lasaga, 1983).

5.4.2 Amphibolite

Garnet formation in metabasites requires high pressures, low f_{O2}, and high (Fe/Mg)bulk rock

compositions (Miyashiro, 1975); the amphibolites in the map area meet these criteria. Garnet exists only in the high-grade (kyanite zone) amphibolites, where f_{O2} is presumably low and lithostatic pressure is high relative to the low- and medium-grade rocks, in samples with (Fe/Mg) almost twice that of garnet-free amphibolites (compare 85-245 and 85-345, Table 2.2).

$(X_{Fe})^{Gt}$ and $(X_{Ca})^{Gt}$ in the garnet amphibolites are high, reflecting the more calcic bulk composition of the amphibolites relative to an average pelite (Figure 5.8, Table 5.5). Modal percentages of the major phases in the garnet amphibolites (Table 5.6) indicate that sample 85-245 contains more apatite and significantly more amphibole than either sample 85-280 or 85-343A and is therefore the most calcic. High $(X_{Ca})^{Gt}$ and $(X_{Mn})^{Gt}$ in this sample therefore probably reflect bulk composition.

5.5 BIOTITE

Commonly reported compositional variations in biotite (Table 5.7) with increasing metamorphic grade include: increasing Ti^{4+} (eg. Yardley et al., 1980; Frank, 1983) and increasing Mg/(Mg+Fe) (eg. Atherton, 1968), and decreasing Al^{vi} (Guidotti, 1984). Guidotti (1984) noted that the most significant increase in Ti-

Table 5.7. Average compositions (Mean) and standard deviations (S.D.) for microprobe analyses of biotite. "Rim" and "X rim" analyses refer to those where biotite is in contact with, and isolated from garnet, respectively. Analyses for 85 - 441 are distinguished as in Table 5.5. Host phases for inclusions are given in brackets. H_2O calculated on the basis of listed OH values. All Fe as Fe^{2+}. n = number of analyses.

SAMPLE ANALYSIS	85 - 698c core & rim		85 - 659b core		85 - 659b rim - 1		85 - 659b rim - 2		85 - 659b X rim		85 - 700b core & rim		85 - 700b rim
	Mean	S.D.	Mean	S.D.	Mean	S.D.	Mean	S.D.	Mean	S.D.	Mean	S.D.	
SiO_2	37.05	0.41	36.17	0.52	36.17	0.20	36.34	0.38	36.62	0.50	36.86	0.62	37.11
TiO_2	1.43	0.17	1.19	0.05	1.45	0.01	1.51	0.05	1.44	0.19	1.65	0.07	1.72
Al_2O_3	17.73	0.40	19.79	0.07	19.65	0.25	19.63	0.26	19.63	0.13	19.58	0.19	19.98
FeO	17.23	0.48	17.81	0.42	17.85	0.37	17.55	0.07	17.98	0.49	16.90	0.27	16.17
MnO	0.12	0.08	0.08	0.00	0.05	0.00	0.08	0.00	0.03	0.02	0.06	0.05	0.13
MgO	11.97	0.23	10.67	0.04	11.31	0.01	11.06	0.07	10.97	0.27	11.60	0.18	11.49
CaO	0.06	0.03	0.04	0.00	0.00	0.00	0.00	0.00	0.03	0.01	0.03	0.00	0.00
Na_2O	0.31	0.13	0.37	0.04	0.24	0.00	0.18	0.11	0.31	0.06	0.24	0.04	0.26
K_2O	8.88	0.29	8.81	0.01	8.19	0.08	8.33	0.08	8.91	0.17	8.84	0.34	9.27
H_2O	3.98	0.03	3.98	0.02	4.01	0.01	3.99	0.04	4.02	0.05	4.04	0.05	4.06
Total	98.76		98.91		99.32		98.67		99.13		99.80		100.19
n	4		2		2		2		4		10		1
Si	5.596	0.029	5.451	0.047	5.461	0.01	5.463	0.008	5.460	0.027	5.472	0.036	5.477
Al^{iv}	2.414	0.050	2.549	0.008	2.539	0.03	2.537	0.015	2.540	0.056	2.528	0.025	2.523
Al^{vi}	0.737		0.967		0.092		0.942		0.912		0.900		0.953
Ti	0.162	0.018	0.135	0.005	0.162	0.00	0.170	0.004	0.161	0.019	0.184	0.006	0.191
Fe	2.173	0.078	2.245	0.066	2.229	0.05	2.207	0.029	2.242	0.051	2.099	0.044	1.996
Mn	0.015	0.010	0.010	0.000	0.006	0.00	0.010	0.000	0.004	0.003	0.008	0.006	0.016
Mg	2.689	0.059	2.306	0.006	2.516	0.00	2.478	0.007	2.438	0.041	2.567	0.047	2.527
Ca	0.010	0.005	0.006	0.000	0.000	0.00	0.000	0.000	0.005	0.002	0.005	0.000	0.000
Na	0.089	0.036	0.108	0.013	0.070	0.00	0.053	0.033	0.090	0.017	0.069	0.011	0.074
K	1.709	0.065	1.694	0.013	1.560	0.02	1.597	0.000	1.695	0.015	1.675	0.057	1.745
O	4		4		4		4		4		4		4
OH	24		24		24		24		24		24		24
Mg/Mg+Fe	0.553		0.516		0.530		0.529		0.521		0.550		0.559
Al^{iv}/Si	0.432		0.468		0.465		0.464		0.465		0.462		0.461
PHLOG	55		52		53		53		52		55		56
ANN	44		48		47		47		48		45		44
MN	1		0		0		0		0		0		0

Table 5.7. (Continued)

SAMPLE	85 - 707b		85 - 722		85-722	85-722	85-723b		85-723	85-732		85-441	85 - 441	
ANALYSIS	core & rim		Middle		rim	inclusion (gt)	core & X rim		rim	core & X rim		core	rim (ky)	
	Mean	S.D.	Mean	S.D.			Mean	S.D.		Mean	S.D.		Mean	S.D.
SiO_2	35.82	0.27	36.20	0.45	36.34	35.06	36.61	0.17	35.48	36.23	0.35	36.44	36.38	0.13
TiO_2	1.87	0.14	1.70	0.09	1.35	1.09	1.36	0.19	1.45	1.70	0.28	1.84	2.41	0.01
Al_2O_3	19.32	0.24	19.46	0.42	19.72	18.71	19.58	0.33	20.32	19.07	0.31	19.34	19.39	0.06
FeO	19.24	0.41	17.16	0.36	17.89	20.01	16.73	0.32	17.20	18.49	0.55	17.59	18.02	0.09
MnO	0.07	0.07	0.10	0.05	0.11	0.01	0.08	0.02	0.03	0.10	0.09	0.21	0.24	0.02
MgO	9.39	0.09	10.72	0.18	11.23	10.51	10.97	0.15	11.18	10.48	0.22	10.82	10.27	0.02
CaO	0.04	0.02	0.04	0.02	0.00	0.03	0.03	0.02	0.00	0.06	0.02	0.00	0.00	0.00
Na_2O	0.26	0.04	0.37	0.07	0.03	0.14	0.37	0.02	0.12	0.30	0.08	0.18	0.21	0.11
K_2O	9.43	0.26	9.16	0.63	8.56	8.68	9.09	0.23	7.54	9.03	0.17	8.78	9.27	0.08
H_2O	3.95	0.03	3.98	0.04	4.00	3.89	3.99	0.01	3.95	3.97	0.03	3.99	4.02	0.01
Total	99.42		98.84		99.23	98.13	98.81		99.27	99.43		99.19	100.21	
n	6		8		1	1	6		1	12		1	2	
Si	5.432	0.016	5.455	0.031	5.444	5.395	5.499	0.025	5.380	5.461	0.027	5.467	5.432	0.008
Al^{iv}	2.568	0.028	2.545	0.042	2.556	2.605	2.501	0.050	2.620	2.539	0.045	2.533	2.568	0.003
Al^{vi}	0.887		0.913		0.927	0.790	0.966		1.013	0.850		0.888	0.845	
Ti	0.214	0.016	0.192	0.009	0.152	0.126	0.154	0.021	0.165	0.193	0.031	0.208	0.271	0.002
Fe	2.440	0.053	2.163	0.045	2.241	2.575	2.102	0.043	2.181	2.330	0.069	2.207	2.250	0.016
Mn	0.009	0.009	0.013	0.006	0.014	0.001	0.010	0.003	0.004	0.012	0.011	0.027	0.030	0.003
Mg	2.122	0.020	2.408	0.036	2.507	2.410	2.455	0.038	2.527	2.354	0.045	2.419	2.285	0.009
Ca	0.006	0.004	0.007	0.004	0.000	0.005	0.005	0.003	0.000	0.010	0.003	0.000	0.000	0.000
Na	0.075	0.010	0.109	0.020	0.009	0.042	0.106	0.005	0.035	0.088	0.023	0.052	0.059	0.030
K	1.824	0.042	1.763	0.136	1.636	1.704	1.743	0.040	1.459	1.736	0.034	1.681	1.765	0.018
O	4		4		24		24		24	24		24	24	
OH	24		24		4		4		4	4		4	4	
Mg/Mg+Fe	0.465				0.515	0.484	0.539		0.547	0.503		0.523	0.503	
Al^{iv}/Si	0.473				0.471	0.483	0.455		0.465	0.465		0.463	0.472	
PHLOG	46		52		51	48	54		55	50		52	50	
ANN	53		47		48	52	46		45	50		47	49	
MN	1		1		1	0	0		0	0		1	1	

Table 5.7. (Continued)

SAMPLE	85 - 441		85 - 441		85 - 446		85 - 446		85 - 535		85 - 535		85 - 535	
ANALYSIS	rim (matrix)		inclusion(ky)		core + X rim		rim		X rim & core		rim		inclusion (gt)	
	Mean	S.D.	Mean	S.D.	Mean	S.D.	Mean	S.D.	Mean	S.D.	Mean	S.D.	Mean	S.D.
SiO_2	36.62	0.12	37.05	0.17	35.77	0.12	35.93	0.28	36.31	0.24	35.57	0.21	36.36	0.30
TiO_2	2.01	0.03	2.45	0.06	2.12	0.02	2.11	0.21	2.22	0.29	1.96	0.09	1.71	0.62
Al_2O_3	19.60	0.18	19.25	0.20	18.74	0.09	18.95	0.18	19.11	0.37	19.59	0.35	19.54	0.27
FeO	17.36	0.12	17.59	0.13	16.95	0.07	16.98	0.21	16.78	0.43	16.76	0.35	16.88	0.39
MnO	0.20	0.08	0.22	0.02	0.19	0.07	0.29	0.05	0.12	0.03	0.16	0.02	0.16	0.09
MgO	10.62	0.27	10.37	0.11	11.00	0.24	10.97	0.15	10.84	0.19	11.16	0.11	11.17	0.34
CaO	0.00	0.00	0.00	0.00	0.00	0.00	0.01	0.00	0.03	0.02	0.04	0.02	0.04	0.03
Na_2O	0.24	0.09	0.28	0.02	0.23	0.01	0.08	0.06	0.30	0.11	0.35	0.02	0.36	0.08
K_2O	9.22	0.38	8.98	0.22	9.69	0.19	9.68	0.10	9.66	0.34	9.23	0.13	9.17	0.22
H_2O	4.02	0.02	4.04	0.02	3.95	0.02	3.97	0.02	3.99	0.03	4.03	0.02	4.00	0.03
Total	99.89		100.53		98.64		98.97		99.36		98.85		99.39	
n	3		4		3		3		5		4		5	
Si	5.460	0.016	5.501	0.020	5.427	0.026	5.428	0.022	5.452	0.016	5.445	0.018	5.442	0.027
Al^{iv}	2.540	0.029	2.499	0.023	2.573	0.005	0.572	0.022	2.548	0.049	2.555	0.051	2.558	0.041
Al^{vi}	0.905		0.087		0.779		2.804		0.835		0.883		0.890	
Ti	0.226	0.004	0.273	0.007	0.242	0.003	0.240	0.024	0.251	0.033	0.220	0.011	0.193	0.070
Fe	2.165	0.024	2.184	0.013	2.151	0.004	2.146	0.018	2.107	0.054	2.087	0.051	2.113	0.037
Mn	0.025	0.009	0.028	0.003	0.024	0.009	0.038	0.006	0.015	0.003	0.021	0.003	0.020	0.012
Mg	2.360	0.053	2.295	0.029	2.488	0.047	2.471	0.032	2.246	0.040	2.476	0.018	2.492	0.074
Ca	0.000	0.000	0.000	0.000	0.000	0.000	0.002	0.000	0.004	0.002	0.006	0.003	0.007	0.005
Na	0.070	0.025	0.081	0.006	0.067	0.003	0.023	0.016	0.086	0.031	0.100	0.005	0.104	0.022
K	1.753	0.064	1.701	0.037	1.876	0.034	1.866	0.029	1.851	0.074	1.753	0.023	1.751	0.050
O	24		24		24		24		24		24		24	
OH	4		4		4		4		4		4		4	
Mg/Mg+Fe	0.522		0.512		0.536		0.536		0.535		0.470		0.541	
Al^{iv}/Si	0.465		0.454		0.475		0.474		0.467		0.469		0.470	
PHLOG	52		51		53		53		53		54		54	
ANN	48		48		46		46		46		45		46	
MN	0		1		1		1		1		1		0	

Table 5.7. (Continued)

SAMPLE	85 - 565		85 - 565	
ANALYSIS	X rim & core		rim	
	Mean	S.D.	Mean	S.D.
SiO_2	36.95	0.27	37.00	0.28
TiO_2	1.86	0.21	1.74	0.12
Al_2O_3	16.62	0.34	16.76	0.32
FeO	18.72	0.26	19.00	0.24
MnO	0.42	0.15	0.39	0.00
MgO	10.29	0.18	10.43	0.04
CaO	0.04	0.02	0.06	0.01
Na_2O	0.05	0.04	0.06	0.06
K_2O	10.05	0.25	10.17	0.17
H_2O	3.92	0.02	3.94	0.04
Total	98.92		99.55	
n	9		2	
Si	5.649	0.035	5.629	0.011
Al^{iv}	2.351	0.048	2.371	0.028
Al^{vi}	0.644		0.634	
Ti	0.214	0.025	0.199	0.012
Fe	2.393	0.035	2.418	0.008
Mn	0.054	0.020	0.051	0.001
Mg	2.344	0.040	2.364	0.031
Ca	0.007	0.003	0.010	0.002
Na	0.015	0.011	0.016	0.018
K	1.959	0.046	1.974	0.052
O	24		24	
OH	4		4	
Mg/Mg+Fe	0.495		0.494	
Al^{iv}/Si	0.416		0.421	
PHLOG	49		49	
ANN	50		50	
MN	1		1	

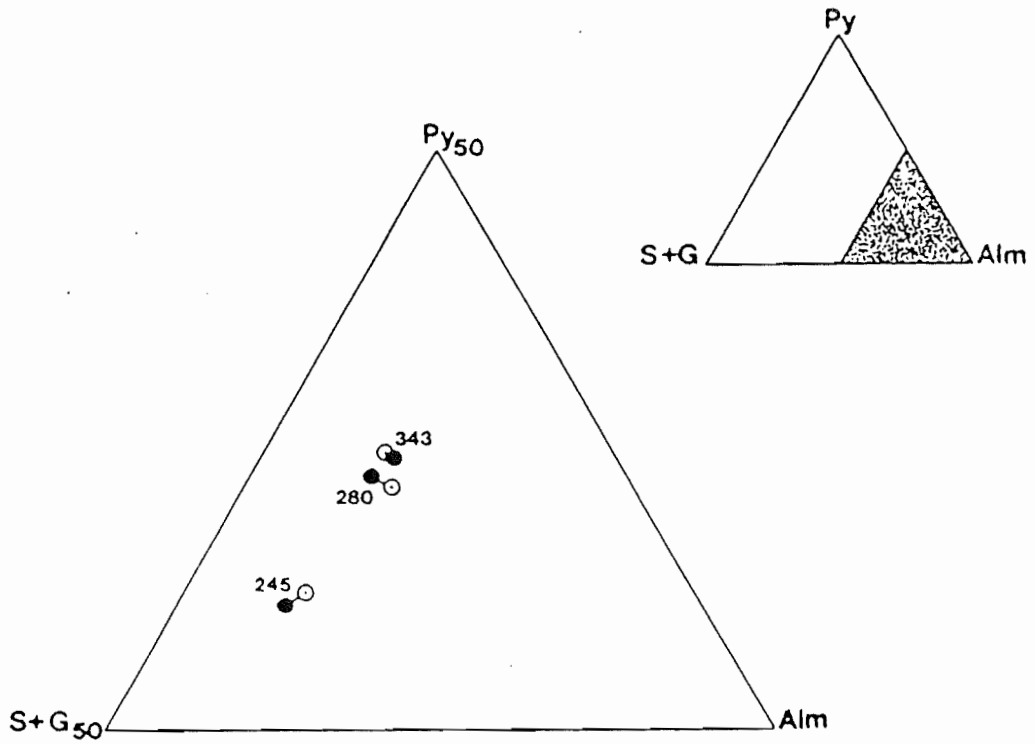

Figure 5.8. Garnet compositions in the garnet amphibolites as a function of pyrope (Py), spessartine and grossular (S + G), and almandine end-members. Closed and open symbols represent core and rim compositions, respectively. Weak normal zonation is shown by garnet in samples 85-280 and 85-245.

TABLE 5.6. Modal analyses (volume %) of three garnet amphibolite samples based on 1000 points counted in thin section.

MINERAL PHASE	85-245	85-280	85-343a
Hornblende	60.7	49.0	35.6
Plagioclase	32.2	40.0	56.8
Garnet	1.2	3.7	2.7
Epidote	2.3	3.3	1.9
Apatite	1.2	0.3	0.8
Quartz	1.8	1.7	1.0
Opaque Minerals	0.6	2.0	1.2
TOTAL	100.0	100.0	100.0

content in biotite coincides with muscovite breakdown in the upper sillimanite zone. Consequently, in the amphibolite grade rocks of the map area, significant variation in Ti-content is unlikely. The presence of ilmenite or sphene in all samples in which biotite was analysed, indicates TiO_2-saturation and any increase in Ti in biotite is therefore a function of metamorphic grade (cf. Frank, 1983; Guidotti, 1984). A general increase in Ti is observed with increasing metamorphic grade although the variation is not large.

The Mg/(Mg+Fe) in biotite varies randomly relative to metamorphic grade (Figure 5.9). This random variation probably reflects slight differences in bulk composition and different degrees of retrograde Fe-Mg exchange and re-equilibration with garnet. The Al^{vi} shows a slight decrease increases from the garnet, to the staurolite-kyanite, to kyanite zones.

In samples showing retrograde diffusion effects in garnet, $(X_{Mg})^{Bi}$ is consistent for grains both in contact with and isolated from garnet (Table 5.7). This suggests that biotite completely homogenized during retrogression (cf. Stephenson, 1979), which is consistent with the higher diffusivities of Mg in biotite relative to garnet (Freer, 1981) and microstructures which suggest recrystallization of micas. However, $(X_{Mg})^{Bi}$ of the

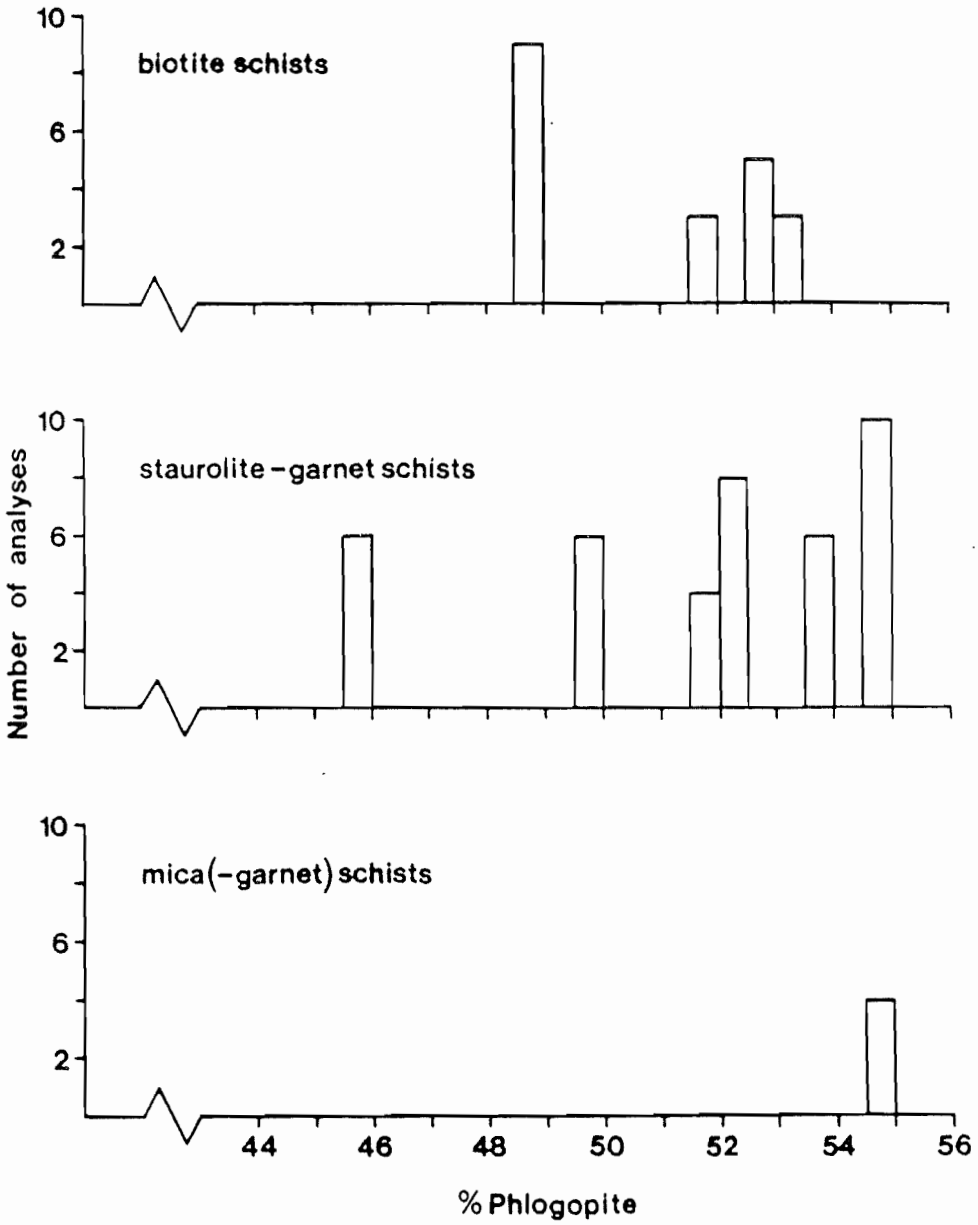

Figure 5.9. Histogram of biotite compositions as a function of the phlogopite end-member, relative to metamorphic grade, indicating no regular variation in (Mg/Mg+Fe) with metamorphic grade.

biotite-garnet pair enclosed in kyanite ($(X_{Mg})^{Bi}$= 0.503) is marginally less than for co-existing matrix biotite ($(X_{Mg})^{Bi}$=0.523) suggesting that $(X_{Mg})^{Bi}$ increased during retrogression. This is consistent with the observed retrograde Mg decrease and Fe increase in garnet and experimental data on Fe-Mg exchange between biotite and garnet (eg. Ferry and Spear, 1978).

5.6 STAUROLITE

Staurolite is homogeneous, iron-rich ($\sum$Fe = 78.4 to 83.8, Table 5.8), and contains trace amounts of Zn. Average staurolite compositions closely approximate the composition of common ferroan staurolite (Deer et al., 1978).

A sample of semipelitic garnet-biotite schist (85-659B) interlayered with staurolite-garnet schists contains relict staurolite pseudomorphed by chlorite and an iron + ?titanium oxide (Figure 5.10). Staurolite relicts contain 8 to 16 times more Zn than fresh ferroan staurolite in similar rocks. This compositional variation, therefore, appears to be related to retrogression; Zn released by staurolite breakdown cannot be incorporated by chlorite and is concentrated in the residual staurolite.

Table 5.8. Average compositions (MEAN) and standard deviations (S.D.) for microprobe analyses of staurolite. H_2O calculated on the basis of listed OH values. All Fe as Fe^{2+}. n = number of analyses. $\sum Fe = [(Fe^{TOT} + Mn)/(Mg + Mn)] \times 100$.

SAMPLE	85 - 700b		85 - 722		85 - 723b		85 - 732		85 - 659b
ANALYSIS	core & rim		core & rim		core & rim		core & rim		relict
	Mean	S.D.	Mean	S.D.	Mean	S.D.	Mean	S.D.	
SiO_2	27.46	0.20	27.44	0.44	27.36	0.16	27.01	0.20	27.35
TiO_2	0.69	0.04	0.70	0.05	0.70	0.05	0.69	0.04	0.53
Al_2O_3	54.24	0.31	53.63	0.31	53.88	0.32	53.45	0.56	53.38
FeO	13.34	0.38	12.97	0.49	13.22	0.26	13.64	0.15	12.15
MnO	0.13	0.02	0.10	0.04	0.11	0.04	0.08	0.03	0.00
MgO	1.70	0.19	1.52	0.17	1.94	0.09	1.78	0.05	1.64
CaO	0.03	0.02	0.03	0.03	0.04	0.03	0.03	0.01	0.00
ZnO	0.22	0.04	0.23	0.14	0.14	0.12	0.12	0.08	1.99
H_2O	1.06	0.01	1.05	0.01	1.05	0.01	1.04	0.01	1.05
Total	98.87		97.67		98.44		97.84		100.08
n	6		9		25		9		1
Si	7.786	0.050	7.857	0.116	7.784	0.043	7.751	0.081	7.840
Al^{iv}	0.214	0.103	0.143	0.092	0.216	0.052	0.249	0.107	0.160
Al^{vi}	17.917		17.958		17.857		17.832		17.879
Ti	0.146	0.009	0.150	0.011	0.150	0.000	0.149	0.008	0.114
Fe	3.137	0.162	3.106	0.121	3.147	0.056	3.273	0.034	2.913
Mn	0.020	0.000	0.023	0.009	0.027	0.010	0.019	0.007	0.000
Mg	0.807	0.010	0.648	0.072	0.823	0.039	0.761	0.022	0.701
Ca	0.010	0.006	0.010	0.008	0.012	0.008	0.010	0.003	0.000
Zn	0.000	0.000	0.049	0.029	0.030	0.024	0.025	0.017	0.421
O	48		48		48		48		48
OH	2		2		2		2		2
$\sum Fe$	79.6		83.0		81.2		81.2		80.6

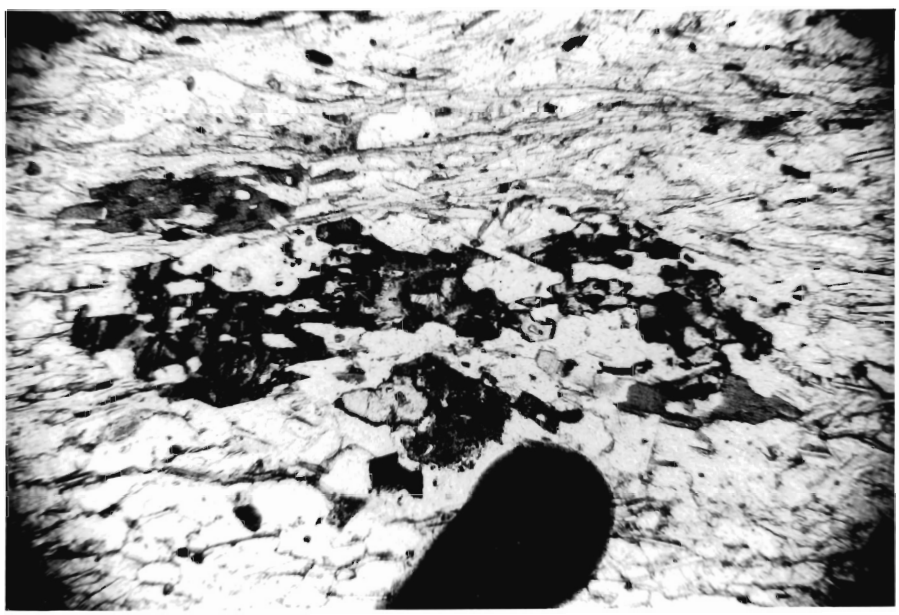

Figure 5.10. Photomicrograph of Zn-rich staurolite relict in a sample of semipelitic garnet-biotite schist. Field of view is 2.25 mm.

5.7 PLAGIOCLASE

Anorthite (An) content in plagioclase commonly increases with metamorphic grade by the substitution Si, Na = Al, Ca (Miyashiro, 1975). Oligoclase is typical of epidote-amphibolite facies and oligoclase-andesine is typical of the amphibolite facies. Although there is no regionally consistent pattern of increasing An content, plagioclase rims are generally more calcic than cores consistent with increasing An content with increasing metamorphic grade in a given sample.

5.7.1 Metasedimentary Phyllites and Schists

Plagioclase in all pelitic and semipelitic schists (Figure 5.11) is homogeneous or weakly zoned oligoclase (An_{22}-An_{23}; Table 5.9). Rarely, zoning is visible in the oligoclase porphyroblasts of the staurolite-garnet schists. Two samples (85-659, 85-535) show a weak increase in Na towards the rims suggesting plagioclase growth with decreasing temperature. However, microstructures suggest that plagioclase growth in 85-659b was prograde and therefore this compositional zoning may reflect complex continuous reactions. Zoning in

Table 5.9. Average compositions (Mean) and standard deviations (S.D.) for microprobe analyses of plagioclase. All Fe as Fe^{2+}. n = number of analyses.

SAMPLE	85-659b	85-659b	85-700b		85-700b	85-700b	85-708b	
ANALYSIS	core	rim	core		rim	inclusion (gt)	rim	
			Mean	S.D.			Mean	S.D.
SiO_2	62.38	62.02	60.53	0.41	61.26	61.59	60.98	0.39
Al_2O_3	23.46	24.38	24.97	0.65	24.75	24.39	25.19	0.28
FeO	0.08	0.09	0.10	0.05	0.13	0.43	0.20	0.04
MgO	0.01	0.00	0.03	0.00	0.02	0.03	0.01	0.00
CaO	4.91	5.26	6.23	0.59	5.97	5.85	6.29	0.11
Na_2O	8.83	8.47	7.91	0.41	7.89	7.94	7.28	0.35
K_2O	0.06	0.06	0.03	0.02	0.01	0.07	0.06	0.05
Total	99.71	100.28	99.80		100.03	100.30	100.01	
n	1	1	3		1	1	2	
Si	11.079	10.958	10.780	0.104	10.862	10.90	10.811	0.038
Al	4.912	5.078	5.242	0.122	5.174	5.09	5.264	0.073
Fe	0.012	0.013	0.015	0.007	0.019	0.06	0.029	0.006
Mg	0.003	0.000	0.008	0.000	0.005	0.00	0.003	0.000
Ca	0.934	0.996	1.188	0.109	1.134	1.11	1.194	0.024
Na	3.041	2.902	2.733	0.151	2.712	2.72	2.503	0.114
K	0.009	0.014	0.007	0.005	0.002	0.01	0.013	0.011
O	32	32	32		32	32	32	
An	24	25	30		30	29	32	
Ab	76	74	70		70	71	67	
Or	0	1	0		0	0	1	

Table 5.9. (Continued)

SAMPLE ANALYSIS	85 - 722 core		85-722 middle	85-722 rim		85-723b core		85-723b rim		85 - 732 core		85 - 732 rim	
	Mean	S.D.		Mean	S.D.	Mean	S.D.	Mean	S.D.	Mean	S.D.	Mean	S.D.
SiO_2	62.54	0.48	62.47	61.95	0.45	62.03	0.45	60.70	0.77	61.15	2.42	62.16	0.16
Al_2O_3	23.92	0.45	23.15	23.76	0.32	24.12	0.01	24.73	0.43	23.25	0.54	23.85	0.14
FeO	0.08	0.04	0.13	0.10	0.04	0.07	0.00	0.08	0.03	0.04	0.03	0.13	0.08
MgO	0.00	0.00	0.00	0.02	0.00	0.03	0.00	0.01	0.00	0.03	0.02	0.02	0.01
CaO	5.15	0.25	4.63	5.19	0.13	5.41	0.18	6.26	0.50	4.89	0.15	5.19	0.06
Na_2O	8.40	0.56	8.52	8.22	0.17	8.26	0.23	8.13	0.27	8.40	0.24	8.20	0.17
K_2O	0.06	0.04	0.08	0.07	0.02	0.12	0.00	0.09	0.02	0.04	0.02	0.05	0.02
Total	100.15		98.98			100.04		100		97.80		99.60	
n	3		1	4		2		5		4		3	
Si	11.048	0.027	11.152	11.038	0.062	10.989	0.026	10.802	0.105	11.061	0.083	11.041	0.017
Al	4.981	0.057	4.872	4.990	0.065	5.037	0.023	5.188	0.100	4.959	0.049	4.993	0.021
Fe	0.012	0.006	0.019	0.015	0.005	0.010	0.000	0.011	0.005	0.006	0.005	0.020	0.012
Mg	0.000	0.000	0.000	0.005	0.000	0.008	0.000	0.003	0.000	0.008	0.004	0.006	0.004
Ca	0.974	0.041	0.886	0.991	0.026	1.026	0.028	1.193	0.100	0.949	0.035	0.988	0.012
Na	2.877	0.214	2.949	2.841	0.063	2.838	0.091	2.807	0.090	2.949	0.153	2.824	0.048
K	0.014	0.008	0.018	0.016	0.006	0.027	0.000	0.021	0.005	0.008	0.004	0.012	0.005
O	32		32	32		32		32		32		32	
An	25		23	26		73		70		24		26	
Ab	75		75	74		26		30		75		74	
Or	0		1	0		1		0		1		0	

Table 5.9. (Continued)

SAMPLE ANALYSIS	85-441 core		85-441 rim		85 - 441 middle	85 - 446 core		85 - 446 rim		85 - 446 inclusion (gt)	85 - 535 core		85 - 535 middle
	Mean	S.D.	Mean	S.D.		Mean	S.D.	Mean	S.D.		Mean	S.D.	
SiO_2	62.81	0.35	62.63	0.43	62.45	63.16	0.67	63.16	0.01	69.18	62.17	0.16	62.39
Al_2O_3	23.51	0.21	23.75	0.49	23.54	23.34	0.10	23.32	0.13	19.80	23.69	0.21	23.50
FeO	0.09	0.00	0.14	0.05	0.02	0.09	0.06	0.06	0.01	0.34	0.06	0.00	0.11
MgO	0.00	0.00	0.03	0.01	0.00	0.02	0.01	0.02	0.01	0.00	0.01	0.00	0.00
CaO	4.57	0.09	4.87	0.19	4.67	4.44	0.29	4.49	0.58	0.02	4.93	0.03	4.72
Na_2O	8.45	0.09	8.66	0.18	8.83	8.62	0.10	8.52	0.19	10.92	8.74	0.16	8.81
K_2O	0.15	0.03	0.07	0.02	0.12	0.13	0.04	0.10	0.07	0.06	0.18	0.05	0.16
Total	99.58		100.15		99.63	99.80		99.67		100.32	99.78		99.69
n	2		5		1	3		2		1	2		1
Si	11.141	0.044	11.069	0.070	11.091	11.174	0.063	11.181	0.012	12.011	11.044	0.024	11.084
Al	4.916	0.051	4.949	0.084	4.929	4.868	0.045	4.870	0.033	4.053	4.962	0.047	4.922
Fe	0.013	0.000	0.020	0.008	0.003	0.014	0.009	0.009	0.002	0.049	0.009	0.000	0.016
Mg	0.000	0.000	0.007	0.003	0.000	0.004	0.001	0.006	0.004	0.000	0.003	0.000	0.000
Ca	0.867	0.019	0.923	0.036	0.889	0.842	0.060	0.852	0.109	0.004	0.938	0.005	0.898
Na	2.905	0.027	2.967	0.057	3.041	2.956	0.021	2.923	0.069	3.676	3.011	0.052	3.035
K	0.034	0.006	0.016	0.006	0.027	0.030	0.009	0.022	0.016	0.013	0.040	0.011	0.036
O	32		32		32	32		32		32	32		32
An	23		23		22	22		22		0	24		23
Ab	76		76		77	77		77		100	75		76
Or	0		1		1	1		1		0	1		1

Table 5.9. (Continued)

SAMPLE. ANALYSIS	85 - 535 rim		85-565 core	85-565 rim		85-245 core		85-245 middle		82-245 rim	85-280 rim	
	Mean	S.D.		Mean	S.D.	Mean	S.D.	Mean	S.D.		Mean	S.D.
SiO_2	62.42	0.39	60.40	59.84	0.73	57.51	0.74	57.65	1.19	59.64	58.60	0.08
Al_2O_3	23.71	0.25	24.03	24.90	0.55	27.09	0.53	27.08	0.57	25.84	26.11	0.05
FeO	0.12	0.07	0.10	0.11	0.05	0.12	0.02	0.13	0.00	0.25	0.09	0.06
MgO	0.02	0.00	0.05	0.03	0.01	0.02	0.01	0.02	0.00	0.00	0.04	0.00
CaO	4.61	0.21	6.56	6.98	0.56	9.32	0.77	9.17	0.67	7.61	7.80	0.26
Na_2O	9.04	0.08	7.45	7.20	0.27	6.31	0.58	6.07	0.54	7.08	7.10	0.24
K_2O	0.11	0.04	0.44	0.32	0.07	0.10	0.01	0.09	0.01	0.12	0.15	0.02
Total	100.03		99.03	99.38		100.47		100.21		100.54	99.89	
n	4		4	6		3		2		1	3	
Si	11.057	0.060	10.859	10.729	0.116	10.269	0.115	10.302	0.144	10.586	10.487	0.017
Al	4.951	0.055	5.093	5.263	0.113	5.702	0.119	5.706	0.158	5.407	5.510	0.002
Fe	0.018	0.010	0.015	0.017	0.007	0.018	0.003	0.020	0.001	0.037	0.013	0.009
Mg	0.005	0.000	0.013	0.007	0.002	0.005	0.003	0.005	0.000	0.000	0.011	0.000
Ca	0.875	0.040	1.264	1.340	0.108	1.783	0.150	1.755	0.141	1.447	1.496	0.046
Na	3.104	0.025	2.597	2.504	0.093	2.184	0.199	2.103	0.172	2.437	2.465	0.087
K	0.025	0.008	0.101	0.072	0.017	0.024	0.001	0.019	0.001	0.027	0.034	0.005
O	32		32	32		32		32		32	32	
An	22		32	34		44		45		37	37	
Ab	77		66	64		55		54		62	62	
Or	1		2	2		1		1		1	1	

Table 5.9. (Continued)

SAMPLE ANALYSIS	85-280 rim		85-343a core		85-343a rim	
	Mean	S.D.	Mean	S.D.	Mean	S.D.
SiO_2	57.22	0.59	56.80	0.07	53.36	2.53
Al_2O_3	27.08	0.34	27.69	0.12	27.96	1.38
FeO	0.11	0.03	0.13	0.06	0.17	0.05
MgO	0.02	0.01	0.01	0.00	0.04	0.01
CaO	9.02	0.35	9.59	0.25	9.80	1.91
Na_2O	6.68	0.31	6.36	0.12	6.23	1.24
K_2O	0.10	0.01	0.13	0.04	0.06	0.07
Total	100.23		100.71		97.62	
n	4		2		2	
Si	10.250	0.070	10.144	0.013	10.079	0.357
Al	5.719	0.076	5.829	0.011	5.896	0.346
Fe	0.016	0.005	0.019	0.009	0.025	0.008
Mg	0.006	0.003	0.003	0.000	0.010	0.002
Ca	1.731	0.070	1.834	0.042	1.880	0.383
Na	2.319	0.107	2.201	0.047	2.157	0.409
K	0.022	0.003	0.029	0.008	0.014	0.016
O	32		32		32	
An	42		45		46	
Ab	57		57		53	
Or	1		1		1	

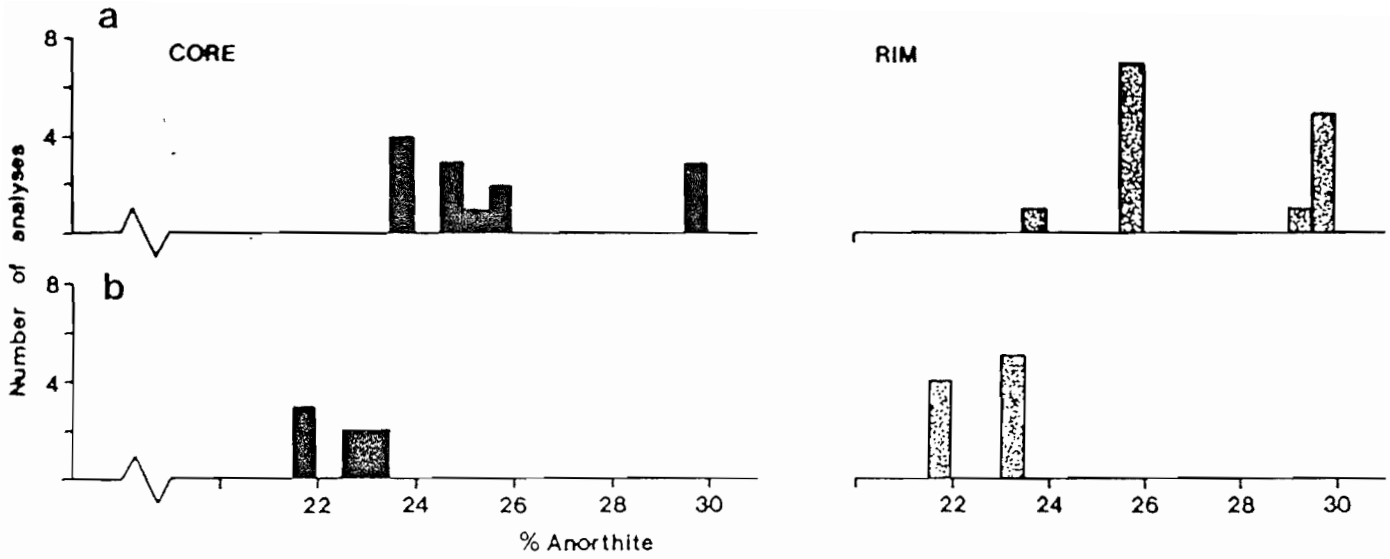

Figure 5.11. Histogram of plagioclase compositions in metasedimentary schists for (a) staurolite-kyanite zone (medium grade) and (b) kyanite zone (high-grade).

sample 85-535 may reflect relict calcic plagioclase cores or the absence of other Ca-bearing phases to consume Ca.

5.7.2 Amphibolite and Hornblende-Biotite Schist

Plagioclase in the amphibolites is andesine (An_{37-45}, core and An_{37-47}, rim; Table 5.9), indicating that these are amphibolite grade rocks. Zoning is visible in samples 85-245 and 85-280. Samples 85-708 and 85-565 are zoned with oligoclase cores (An_{22}) and andesine rims (An_{32-34}).

5.8 AMPHIBOLE

Amphibole chemistry is a complex function of pressure, temperature, f_{O2}, and bulk rock chemistry unless it is part of the buffered "common assemblage" which consists of: amphibole-chlorite-epidote-plagioclase -quartz $\pm$ Ti-phase oxide $\pm$ Fe^{3+} $\pm$ carbonate $\pm$ K-mica (Laird and Albee, 1981). The amphibolites analysed do not always contain this buffered assemblage and therefore separating the effects of the above variables is difficult. Bulk chemistry is available for samples 85-245, 85-706b, and 85-345 (Table 2.2) but f_{O2} is unknown.

An increase in Ti, Al, and (Na+K) contents and decrease in Si in amphiboles have been attributed to

increasing metamorphic grade (Leake, 1965; Brady, 1974; Hynes, 1982) and to an associated decrease in f_{O2} (Spear, 1976). The relationship of amphibole chemistry to metamorphic pressure is controversial. Some authors hold that low Al^{vi} (Leake, 1965, Raase, 1974, Laird and Albee, 1981) and high Na^{A_site} (Graham, 1974; Holland and Richardson, 1979; Laird and Albee, 1981) which are predominantly temperature-related effects are diagnostic of low pressure amphiboles, while others find no such relationship (eg. Hynes, 1982).

Amphiboles were analysed in three garnet amphibolites and one late, synmetamorphic, epidote-rich vein exposed in the George Brook amphibolite. All analysed amphiboles are hornblende, showing combined Tschermakite and pargasite substitution, with the exception of those in the vein sample (85-643c) which are mainly tremolite (average $(X_{Mg})^{Am}$=0.7), locally as patchy intergrowths with hornblende (Figure 5.12, Table 5.10). Average $(Na + K)^{A\_site}$ and Ti of approximately 0.50 and 0.07, respectively (Table 5.10) indicate that hornblende is metamorphic as opposed to igneous (Jamieson, 1981).

Assuming constant f_{O2}, amphiboles show an increase in Ti and in (Na + K) and decrease in Si with metamorphic grade, but show no increase in Al^{vi} (Figure 5.12a and b). The latter observation may reflect the small database,

Table 5.10. Average compositions (Mean) and standard deviations (S.D.) for microprobe analyses of amphibole. Structural formulae calculated on anhydrous basis of 23 oxygens. All Fe as Fe^{2+}. n = number of analyses. Na^T indicates total Na.

SAMPLE	85 - 706b		85 - 245		85 - 280		85 - 343a		85 - 345		85 - 643c		85 - 643c		85 - 643c
ANALYSIS	core & rim		core & rim		core & rim		core & rim		core & rim		core		rim		intergrowth
	Mean	S.D.	Mean	S.D.	Mean	S.D.	Mean	S.D.	Mean	S.D.	Mean	S.D.	Mean	S.D.	Mean
SiO_2	44.00	0.33	40.44	0.42	40.45	0.22	40.58	0.17	43.72	0.35	53.01	0.89	51.58	0.91	43.83
TiO_2	0.37	0.09	0.80	0.15	0.49	0.12	0.55	0.06	0.70	0.10	0.32	0.32	0.24	0.14	0.35
Al_2O_3	16.46	0.52	17.48	0.06	16.00	0.19	15.62	0.17	13.95	0.58	3.50	0.17	4.48	0.63	14.18
FeO	13.68	0.19	18.85	0.13	20.26	0.36	20.53	0.28	14.89	0.16	12.02	0.11	12.61	0.12	16.04
MnO	0.29	0.05	0.19	0.02	0.34	0.10	0.33	0.03	0.26	0.05	0.32	0.08	0.24	0.09	0.35
MgO	10.45	0.35	7.35	0.09	6.67	0.31	6.57	0.17	10.93	0.32	15.76	0.22	15.02	0.57	9.67
CaO	11.07	0.18	11.58	0.28	11.76	0.26	11.80	0.15	12.04	0.21	12.71	0.35	12.73	0.28	12.12
Na_2O	1.30	0.11	1.46	0.08	1.36	0.09	1.48	0.05	1.22	0.16	0.46	0.05	0.60	0.09	1.54
K_2O	0.10	0.03	0.70	0.09	0.59	0.06	0.49	0.03	0.20	0.13	0.05	0.06	0.09	0.07	0.35
Total	97.72		98.85		97.92		97.95		97.91		98.15		97.59		98.43
n	6		3		6		5		11		2		3		1
Si_{iv}	6.399	0.046	6.034	0.029	6.146	0.021	6.171	0.025	6.420	0.051	7.593	0.059	7.469	0.071	6.458
Al_{vi}	1.601	0.088	1.696	0.021	1.854	0.038	1.829	0.024	1.580	0.099	0.407	0.034	0.531	0.114	1.542
Al	1.220		1.378		1.012		0.971		0.836		0.184		0.234		0.921
Ti	0.040	0.100	0.090	0.017	0.056	0.013	0.063	0.007	0.079	0.008	0.035	0.035	0.026	0.015	0.039
Fe	2.663	0.075	2.352	0.027	2.574	0.047	2.610	0.043	2.398	0.068	1.440	0.027	1.527	0.027	1.977
Mg	1.664	0.025	1.634	0.017	1.510	0.069	1.489	0.033	1.829	0.019	3.364	0.016	3.241	0.099	2.124
Mn	0.035	0.006	0.024	0.003	0.044	0.012	0.042	0.004	0.033	0.006	0.038	0.010	0.029	0.010	0.044
Ca	1.725	0.025	1.851	0.055	1.914	0.043	1.923	0.023	1.903	0.028	1.950	0.036	1.975	0.060	1.914
Na	0.275	0.031	0.149	0.020	0.086	0.026	0.077	0.014	0.097	0.050	0.050	0.015	0.025	0.025	0.086
Na	0.092		0.273		0.313		0.359		0.237		0.076		0.144		0.354
K	0.019	0.005	0.134	0.170	0.115	0.011	0.095	0.006	0.039	0.023	0.010	0.011	0.017	0.013	0.066
O_T	23		23		23		23		23		23		23		23
$Na^T + K$	0.386		0.556		0.514		0.531		0.373		0.136		0.186		0.506

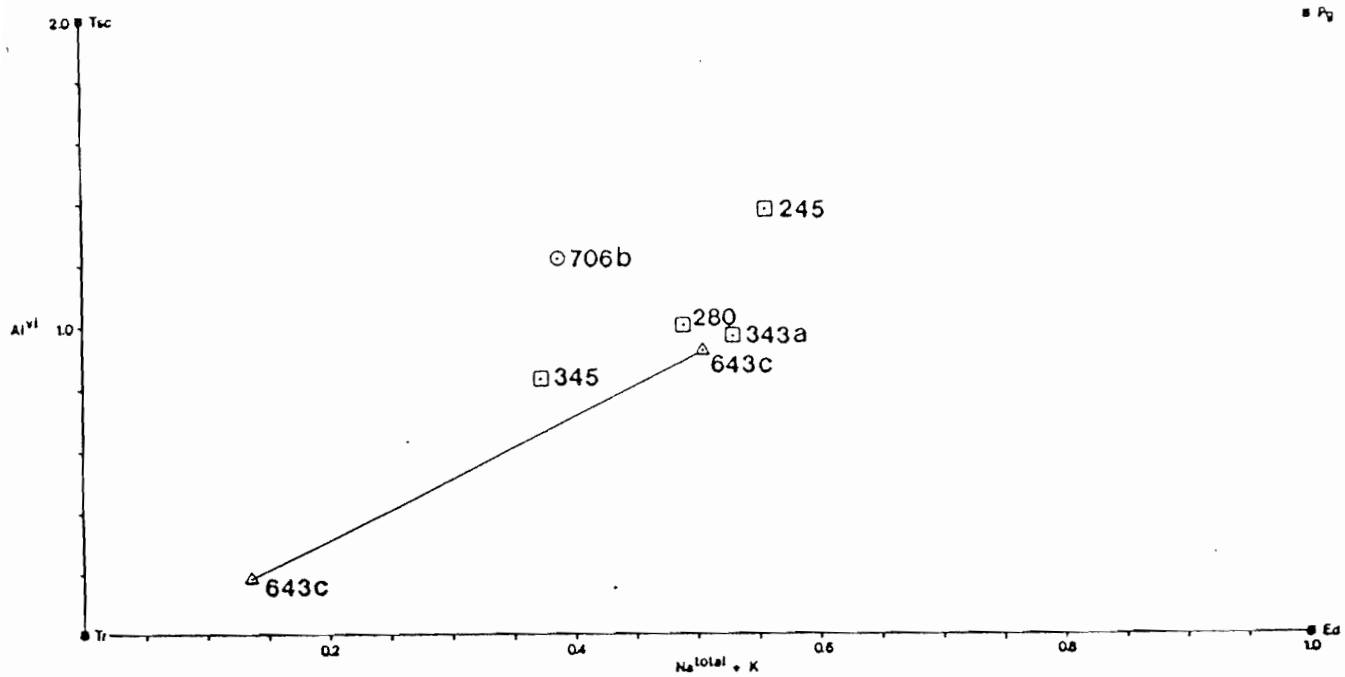

Figure 5.12. (a) Plot of Al^{Vi} versus (Na^{Total} + K) for average amphibole compositions in the George Brook amphibolite and from a late vein cross-cutting the George Brook amphibolite. Note general increase in (Na^{Total} + K) with metamorphic grade with the exception of sample 85-345. (b) Plot of Al^{Vi} versus Si for average amphibole compositions in the garnet amphibolites and from a late synmetamorphic vein cross-cutting the George Brook amphibolite. Note the decrease in Si with metamorphic grade with the exception of 85-345. For (a) and (b): circle = st-gt zone samples, squares = ky zone samples, and tieline joins intergrown amphiboles from late synmetamorphic vein.

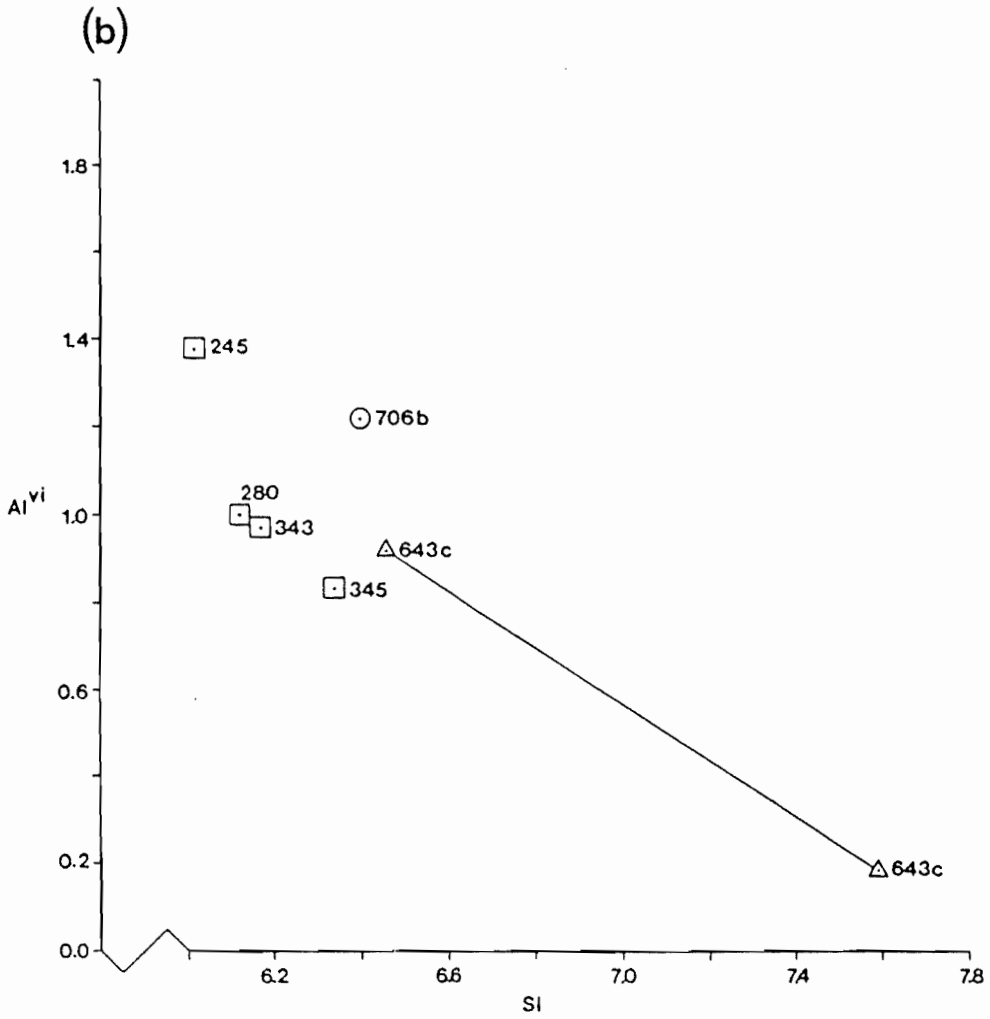

Figure 5.12 (continued)

since only one sample from the garnet zone, and one from the staurolite-kyanite zone, were analysed, whereas all other samples are from the kyanite zone. However, if oxidation states vary, Al^{vi} would vary inversely to Fe^{3+} resulting in the observed uneven distribution of Al^{vi}.

Although Ti-phases are absent in some samples, suggesting a lack of Ti-saturation, the Ti increase observed with increasing grade is regular and therefore probably a real correlation and not due to bulk composition. Amphiboles in sample 85-345 are anomalous, having low (Na+K) and Al^{vi} and high Si relative to the other high-grade amphibolites (85-245, 85-280, 85-343a). Bulk chemistry available for three of these amphibolites (85-345, 85-706B, 85-245) reveals that sample 85-345 is low in (Na+K) relative to the other samples thus accounting for the observed hornblende compositions in this sample.

Despite the controversy surrounding the affects of pressure on amphibole composition, comparison of the amphibole chemistry in the amphibolites with pressure-discrimination diagrams of Raase (1974) and Laird and Albee (1981) indicate that these amphiboles formed at moderate pressures. This is consistent with quantitative pressure estimates based on other techniques (see Table 6.6).

5.9 EQUILIBRIUM ASSESSMENT

Assessment of whether equilibrium has been obtained and retained by a mineral assemblage is important for meaningful interpretations of P and T estimates based on mineral equilbria. Use of geobarometry and geothermometry to obtain quantitative P-T estimates requires chemical equilibration. However, incomplete textural and chemical equilibration is essential for preservation of prograde and retrograde mineral assemblages and reaction textures and hence for determination of a complete P-T-t path. This is a fundamental problem in determining P-T-t paths and thus a well constrained prograde P-T-t path means poorly constrained peak metamorphic conditions and vice versa.

Textural and chemical disequilibrium in the Jumping Brook metamorphic suite are discussed below. Commonly cited textural and chemical criteria for determination of an equilbrium metamorphic mineral assemblage are listed in Table 5.11.

5.9.1 Textural Disequilibrium

Strong evidence for microscopic textural disequilbrium in the Dauphinee Brook and Corney Brook schists comes from internal-external fabric relations

Table 5.11. Summary of commonly cited criteria for textural and chemical equilibrium taken from Best (1982) and Vernon (1976).

TEXTURAL CRITERIA

1. All phases are in mutual contact with one another and lack evidence of one mineral replacing another. (Phases inside a corona structure or present only as inclusions are unlikely part of the equilbrium assemblage.)

2. Absence of known incompatible mineral pairs (eg. hematite and graphite).

3. Limited number of different mineral phases in the rock so that the assemblage obeys the phase rule.

4. Presence of stable shapes of grains and inclusions.

CHEMICAL CRITERIA

1. Lack of compositional zoning or inhomogeneity in mineral phases. If phases are zoned, rim compositions should be similar.

2. Regular partitioning of elements between co-existing phases and hence the absence of intersecting tielines on graphic representations such as Thompson AFM plots.

3. Similar compositions between grains of the same phase on the scale of investigation (generally taken to be thin section scale).

---

which indicate a progression of porphyroblast growth during crenulation. Garnet enclosed in staurolite is idioblastic whereas that in the matrix of the staurolite-garnet schists is commonly subidioblastic to xenoblastic suggesting it is unstable in the matrix mineral assemblage kyanite-biotite-staurolite-plagioclase-muscovite. Disequilibrium is further supported by optically visible zoning in oligoclase in the staurolite-garnet schists, partial muscovite pseudomorphs after kyanite in the pelitic biotite schists, and the preservation of compositional layering even in the highest grade schists.

5.9.2 Chemical Disequilibrium

To assess the degree of chemical equilibration in the Jumping Brook metamorphic suite, Thompson (1957) AFM (pelitic rocks) and Eskola (1915) ACF (mafic rocks) ternary plots were constructed. Unfortunately, sufficient data for the major mineral phases are available only for the staurolite-garnet schists and biotite schists (refer to Table 5.1) and therefore, AFM plots were not constructed for the low-grade pelitic phyllites. Kyanite contains only trace amounts of Fe and K (Conrod, 1984) and is therefore plotted as pure Al_2SiO_5 on the AFM diagrams.

(i) AFM Diagrams

Evidence of retrograde exchange between garnet and biotite is observed within several microns of grain boundaries where the two phases are in contact, whereas isolated garnet rims and biotite are homogeneous on a thin section scale. Rim compositions of garnet and biotite in contact with one another are assumed to reflect re-equilibration on a micron scale, and are joined by tielines on the AFM diagrams. These are the compositions used in geothermometry calculations. The isolated garnet rims and biotite may or may not reflect prograde equilibrium compositions and are joined by dashed (for reference) or solid tielines where disequilibrium or equilibrium, respectively, are inferred.

Figures 5.13 and 5.14 present AFM diagrams for the staurolite-garnet schists and the biotite schists, respectively. Two observations indicate disequilibrium on a thin section scale. Firstly, the existence of a four phase apparent equilibrium assemblage on the AFM diagram requires either a bulk composition that lies on the staurolite-biotite join, the persistence of a metastable phase, or an extra independent component is involved. No bulk rock chemistry is available for the Corney Brook and

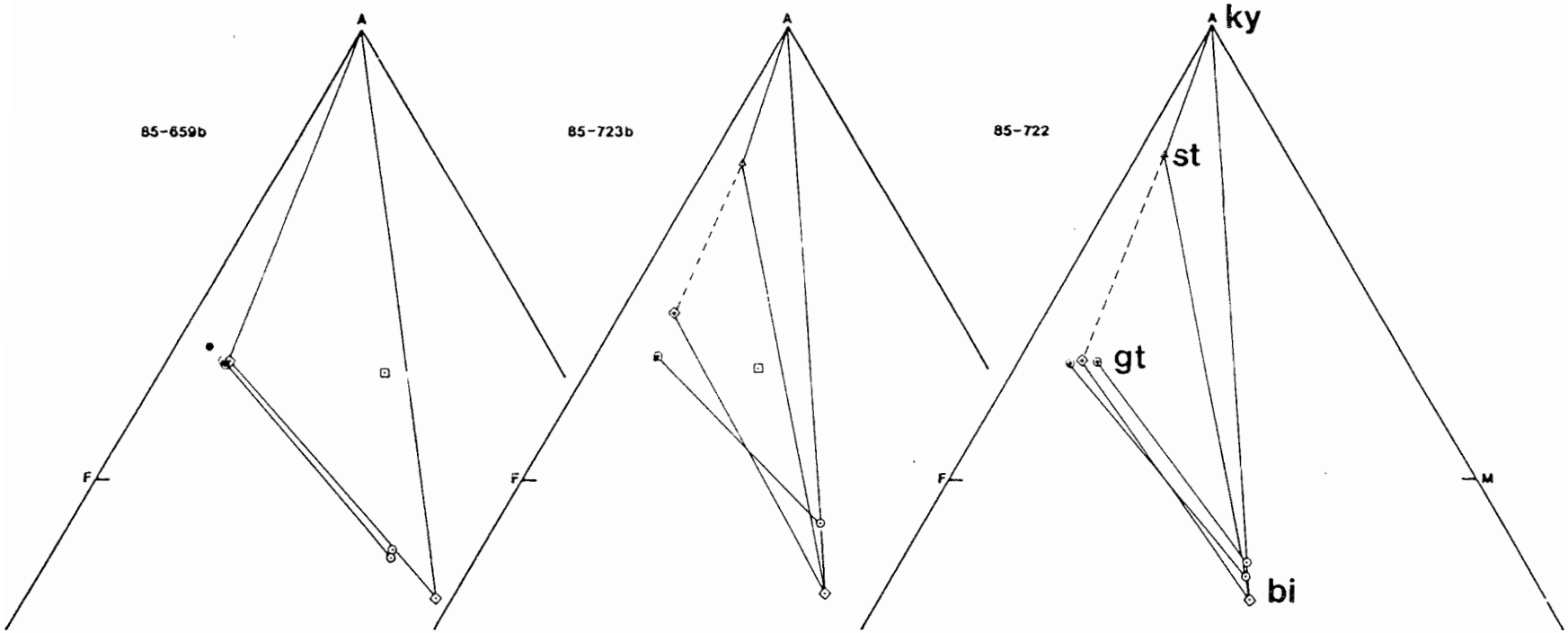

Figure 5.13. Thompson (1957) AFM diagrams for the staurolite-garnet schists. Closed symbols and single point are garnet cores. Circles are rim compositions of biotite and garnet in contact with one another.Diamonds are rim compositions of mineral phases not in contact. Squares are late chlorite prophyroblasts.
Garnet and biotite are not in equilibrium. Note increase in Fe in garnet in contact with biotite except for one pair (85-722). Mineral fields for all AFM plots shown on that for 85-722.

Figure 5.14. Thompson (1957) AFM diagrams for the high-grade biotite schists. Sample 85-441: ○ indicate garnet and biotite in contact and included in kyanite. △ indicate garnet and biotite in contact in matrix. ◇ indicate garnet and biotite isolated from one another in the matrix, + and ▼ indicate garnet cores and isolated biotite inclusion in kyanite, respectively. 85-446: ○ indicate garnet and biotite in contact in the matrix, ◇ indicate isolated matrix garnet and biotite, □ represents composition of the late chlorite porphyroblasts. Garnet and biotite are not in equilibrium. Note increase in Fe in garnet in contact with biotite. Mineral fields for all AFM plots are shown on that for 85-446.

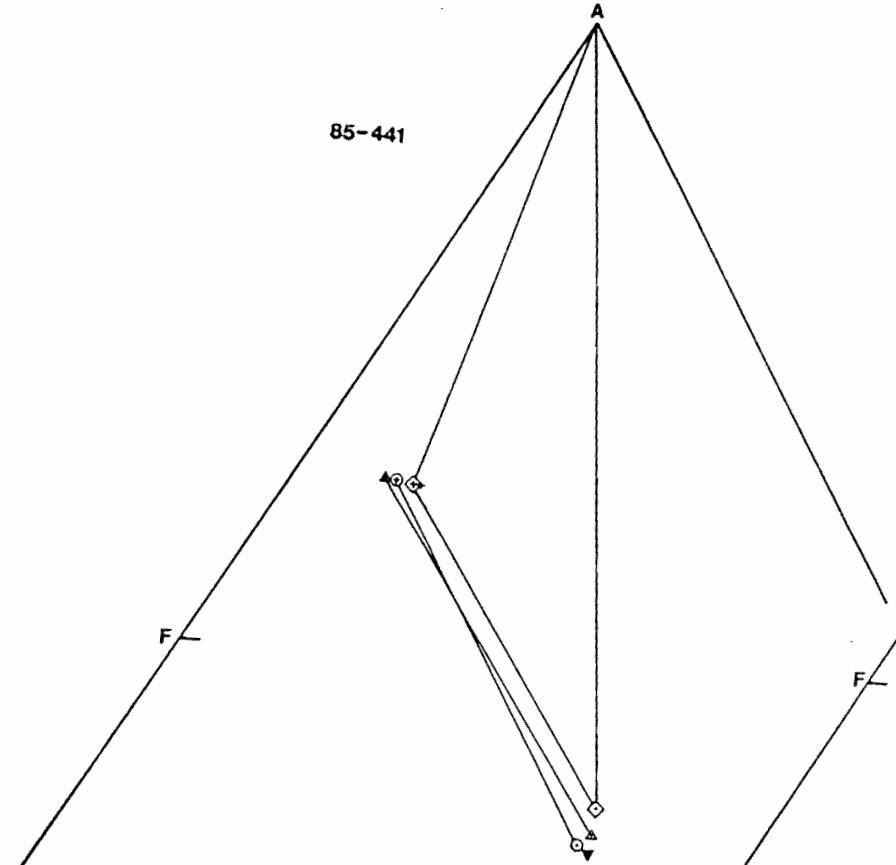
A
85-441
F

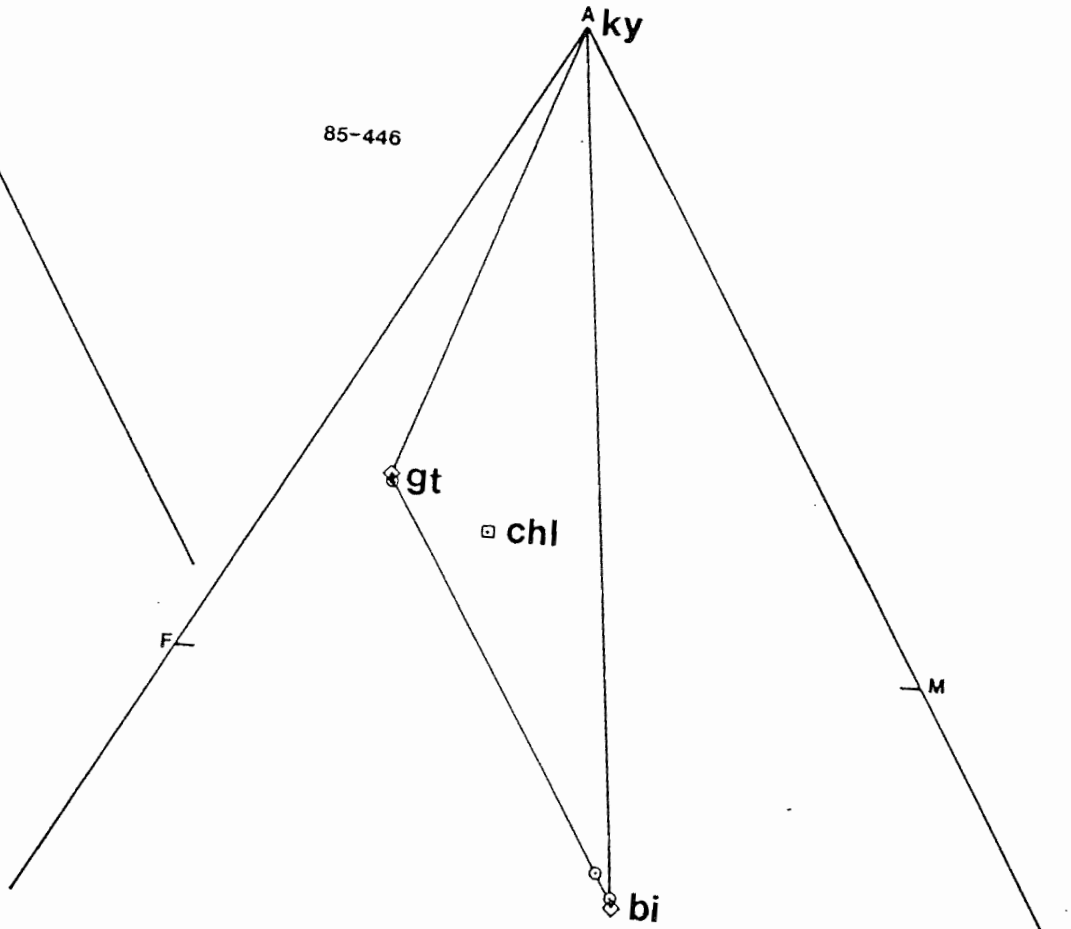
A
ky
85-446
gt
chl
F
M
bi

Fishing Cove River schists but this common pelitic assemblage is generally attributed to the metastable persistence of refractory garnet (eg. Atherton and Smith, 1979; Evirgen and Ashworth, 1984). This interpretation is supported by microstructures that show that garnet formed prior to staurolite and kyanite, and that matrix garnet is commonly subidioblastic to xenoblastic, and therefore presumably unstable. Secondly, tielines between co-existing phases cross or converge in all the AFM plots indicating inconsistent K_D^{Fe-Mg}, and hence disequilibrium, among the ferromagnesian phases.

Tie line configurations in the AFM plots are best considered in terms of 3 cases: (1) garnets that show good growth zonations and no retrograde cation exchange with biotite (that is, no decrease in Mg and increase in Fe (sample 85-659B, Figure 5.13), (2) garnets that are homogeneous, co-exist with apparently stable biotite, staurolite, kyanite, muscovite, and quartz, and exhibit evidence of retrograde cation exchange with biotite (samples 85-722 and 85-723B) and (3) garnets that are homogeneous or weakly normally zoned, co-exist with biotite, kyanite, muscovite and quartz, and exhibit evidence of retrograde cation exchange with biotite unless included in kyanite, where they preserve growth

zonations and show no retrograde exchange (samples 85-441 and 85-446, Figure 5.14).

Case (1) The preservation of growth zonation in these garnets indicates that no volume diffusion has occurred. However, tielines between co-existing phases in sample 85-659b intersect, indicating disequilibrium. Garnet shows no signs of retrograde exchange with biotite as in cases 2 and 3. Therefore, disequilibrium in this case probably reflects equilibration of biotite with staurolite and kyanite at peak metamorphic conditions, whereas garnet remained metastable.

Case (2) The absence of growth zonation in garnets in samples 85-722 and 85-723b indicates that volume diffusion occurred. Garnet-biotite tieline intersections on AFM plots indicate disequilbrium between these phases. As in case 1, the presence of a four phase assemblage suggests garnet persists metastably and it is therefore unlikely that garnet and biotite are in equilibrium. However, garnet and biotite show evidence of retrograde cation exchange. Also evident in the AFM diagrams for Case 2 (and Case 3) samples is a higher $(X_{Fe})^{Gt}$ for garnets in contact with biotite compared to rims of

isolated garnets. One exception to this trend is observed in sample 85-722.

Case (3) The absence of staurolite in samples 85-441 and 85-446 means that garnet forms part of the stable assemblage garnet-biotite-kyanite. Inclusion-free garnet rims, interpreted to result from late prograde growth on earlier garnets, further supports the possibility that garnet rims are part of an equilibrium assemblage. Several garnet-biotite pairs are shown in Figure 5.14. Intersecting tielines indicate that the garnet-biotite pair enclosed in kyanite is in disequilibrium with garnet-biotite pairs in the matrix.

(ii) ACF Diagrams

ACF diagrams of garnet, hornblende, and plagioclase core and rim compositions, for phases in contact with and isolated from each other, are shown in Figure 5.15. The garnet-hornblende rims in contact are the same compositions used in garnet-hornblende geothermometry calculations. In all but sample 85-343a, only one garnet-hornblende pair was analysed and thus the degree of equilibration is difficult to assess. Converging tielines between two garnet-hornblende pairs in sample 85-343a indicates thin-section scale disequilibrium in this

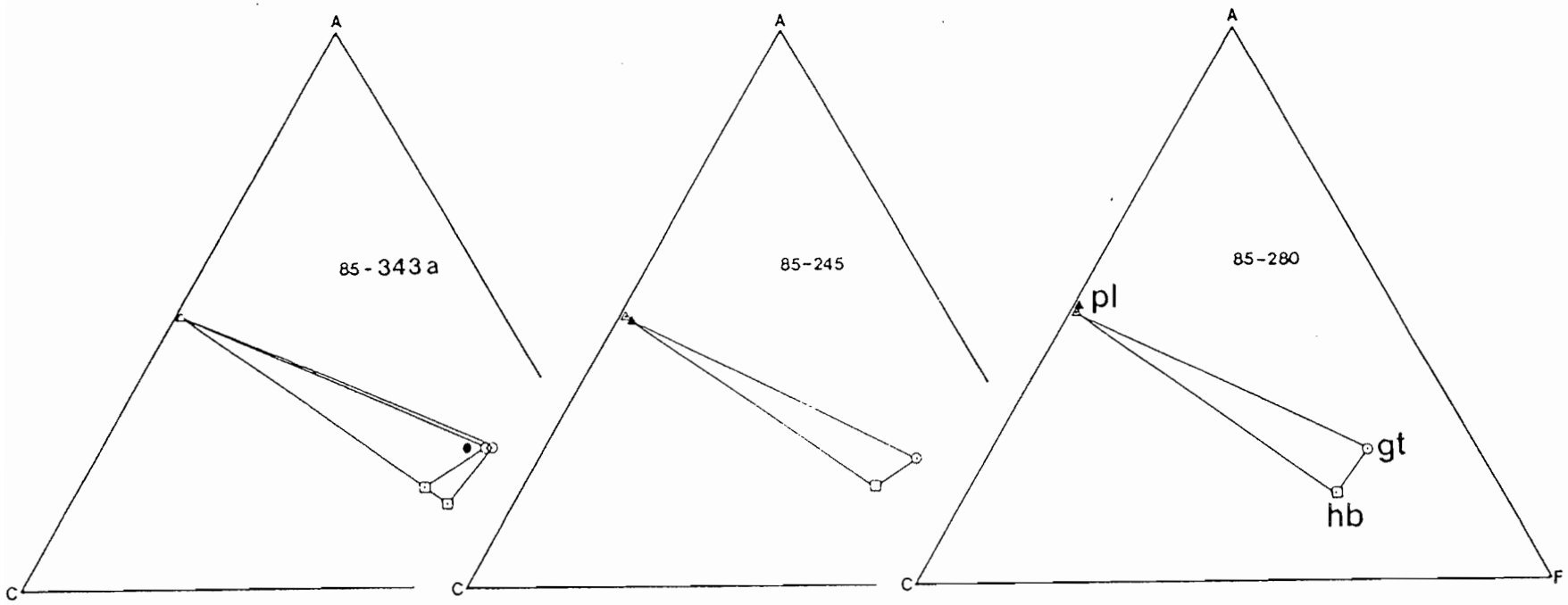

Figure 5.15. Eskola ACF diagram. Closed and open symbols represent core and rim compositions, respectively. ▲ △ are plagioclase, ■ □ are hornblende, ● ○ are garnet. Note apparent lack of chemical equilibrium between garnet and hornblende in 85-343a. Mineral fields for all ACF plots are shown on that for 85-280.

sample, which is not surprising considering the disequilibrium displayed by the ferromagnesian minerals in the pelitic schists.

5.10 SUMMARY

Mineral chemistry generally supports an east-northeasterly increase in metamorphic grade: Ti-content in biotite increases towards the east-northeast; garnets are compositionally zoned in the west and central parts of the map area and homogeneous in the east; hornblende is the only amphibole observed in the mafic rocks in the eastern part of the study area, as opposed to the tremolite-actinolite which is observed in the low-grade mafic rocks.

Chlorite is dominantly ripidolite although post-S_2 porphyroblasts in the staurolite-garnet and biotite schists are more magnesian, suggesting a higher temperature of formation relative to chlorite in the low-grade phyllites and schists. Muscovite is homogeneous on a thin section scale, and no apparent relationship exists betwen $(X_{Na})^{Pl}$ and $(X_{Na})^{Mu}$ in samples containing the limiting assemblage muscovite-kyanite-plagioclase. Staurolite is iron-rich and homogeneous.

Maximum mean temperatures experienced by samples preserving garnet growth zonation is probably less than approximately 600°C, whereas samples containing garnets with homogeneous cores experienced temperatures in the range of 600° and 700°C (cf. Woodsworth, 1977; Yardley, 1977). These temperature estimates are consistent with geothermometry calculations (Chapter 6).

Abundant evidence exists in the staurolite-garnet and biotite schists for textural and chemical disequilibrium. Tielines between co-existing phases on Thompson AFM plots commonly intersect one another, and garnet locally shows a Mg decrease and Fe increase at rims in contact with biotite. Mn increase and some Mg decrease in inclusion-free overgrowths on high-grade garnets is attributed to late prograde growth in response to staurolite breakdown.

CHAPTER 6

CONDITIONS OF METAMORPHISM

6.1 INTRODUCTION

Metamorphic pressure and temperature estimates are commonly derived by comparing natural assemblages to experimental and theoretical petrogenetic grids. Ideally, phase equilibria in metamorphic rocks can be inferred from arrested reaction textures (eg. Kwak, 1974) but this approach is complicated by the tendency of prograde reactions to go to completion (Vernon, 1976, p.97). Many researchers rely on observed phase changes across isograds. However this approach neglects continuous reactions which involve changes in mineral chemistry and modal abundances, rather than changes in the mineral phases present. As well, bulk rock and metamorphic fluid compositions affect the mineral assemblages observed (eg. Liou et al., 1974; Atherton and Smith, 1979; Evirgen and Ashworth, 1984) and commonly differ from those for which experimental phase equilbria are derived. Consequently, determining phase equilibria in natural assemblages is difficult. However, a well-established sequence of metamorphic mineral growth based on porphyroblast-matrix

relations can provide restrictions on applicable mineral reactions.

In order to constrain the P-T ranges for prograde and retrograde metamorphism, petrogenetic grids and phase equilibria have been applied to the mineral assemblages of the Jumping Brook metamorphic suite. Pelitic and mafic rocks are considered in separate sections. Mineral assemblages of specific units are given in Table 4.1 and a paragenetic summary diagram of the metamorphic mineral assemblages of general lithologies (that is, metabasic, felsic metavolcanic, pelitic, and calcareous) is given in Table 6.1.

6.2 PROGRADE METAMORPHISM

The Jumping Brook metamorphic suite shows a Barrovian metamorphic progression from the biotite and garnet zones in the low-grade exposures of the Dauphinee Brook schist exposed along the Cabot Trail and western part of Corney Brook through a staurolite-kyanite zone in exposures along Corney Brook and Robert Brook to the kyanite zone along Fishing Cove River, Benjies Lake Brook, and the upper reaches of Corney Brook and Robert Brook in the eastern part of the map area (Appendix 1,

Table 6.1. Metamorphic mineral assemblages in the rocks of the Jumping Brook metamorphic suite. (P) & (R) refer to prograde and retrograde phases, respectively where the distinction is necessary. Solid lines = abundant phases, dashes lines = locally present phases, dotted lines = rarely present phases. Sillimanite is metastable in the kyanite zone.

METASEDIMENTARY ROCKS

FACIES:	EPIDOTE-AMPHIBOLITE		AMPHIBOLITE		
ZONE:	BIOTITE	ALMANDINE	ST-KY	KYANITE	
MINERAL					COMMENTS
PELITES TO PSAMMITES					
chlorite (P)	———	———			commonly, as porphyroblasts, also after bio, gt, st, ky
chlorite (R)	- - - - - - - -	- - - - - - - - - -	- - - - - - -	- - - - - - - - -	
chloritoid	- - - - - - - -				
biotite	- - - - - - - -	———	———	———	
muscovite	———	———	———	———	
garnet	———	———	———	———	
staurolite			———	——— - - - -	
kyanite			———	———	
sillimanite				. . . . .	
plagioclase	———	———	———	———	
K-spar	. . . . .	. . . . .	. . . . .	. . . . .	porphyroblasts in feldspar schist (chapter 2)
hornblende		. . . . .	. . . . .	. . . . .	
opaque minerals	- - - - - - - -	- - - - - - - - - -	- - - - - - -	- - - - - - - - -	
zircon	- - - - - - - -	- - - - - - - - - -	- - - - - - -	- - - - - - - - -	
carbonate	- - - - - - - -	- - - - - - - - - -	- - - - - - -	- - - - - - - - -	
MARBLES					only exposed in almandine to staurolite-kyanite zone transition
carbonate		———	———		
garnet		———	———		
wollastonite		- -	- - - - - - -		
diopside		- -	- - - - - - -		

Table 6.1. (Continued)

MAFIC ROCKS

FACIES:	EPIDOTE-AMPHIBOLITE		AMPHIBOLITE FACIES		
ZONE:	BIOTITE	ALMANDINE	ST-KY	KYANITE	
MINERAL					COMMENTS
chlorite (P)	———	———			
chlorite (R)		-------	-------	---------	-after biotite, chloritoid
epidote (P)	———	——— -------	----		
epidote (R)		----------	...?...	———	
actinolite	--------	----			
zoned amphibole (P)	--------	----			-actinolitic cores, blue-
hornblende (P)		———	———	———	green hb rims
biotite (P)	.....	.....	.....	.....	
garnet				----------	
plagioclase	———	———	———	———	
K-feldspar	.....	.....	.....	.....	
sphene				.....	-locally rims opaque minerals
pyrite	.....	.....	.....	.....	
?magnetite			-------	----------	
ilmentite	———	----------	- - - -	---------	
carbonate	--------				
apatite			-------	----------	
zircon	.....	.....	.....	.....	-as inclusions in biotite
white mica	--------				-after plagioclase porphyro-
rutile	--------				clasts

Figure A1.1; Map 1). Rare fibrolite is developed in the high-grade rocks. Retrogression is locally strong in the high-grade biotite schist but is otherwise minor.

6.2.1 Pelitic Rocks

Absence of bulk rock chemical analyses for the Dauphinee, Corney Brook, and Fishing Cove River schists and rare preservation of arrested reaction textures preclude quantitative definition of metamorphic reactions for the pelitic rocks. Yardley et al. (1980) found that most pelitic reactions take place initially by continuous reactions (that is, divariant equilibria) and that discontinuous reactions (univariant equilibria) are rare because one or more of the reactants (commonly chlorite or muscovite) is used up during the continuous reaction. They concluded that univariant reactions can provide P-T limits of natural assemblages but generally are not the reactions that have occurred. Thus, the discontinuous reactions proposed in this work, while consistent with mineral assemblages and textures, are used only to place some restriction on P-T conditions of metamorphism.

The assumption $P_{H2O} = P_{TOTAL}$, $X_{H2O} = 1.0$ is made for phase equilibria considerations in the Dauphinee Brook and Corney Brook schists, although in the vicinity of the

marble, and where the schists are carbonate-bearing, X_{H2O} was probably < 1.0. Since carbonate-bearing assemblages have not been used in P-T determinations this is not a serious problem.

Graphite in pelitic rocks acts as an f_{O2} buffer (Miyashiro, 1964) and hence, most pelitic rocks exhibit a characteristic sequence of reactions suggesting fairly uniform and low f_{O2} (Hoschek, 1969). Carbonaceous material is observed in the low-grade pelites but is not optically detectable in the medium to high-grade rocks. Consequently, f_{O2} is assumed to be uniform throughout the Dauphinee schist, and in the absence of data to indicate otherwise, for the Corney Brook schist. In any case, for P = 2-10 kb, temperatures of some reactions involving staurolite and chloritoid vary by only 20°C if f_{O2} varies between that of the C-buffer and the FMQ buffer (Hoschek, 1969). In addition, f_{O2} variation is only important where major minerals, such as biotite, have significant amounts of Fe^{3+} which is unlikely, at least in the medium to high-grade rocks. Therefore, the effects of f_{O2} variation on phase equilibria for these rocks are assumed to be negligible.

Mineral assemblages in the pelitic phyllites of the Dauphinee Brook schist (chl-mu-fsp-ilm$\pm$chtd and/or bi$\pm$

gt($Alm_{70}Sp_{20}Gr+Py_{10}$)) are characteristic of the biotite and garnet zones (Turner, 1981). Generally, almandine garnet remains stable to upper amphibolite facies, biotite is stable from greenschist to amphibolite facies conditions, and chloritoid may persist into the greenschist-amphibolite facies transition (Turner, 1981). Thus, the Dauphinee Brook schist reflects transitional greenschist-amphibolite facies conditions.

Mineral assemblages in the Corney Brook and Fishing Cove River schists indicate that metamorphic grade ranges from the staurolite-kyanite zone to the kyanite zone of the amphibolite facies (Turner, 1981; Elhers and Blatt, 1982). Rare fibrolite has grown in muscovite in the biotite schists.

The sequence of porphyroblast growth deduced from internal-external fabric relations provides important constraints on the metamorphic reactions that could have taken place in the Dauphinee Brook, Corney Brook, and Fishing Cove River schists. All experimentally determined and thermodynamically calculated reactions discussed below are shown in Figures 6.1 or 6.2.

The restriction of chloritoid to Fe-rich bulk compositions (Atherton, 1977) is reflected by its localized occurrence in the Dauphinee Brook schist. A

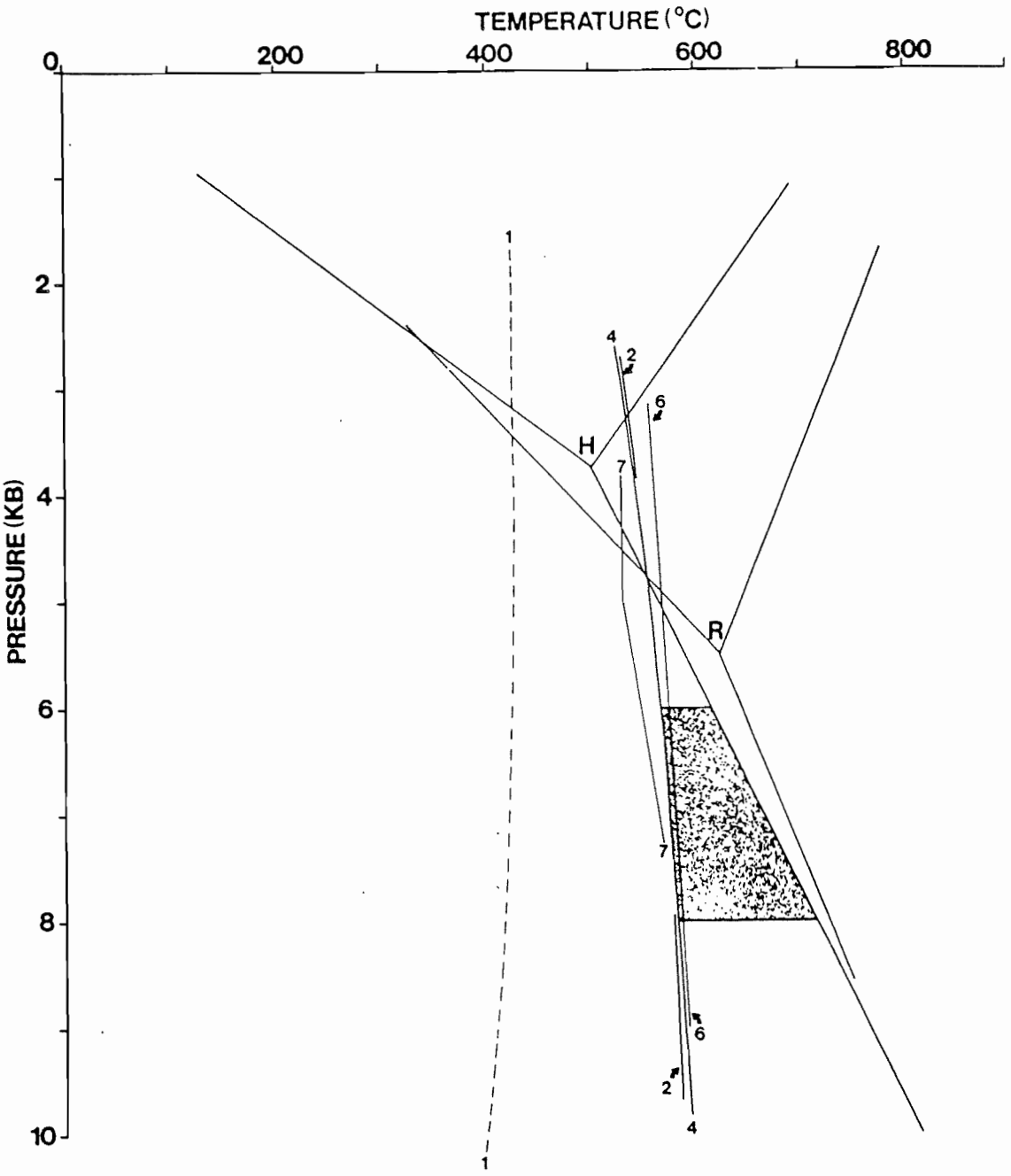

Figure 6.1. Experimental and theoretical pelitic phase equilibria for chloritoid and staurolite production. Preferred reactions for chloritoid and staurolite production are (4) and (5). Numbers for reactions consistent with text. The boundary for reaction (5) has not been determined but Hoschek (1969) suggested it occurs between (6) and (7). Shaded area denotes the temperature conditions inferred from phase equilibria for the staurolite-garnet schists for 6 to 8 kb. High temperature boundary defined by the kyanite= sillimanite boundary of Holdaway (1971). H and R indicate the Al_2SiO_5 triple point after Holdaway (1971) and Richardson et al. (1969), respectively.

number of chloritoid-producing reactions have been proposed by Hoschek (1969) for paragonite-free, chloritoid-bearing rocks such as those of the Dauphinee Brook schist:

(1) chl + Al-silicate (kaolinite or pyrophyllite) = chtd + qtz + H2O

(2) chl + mu = chtd + bi + qtz + H_2O

Reaction (2) occurs in pelitic rocks in the upper greenschist facies (Hoschek, 1969). No kaolinite or pyrophyllite has been detected by X-ray diffraction or microprobe analyses in the chloritoid phyllites. These phases are unstable at epidote-amphibolite conditions and it is probable the reaction has gone to completion. Reaction (2) may have operated at the margins of the graphitic, pelitic, garnet-biotite lenses that occur locally in the chloritoid-bearing semipelitic layers of the Dauphinee Brook schist (Figure 4.2).

The stability of chloritoid and absence of staurolite in the low-grade pelites indicates metamorphic

temperatures in the range of about 425°C to a maximum of 525° to 575°C. The upper temperature limit is partially dependent on P_{H2O} and the staurolite-forming reaction (Figure 6.1).

Garnet-forming reactions in the low-grade pelites, like those for chloritoid, have apparently gone to completion. Microstructures indicate that garnet and chloritoid or biotite grew concurrently. Therefore, chloritoid and biotite are not involved in garnet production in the low-grade rocks (cf. Thompson and Norton, 1968; Karabinos, 1985). Considering the muscovite- and chlorite-rich nature of the pelitic rocks and that garnet has commonly nucleated on quartz porphyroclasts, it is probable that garnet formed via a reaction such as

(3) $\quad chl + mu + qtz = alm + bi + H_2O.$

Whether biotite or chloritoid forms as a result of reaction (3) depends on the Fe/Mg ratio and K-content of the host rock.

Garnet-forming reactions in the Corney Brook schist are either continuous or have gone to completion, as no

arrested reaction textures are observed. However, chlorite is commonly included in garnet and is absent from the matrix except as a retrograde phase. Therefore, garnet probably formed by the same reaction as in the Dauphinee Brook schist.

Hoschek (1969) experimentally determined a number of discontinuous staurolite-producing reactions. For rocks containing no chloritoid or garnet, the following reaction may occur:

(4) chl + mu = st + bi + qtz + H_2O

For the more common situation where lower grade rocks contain chloritoid and/or garnet, the following reactions may form staurolite:

(5) chtd + chl + mu = st + bi + qtz + H_2O

(6) chtd + qtz = st + gt + H_2O

(7) chtd + Al_2SiO_5 = st + qtz + H_2O

The reaction boundary for equilibrium (5) has not been determined but Hoschek (1969) suggested it occurs between

reaction (6) and (7). Baltatzis (1979) suggested reactions (6) and (7) may apply to biotite-free, Fe-rich rocks. Yardley et al. (1980) and Bell and Rubenach (1983) suggested the following reaction based on mineral chemistry and phase assemblages and on microstructure, respectively:

(8) $mu + gt + chl = st + bi + qtz + H_2O$

This reaction has not been experimentally determined but likely occurs within the P-T range defined by reactions (4) and (5).

Reactions (6) and (7) can be eliminated as possible staurolite-producing reactions for the staurolite-garnet schist, which contain biotite and microstructures that show garnet grew before staurolite. Where inclusion trails are well developed in biotite, co-existing staurolite overgrows the same crenulation stage (generally stage 5-6), and both may include garnet, indicating concurrent staurolite and biotite growth. Garnet included in staurolite is commonly idioblastic, but is subidioblastic to xenoblastic in the matrix, suggesting that it was initially stable during staurolite growth but subsequently became unstable. Chlorite

inclusions are common in garnet and locally present in staurolite. Chlorite is absent from the matrix except as an obviously retrograde phase. These observations support reaction (4) for staurolite formation in the Corney Brook schist. However, chloritoid is never present in the Corney Brook schist and an apparent chloritoid "ghost" is observed in one sample of the staurolite-garnet schists (Figure 4.18). Therefore, it is probable that reactions (4) and (5) may have formed staurolite in originally chloritoid-free and chloritoid-bearing rocks of the Corney Brook schist but reaction (5) is favoured for the staurolite-garnet schist.

Phase equilibria define a temperature range of approximately 555° to 720°C for a pressure range of 6 to 8 kb (see Figure 6.1 and section 6.5.2). The upper temperature limit is dependent on the staurolite breakdown reaction (Figure 6.2). The disappearance of zoning in garnet suggests temperatures exceeded approximately 600°C (Woodsworth, 1977; Yardley, 1977) in the staurolite-garnet schists, consistent with the suggested temperature range.

In the biotite schists of the Fishing Cove River schist, garnet phase equilbria are more complex than in the Dauphinee Brook and Corney Brook schists. Unlike the

Figure 6.2. Experimental and theoretical phase equilibria for staurolite breakdown. Reactions are:
(9) st + mu + qtz = Al_2SiO_5 + bi + gt + H_2O (Hoschek, 1969)
(10) st + mu + qtz = Al_2SiO_5 + bi + H_2O (Hoschek, 1969)
(11) st + qtz = Al_2SiO_5 + gt + H_2O
(a, Bickle and Archibald, 1984; b, Hoschek, 1969; c, Rao and Johannes, 1979)
(12) chl + mu = ky + phlg + qtz + H_2O
(Bird and Fawcett, 1973)
No reaction boundary has been determined for reaction (9) but is thought to occur between reactions (10) and (11b) (Hoschek, 1969). Also shown are reaction curves for muscovite breakdown (M): mu + qtz = ksp + Al_2SiO_5 + L and for granite melting (G) for $P_{H2O}=P_{TOTAL}$ (G-1), $P_{H2O}=0.5P_{TOTAL}$ (G-2), and $P_{H2O}=0.3P_{TOTAL}$ (G-3) after Binns (1969). Shaded area defines the interpreted peak temperature range for 6 to 8 kb. H and R indicate the Al_2SiO_5 triple point after Holdaway (1971) and Richardson et al. (1969), respectively.

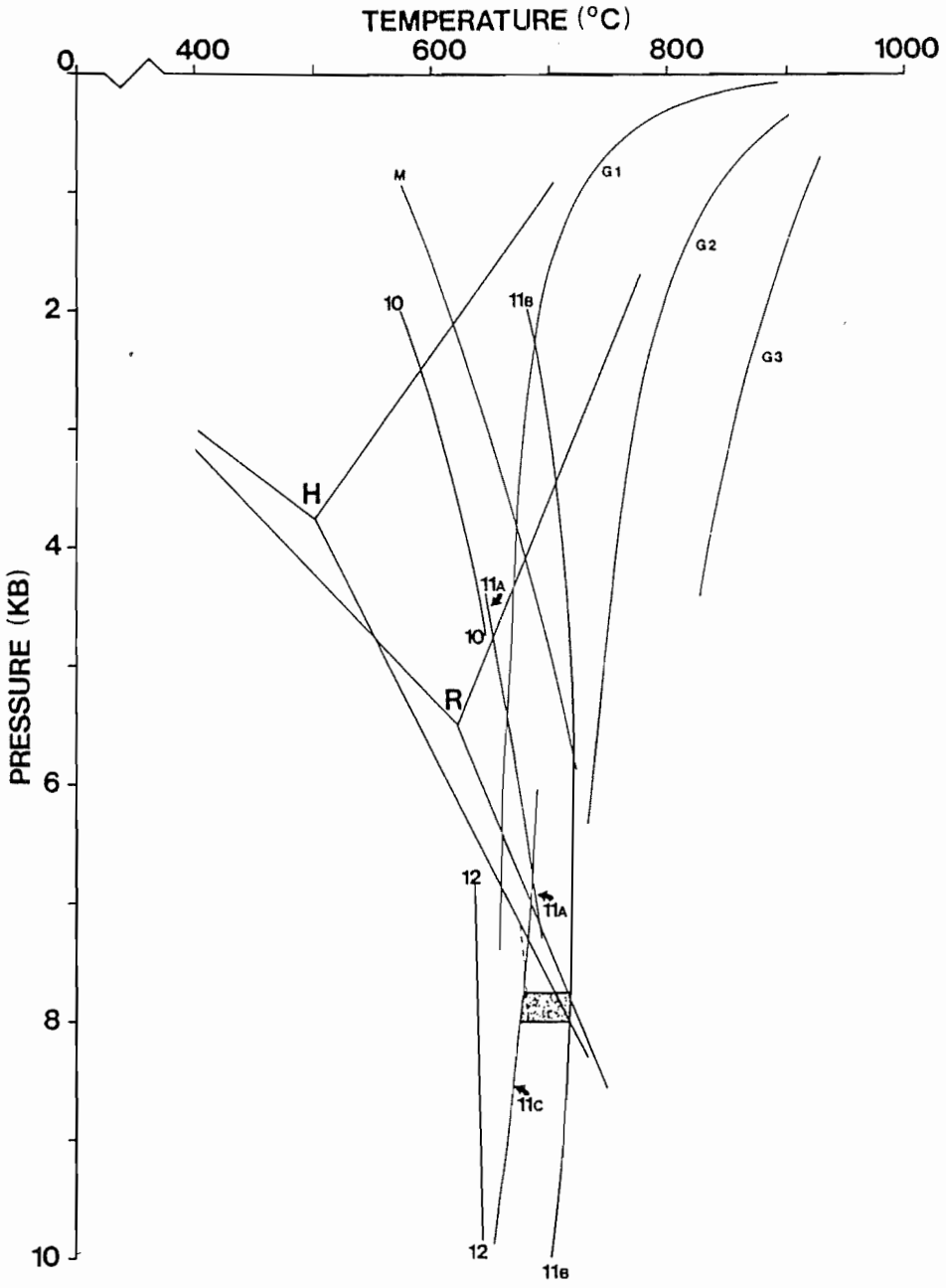
TEMPERATURE (°C)
400
600
800
1000
0
2
4
6
8
10
PRESSURE (KB)
M
G1
G2
G3
10
11B
H
11A
10
R
12
T1A
11C
12
11B

Figure 6.2

staurolite-garnet schists, some garnet growth in biotite schists occurred after staurolite growth. In almost all samples of the biotite schists, garnet contains distinct inclusion-free rims mantling an inclusion-rich core (Figure 4.21). Inclusion trails in garnet cores are commonly straight and at a high angle to the matrix fabric. Co-existing staurolite (where present) is (1) included in, or partially replaced by garnet (Figure 4.22) and possibly by plagioclase, (2) is included in kyanite, or (3) is partially replaced by submicroscopic intergrowths of phyllosilicates. In several samples, garnet has partially replaced muscovite in quartz-rich layers also containing minor plagioclase, apatite, and biotite (Figure 6.3). These observations indicate a reaction involving staurolite, muscovite, and quartz to form garnet, such as

(9) st + mu + qtz = Al_2SiO_5 + bi + gt + H_2O

(Hoschek, 1969).

This reaction was suggested by Hoschek (1969) as a possible intermediate reaction between two experimentally derived Al_2SiO_5-producing reactions:

(10) st + mu + qtz = Al_2SiO_5 + bi + H_2O and

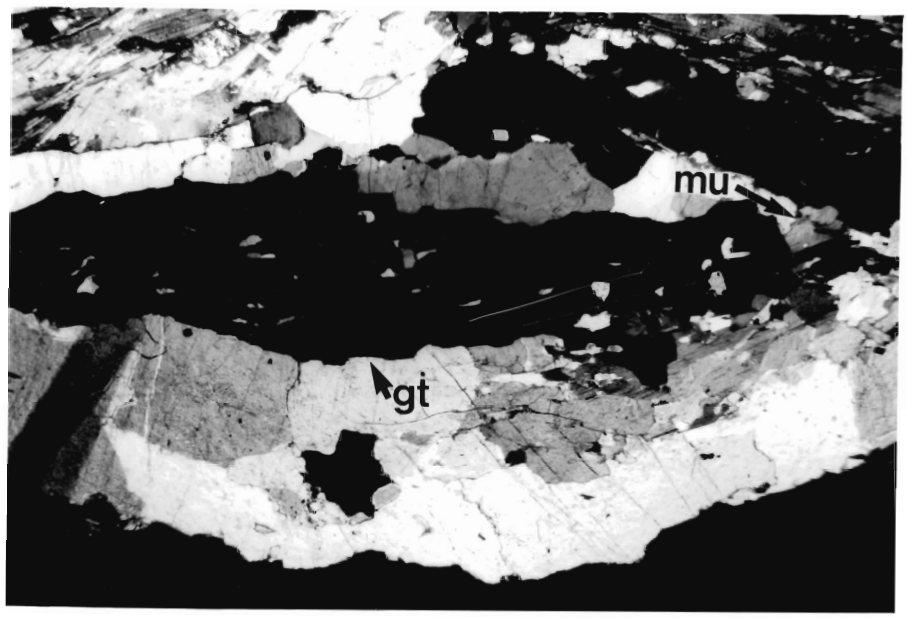

Figure 6.3. High-grade garnet replacing muscovite in a quartz-rich segregation in the Fishing Cove River schist.

(11) st + qtz = Al_2SiO_5 + alm + H_2O

(see Figure 6.2).

Presumably, kyanite is also produced by reaction (9). Based on its scarcity, fibrolite in the high-grade rocks is interpreted to be metastable. This interpretation is supported by experimental results of Salje (1986) which show that fibrolite is stable at temperatures > 900°C for moderate pressures.

Kyanite-producing reactions in the staurolite-garnet schists are unclear. Kyanite in these rocks may have developed by reaction (9) as suggested by the AFM plots where staurolite lies on the tie line between garnet and kyanite. However, internal-external fabric relations indicate that, despite some overlap, kyanite growth generally outlasted that of staurolite and was concurrent with oligoclase growth. Kyanite has preferentially grown along the muscovite-rich S_2 cleavage domains in the staurolite-garnet schists. In some sections, oligoclase appears to have replaced biotite. There is no textural evidence for staurolite-breakdown to form kyanite or for garnet growth after staurolite. Therefore, in the staurolite-garnet schists, kyanite may have formed by reactions such as,

(12) chl + mu = ky + phlg + qtz + H_2O

(Bird and Fawcett, 1973)

or

(13) mu + qtz + Na^+ = ab + Al_2SiO_5 + K^+ + H_2O

(Chinner, 1967).

Chlorite was consumed during garnet- and staurolite-producing reactions and thus was probably not available for kyanite formation. Therefore, reaction (12) could not have produced kyanite in the staurolite-garnet schist. Textural observations suggest that a reaction similar to (13), but involving biotite and Ca^+ as reactants with quartz, formed kyanite and oligoclase.

6.2.2 Mafic Rocks

Reactions in mafic schists are generally continuous, and thus chemical analyses of all co-existing phases are required to understand fully phase equilibria in these rocks (Laird, 1980). Consequently, reactions in the mafic rocks were not examined in detail, although reactions consistent with observed changes in mineral assemblages can be used to constrain general P-T conditions. P_{H2O} is assumed equal to P_{TOTAL} although in some cases this may

be invalid (see below). Oxygen fugacity cannot be estimated as buffering assemblages are not present in any of the mafic rocks.

The lowest grade mineral assemblage observed in the Faribault Brook metavolcanics (chl-ep-act-pl-qtz-ilm ± hb) is characteristic of the epidote-amphibolite facies. Microtextures in the low-grade metavolcanic rocks are generally equivocal, although epidote has grown in plagioclase porphyroclasts, amphibole has overprinted chlorite, and where actinolite and blue-green hornblende co-exist, hornblende has overprinted the former. Microprobe analyses of the minerals in the Faribault Brook metavolcanics were not obtained in this study although Craw (1984, and unpublished data) identified oligoclase (An_{19-22}) and magnesian chlorite, consistent with epidote-amphibolite facies conditions (Turner, 1981; Cooper, 1972).

Figure 6.4 shows experimental phase equilibria for chlorite, epidote, and tremolite stability at different f_{O2} and phase equilibria for basaltic systems at amphibolite and granulite facies conditions. Phase equilibria governing the prehnite-pumpellyite to greenschist facies transition for various f_{O2} were experimentally and theoretically determined by Liou et

Figure 6.4. Experimental and theoretical phase equilibria for mafic rocks. References for reactions are (1), (2), and (3) Liou et al., 1985; (4) and (7) Liou, (1973); (5) and (6a,b) Liou et al., 1974; (8a,b) Spear, 1976; (8c,d) and (9) Binns, 1969; (10) Yoder and Tilley, 1962. Reaction (1) is referred to as reaction (17) in the text. Arrow shows the direction this reaction boundary shifts for increasing Fe^{3+} in epidote. Reaction numbers do not correspond to those referred to in text. Oxygen buffers: HM=hematite-magnetite; QFM=quartz-fayalite-magnetite; NNO=Ni-NiO. Dark shading = estimated peak temperature range for the Faribault Brook metavolcanics at 6-8 kb. Stippled area = estimated peak temperatures for the garnet amphibolites at 6-8 kb.

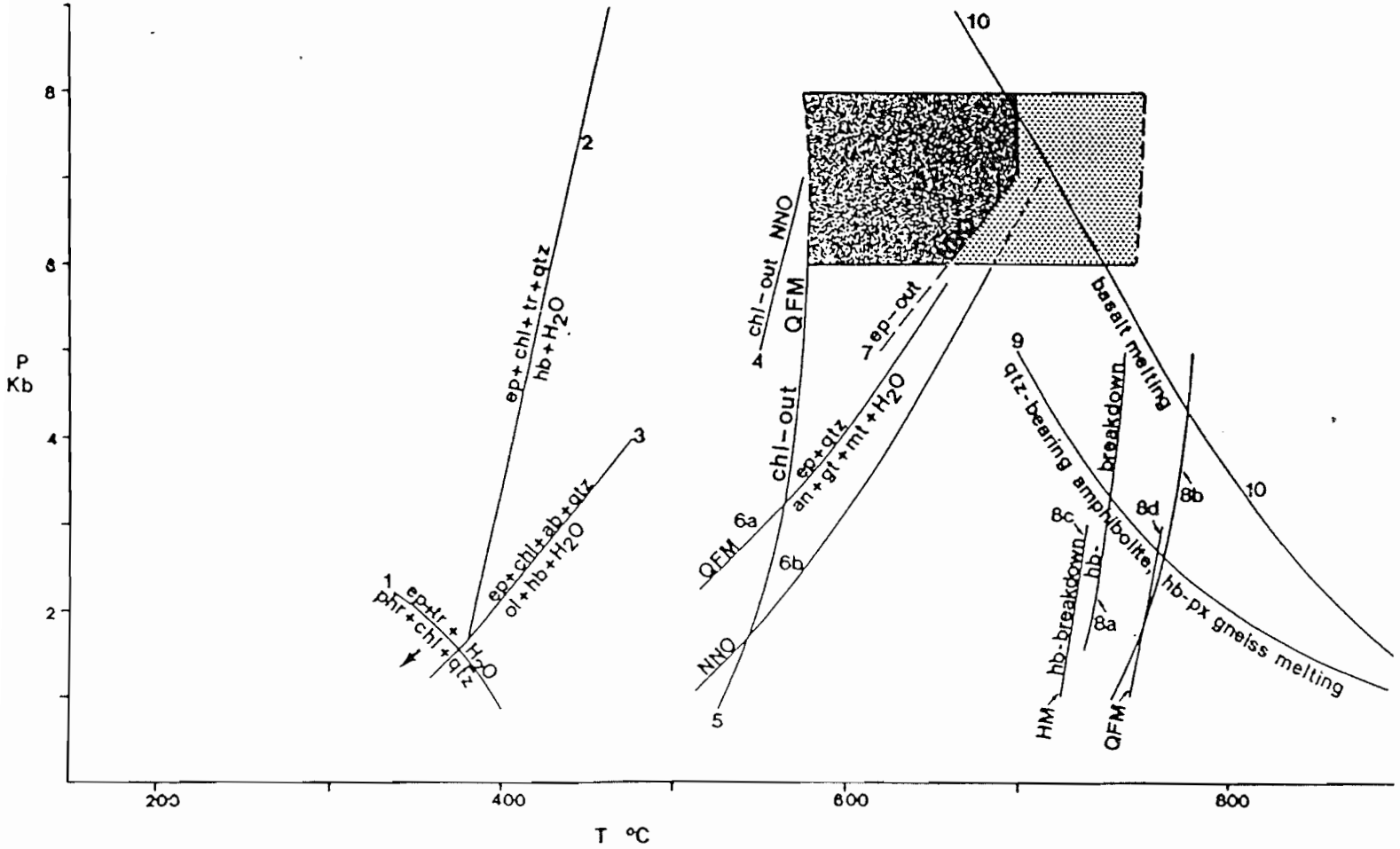
P
Kb
8
6
4
2
200
400
600
800
T °C
1
ep+tr+
phr+chl+qtz
H2O
2
ep+chl+tr+qtz
hb+H2O
3
ep+chl+ab+qtz
ol+hb+H2O
4
chl-out
NNO
QFM
5
6a
6b
chl-out
ep+qtz
an+gt+ml+H2O
ep-out
QFM
NNO
9
qtz-bearing amphibolite
hb-px gneiss melting
basalt melting
breakdown
10
8a
8b
8c
8d
hb-breakdown
hb-
HM
QFM

Figure 6.4.

al. (1985) in a model basaltic system Na_2O - CaO - MgO - Al_2O_3 - SiO_2 (NCMAS) (Figure 6.4).

The lack of mineral analyses for the Faribault Brook metavolcanics precludes assessment of any continuous reactions which may have operated during metamorphism, although microtextures indicate hornblende production from the assemblage epidote-chlorite-tremolite supporting the reaction

(14) ep + chl + tr = hb + H_2O (Liou et al., 1985).

The co-existence of chlorite and epidote with hornblende suggests temperatures in the range of about 400° to 575°C depending on pressure, f_{O2} and P_{H2O} (Figure 6.4). Ilmenite is the major oxide in the Faribault Brook metavolcanics which suggests low f_{O2} during prograde metamorphism. Phase equilibria in Figure 6.4 are based on the assumption that $P_{H2O} = P_{TOTAL}$ but whether this is valid for the Faribault Brook metavolcanics is uncertain. Synmetamorphic carbonate veins in the Faribault Brook metavolcanics suggest $P_{TOTAL} = P_{CO2} + P_{H2O}$ in which case the temperatures of the dehydration equilibria in Figure 6.4 would be lowered. Consequently, the temperature range of 400° to 575°C provides a qualitative estimate of

metamorphic conditions, and the upper temperature limit is a maximum if $P_{H2O} < P_{TOTAL}$. These temperatures agree well with those estimated for the interlayered Dauphinee Brook schist.

Mineral assemblages in the George Brook amphibolite do not vary significantly with metamorphic grade. The most notable change is the disappearance of zoned amphibole (tremolitic cores, blue-green hornblende rims) between the most westerly George Brook amphibolite exposures and the next exposures of this unit eastward along Corney Brook.

The amphibolites interlayered with the staurolite-garnet schists consist of hornblende, plagioclase, quartz, pyrite, ?ilmenite (rimmed by sphene), and locally, epidote. The hornblendites interlayered with the staurolite-garnet schists consists of hornblende, plagioclase, and rare opaque minerals (Appendix 1, Table A1.3). Epidote in the amphibolites locally defines isoclinal folds to which the pervasive foliation is axial planar. As these folds are interpreted to be synmetamorphic (section 4.3), epidote is interpreted to be prograde. Although oxides are lacking in this particular sample, epidote and hornblende stability suggests a range of approximately 550^{o} to 650^{o}C for 6 to

8 kb and range of f_{O2} between different buffers, and for $P_{H2O} = P_{TOTAL}$ (Liou et al., 1974 and Figure 6.4). This temperature range is consistent with conditions inferred for the associated staurolite-garnet schists.

The stable mineral assemblage of the garnet amphibolites is hb+pl+gt+qtz+?ilm. Retrograde epidote after hornblende and plagioclase is common. Oxygen fugacity is not constrained by this assemblage.

No evidence for partial melting is found in the garnet amphibolite (see later). Determination of a temperature range for the garnet amphibolite is difficult because most phase equilibria are not been experimentally determined in the range 6 to 8 kb. Extrapolation of hornblende breakdown reactions up to 6 to 8 kb suggests a temperature range of approximately 660° to 760°C for $P_{H2O} = P_{TOTAL}$ ($X_{H2O} = 1$, f_{O2} = QFM buffer) is applicable. This is consistent for the temperature range estimated for elimination of garnet zonation. However, if melting of garnet amphibolite ($P_{H2O} = P_{TOTAL}$) occurs at similar P-T conditions to melting of quartz-bearing amphibolite and hornblende-pyroxene gneiss, then an upper limit of about 680°C is more probable (Figure 6.4).

6.3 RETROGRADE METAMORPHISM

6.3.1 Pelitic Rocks

Biotite in the mica(-garnet) schist of the Dauphinee Brook schist is commonly replaced by chlorite and K-feldspar whereas in the staurolite-garnet schists it is commonly pristine and locally replaced by chlorite. Chayes (1955) proposed the reaction

(15) $\quad chl + K\text{-}fsp = bi + H_2O$

which may govern biotite retrogression in the Dauphinee Brook schist, but this reaction has not been experimentally determined.

Post-S_2 chlorite porphyroblasts have nucleated on biotite in all the medium- and high-grade rocks of the Dauphinee Brook, Corney Brook, and Fishing Cove River schists. Based on microstructures and mineral assemblages these porphyroblasts are interpreted to be retrograde.

Jamieson (1987, unpublished data) has documented a reaction related to the intrusion of the 365 Ma Salmon Pool pluton which has effectively caused retrogression of the high temperature, regional metamorphic mineral

assemblages in the staurolite-garnet schists exposed along the Cheticamp River. The inferred reaction,

(16) st + qtz = cd + Al_2SiO_5 (andalusite) + H_2O

was proposed by Bickle and Archibald (1984). The temperature range of this reaction (approximately 500 ^{o} to 600^{o}C) is related to contact metamorphism, and thus has no bearing on the regional metamorphic cooling, but does provide a pressure-time constraint for the region of 2 to 3 kb at 365 Ma.

6.3.2 Mafic Rocks

Retrogression of the major minerals in the Faribault Brook metavolcanics is difficult to separate from the prograde effects. Retrogression in the George Brook amphibolite and and hornblendites consists mainly of sericitization of plagioclase and minor chloritization of hornblende. This does little to constrain the retrograde P-T conditions except that chlorite is stable below about 550^{o}C in metabasites (Figure 6.4).

However, a late synmetamorphic vein in epidote-amphibolite grade George Brook amphibolite on Corney Brook does provide some constraint on retrograde P-T

conditions. It consists primarily of a patchy intergrowth of tremolite with minor hornblende (Table 5.10), epidote, prehnite, and chlorite. This assemblage suggests P-T conditions transitional between the prehnite-actinolite and greenschist facies (Liou et al., 1985) which is governed by the reaction:

(17) pr + chl + qtz = ep + tr + H_2O

This reaction limits the retrograde path to approximately 2.0 kb or less at 400°C or less, depending on f_{O2} and P_{H2O} (Figure 6.4).

6.4 ISOGRADS

Discontinuous exposure precludes well constrained regional definition of isograds across the map area. The first appearance of metamorphic index minerals depends on bulk composition as well as pressure, temperature, and fluid composition. For example, in the garnet-biotite zone, garnet-free and garnet-bearing pelitic and semipelitic schists are interlayered. Similarly, in the staurolite-kyanite zone, semipelitic to psammitic schists lack kyanite and locally staurolite, which are present in

the interlayered staurolite-garnet schists. Hence, in the absence of whole rock composition data, true isograds cannot be defined and those shown on Map 1 (back pocket) are approximate.

Hornblende-bearing semipelites and ?wollastonite-diopside marbles exposed approximately 75 m and 375 m, respectively (horizontal distance), structurally below the staurolite-garnet schists suggest the transition from epidote-amphibolite to amphibolite facies conditions occurs west of the staurolite-garnet schists. Therefore, although partly controlled by bulk rock composition, staurolite and kyanite development in the staurolite-garnet schists marks an approximate staurolite+kyanite-in isograd. The staurolite-out isograd marks the staurolite-kyanite zone to kyanite zone transition. The garnet isograd is defined on the first appearance of almandine garnet with low $(X_{Mn})_{Gt}$ rims. The garnet co-existing with chloritoid or biotite in the low-grade phyllites is relatively spessartine-rich, and therefore, these rocks are placed in the biotite zone. The appearance of biotite before garnet is consistent with the Dalradian Barrovian sequence (eg. Atherton, 1977).

6.5 GEOTHERMOMETRY AND GEOBAROMETRY

Geothermometry and geobarometry based on mineral exchange equilbria have gained wide acceptance in metamorphic petrology (Essene, 1982) but are still subject to many limitations (eg. Powell, 1985). Aside from commonly encountered problems of disequilibrium, retrograde re-equilibration, and uncertain cation site-distribution, one of the major weaknesses in geobarometry and geothermometry is the scarcity of reliable thermodynamic data on the effects of non-ideal solid solutions.

Exchange geothermometers and solid-solid reaction geothermobarometers generally involve solid solutions. Assessment of the effect of solid solution on equilibrium requires a knowledge of the relevant activity coefficient (γ) and the mixing or Margules parameter (W). These are rarely known for P and T of geologic interest (eg. Orville, 1972). In addition, the nature of the non-ideal solution model (symmetrical, regular binary, ternary, or quaternary) must be assumed (eg. Ghent et al., 1979; Hodges and Spear, 1982). To avoid these unknowns, geothermometers and geobarometers have been calibrated with synthetic minerals of known composition (Ferry and

Spear, 1978), and assuming ideality (eg. Ghent, 1976; Ferry and Spear, 1978; Graham and Powell, 1984). Other workers have estimated W and γ empirically, experimentally, or thermodynamically (eg. Hodges and Spear, 1982). However, the problem of which values to use for these parameters still remains. Most authors employ the reasoning that if a T or P calculated with certain W and γ agrees within error with an independently determined T or P, the parameters are acceptable. This is a reasonable argument considering the present state of thermodynamics but does not validate these parameters considering the error ($\pm$ 50°C and approximately 2 kb) in most geothermometers and geobarometers. Yet to assume ideality is clearly in error.

Application of solid-solid (fluid-absent) equilibria to the schists of the Jumping Brook metamorphic suite (quartz-Al_2SiO_5-plagioclase-garnet, Ghent, 1976 and garnet-biotite-muscovite-plagioclase, Ghent and Stout, 1981) requires assessment of non-ideality and a temperature estimate. Most workers use temperatures derived from a cation exchange geothermometer, such as the biotite-garnet geothermometer. However, most exchange geothermometers require a pressure estimate in order to calculate a temperature, and so a circular problem arises

in which a pressure is required to calculate a temperature and vice versa. In addition, the garnet-biotite-muscovite-plagioclase geobarometer is calibrated against, and therefore dependent on, garnet-biotite and garnet-plagioclase-Al_2SiO_5-quartz equilibria.

As no universally accepted solution to these problems exists, temperatures for the Jumping Brook metamorphic suite have been calculated using empirical geothermometers or those where ideality is assumed. Metamorphic pressures are calculated using the garnet-plagioclase-Al_2SiO_5-quartz (Ghent, 1976; Ghent et al., 1979). Calculated pressures are compared to those documented in the literature for Barrovian terranes, to estimates made by comparison of calculated temperatures to the Al_2SiO_5 phase diagram, and to mineralogical considerations. Tables 6.2 and 6.3 list the definitions of the parameters used in geobarometry and geothermometry calculations.

6.5.1 Temperature Estimates

Metamorphic "equilibrium" temperatures for 3 samples of the Corney Brook schist and 2 samples of Fishing Cove River schist (Table 6.4) were calculated using the calibrations of the garnet-biotite exchange

Table 6.2. Definitions of mole fractions used in geobarometry and geothermometry calculations (see Table 6.3).

$(X_{Fe})^{Gt} = Fe/(Fe + Mg + Ca + Mn)$

$(X_{Ca})^{Gt} = Ca/(Fe + Mg + Ca + Mn)$

$(X_{Mg})^{Gt} = Mg/(Fe + Mg + Ca + Mn)$

$(X_{Mn})^{Gt} = Mn/(Fe + Mg + Ca + Mn)$

$(X_{Fe})^{Hb} = Fe/(Mg + Mn + Fe + Ti + Al^{vi})$

$(X_{Mg})^{Hb} = Mg/(Mg + Mn + Fe + Ti + Al^{vi})$

$(X_{Fe})^{Bi} = Fe/(Fe + Mg + Ti + Al^{vi})$

$(X_{Mg})^{Bi} = Mg/(Fe + Mg + Ti + Al^{vi})$

$(X_{Ca})^{Pl} = Ca/(Ca + Na + K)$

$(X_{Na})^{Pl} = Na/(Ca + Na + K)$

Table 6.3. Summary of the distribution coefficients and equations used in geobarometry and geothermometry. Chemical formulae of minerals are given in the text. Definitions of the mole fractions are listed in Table 6.2. References are (1) Ferry and Spear (1978), (2) Hoinkes (1986), (3) Graham and Powell (1984), and (4) Ghent et al. (1979). Pressure in bars, temperature in Kelvin for all equations.

EQUILIBRIA	K_D	EQUATION	REFERENCE
almandine + phlogopite = pyrope + annite	$\frac{(X_{Mg})^{Gt}\,(X_{Fe})^{Bi}}{(X_{Fe})^{Gt}\,(X_{Mg})^{Bi}}$	$0=12{,}454-4.662(T)+0.057(P)+3RT\ln K_D$	1
as above	as above	$T=\frac{2089+0.00956(P)}{0.7821-\ln K_D-2.978(X_{Ca})^{Gt}+5.906((X_{Ca})^{Gt})^2}$	2
1/4 ferro-pargasite + 1/3 pyrope = 1/4 paragasite + 1/3 almandine	$\frac{(X_{Fe})^{Gt}/(X_{Mg})^{Gt}}{(X_{Fe})^{Hb}/(X_{Mg})^{Hb}}$	$T=\frac{2880+3280\,(X_{Ca})^{Gt}}{\ln K_D+2.426}$	3
3 anorthite = grossular + $2Al_2SiO_5$ + quartz	$K_D=K_S K\gamma$ $K_S=\frac{((X_{Ca})^{Gt})^3}{((X_{Ca})^{Pl})^3}$ $K\gamma=\frac{((\ Ca)^{Gt})^3}{((\ Ca)^{Pl})^3}$	$0=-\frac{3272}{T}+8.3969-\frac{3448(P-1)}{T}+\log K_s-\log K\gamma$	4

Table 6.4. Garnet-biotite temperatures calculated for the Dauphinee Brook, Corney Brook, and Fishing Cove River schists. T_1 = Thompson (1976) calibration, T = Ferry and Spear (1978) calibration, T_3 = Hoinkes (1986) calibration. Error on all calculated temperatures is ±50°C. K_D as defined in Table 6.3. Mole fractions as defined in Table 6.2. Pressures calculated by comparison of T_1 to the Al_2SiO_5 - diagram of Holdaway (1971) for kyanite-bearing samples. "CT" samples are those collected and analysed by Conrod (1984).

SAMPLE	PAIR	K_D	T_1°C	T_2 °C	T_3 °C	P kb	$(X_{Mn})^{Gt}$	$(X_{Ca})^{Gt}$	$\frac{(Ti+Al^{Vi})}{(Ti+Al^{Vi}+Fe+Mg)^{Bi}}$	$\frac{(Ca+Mn)^{Gt}}{(Ca+Mn+Fe+Mg)}$
85-659	1	0.1590	537	542-548	616-622	5	0.004	0.0888	0.19	0.09
(st-ky)	2	0.1550	529	535-540	620-626	5	0.003	0.1090	0.05	0.11
85-723b (st-ky)	1	0.1626	546	549-555	628-634	5	0.033	0.0940	0.20	0.13
85-722	1	0.1012	444	423-427	464-469	4	0.045	0.0670	0.19	0.11
(st-ky)	2	0.1563	539	537-542	613-619	5	0.031	0.0807	0.19	0.11
85-441	1	0.1870	581	596-602	647-653	5	0.075	0.0508	0.20	0.13
(ky)	2	0.2469	660	709-715	777-785	6	0.051	0.0553	0.20	0.11
85-446	1	0.2030	600	626-632	683-690	6	0.099	0.0534	0.19	0.15
(ky)	2	0.2100	611	639-645	701-707	6	0.097	0.0455	0.18	0.14
CT-24 (bio)	1	0.1699	559	564-567	612-618		0.012	0.0524	0.20	0.06
CT-3T (gt)	1	0.1396	509	504-509	575-581		0.030	0.0960	0.19	0.13
CT-81 (st-ky)	1	0.1470	514	519-524	678-684	4	0.008	0.1220	0.19	0.13
CT-57B (ky)	1	0.2125	611	644-650	685-691	6	0.033	0.0361	0.20	0.07

geothermometer by Thompson (1976), Ferry and Spear (1978), and Hoinkes (1986). The latter applies a correction for Ca in garnet to the Ferry and Spear (1978) calibration. Temperatures were also calculated for two medium-grade garnet-biotite schists (Dauphinee Brook schist, CT24 and CT31), one staurolite-garnet schist (Corney Brook schist, CT81) and a high-grade biotite-(kyanite) schist (Fishing Cove River schist, CT54B) from French Mountain collected and analysed by Conrod (1984). Temperatures for the garnet amphibolite (Table 6.5) were calculated using the garnet-hornblende geothermometer of Graham and Powell (1984). Estimated error for all calibrations is $\pm$ 50°C.

(i) Garnet - Biotite Geothermometry

Garnet-biotite geothermometry is based on the temperature dependence of Fe^{2+}-Mg^{2+} exchange between these phases. The governing reaction is:

(18) $\underset{\text{almandine}}{Fe_3Al_2Si_3O_{12}} + \underset{\text{phlogopite}}{KMg_3AlSi_3O_{10}(OH)_2}$

$$= \underset{\text{pyrope}}{Mg_3Al_2Si_3O_{12}} + \underset{\text{annite}}{KFe_3Si_3O_{10}(OH)_2}$$

The equilibrium constant (K_{EQ}) for this reaction can be written as

Table 6.5. Garnet-hornblende temperatures calculated using the calibration of Graham and Powell (1985).

SAMPLE	K_D	$(X_{Ca})_{Gt}$	T (^oC)	$Ca(x\text{-site})_{Hb}$
85-245	2.33	0.233	841 ± 50	1.957
85-343a	2.05	0.224	877 ± 50	2.023
	1.82	0.232	931 ± 50	1.890
85-280	2.71	0.221	780 ± 50	1.898

$$K_{EQ} = \frac{(X_{Mg})^{Gt}.(X_{Fe})^{Bi}}{(X_{Fe})^{Gt}.(X_{Mg})^{Bi}}$$

and, assuming ideality, $K_{EQ} = K_D$. Ca and Mn substitution in garnet results in preferential Fe^{2+} substitution in garnet (Dallmeyer, 1974), causing a systematic decrease in K_D and a corresponding apparent temperature increase. Conversely, an increase in octahedral Ti, Al, and Fe^{3+} in biotite causes preferential Fe^{2+} substitution in biotite (Dallmeyer, 1974) and hence an increase in K_D and a corresponding temperature decrease.

Generally, the Thompson calibration yields temperatures that are lower than, but agree within error with, the Ferry and Spear calibration (eg. Ferry and Spear, 1978; Ghent et al., 1979; Barber and Yardley, 1985; Treloar, 1985). This is probably due to substitutions in garnet and biotite (as discussed above) in the natural garnet-biotite pairs used in the Thompson (1976) calibration. Ferry and Spear (1978) used synthetic garnets ($Alm_{80}Py_{20}$ and $Alm_{90}Py_{10}$) thereby avoiding this problem. Hoinkes' (1986) correction to Ferry and Spear's (1978) calibration is based on an empirical relationship between $\ln K_D$ and $(X_{Ca})^{Gt}$ and gives higher temperatures

than those calculated using the Ferry and Spear (1978) and the Thompson (1976) calibrations (Hoinkes, 1986).

The pressure range used in the temperature calculations is 5.0 to 6.5 kb based on estimates discussed in a later section. Calculated temperatures generally increase in order of calibrations by Thompson (1976), Ferry and Spear (1978), and Hoinkes (1986) (Table 6.4). Figure 6.5 shows that, although some correlation between $\ln K_D$ and $(X_{Ca})^{Gt}$ exists in the Corney Brook and Fishing Cove River schists, it is not the same as that determined by Hoinkes (1986). Therefore the Hoinkes (1986) correction is inapplicable to these rocks and resulting temperatures (Table 6.4) have been disregarded.

Table 6.4 shows no clear correlation between temperature and $(X_{Mn})^{Gt}$ or $(X_{Ca})^{Gt}$. All garnet-biotite pairs border on or exceed the limits for $(X_{Mn+Ca})^{Gt}$, $(X_{Ti+Al^{vi}})^{Bi}$ suggested by Ferry and Spear (1978) (Table 6.4). However, the temperatures calculated by the Thompson (1976) and Ferry and Spear (1978) calibrations agree within error and are inferred to be reliable. The temperature range (423° to 715°C) calculated by the Ferry and Spear calibration is used for convenience, in subsequent calculations and geological interpretations.

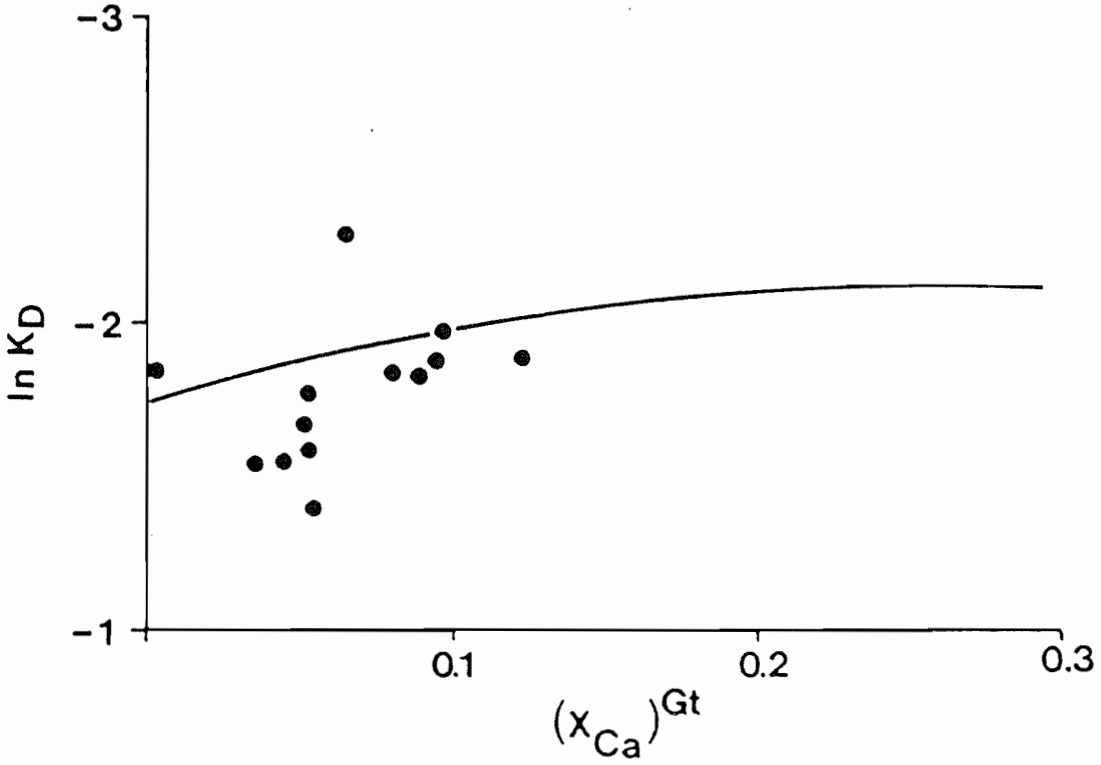

Figure 6.5. Plot of $\ln K_D$ versus $(X_{Ca})^{Gt}$ for samples used in garnet-biotite geothermometry compared to the correlation observed by Hoinkes (1986) (solid line), showing the absence of a simple relationship between $\ln K_D$ and garnet composition in the Jumping Brook metamorphic suite.

(ii) Garnet-Hornblende Geothermometry

Fe^{2+}-Mg^{2+} exchange between garnet and hornblende is governed by the reaction:

(19) $$1/4\ \underset{\text{(ferro-pargasite)}}{NaCa_2Fe_4Al_3Si_6O_{22}(OH)_2} + 1/3\underset{\text{(pyrope)}}{Mg_3Al_2Si_3O_{12}} =$$

$$1/4\ \underset{\text{(pargasite)}}{NaCa_2Mg_4Al_3Si_6O_{22}(OH)_2} + 1/3\ \underset{\text{(almandine)}}{Fe_3Al_2Si_3O_{12}}$$

(Graham and Powell, 1984). Assuming garnet and hornblende are ideal solid solutions and Fe^{2+}-Mg^{2+} distribution in the octahedral sites is disordered, the equilibrium constant is equivalent to the distribution coefficient:

$$K_{EQ} = K_D = \frac{(X_{Fe})^{Gt}/(X_{Mg})^{Gt}}{(X_{Fe})^{Hb}/(X_{Mg})^{Hb}}$$

Graham and Powell (1984) calibrated this geothermometer against the clinopyroxene-garnet geothermometer of Ellis and Green (1979), which is relevant mainly to eclogitic rocks and has problems of non-ideal Ca-Mg substitutions in garnet and clinopyroxene. Since activity-composition relationships for end-member components in calcic amphibole solid solutions are unknown, Graham and Powell (1984) assumed that all non-ideality in the geothermometer is due to Ca-substituion in garnet. This assumption is probably

invalid but no better model is available. They also assume that all Fe in the amphibole is Fe^{2+} and therefore, the calculated temperatures are maxima. The garnet-hornblende thermometer is best applied to:

(1) rocks of amphibolite grade (i.e. 600° to 850°C), to validate the assumption that diffusion between garnet and hornblende closes near the thermal maximum,

(2) rocks with low f_{O2} so that Fe^{3+} in amphibole will be low

(3) $(X_{Mn})^{Gt} < 0.1$, thereby eliminating any need for an Mn-correction

(Graham and Powell, 1984). $(X_{Mn})^{Gt}$ is always <0.1. Since regional metamorphism is commonly a reducing process, Fe^{3+} should be low in most mineral phases. Thus, the garnet amphibolites of the Fishing Cove River schist meet these criteria.

Temperatures calculated for the garnet amphibolites (780° to 931°C, Table 6.5), using the garnet-hornblende geothermometer are up to 216°C higher than the garnet-biotite temperatures calculated for the high-grade biotite schists (samples 85-441, 85-446, Table 6.4), and are too high for the observed mineral assemblages.

Cation sums for the Y-site exceed 5.0 in analysed amphiboles from all the garnet amphibolite samples by about 0.4 cations (Table 5.10). This is commonly interpreted to reflect the presence of Fe^{3+} in amphibole, since if significant Fe^{3+} is present, calculation of the structural formula with all Fe as Fe^{2+} results in too much Fe in the Y-site (Hawthorne, 1981). It may also be due to some Fe^{2+} substitution into the X-site since Mg-substitution into the X-site is uncommon (Hawthorne, 1981). In either case, the result is to lower Fe^{2+}/Mg^{2+} in the hornblende Y-site, thus decreasing K_D and increasing calculated temperature (eg. Graham and Powell, 1984). For example, re-calculation of the garnet-hornblende temperature for 85-245, assuming 25% of the Fe is Fe^{3+}, yields a temperature of 750°C, 90°C less than that calculated assuming all Fe as Fe^{2+}.

Graham and Powell (1984) also noted a correlation between high $Ca(X\text{-site})_{Hb}$ and anomalously high temperatures. The anomalous samples excluded by Graham and Powell (1984) from their calibration database contain $Ca(X\text{-site})_{Hb} \geq 1.94$ based on cations/23 oxygens. This apparent correlation is due to calibration against the garnet-clinopyroxene geothermometer which is applicable to high pressure rocks, and thus to low Ca amphiboles.

Although no direct correlation with $Ca(X\text{-site})_{Hb}$ and garnet-hornblende temperatures is observed due to intersample variation in hornblende Y-site composition, all but one sample (85-343A) have >1.94 $Ca(X\text{-site})_{Hb}$ (Table 6.5). Therefore, high $Ca(X\text{-site})_{Hb}$ may be partly responsible for the high garnet-hornblende temperatures presumably by causing non-ideal Fe-Mg exchange between garnet and hornblende. Similarily, $(X_{Ca})^{Gt}$ is high, averaging about 0.23, which may cause non-ideality in Fe-Mg exchange. In addition, the lack of apparent chemical equilibrium (Figure 5.15) in the garnet-amphibolite may also contribute to the anomalous temperatures.

(iii) Geological Significance of Temperature Estimates

Calculated temperatures show a systematic increase with increasing metamorphic grade. However, garnet-biotite temperatures calculated for the staurolite-garnet schists (samples 85-659, 722,723, and CT81) may be meaningless as garnet and biotite apparently do not retain peak metamorphic compositions (case 1, section 5.9.2). Garnet-biotite temperatures calculated for case 2 samples (85-722 and 85-723B, Chapter 5) are too low or marginally acceptable for staurolite-kyanite zone rocks. However, the chemical evidence for retrograde cation

exchange between garnet and biotite, the inter-sample temperature variation between closely spaced samples (eg. 85-722 and 85-723b), and the higher temperatures recorded by biotite included in garnet (537° to 542°C; Table 6.4, 85-722, pair 2) relative to biotite in the matrix (423° to 444°C; Table 6.4, 85-722, pair 1) indicate that these temperatures reflect differential, retrograde re-equilibration.

The best evidence for peak metamorphic temperatures comes from a garnet-biotite pair included in kyanite in the biotite schist (Figure 5.6c). This pair records a temperature of 660°C based on Thompson's calibration and a range of 709°c to 715°C ± 50°C using the Ferry and Spear (1978) calibration (Table 6.4, pair 2), consistent with temperature estimates for kyanite zone rocks based on phase equilibria, and with that for volume diffusion in garnet. The re-equilibration temperatures for biotite schist samples calculated using matrix garnet-biotite pairs range from 581° to 645°C ± 50°C (Table 6.4, 85-441, pair 1 and 85-446, pair 1&2).

6.5.2 Pressure Estimates

Few metamorphic reactions closely constrain in metamorphic pressures. Pressure estimates for Barrovian

metamorphic terranes commonly range between 5 and 10 kb (eg. Ghent et al., 1979; Moles, 1985). Minimum pressure estimates can be derived by comparing temperatures calculated using the P-independent empirical calibration for garnet-biotite Fe-Mg exchange (Thompson, 1976 - see below) with the Al_2SiO_5 diagram of Holdaway (1971). Clearly, errors in Thompson's (1976) calibration and the well documented uncertainty in the Al_2SiO_5 triple point (Althaus, 1967; Richardson et al., 1969; Holdaway, 1971; Salje, 1986) compound the error of these minimum pressure estimates. Since these samples must be within the stability field of kyanite, these estimates are minima for kyanite-bearing rocks. However, this approach avoids the circular problem previously discussed and provides a first-order approximation to minimum metamorphic pressures in the kyanite-bearing schists of the Jumping Brook metamorphic suite.

Estimated minimum pressures range from about 3.5 to 6.5 kb (rounded to the nearest integer in Table 6.4). The lowest pressure is determined for a sample which shows retrograde cation exchange between garnet and biotite. The upper pressure limit is estimated from the garnet-biotite pair interpreted to preserve "peak" compositions. Therefore, the minimum pressure range used in the

temperature calculations is 5.0 to 6.5 kb, consistent with general lower pressure limits for Barrovian terranes and the upper pressure limit estimated above (Table 6.4). The choice of this pressure range is further supported by experimental data (Hoschek, 1969; Richardson, 1968; Thompson, 1976) which suggest co-existence of kyanite and staurolite at 650 ^{o} to 700 ^{o}C and 6 to 8 kb (Figure 6.1 and 6.2). Temperature calculations are relatively insensitive to the pressure estimates. For example, a change in pressure of 1 kb translates into a temperature range of 3^{o}C for the Ferry and Spear (1978) calibration.

(i) Garnet-Plagioclase-Al_2SiO_5-Quartz Geobarometer

The plagioclase-garnet-Al_2SiO_5-quartz geobarometer (Ghent, 1976; Ghent et al., 1979) is based on Ca-exchange between garnet and plagioclase by the reaction:

(20) $$\underset{\text{anorthite}}{3CaAl_2Si_2O_8} = \underset{\text{grossular}}{Ca_3Al_2Si_3O_{12}} + 2Al_2SiO_5 + \underset{\text{quartz}}{SiO_2}$$

Various estimates of the relevant mixing parameters and activity coefficients have been reported (eg. Hodges and Spears, 1982; Ghent, 1976; Ghent et al. 1979) but no values are universally accepted. Ghent et al. (1979) used an empirical estimate of the activity coefficient product

(K_γ) of log K = -0.4 for kyanite-bearing samples near the kyanite-sillimanite boundary. In the absence of any better estimate, this value is used here.

Pressures of 4 to 8 kb (Table 6.6) were calculated for kyanite-bearing samples using the minimum and maximum garnet-biotite temperatures (Ferry and Spear, 1978). Ghent et al. (1979) quote an error of $\pm$ 1.6 kb for this geobarometer. This pressure range is consistent with the estimated minimum range of 5.0 to 6.5 kb. As most of the garnet-biotite temperatures used in the pressure calculations are re-equilibrated and therefore minima, these pressures are also minima. The most reliable are those calculated using the apparent peak temperatures which give a range of about 7.5 to 8.0 kb. The complete P-T ranges calculated using pressures estimated from both techniques and temperatures from the Ferry and Spear (1980) calibration are shown in Figure 6.6.

6.6 PARTIAL MELTING

The estimated peak temperatures of 660° to 715 °C $\pm$ 50 °C at 6 to 8 kb are sufficiently high for "wet" melting ($P_{H2O}=P_{TOTAL}$, $X_{H2O}=1.0$) of muscovite-bearing pelites (Thompson, 1982), but temperatures of >700 °C are

Table 6.6. Pressures calculated using the plagioclase-garnet-Al_2SiO_5-quartz geobarometer of Ghent (1976) and Ghent et al. (1979). T_1 = lower temperature and T_2 = higher temperature calculated by Ferry and Spear (1978) calibration of the garnet-biotite geothermommeter. P_1 and P_2 are the calculated pressures corresponding to T_1 and T_2. $K\gamma$ from Ghent et al. (1979). Kyanite is the stable Al_2SiO_5 polymorph in all samples. Temperatures in Kelvin, pressures in kilobars.

SAMPLE	log K_s	log $K\gamma$	T_1	P_1	T_2	P_2
85-722	-1.44	-0.4	696	3.8	815	6.0
85-723b	-1.50	-0.4	822	6.0	828	6.1
85-441	-1.89	-0.4	869	6.0	988	8.0
85-446	-2.24	-0.4	899	5.5	418	5.7

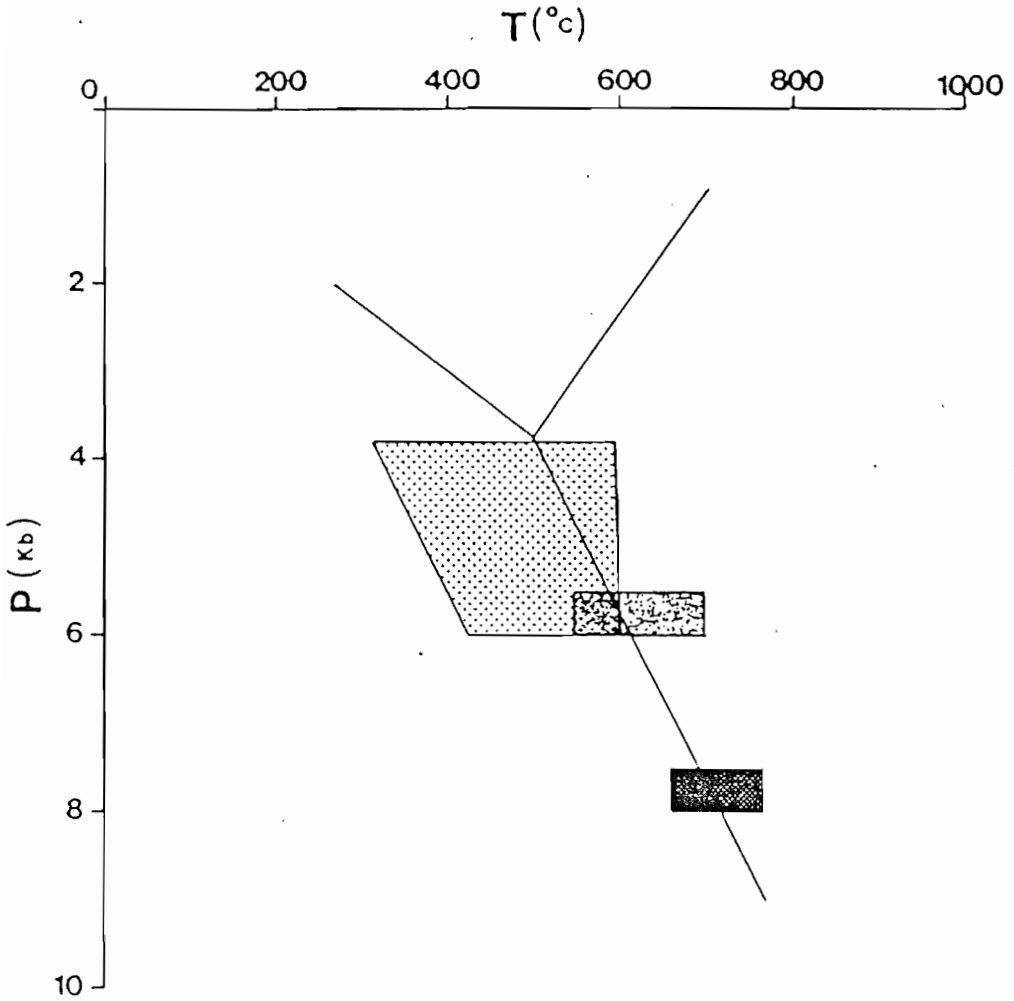

Figure 6.6. Range of P-T estimates determined using the garnet-biotite geothermometer and garnet-plagioclase-Al_2SiO_5-quartz geobarometer for the staurolite-garnet schists and the biotite schists. Dark stipple = peak P-T range for biotite schists, Medium grey shading = re-equilibrated P-T range for biotite schists, light stipple = re-equilibrated P-T range for the staurolite-garnet schists. Al_2SiO_5-triple point after Holdaway (1971) and Richardson et al. (1969) denoted by H and R, respectively.

required to produce a melt from a biotite-plagioclase (An_{50})-quartz mixture which contains significant amounts of potassic feldspar (Hoschek, 1976). Thus, it appears that the higher grade rocks of the Jumping Brook metamorphic suite border on the lower temperature limit required for melting.

Felsic layers and veins (leucosomes) in the high-grade biotite schists consist of strongly foliated, concordant, granitic pegmatites, interpreted by Currie (1987) as anatectic, and concordant and discordant centimetre-scale quartzo-feldspathic veins. However, it is unlikely that metamorphic segregation could produce the large volume of granite pegmatite observed. These pegmatites are more probably related to plutonism and may well be genetically related to the unnamed foliated felsic muscovite(-garnet) orthogneiss exposed in the upper reaches of Corney Brook and along Fishing Cove River, to the MacKenzie River orthogneiss, or to other plutons in the area.

The quartzo-feldspathic veins are composed of quartz, plagioclase, and minor apatite and biotite, and lack mafic selvages (melanosomes). However, the absence of K-feldspar in the leucosomes and associated melanosomes, and the stability of muscovite in the

highest grade rocks supports Craw's interpretation of hydrothermally induced metamorphic segregation for their origin. If $X_{H2O} < 1.0$ (see Figure 6.2) then melting of muscovite-bearing pelites is not possible at the temperatures estimated for the Jumping Brook metamorphic suite (Thompson, 1982).

6.7 PRESSURE-TEMPERATURE-TIME (P-T-t) PATH

Figure 6.7 illustrates the different ranges of P and T defined by phase equilibria, geobarometry and geothermometry, and garnet chemistry. A P-T-t path for the biotite schists of the Fishing Cove River schist constrained by these P-T ranges, is also shown in Figure 6.7.

Definition of the prograde P-T path of the Fishing Cove River schist is hindered by the lack of preservation of very early mineral assemblages. Assuming the metamorphic field gradient represents a locus of peak metamorphic P-T points for the Jumping Brook metamorphic suite, then the prograde path for the biotite schists was one of increasing pressure and temperature. Increasing temperature and probably pressure with time is also supported by the determined sequence of metamorphic

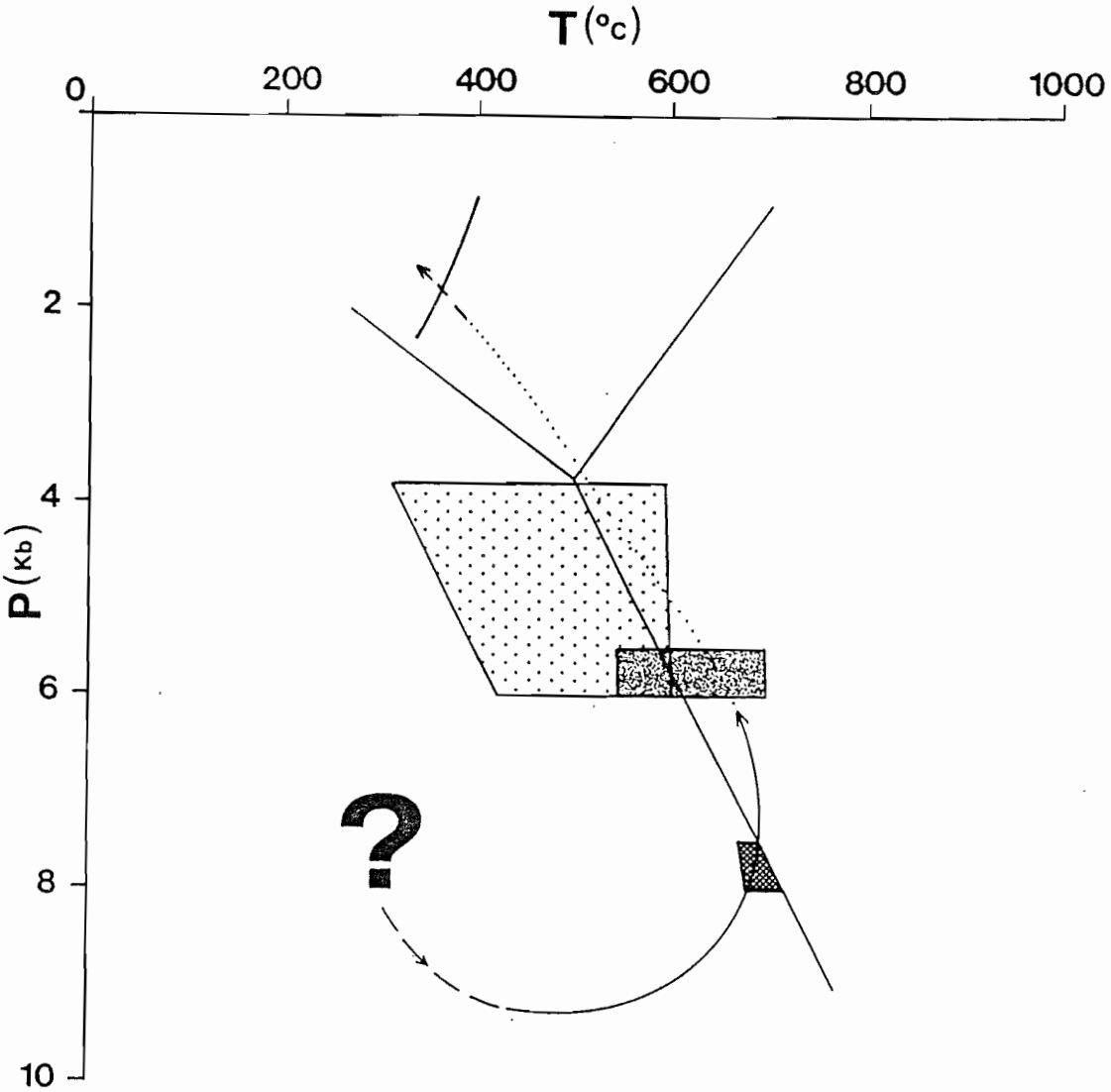

Figure 6.7. P-T-(relative) path for the Fishing Cove River schist (high-grade biotite schists) derived from porphyroblast-matrix relations, mineral reactions, mineral chemistry, geothermometry, and geobarometry. The prograde path is schematic. Peak P-T conditions are constrained by the kyanite=sillimanite boundary from Holdaway (1971), reaction (10), and pressures pf 7.75-8.0 kb calculated using the pl-gt-Al_2SiO_5-qtz geobarometer. P-T ranges (based on reset equilibria) for the Fishing Cove River (grey shading) and Corney Brook schist (light stipple) are shown for reference (see Figure 6.6). The retrograde path is partly constrained by reaction (17).

mineral growth, but dP/dT is unknown and therefore the prograde path shown in Figure 6.7 is schematic. Decreasing temperatures and pressures following peak metamorphism are suggested by re-equilibrated garnet-biotite exchange temperatures, retrograde mineral assemblages, and reaction (17), although dP/dT is not well constrained. The time component in Figure 6.7 is strictly relative and based on the interpreted sequence of metamorphic mineral growth. The general form of the P-T path is characteristic of metamorphism by crustal thickening (eg. overthrust terranes; Figure 6.8).

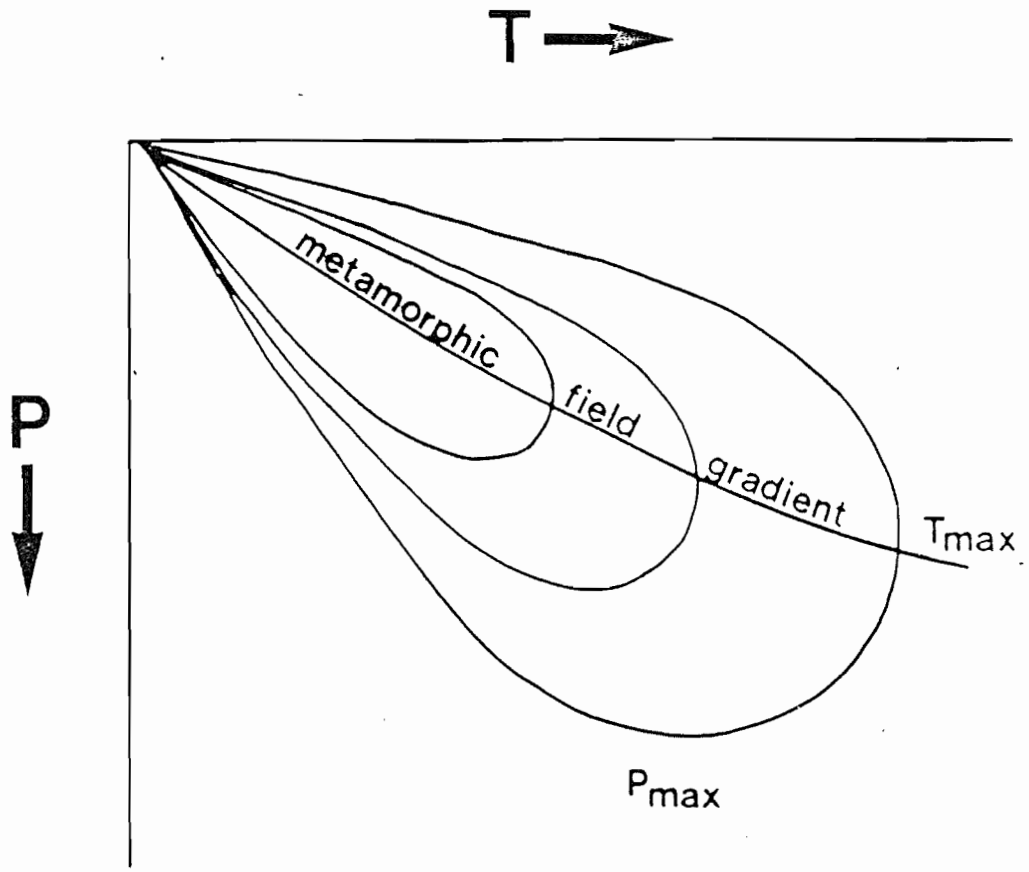

Figure 6.8. Generalized form of a P-T-t path for an overthrust region modified from Spear et al. (1984). Note that peak pressure conditions pre-date peak temperature conditions. Metamorphic field gradient= locus of "peak" P-T conditions for samples through a metamorphic belt.

CHAPTER 7

IMPLICATIONS FOR REGIONAL TECTONICS

7.1 INTRODUCTION

Quantitative thermal models, when combined with petrologic P-T-t paths and geochronology, can provide significant constraints on timing of metamorphism, uplift rates, and initial thermal conditions of the metamorphic rocks and hence, provide information on the tectonothermal history of the region. Cooling ages for the medium- to high-grade rocks of the Jumping Brook metamorphic suite are presented below. These ages and the partial P-T-t path derived in Chapter 6 are compared to P-T-t paths generated using a simple, one-dimensional computer model for overthrusting. The results have important implications for the tectonothermal history of the Jumping Brook metamorphic suite and its place in the tectonostratigraphic framework of the Appalachians.

7.2 METAMORPHIC COOLING AGES

In order to determine the timing and rate of metamorphic cooling in the Jumping Brook metamorphic suite, hornblende and biotite separates were analysed by

the ^{40}Ar-^{39}Ar age-spectrum method (Apppendix 2). Ideally, to gain information on metamorphic cooling rates, mineral separates of different phases (eg. hornblende, biotite, muscovite, K-feldspar) from the same rock, or from closely spaced samples that have experienced the same metamorphic history, should be analysed (eg. Cliff, 1985). However, amphibolites in the Jumping Brook metamorphic suite rarely contain biotite and in associated metasedimentary schists, biotite is commonly retrograded to chlorite and K-feldspar. In the biotite schists, where biotite is reasonably fresh, no closely spaced samples of biotite schists and amphibolites were collected. Consequently, only one hornblende-biotite pair from closely spaced samples was analysed.

Two hornblende separates were taken from 1 to 3 metre thick amphibolite layers in schlieren of the Fishing Cove River schist in the MacKenzies Mountain megacrystic orthogneiss of the Pleasant Bay Complex (samples 85-245 and 85-345). One hornblende separate was taken from a medium-grained amphibolite (sample 85-708b) which occurs approximately 15 metres (horizontal distance) from an exposure of George Brook amphibolite. The biotite separate comes from a biotite-muscovite-garnet schist (sample 85-707b) exposed approximately 25

metres (horizontal distance) structurally below sample 85-708b.

7.2.1 Age Spectra

Figure 7.1 presents the age spectra and corresponding plateau ages obtained for samples 85-245, 85-345, 85-708b, and 85-707b. A "reliable" plateau is that in which five contiguous gas fractions give consistent ages within 2σ error (eg. Berger and York, 1981). Some authors consider any number of contiguous gas fractions, representing 50% of the total ^{39}Ar-released and with corresponding ages that agree within 2σ, to define a "reliable" plateau (eg. Fleck et al., 1977). Based on these definitions, the hornblende spectrum for sample 85-345 shows a "reliable" plateau over 5 steps for 83.6% of argon released and a corresponding age of 383 Ma. Although not strictly "reliable", the hornblende spectrum for sample 85-245 shows a plateau over 2 steps for 41.8% Ar released at 2σ error corresponding to an age of 383 Ma, whereas that for sample 85-708b shows a plateau over 79.8% Ar released at 3σ with an age of 389 Ma. Since estimated error based on variation in J-values (Appendix 2) is approximately 4 Ma, these ages are remarkably consistent.

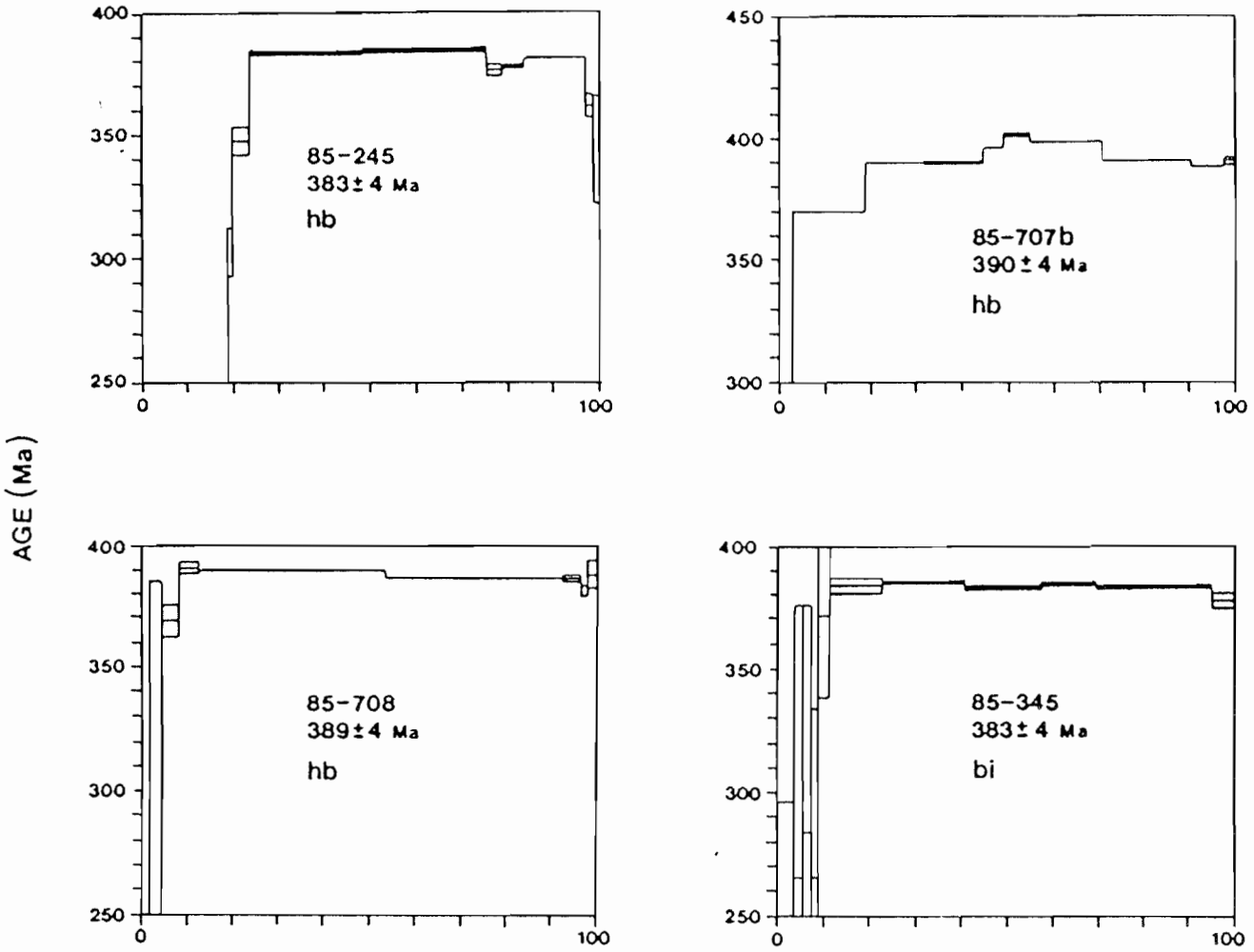

Figure 7.1. ^{40}Ar-^{39}Ar age spectra for three hornblende and one biotite separates. Plateau ages shown are weighted averages of all steps defining the plateau.

The biotite spectrum for sample 85-707b is disturbed and shows a small "hill" in the middle of the spectrum. This feature is very common in biotite but its cause is unknown (Reynolds, 1986, person. comm.). However, the spectrum age estimated by excluding the disturbed section of the spectrum is 390 Ma $\pm$ 4 Ma which agrees well with the hornblende ages obtained in this study and hornblende and biotite ages obtained in other work (see below). Therefore, this age is considered to be geologically significant.

7.2.2 Geological Interpretation of Cooling Ages

Since peak metamorphic temperatures are well above blocking temperatures for hornblende (500 $\pm$ 50°C) and biotite (300 $\pm$ 50 °C), the ages obtained are metamorphic cooling ages. Apparent ages for the hornblende and biotite from samples 85-708b and 707b, respectively, agree within error at approximately 385 Ma, suggesting rapid early Devonian cooling between 500 $\pm$ 50°C and 300 $\pm$ 50°C.

Similar cooling ages have been obtained in the Middle River area (Doucet, 1983) and the Money Point area (Plint, 1985, unpublished data; Reynolds, 1986, unpublished data) (Table 7.1). These regional similarities in metamorphic cooling ages in the western

Table 7.1. ^{40}Ar-^{39}Ar plateau ages for other parts of the western Highlands volcanic-sedimentary belt. Age-1 and -2 refer to original and duplicate analyses. Original and duplicate samples were irradiated separately. Hornblende spectra for the Money Point Group are highly discordant and therefore quoted ages are based on the highest temperature steps and require further investigation to assess their reliability. Cape North age-1 data from Plint (1985, unpublished), Cape North age-2 data and Middle River hornblende age from Reynolds (1986, unpublished). Middle River biotite age from Doucet (1983).

AREA	UNIT	MINERAL	AGE-1 (Ma)	AGE-2 (Ma)
Cape North	Money Pt Group	hornblende	410 ± 4	413 ± 4
Cape North	Money Pt Group	biotite	383 ± 4	389 ± 4
Middle River	Middle R. unit	hornblende	386 ± 9	-------
Middle River	Middle R. unit	biotite	390 ± 4	-------

Cape Breton Highlands indicate that the timing of metamorphic cooling was similar throughout the belt.

7.3 THERMAL MODELS

Quantitative thermal models for overthrust terranes based on the heat flow equation have been developed by various workers (eg. Oxburgh and Turcotte, 1974; England, 1978; England and Thompson, 1984; Royden and Hodges, 1984). These models calculate theoretical P-T-t paths for set thermal and physical conditions, such as slab thickness, erosion rate (linear or exponential), and heat flux from the mantle and due to decay of radiogenic crustal elements. Hence, these models provide a means of constraining the above parameters in overthrust terranes where geological P-T-t paths have been derived (eg. Droop, 1985).

A theoretical model for computing P-T-t paths (THRUST; Issler, 1985, unpublished) was applied to the Jumping Brook metamorphic suite in order to:

(1) reproduce the peak metamorphic conditions with the simplest possible combination of parameters,
(2) compare computed times of metamorphism and uplift with geochronological data, and

(3) constrain values of physical and thermal parameters of possible tectonic significance, such as burial depths, uplift rates, and heat flux.

The model assumes crustal thickening by thrusting of a single slab. Although there is no geological evidence supporting this assumption, variations in P-T-t paths generated by other thickening geometries (eg. homogeneous thickening, multiple thrust slabs) are within the detection limits of the available data.

7.3.1 The Model

The model assumes heat transfer by conduction in one dimension (vertical), and instantaneous thrusting of a single slab onto continental crust with a steady-state geotherm. Erosion begins immediately after thrusting and continues until the thrust slab is completely eroded (cf. England and Thompson, 1984). Surface temperature is fixed at $0^{o}C$ and a constant mantle heat flux (q_{*}) is prescribed at the base of the lithosphere (d_1 = 150 km). THRUST is similar to the model developed by England and Thompson (1984) but uses the finite element method to solve the heat conduction equation.

P-T-t paths are generated for constant depth points (10, 20, 30, 40 km) below the initial (post-thrusting)

surface. The factor affecting the burial depth of a given depth point is the thrust slab thickness. The thermal and physical parameters required by THRUST are listed in Tables 7.2 and 7.3.

7.3.2 Parameters

Table 7.2 lists the thermal parameters for the different heat source distributions (I, II, III) used by England and Thompson (1984) and used here for initial model runs. Given the wide range of rock compositions in the Jumping Brook metamorphic suite, their intermediate value for thermal conductivity (2.25 $Wm^{-1}K^{-1}$) was chosen for all model runs. Table 7.3 lists the physical parameters used in the study. The thicknesses of the radiogenic heat-producing layer (d_r), of the crust (d_c), and of the subcrustal lithosphere (d_l - d_c) are taken from England and Thompson (1984). The initial time of thrusting, thickness of the thrust slab, erosion rate, and erosion time constant are constrained by geology.

The initial time of thrusting is taken to be 430 Ma based on the zircon age of 433 Ma $\pm$ 20 Ma obtained for the apparently syntectonic Belle Cote Road orthogneiss (Jamieson et al., 1986). Slab thicknesses of 10, 15, and 20 km were used in initial model runs to determine the effect of variation in slab thickness on resultant P-T-t

Table 7.2. Thermal parameters used in model runs.

PARAMETER	SYMBOL	I	II	III
Thermal conductivity ($Wm^{-1}K^{-1}$)	K	1.5	2.25	3.0
Thermal diffusivity (m^2s^{-1})	k	$6*10^{-7}$	$9*10^{-7}$	$1.2*10^{-6}$
Heat content ($JK^{-1}m^{-3}$)		-------- $2.25*10^6$ --------		
Radiogenic heat production (μWm^{-3})	r	1.666	2.000	2.333
Mantle heat flow (mWm^{-2})	q*	20	30	40

Table 7.3. Physical parameters used in the model runs.

PARAMETER	SYMBOL	VALUE
Thickness of radiogenic heat producing layer	d_r	15 km
Thickness of crust	d_c	35 km
Thickness of subcrustal lithosphere where d_l = thickness of lithosphere	$d_l - d_c$	150 km
Initial time of thrusting		430 Ma
Thickness of thrust slab	S	10, 15, 20 km
Erosional time constant	τ	60 Ma

Exponential Erosion

$S = S_o e^{-t/\tau}$

where S(t) = thickness of overthrust at time t
S_o = initial thrust slice thickness
τ = time constant (Ma)

Linear Erosion

$S = S_o - Et$

where E = erosion rate (m/Ma)

paths. An exponential erosion rate is assumed and a time constant of 60 Ma is used to allow erosion back to approximately pre-thrust thickness in 430 Ma. Therefore, the parameters varied in the the model runs are (1) radiogenic heat production (r), (2) mantle heat flux (q_*), and (3) thrust slab thickness (S). Mantle heat flux and radiogenic heat production are referred to collectively as the heat source distribution.

7.3.3 Effects of Parameter Variation

Figure 7.2 shows P-T-t paths for the heat source distributions I, II, III (Table 7.2 and 7.3) used by England and Thompson (1984) for slab thicknesses of 10, 15, 20 km. Figure 7.2 shows that variation in slab thickness affects the general shape of the P-T-t path due to its effect on erosion rate and hence on dP/dT. Erosion back to pre-thrusting crustal thicknesses must occur in 430 Ma and thus the thicker the thrust slab, the higher the erosion rate. This is reflected in the broader P-T-t curve derived for a thick thrust slab (20 km) relative to that for a thinner slab (10 km). For a well defined petrological P-T-t path, this variation might be distinguishable for a minimum difference in slab thickness of 10 km where resultant pressure differences are approximately 2 to 3 kb (200-300 MPa) and temperature

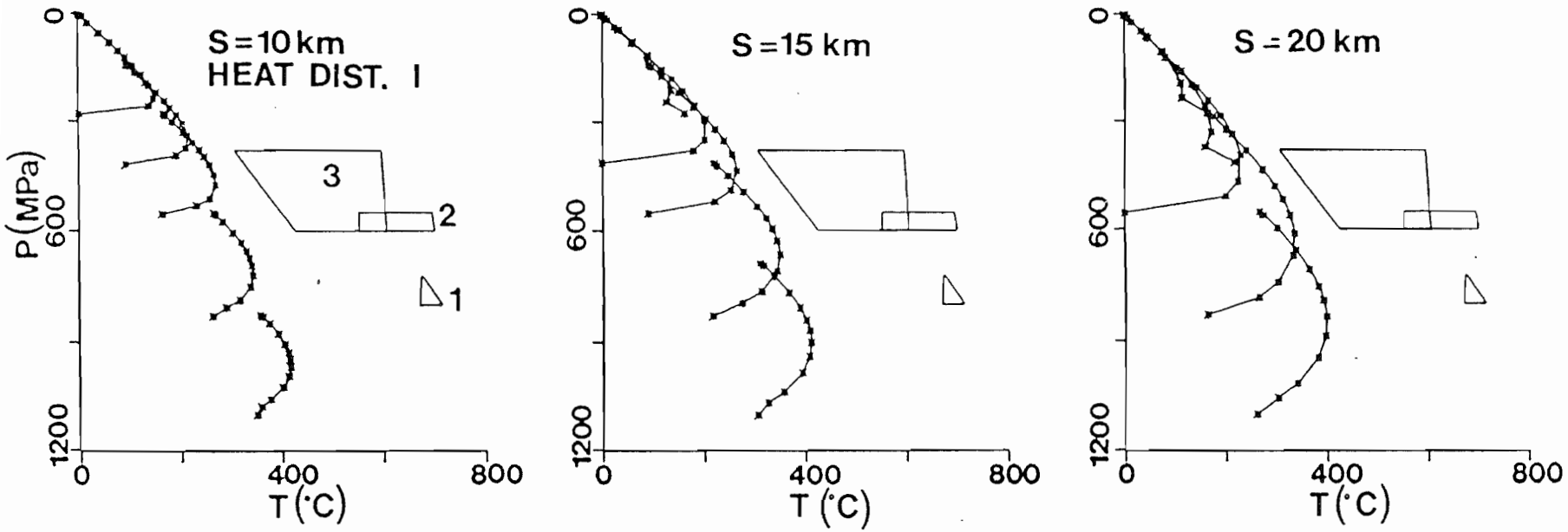

Figure 7.2. P-T-t paths derived using program THRUST (Issler, 1986, unpublished) for heat distributions I, II, III as listed in Table 7.3 for a thrust slab thickness of 10, 15, and 20 km. Boxed and triangular areas indicate the range of P-T conditions for (1) metamorphic peak in the Fishing Cove River schist determined by from phase equlibria, geobarometry, and geothermometry (see Figure 6.2 and 6.6), (2) reset equilibria in the Fishing Cove River schist, and (3) reset equilibria in the staurolite-garnet schists as shown in Figure 6.5. Note that observed peak P-T conditions are approached by P-T-t paths generated for heat distribution III.

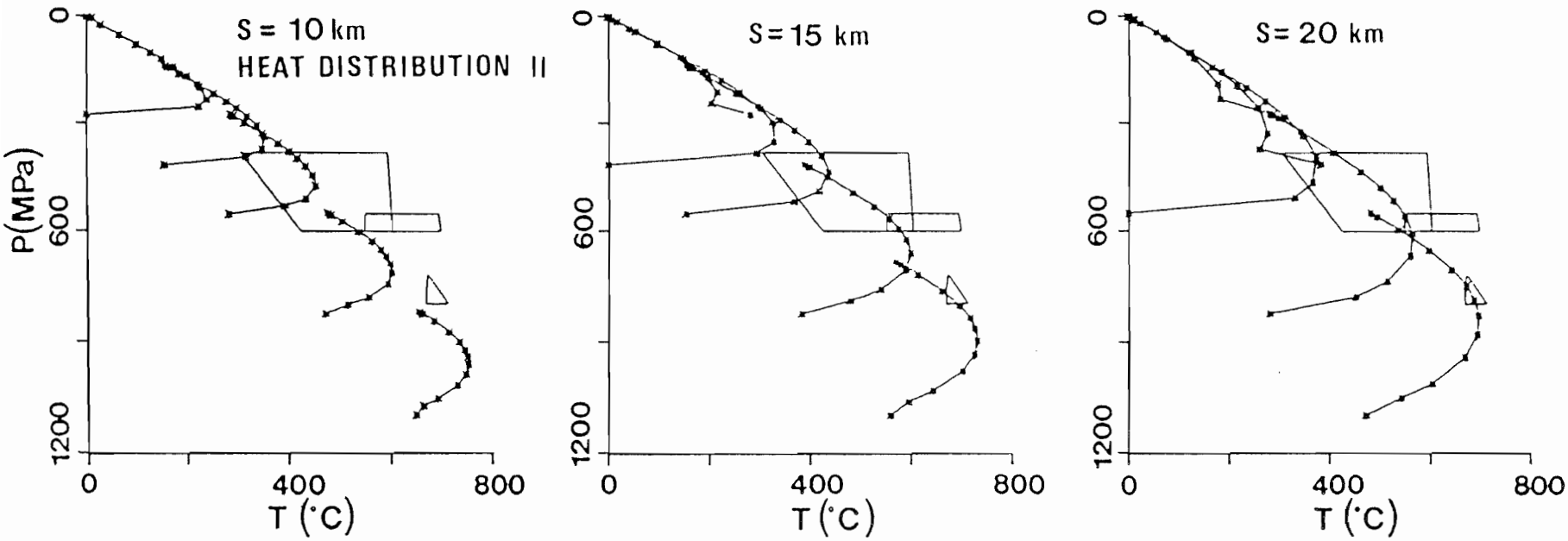

Figure 7.2. (Continued)

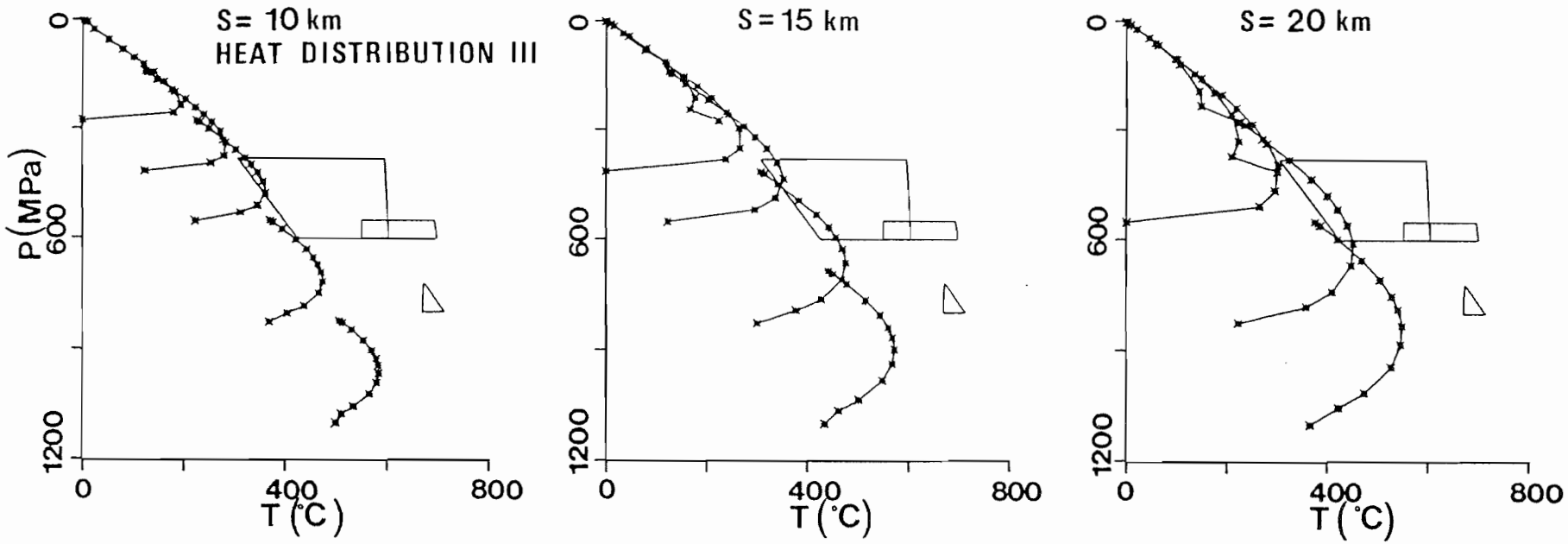

Figure 7.2. (Continued)

differences are approximately 100° to 150°C. However, for a difference in slab thickness of less than about 10 km, temperature and pressure differences are approximately 40° to 50°C and 1 to 1.5 kb (100-150 MPa), well within the errors of geobarometry and geothermometry. Peak pressures are consistent for a given depth below the initial surface, but temperatures vary slightly depending on the depth point location relative to the thrust plane. The latter depends on the thrust slab thickness. However, these variations at peak conditions are less than 50°C and therefore, negligible in terms of comparison to geological P-T-t paths.

In contrast, the heat source distribution has a profound effect on the peak temperatures reached at a given depth (compare Ia,b,c; IIa,b,c; IIIa,b,c in Figure 7.2). In order to assess the effect of variations in q_* and r on the peak conditions obtained, model III was run for a constant surface heat flux (q_s) of 75 mWm^{-2} at (1) r=3.000 μWm^{-3}, q_*=30 mWm^{-2} (Figure 7.3a) and (2) r=1.666 μWm^{-3}, q_*=50 mWm^{-2} (Figure 7.3b). Figure 7.3 shows that an increase in q_* and a decrease in r yields higher peak temperatures and geothermal gradients than increasing r and decreasing q_*. For example, 30 km below the initial surface at 30 Ma after thrusting (i.e. approximately at peak metamorphism), the temperatures obtained for cases

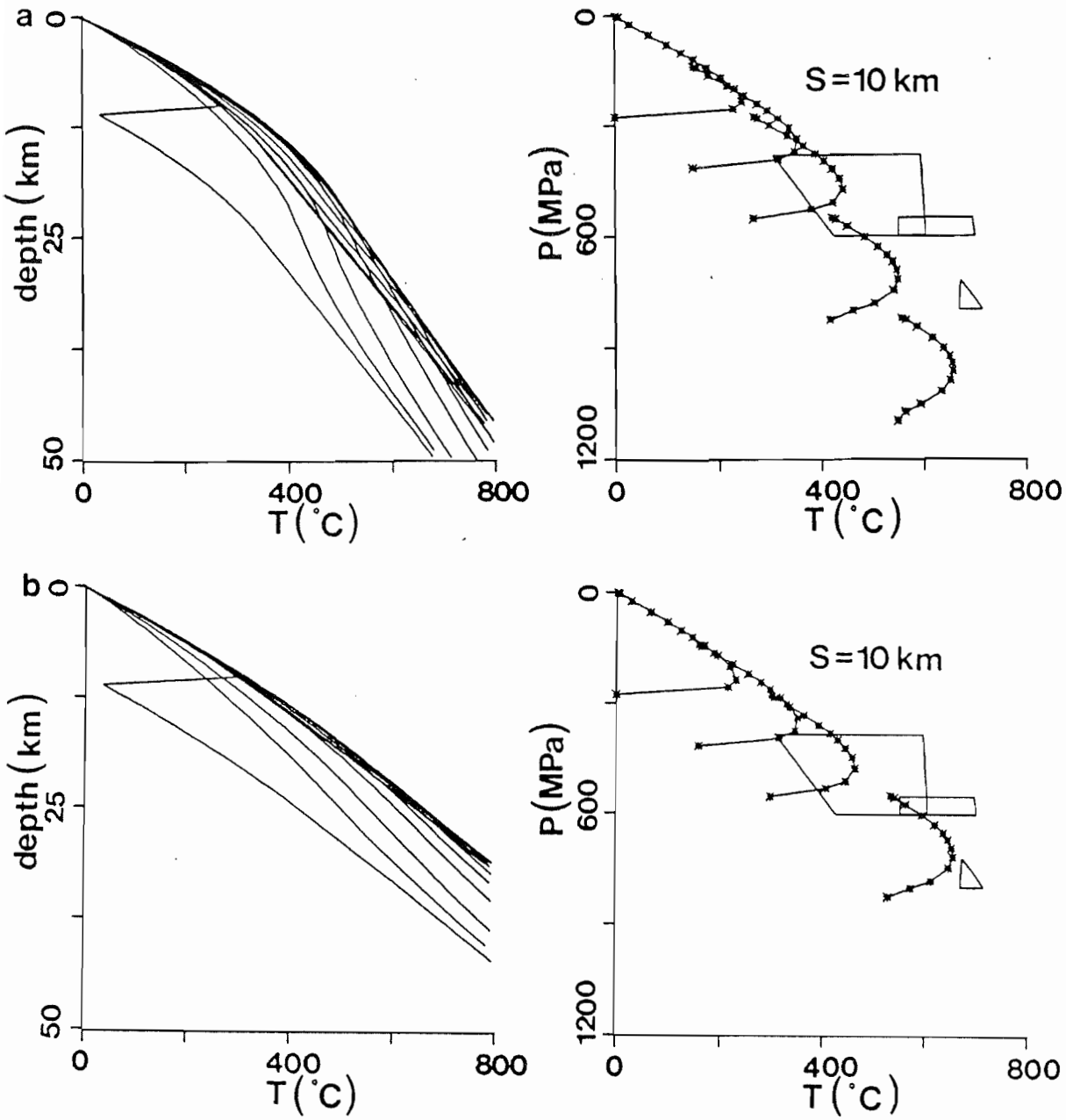

Figure 7.3. Effects of variations in the mantle heat flux (q_*) and radiogenic heat production (r) for a constant surface heat flux (q_s) and slab thickness (S). (a) P-T-t paths for points 10, 15, 20, 30, and 40 km below the initial (post-thrusting) surface and the geothermal gradient generated for a constant q_s of 75 mWm^{-2}, r=3μ Wm^{-3} and q_*=30 mWm^{-2}. (b) As for (a) but r=1.666, μWm^{-3} and q_*= 50 mWm^{-2}. Boxed and triangular areas as in Figure 7.2. Note that an increase in q_* and the corresponding decrease in r for a constant surface heat flux results in higher peak temperatures and geothermal gradients for a given depth point. The difference in peak temperatures between (a) and (b) is approximately 100°C.

(1) and (2) above are approximately 550° and 650°C with a corresponding P of approximately 7.0 kb (700 MPa). This effect results from the solution to the steady-state heat conduction equation which defines the initial (pre-thrust) thermal state of the lithosphere:

$$(21\text{ a}) \qquad T(z) = \frac{q_* + rd_r}{K} - \frac{rz^2}{2K} \qquad 0 \leq z \leq d_r$$

$$(21\text{ b}) \qquad = \left(\frac{q_*}{K}\right) z + \frac{rd_r^2}{2K} \qquad d_r \leq z \leq d_1$$

where T is the temperature at depth (z) and r is assumed constant to depth (dr). All other variables are as defined above. At a given depth within the radiogenic heat producing layer (equation 21a), and a constant q_s (and hence, constant $q_* + r$), the first term in equation 21a is a constant. Thus, if r increases (and q_* decreases), T(z) in equation (21a) must decrease. Similarly, below the radiogenic heat-producing layer (equation 21b), the term with radiogenic heat production is constant and T(z) varies linearily with q_*. Thus, an increase in q_* and corresponding decrease in r results in higher peak temperatures.

Figures 7.2 and 7.3 illustrate the need for the high heat source distribution, such as III which applies to

geologically young regions (<250 Ma, England and Thompson, 1984), to account for the observed data. Assuming the Jumping Brook metamorphic suite is younger than the Cheticamp pluton (cf. Currie et al., 1982), then the sequence could have been no older than approximately 100 Ma at the onset of metamorphism (about 430 Ma) which supports the required high heat source distribution. Based on these observations and the probable island arc affinities of the Faribault Brook metavolcanics (Connors, 1986), published surface heat flow data for young marginal basins were applied to the model. Published values for radiogenic heat production in volcanic-sedimentary and sedimentary sequences of similar lithologies to the Jumping Brook metamorphic suite range from approximately 1.0 to 2.0 μWm^{-3} (Wright et al., 1980; Keen and Lewis, 1982). These values were used to calculate q_*.

7.3.4 Preferred Model

The best fit between the peak conditions predicted by the model and the observed geological data (Figure 7.4) was obtained for a q_s of 75 mWm^{-2} (similar to values for 9 to 35 Ma old marginal basins, Sclater et al., 1980) for q_* of 45 mWm^{-2} and r of 2.0 μWm^{-3}. The depths at which these conditions were obtained at 33, 35, and 38 km

Figure 7.4. Preferred model for the heat distribution required to fit the geological data. P-T-t paths were generated for a heat source distribution of q_*=45 mWm^{-2}, r=2.000 μWm^{-3}, S=20km using exponential erosion (τ =60 Ma) at 10, 15, 20, 30, and 40 km below the initial (post-thrusting) surface. Boxed and triangular areas as in Figure 7.2. Heavy dashed line and dots define the P-T-t path (38 km depth) which best fits the observed peak P-T conditions. Dots are time reference points along the path - corresponding times for peak and near peak metamorphism are shown. T-t lines based on ^{40}Ar-^{39}Ar data and P-t line based on reaction (16) are also shown. The ages indicated on the T-t lines are based on the approximate maximum age difference for the biotite - hornblende pair, including an error $\pm$ 4 Ma. Note that the observed peak P-T conditions can be obtained for this heat source distribution at 38 km, but that exponential erosion does not account for the rapid cooling and uplift rates which are suggested by the P-t and T-t lines.

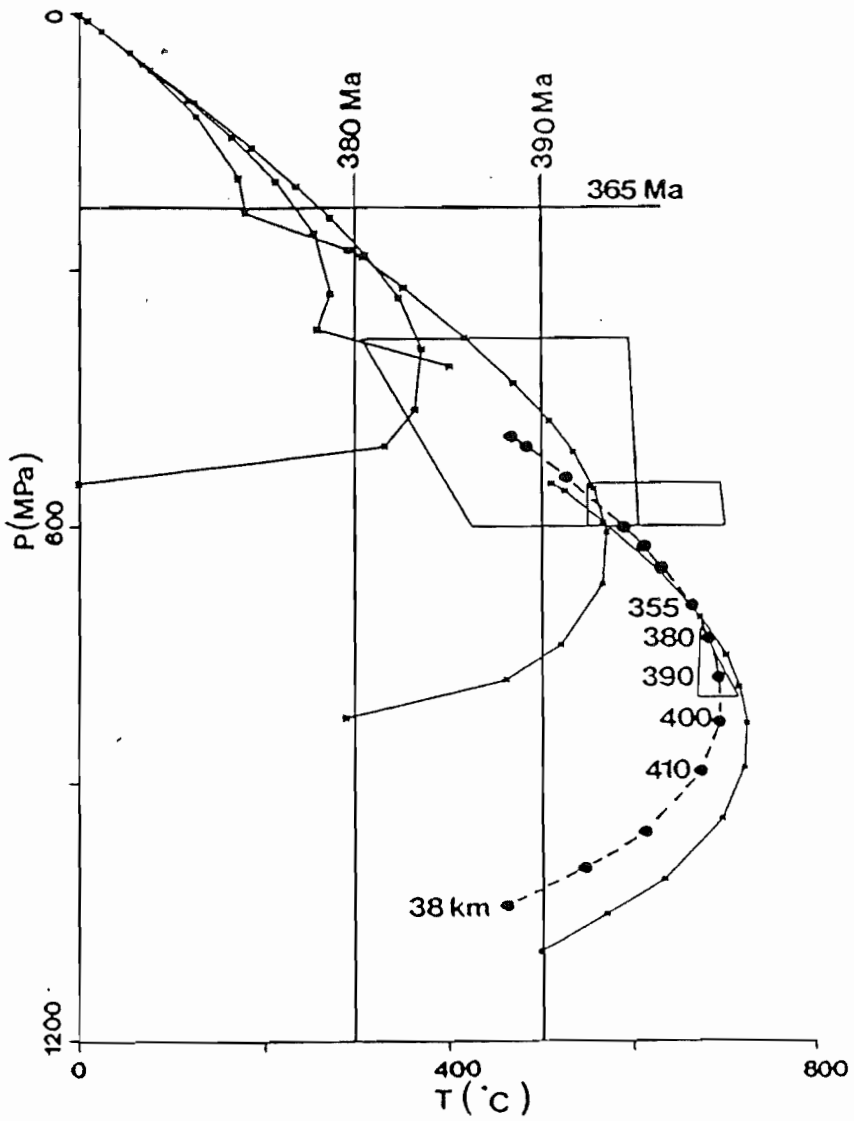
0
380 Ma
390 Ma
365 Ma
P(MPa)
600
355
380
390
400
410
38 km
1200
0
400
800
T(°C)

Figure 7.4.

below the surface of 10, 15, and 20 km thick thrust slabs respectively. These model results suggest peak metamorphic conditions were reached at approximately 400 Ma.

The calculated retrograde path, however, does not agree with the geological observations (Figure 7.4). Shown in Figure 7.4 are the T-t lines based on the maximum age difference (rounded off to the nearest 10Ma) between ^{40}Ar-^{39}Ar cooling ages for the hornblende-biotite pair and the P-t line determined from reaction (16) (section 6.3.1). The ^{40}Ar-^{39}Ar data suggest a very rapid, presumably nearly isobaric cooling between 500^{o} and 300^{o}C which is not accounted for by the exponential erosion model. (Figure 7.4). Since cooling accompanies uplift or succeeds it if uplift is very rapid (isothermic decompression), the age data imply that uplift of the Jumping Brook metamorphic suite was rapid.

Assuming peak metamorphism occurred at approximately 400 Ma as suggested by the preferred model (Figure 7.4), and that uplift was continuous, then the high-grade rocks of the Jumping Brook metamorphic suite were uplifted from approximately 24 km (8 kb) at 400 Ma to approximately 7.5 km (2.5 kb) by 365 Ma. This corresponds to a rate of 470 m/Ma which is slow relative to rates of 1 to 4 km/Ma determined in the Alps (eg. Cliff et al., 1985). Since

cooling was rapid (at least between 500° and 300°C), uplift must have occurred in a time interval less than 35 Ma. Thus, either very rapid erosion or tectonic exhumation is required.

Figure 7.5a and b show the P-T-t paths obtained by forward modelling using different uplift histories in an attempt to account for the retrograde P-T-t data. Figure 7.5a shows the P-T-t paths obtained for the same heat distribution (q_*=45 mWm^{-2}, r=μWm^{-3}) as those if Figure 7.4 but for a faster erosion rate (erosion time constant, τ = 15 Ma). Rocks at 44 km depth experience the peak conditions observed in the high-grade rocks of the study area, but the retrograde path is inconsistent with observed data.

In order to approximately fit the observed retrograde P-T-t data, a time delay of approximately 25 Ma before the onset of uplift, followed by very rapid (5 Ma) nearly isothermic decompression (using a linear erosion rate) for rocks buried to 32 km, and subsequent rapid, nearly isobaric cooling, is required. However, the cooling rate between 390 and 380 Ma is slower (3°C/Ma) than the maximum cooling rate calculated from the observed data. Uplift of 16.5 km in 5 Ma suggests tectonic exhumation as opposed to uplift by erosion for the Jumping Brook metamorphic suite. This is further

Figure 7.5. P-T-t paths generated for the same heat source distribution and slab thickness as that in Figure 7.4. but for (a) rapid exponential erosion (τ = 15 Ma) and (b) a time delay of 25 Ma followed by linear erosion of the thrust slab in 5 Ma. T-t and P-t lines as in Figure 7.4. P-T-t paths are shown for depths of 10, 15, 20, 30 and 40 below the post-thrusting initial surface. P-T-t path at depth point 40 km in (b) is off scale and omitted for clarity. Heavy lines and dots in (a) and (b) define the P-T-t path which best fits the observed peak P-T conditions at depths of 32 km for (a) and 44 km for (b). (a) indicates that rapid erosion can not account for the observed P-t and T-t data. (b) suggests that very rapid uplift (i.e. tectonic exhumation) is required to account for observed peak P-T conditions and a rapid cooling although the rate of cooling in this model is slower than that suggested by observed data. The exact nature of the uplift path is unclear due to the lack of constraint on P in the retrograde path.

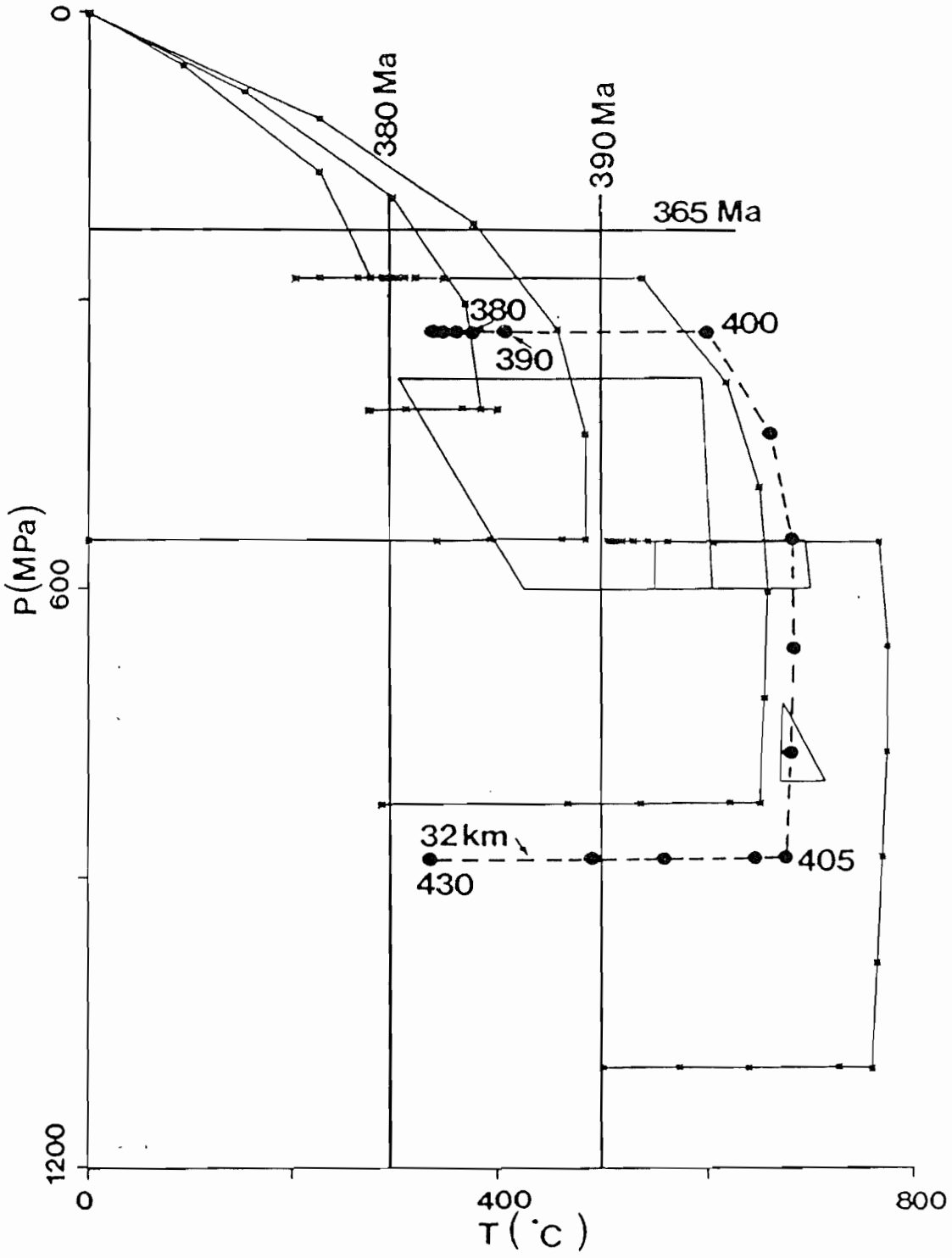
0
380 Ma
390 Ma
365 Ma
380
390
400
P(MPa)
600
32 km
430
405
1200
0
400
800
T(°C)

Figure 7.5b

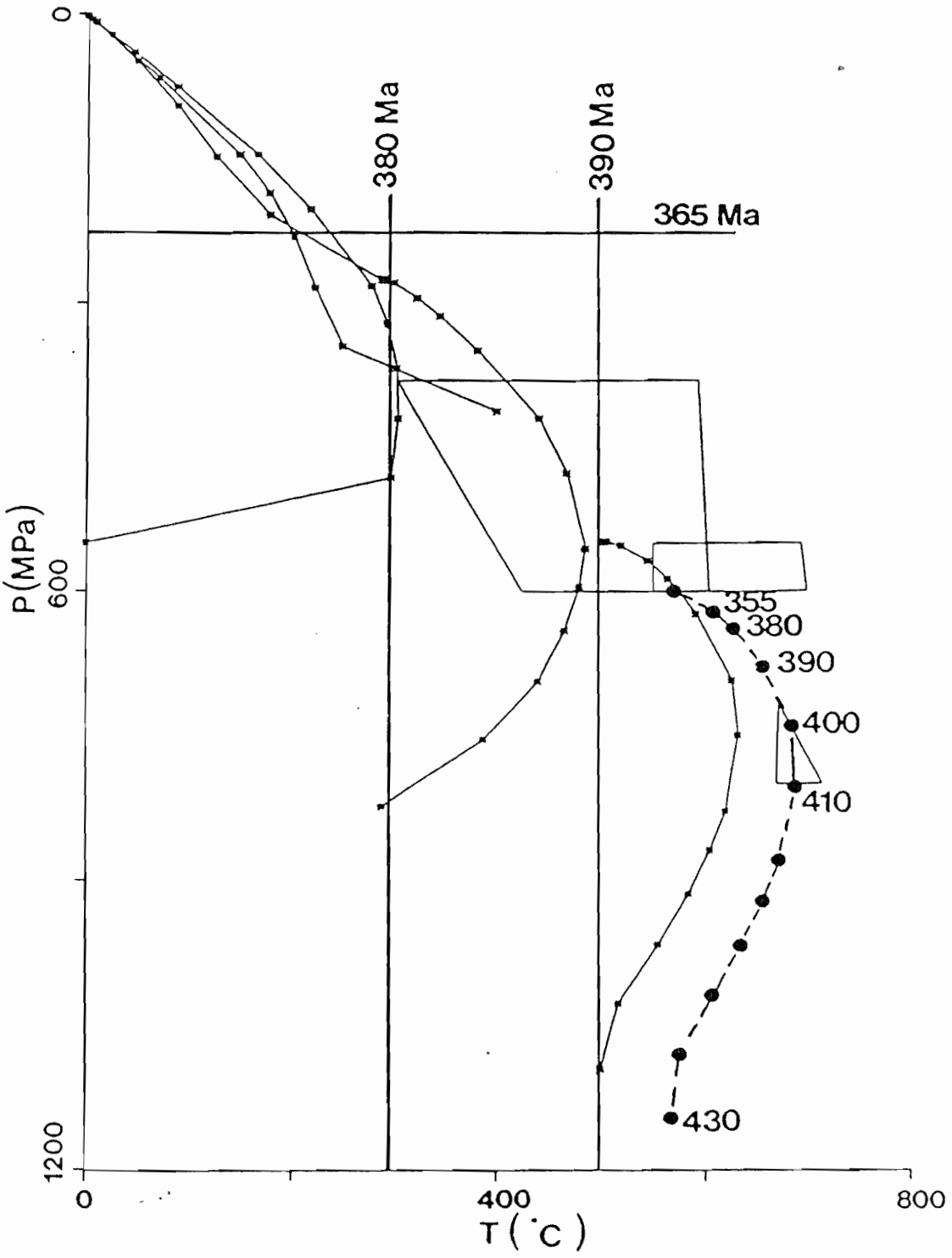
0
380 Ma
390 Ma
365 Ma
P(MPa)
600
1200
355
380
390
400
410
430
0
400
800
T(°C)

Figure 7.5a

supported by the inability of erosion (cf, Figures 7.4, 7.5a) to account for observed cooling ages. It is possible that syn-metamorphic intrusions played some part in heating the Jumping Brook metamorphic suite, thereby making the suggested time delay a maximum value.

The applicability of this model is unclear due to the lack of constraint on P and T in the prograde path and on pressure in the retrograde path. If uplift was rapid, then high temperatures (for diffusion) and hence high-grade mineral compositions may have persisted to lower pressures than suggested by the co-existing kyanite, that is, re-equilibration may have been incomplete. Thus, pressures calculated by the garnet-plagioclase-kyanite-quartz geobarometer may be geologically insignificant. Clearly, the uplift history of the Jumping Brook metamorphic suite is complex and can not be modelled by a simple exponential erosion model, but must have involved rapid Devonian uplift to achieve the rapid cooling indicated by the ^{40}Ar-^{39}Ar ages.

In conclusion, modelling results based on a geologically young region with a surface heat flow of 75 mWm^{-2} overthrust at 430 Ma can account for the observed peak P-T conditions of the Jumping Brook metamorphic suite. However extremely rapid uplift (probably by tectonic exhumation) is required to account for the

nearly identical hornblende and biotite ^{40}Ar-^{39}Ar cooling ages. Assuming the Jumping Brook metamorphic suite is younger than the Cheticamp pluton, these results constrain the depositional age of the suite to Ordovician-Silurian (cf. Currie et al., 1982; Jamieson et al., 1986, 1987).

7.4 REGIONAL CORRELATIONS

Based on the results of this study, possible correlations between the Jumping Brook metamorphic suite and other areas of Cape Breton Island and with Newfoundland are considered.

7.4.1 Correlations within Cape Breton

Barr et al. (1985) correlated the rocks of the Cape North area and the Middle River area with the Jumping Brook metamorphic suite (see Figure 1.1). The Cape North sequence consists of low- to medium-grade, interlayered pelitic to psammitic schist and schistose volcanic and pyroclastic rocks, quartzite, quartz-pebble metaconglomerate, and calc-silicate schist (Money Point Group) structurally overlain by medium- to high-grade pelitic to semipelitic gneiss, marble, calc-silicate

gneiss, and mylonite (Cape North Group) (Macdonald and Smith, 1980). Coarse-grained amphibolites occur in both sequences. Lit-par-lit injected granitoid rocks, including garnetiferous gneissic biotite granite-granodiorite, foliated leucocratic microgranite, aplite and pegmatite are ubiquitous in the Cape North Group and at the western margin of the Money Point Group (Macdonald and Smith, 1980).

The Middle River unit consists of low- to medium-grade metasedimentary rocks with thin metabasite layers interpreted to be volcanic flows (Doucet, 1983). Fine-grained phyllites, schists, and a metaconglomerate layer, exposed in the south of the area, are structurally overlain by medium-grained mica schists and gneisses to the north. Thin marble layers, possible tuffaceous schists, and a deformed rhyolite, are present in the phyllites and schists.

A general lithological sequence of low- to medium-grade mafic to felsic volcanic rocks (flows and pyroclastics) and pelitic to psammitic schists structurally overlain by medium- to high-grade schists and gneisses, locally with marbles, quartzites, and amphibolites is common to the Cape North, Middle River, and Cheticamp areas. Metamorphosed crystal tuffs, rhyolitic flows and epidote concretions similar to those

of the Money Point Group are observed in the Faribault Brook metavolcanics of the Jumping Brook metamorphic suite. The conglomerate layer in the Middle River unit (Doucet, 1983) consists of quartz, siltstone, volcanic and granite clasts in a fine-grained matrix, similar to the metaconglomerate exposed in the Fishing Cove River schist along Robert Brook. Lithologically, the rocks of the Cape North and Middle River areas are thus very similar to those of the Cheticamp area.

Review of literature and investigation of available thin sections from the Middle River and Cape North areas reveals that they are structurally and metamorphically similar to the Cheticamp area, particularly in terms of early, synmetamorphic, progressive crenulation. Table 7.4 summarizes the structure at Money Point, in the Middle River area, and in the Cheticamp region and presents a re-interpretation of early deformation in the Middle River area. Terminology used is that of Macdonald and Smith (1980), Doucet (1983), and this study, respectively.

Macdonald and Smith (1980) defined 5 deformation stages at Money Point. D_1 involved isoclinal folds in compositional layering to which S_1 is axial planar. These folds are not obvious except where strong compositional layering exists. D_2 refolded F_1 folds into gently

Table 7.4 Summary of macroscopic to microscopic structure in Money Point Middle River, and Cheticamp areas and of the re-interpretation of early structures in the Middle River area as discussed in text. A legend for mineral abbreviations is given in Table A1.1. Fabric notation after the references cited.

Area	Macroscopic Structure				Microstructure
		Folds	Planar Fabrics	Lineations	
Money Point (MacDonald and Smith, 1980)	D_1	F_1, mesoscopic, inclined to upright, isoclinal, gentle NNE or SSW plunge, folds compositional layering (S_0)	S_1, axial planar schistosity, dominant planar fabric in area, westward dip	L_1, small scale rodding and S_0-S_1 intersections, L_1 parallel to F_1 axes	S_1 defined by chl, mu and possibly bi. S_2 formed by crenulation of S_1. Syn-crenulation cd (stage 1 S_i), gt (stage 1 S_i), bi (stage 1-2 S_i) growth Post-S_2 (?) growth of st and ky porphyroblasts
	D_2	F_2, mesoscopic gently inclined to upright, close to tight, gentle to moderate plunge to N-NNE or S-SSW, dextral asymmetry looking north, refolds F_1 and approx. co-axial with F_1	S_2, axial planar crenulation cleavage, moderate to steeply dipping (commonly to the east)	L_2, crenulation lineation parallels F_2 axes	
	D_3	F_3, mesoscopic, upright open to close, rounded to chevron folds and kink bands, generally plunge N, steep axial planes, strike N-S or E-NE to WSW			
	D_4	Macroscopic, upright folding about a NW axis ? = F_3			
	D_5	F_5, macroscopic, upright, open to close, 30 -35 °NNE plunge ?=F4			

Table 7.4. (Continued)

Area		Macroscopic Structure			Microstructure
		Folds	Planar Fabrics	Lineations	
Cheticamp (this study)	D_1	F_1, tight to isoclinal, rootless, intrafolial, approx. N-trending axes	S_1, axial planar cleavage	L_1, intersection lineation of S_0* and S_1	Low grade rocks: post-S_1 gt, chtd, and bi growth. Locally, post-incipient S_2 gt growth. Later flattening of S_1 around porphyroblasts and foliation re-orientation. Medium- to high-grade rocks: crenulation of S_1 to form S_2, syn-crenulation gt (stage 1-2 S_i), st (commonly stage 2-3), ol (commonly stage 3 or 5-6), ky (commonly stage 5-6) growth. Locally, ky and st overgrow re-oriented S_2
	D_2	F_2 crenulation	S_2, crenulation cleavage (schistosity)	L_2, mineral stretching lineation	
	D_3	?	S_3 mylonitic banding	?	
	D_4	F_4, upright, open, gently N-plunging, NNE trending macro- to microscopic folds, coaxial to F_1	S_4, incipient crenulation cleavage	L_4, crenulation lineation	
	D_5	F_5, kink folds and crenulations	S_5, incipient axial planar and crenulation cleavage	L_5, crenulation lineation	
	D_6		S_6, fault surfaces	L_6, slickensides	

Table 7.4. (Continued)

Area		Macroscopic Structure			Microstructure
		Folds	Planar Fabrics	Lineations	
Middle River (after Doucet, 1983)	D_1	?	S_{MR1}, schistosity defined by phyllosilicates	?	Pre-S_{GB1} gt porphyroblast growth, pre- to syn- S_{GB1} biotite porphyroblast growth, syn- to post- S_{GB1} chl and chtd growth. Pre- S_{MR2} gt, st, and ky porphyroblast growth S_{MR2} defined by bi and mu.
	D_2	isoclinal crenulation of S_{MR1} mesoscopic, tight, shallowly EW plunging folds, affect S_{MR2}, its relation to S_{GB1} is unknown	S_{GB1} in low-grade schists & phyllites, schistosity S_{MR2} in high-grade rocks, crenulation cleavage	L_{GB1}, associated with development of S_{GB1}, defined by pebble elongation, chl and hb, moderate plunge to NE	
	?	mesoscopic, tight, shallow EW plunging folds, affect S_{MR2} but relation of these folds to S_{GB1} is unknown	S_{GB2} a fine crenulation cleavage, shallowly NE plunging affects S_{GB1} but timing with respect to other deformation events is unclear	L_{GB2}, intersection lineation associated with S_{GB2}, plunges shallowly NE	
	D_3	mesoscopic, open to tight folds and kinks affect S_{GB1} and S_{MR2}, relation to S_{GB2} to steeply to N and NW unknown, plunge moderate			
	D_4	open to close, macroscopic folds, NNE trending, moderate to steep plunge			
	D_5		Shearing & faulting		
	D_6		Post-Mississippian faulting		

Table 7.4. (Continued)

Area		Macroscopic Structure			Microstructure
		Folds	Planar Fabrics	Lineations	
Middle River (re-interpretation this study)	D_1	F_1, isoclinal folds in compositional layering (inferred from microstructure)	S_1, schistosity, defined by phyllosilicates ($= S_{MR1} = S_{GB1}$)	?	isoclinal folds in compositional layering are transposed along S_1 in the low-grade phyllites chtd, chl, cc, gt porphyroblasts overgrow stage 1-2 crenulation of S_1. Ky and st overgrow S_2. Later foliation reorientation of S_2 causes S_2 to wrap around st and ky and locally truncate S_1.
	D_2	crenulation of S_1 to form S_2	S_2, schistosity ($= S_{MR2} = S_{GB2}$)	?	
	D_3 to D_6	as given by Doucet (1983)	as given by Doucet (1983)	as given by Doucet (1983)	

inclined to upright, close to tight folds to which S_2 is axial planar. F_1 and F_2 are co-axial and Macdonald and Smith (1980) suggested that the two deformation phases probably reflect a continuous progressive deformation. Microscopically, S_2 is a crenulation cleavage formed by the progressive crenulation of S_1. Photomicrographs presented by Macdonald and Smith (1980) indicate cordierite and garnet overgrew stage 1 crenulations whereas biotite overgrew stage 1 to 2. Macdonald and Smith (1980) also noted neocrystallization of mica within S_2. A photomicrograph of staurolite shows straight S_i defined by quartz and opaque minerals, oriented approximately parallel to stage 4 matrix foliation (S_2). Textural relations are not clear in this photograph, but it appears that staurolite may have overgrown S_2. Kyanite overgrows a matrix foliation interpreted by Macdonald and Smith to be S_1. Although the textures illustrated in their photomicrographs are ambiguous, there is a strong possibility that this is in fact S_2, by analogy with Cheticamp area.

D_3 as defined by Macdonald and Smith (1980) involved mesoscopic, open to close, upright, rounded to chevron folds and kink bands which plunge gently to the north, possibly contemporaneous with D_4 macroscopic, upright,

northwest-trending folds. D_5 consisted of Carboniferous folding and faulting.

In the Middle River area, Doucet (1983) documented six deformation stages. The effects of D_1 are observed in the medium to high-grade metasedimentary schists as a crenulation schistosity (S_{MR1}). The pervasive foliation is a crenulation cleavage (S_{MR2}). Mesoscopic, tight folds of similar orientation to the crenulation were also reported in the medium- to high-grade rocks (Doucet, 1983). However, neither mesoscopic folds nor crenulations of an earlier fabric were observed in the low-grade phyllites and schists. Doucet (1983) reported a fine crenulation cleavage (S_{GB2}) and lineation (L_{GB2}) that affected the phyllitic schistosity (S_{GB1}) of the low-grade rocks. Examination of thin sections from a transect along Middle River between Second Gold Brook and Falls Brook (Delahay, 1979; Doucet, 1983) reveals two significant features. Firstly, isoclinal folding and transposition of a compositional layering along an axial planar S_{GB1} foliation are locally evident. Secondly, carbonate, chlorite, and garnet porphyroblasts have overgrown the hinge zones of crenulated S_{GB2} which is well preserved in the matrix. The latter observation suggests that the crenulations observed in the low-grade rocks are the early stages of a progressively developed

synmetamorphic crenulation cleavage, best preserved in the medium- to high-grade rocks of the Middle River area. Thus, the pervasive foliation in the low-grade rocks (S_{GB1}) may be equivalent to S_{MR1} (cf. Doucet, 1983) and both the low- and medium- to high-grade rocks have been subjected to a later, crenulation cleavage-producing deformaton.

Review of available photomicrographs of the medium- to high-grade schists, and information given in Doucet (1983) shows that chloritoid overgrew S_{GB1}, and kyanite and staurolite overgrew S_{MR2}. Both foliations were subsequently deformed around the porphyroblasts. Doucet (1983) reported complex helicitic (i.e. sigmoidal) inclusion trails in medium- to high-grade garnets, that are discontinuous with S_{MR2}.

D_3 involved mesoscopic, open to tight folds and kinks which affected both the low-grade (S_{GB1}) and medium- to high-grade schists (S_{MR2}). Macroscopic, nearly upright, moderately north-plunging folds (F_4) deformed the phyllitic schistosity (S_{GB1}) in the low-grade Middle River rocks. D_5 consisted of later faulting and shearing (Doucet, 1983) and D_6, of post-Mississippian, northerly trending faulting.

Comparison and re-interpretation of macroscopic and microscopic structures at Money Point and in the Middle

River area with those of the Cheticamp area, reveal strong similarities in the early deformation sequence and relative timing of deformation and porphyroblast growth:

1. Tight to isoclinal folds deformed compositional layering (S_a) and were associated with development of axial planar cleavage S_b.
2. Crenulation of S_b which formed a crenulation cleavage S_c was accompanied by syndeformational porphyroblast growth. Porphyroblasts overgrew different stages of this crenulation cleavage development.
3. S_c is best developed in the medium- to high-grade, pelitic to semipelitic schists but is present locally in the low-grade phyllites and schists. However, further work is required in the Middle River area to confirm the early sequence interpreted here. Doucet (1983) reports multistage garnet growth based on zonation profiles in the medium-grade garnets which may be equivalent to that documented in the high-grade rocks of the study area, or may reflect early multistage garnet, thus invalidating the application of the "garnet datum" to the Middle River area.

The major differences in deformation histories post-date the formation of S_c. In the Middle River and Money Point areas, mesoscopic folds and kinks are reported to post-date S_c and were followed by upright, macroscopic,

moderately north-plunging folding. S_c development in the Cheticamp area was followed by shearing related to east to west stacking of isoclinal folds (Craw, 1984) and upright, open, gently north-plunging, north-northeast-trending folding.

Based on meso- and micro-stuctures, the Middle River area, Money Point, and the Cheticamp area have experienced similar early deformation histories. Although insufficient data are available to make any firm conclusions, it appears that garnet-staurolite-kyanite is a common sequence of porphyroblast growth in the Jumping Brook metamorphic suite, implying a consistent pattern of progressive syndeformational metamorphism in the Highlands zone.

7.4.2 Correlations in the Appalachians

Traditionally, Cape Breton Island has been correlated with the Avalon Zone of the Appalachians (eg. Williams, 1979). The Avalon Zone in Newfoundland is characterized by late Precambrian sedimentary and volcanic rocks and plutons metamorphosed up to greenschist grade, overlain by undeformed Cambrian-Ordovician platform sedimentary rocks, and minor Devonian plutonism and metamorphism (Williams, 1979). Deformation

in the Avalon Zone is minor relative to the neighbouring polydeformed Gander Zone.

The Jumping Brook metamorphic suite is characterized by a polydeformed volcanic-sedimentary sequence metamorphosed up to amphibolite facies, bounded to the east by paragneisses, amphibolites, and tonaltic to granodioritic orthogneisses (Chapter 2; Jamieson et al., 1987). Thermal modelling, cooling ages, and stratigraphic control suggests the Jumping Brook metamorphic suite is Ordovician-Silurian. These characteristics are not typical of the Avalon Zone of southeastern Cape Breton Island and eastern Newfoundland nor of the Grenvillian rocks of the Humber Zone, Newfoundland and the Northwestern Highlands zone, Cape Breton Island (cf. Barr, 1985; Jamieson et al., 1986; Barr and Raeside, 1986) thus suggesting correlations of the Jumping Brook metamorphic suite with the Central Mobile Belt of Newfoundland.

Without ages of rocks, lithological correlations are tenuous and more data are required before specific correlations can be made. However, the lack of ophiolitic rocks in the Highlands zone suggests the study area is not part of the Dunnage Zone and thus, possibly correlates with the Gander Zone of northeastern and southwestern Newfoundland. The lithologic sequence (low-

to medium-grade volcanic and sedimentary rocks structurally overlain by paragneisses and tonaltic to granodioritic orthogneisses) of the Jumping Brook metamorphic suite resembles that of the Ordovician La Poile, Bay du Nord, and Baie d'Espoir Groups of the Gander Zone (Coleman-Sadd, 1980; Chorlton and Dallmeyer, 1986). However, the rocks are also lithologically similar to the ?Ordovician Pacquet Harbour Group of the Dunnage Zone. Therefore, correlation of the Jumping Brook metamorphic suite with specific areas of the Central Mobile Belt requires further work, but correlation with the Avalon Zone is improbable (cf. Barr et al., 1985; Barr and Raeside, 1986).

CHAPTER 8

CONCLUSIONS AND RECOMMENDATION FOR FUTURE WORK

8.1 CONCLUSIONS

Polyphase deformation in the Jumping Brook metamorphic suite precludes determination of a depositional stratigraphy. The Jumping Brook metamorphic suite comprises a lithological sequence of low-grade mafic and felsic metavolcanic flows and volcaniclastic rocks, locally interlayered with pelitic to psammitic phyllites and schists, structurally overlain by low- to high-grade pelitic to psammitic phyllites, schists, and paragneisses. The Jumping Brook metamorphic suite is bounded to the east by the Pleasant Bay Gneiss Complex which is characterized by quartzo-feldspathic schists, tonialtic to granodioritic orthogneisses, and amphibolites.

The relative ages of the Jumping Brook metamorphic suite and the Cheticamp pluton, and the geological relations between this suite and the Pleasant Bay Gneiss Complex have not been resolved by this study. All exposed contacts between the suite and the Cheticamp pluton are faulted or sheared, obscuring relative age relations.

However, enclaves of the Fishing Cove River schist in the MacKenzies Mountain megacrystic orthogneiss, and the abundance of orthogneiss in the Pleasant Bay Gneiss Complex, suggest the boundary between these divisions was either originally intrusive or has subsequently been obscured by intrusions.

Early deformation in the Jumping Brook metamorphic suite was characterized by tight to isoclinal folding (F_1) of compositional layering (probably bedding) about northerly trending, shallowly plunging axes, and transposition of these folds along an axial planar cleavage (S_1). Crenulation (F_2) of S_1 to form S_2 is common in the medium- to high-grade metasedimentary rocks but is only locally observed in thin section in the low-grade rocks. This crenulation is apparently related to northerly trending extention, although the cause of this deformation is unclear. This was followed by westward-directed thrusting along high strain zones. Differential uplift along these zones is inferred to account for the observed metamorphic progression. Post-metamorphic deformation in the map area is characterized by upright, macroscopic, open folding (F_4), with associated crenulations and mesocopic folds essentially co-axial with F_1 folds, and by later kink folds, crenulations, and Carboniferous faulting.

Metamorphic grade increases east-northeastward in a typical Barrovian sequence. Petrography indicates only one phase of prograde metamorphism in the study area. Garnet, chloritoid, and biotite porphyroblasts have overgrown S_1 in the low-grade rocks, whereas in the medium- to high-grade rocks porphyroblasts of garnet, biotite, staurolite, oligoclase, and kyanite have overgrown different stages of the crenulation of S_1 to form S_2.

Porphyroblast-matrix relationships and included mineral assemblages allow determination of the following sequence of metamorphic mineral growth in the medium- to high-grade rocks: chlorite^1, chloritoid, garnet^1, staurolite, oligoclase and kyanite, garnet^2, chlorite^2. Post-S_2 fibrolite is developed locally in the highest grade rocks and is interpreted to have grown metastably. Biotite and muscovite apparently grew and recrystallized continuously throughout the metamorphism.

Garnet-biotite geothermometry, garnet-plagioclase-kyanite-quartz geobarometry, and phase equilibria suggest peak metamorphic conditions for the highest grade rocks of approximately 700°C at 7.75 to 8 kb although the latter is optomistic considering the 1.6 kb error for the geobarometer. Based on phase equilibria considerations, the prograde metamorphic path was one of increasing P and

T but dP/dT is unclear. Retrograde reactions give some constraint on the retrograde P-T path. The overall form of the P-T-t path is characteristic of metamorphism due to tectonic thickening. ^{40}Ar-^{39}Ar metamorphic cooling ages on biotite of 383 $\pm$ 4 Ma, and on hornblende of 390 $\pm$ 4 Ma, 389 $\pm$ Ma, and 383 $\pm$ 4 Ma indicate rapid, early Devonian cooling of the Jumping Brook metamorphic suite.

Comparison of the geological P-T-t path and cooling ages with theoretical P-T-t paths generated by single-slab, one-dimensional, conductive thermal models for overthrusting requires an initially high heat source distribution (q_s=75mWm^{-2}) and extremely rapid uplift to fit the observed data. Thus the Jumping Brook metamorphic suite is interpreted to have been a geologically young ($\leq$ 100 Ma) region at the time of overthrusting. These results suggest the depositional age of the Jumping Brook metamorphic suite is Ordovician-Silurian (cf. Currie et al., 1982, Jamieson et al., 1986, 1987), although if some heat was added to the system by synmetamorphic intrusions (eg. Belle Cote Road orthogneiss), an older age at the time of overthrusting would also be consistent with the observed data.

Based on age estimates, metamorphic grade, and degree of deformation, the Jumping Brook metamorphic suite more closely resembles parts of the Central Mobile

Belt of Newfoundland than the Avalon Zone of eastern Newfoundland. Whether the Jumping Brook metamorphic suite correlates with the Gander or Dunnage Zone is unclear from existing data. However, the Jumping Brook metamorphic suite bears closer lithological similarities to the Gander Zone.

8.2 RECOMMENDATIONS FOR FUTURE WORK

This study has laid the groundwork for several further research projects which could resolve some still controversial geological questions.

(1) Detailed mapping (1:10,000) of the Robert Brook area should be done to investigate contact relations between the Jumping Brook metamorphic suite and the Cheticamp pluton, and to better constrain the geology between the Corney Brook and Cheticamp River sections through the suite.

(2) Detailed microstructural investigation of carefully oriented thin sections to determine the exact relationship between the crenulations and mineral stretching lineation, and to explore their potential use

as kinematic indicators is required to better constrain the structural history of the area.

(3) Geochemical study of the Dauphinee Brook, Corney Brook, and Fishing Cove River schists may give further indication of the possible mineral reactions and support or discredit those proposed here. In addition, the involvement of oxides and sulphides in metamorphic reactions have not been considered in this work. Thus, the possibility of silicate-sulphide reactions, particularily in mineralized zones south of the study area should be considered.

(4) ^{40}Ar-^{39}Ar age-spectrum dating of feldspars in the foliated pegmatites and fission track work on apatite from the quartz-plagioclase leucosomes and possibly from the foliated pegmatites in the high-grade rocks could give some constraint on the low-temperature part of the retrograde path. Similarily, more zircon dating in the western Highlands volcanic-sedimentary belt could give further constraint on the timing of metamorphism and possibly, timing of deposition.

(5) A detailed study of the structure and metamorphism of the Pleasant Bay Gneiss Complex with emphasis on the

microscopic and the macroscopic structure is required to determine its role in the metamorphic history of the Jumping Brook metamorphic suite.

(6) Studies similar to this work in southwestern Newfoundland and comparison of results from the Highlands zone and Newfoundland to recently acquired seismic data for the Gulf of Saint Lawrence and the Cabot Strait (G.S.C., unpublished data, 1986) could confirm or discredit suggested correlations with the Central Mobile Belt.

APPENDIX 1

SAMPLE DESCRIPTIONS

All samples analysed for whole rock geochemistry, mineral chemistry, and ^{40}Ar-^{39}Ar age are described below. Abbreviations used are those listed in Table A1.1. Where optical determination of feldspar is impossible, and mineral chemistry was not obtained, no distinction of feldspar type is made. In some samples, fine-grain size causes difficulty in deciphering quartz and feldspar and thus the percentage estimate (given in brackets after the mineral) is listed for quartz plus feldspar. Minerals in brackets in thin section descriptions denote minerals defining the foliation specified.

(1) HAND SPECIMEN DESCRIPTION

DAUPHINEE BROOK SCHIST

85-107 very fine-grained, grey pelitic phyllite, well developed slaty cleavage, fissile. Fine crenulation lineation (D_4)

85-K45 very fine-grained, grey-green pelitic phyllite, well developed slaty cleavage, fissile, fine crenulation lineation (D_4)

85-698c fine-grained, grey quartz-feldspar-biotite semipelitic schist with small (average 1 mm diameter or length) subidioblastic garnet and hornblende porphyroblasts

CORNEY BROOK SCHIST

85-659b light greenish white to grey garnet-biotite -muscovite semipelitic schist. Foliation wraps around large subidioblastic garnet (0.5 to 0.7 mm diameter) porphyroblasts. Biotite porphyroblasts average 1 mm diameter.

85-700b fine-grained, well foliated pelitic staurolite -garnet schist. Well developed biotite mineral lineation. Weakly developed fine crenulation parallel to the mineral lineation. Porphyroblast (staurolite, garnet, biotite) are subidio- to idio-blastic and wrapped around by the foliation. Garnet is included in staurolite.

85-707b Muscovite-biotite-garnet pelitic schist, fine-grained, well foliated

85-716A Fine-grained, moderately foliated, semipelitic garnet-biotite schist with strong micaceous sheen. Weakly developed mineral (biotite) lineation. Compositionally layered: contains a 1.5 cm layer of very fine-grained grey, semipelitic schist which is approximately parallel to the foliation and contains subidioblastic garnet porphyroblasts.

85-722 Fine-grained, well foliated, semipelitic schist. Well developed mineral (biotite) lineation. Subidioblastic garnet and staurolite porphyroblasts wrapped around by the foliation. Minor pelitic-rich lamallae (<1 mm wide) at very low angle (1 - 2^{o}) to the foliation.

85-723b Fine-grained, well foliated, silvery grey, pelitic staurolite-garnet schist. Staurolite (0.3 to 0.5 cm diameter), garnet (0.5 to 0.7 cm diameter), biotite (0.3 to 0.7 cm by 0.1 to 0.4 cm) porphyroblasts. Biotite defines the lineation. All porphyroblasts are subidio- to idio-blastic.

FISHING COVE RIVER SCHIST

85-732 Fine-grained, well foliated, semipelitic biotite schist. Subidio- to xeno-blastic garnet and staurolite pophyroblasts (< 1 mm diameter or length). Strong micaceous sheen. Moderately developed mineral (biotite) lineation.

85-441 Medium-grained, well foliated, pelitic biotite -garnet-kyanite schist. Garnet and kyanite are subidioblastic. Garnets average 1 - 2 mm diameter, kyanite averages 2mm long and 1 mm wide. Minor quartz porphyroclasts.

85-445 Medium-grained, well foliated, pelitic, biotite -garnet schist. Subidioblastic garnets average 0.8 mm diameter and are wrapped around by the foliation.

85-446 Medium-grained, moderately foliated, pelitic, biotite schist. Subidioblastic garnet and possibly kyanite porphyroblasts. Quartz and feldspar porphyroclasts.

85-535 Medium-grained, well foliated, semipelitic biotite(-garnet) schist. Feldspar porphyroclast are strung-out along the foliation.

85-565 Medium-grained, well foliated, semipelitic, biotite(-hornblende) schist. Minor xenoblastic garnet. Moderate mineral (biotite) lineation.

GEORGE BROOK AMPHIBOLITE AND CORRELATED GARNET AMPHIBOLITES

85-621d Medium-grained, schistose amphibolite with relict dioritic texture. Acicular to prismatic hornblende porphyroblasts are developed randomly on the foliation surface.

85-631g Medium-grained, moderately foliated amphibolite with relict dioritic textures. Moderately well developed lineation defined by feldspar and hornblende.

85-706b Medium-grained, moderately foliated amphibolite cross cut by ?feldspar-rich veinlets. Rare disseminated pyrite blebs.

85-708b Medium-grained, moderately foliated, gabbroic amphibolite, minor disseminated pyrite blebs.

85-245 Medium-grained, well foliated amphibolite with small (< 1 mm diameter) xenoblastic garnet porphyroblasts. Feldspar and hornbledne define the foliation.

85-280 Medium-grained, moderately foliated, minor garnet porphyroblasts. Quartz (?segregation) veins parallel the foliation.

85-343a Medium-grained, moderately foliated amphibolite, minor subidioblastic garnet porphyroblasts.

85-345 Medium-grained, well foliated amphibolite contains small xenoblastic to subidioblastic garnet.

85-643c Pale green epidote-rich vein (approximately 1 to 2 cm apparent width) containing xenoblastic amphibole porphyroblast which cross cuts well foliated amphibolite with relict dioritic texture.

(2) THIN SECTION DESCRIPTIONS

DAUPHINEE BROOK SCHIST

85-107 Chl(40), mu(32), qtz+fsp(25), ilm(2), chtd (1), Gt(0.5)
retrograde: chl and clay minerals after chtd

Pronounced foliation (mu, chl, ilm). Compositional layering and foliation intersect at 15°. Idioblastic gt and chtd have overgrown foliation. S_i (qtz, ilm) straight to weakly sigmoidal. Hourglass chtd. Moderate fractures in garnet. 1 mm wide mu lamallae and some quartz lamallae isoclinally folded and transposed along foliation. Qtz±chl strain shadows around ilmenite.

85-K45 As for 85-107. See also Connors (1986)

85-698c Qtz(37), fsp(21), bi(30), gt(8), hb(2), chl(1), ap and ep (1)
retrograde: minor chl after bi and gt

Prounounced S_2 (biotite). Elongate-granoblastic texture. Sub-to idio-blastic poikiolblastic garnet and hornblende overgrow S_2. No S_i. Garnet moderately fractured. Minor chlorite after garnet along fractures. Ellipsoidal partially recrystallized quartz porphyroclasts have lobate subgrain boundaries. Late chlorite porphyroblasts overprint biotite.

CORNEY BROOK SCHIST

85-659b mu(40), qtz(35), bi(15), gt(8), pl(5), tm(o.5), chl(0.5), op(1), st (trace)
retrograde: minor iron oxide on fractures in gt, chlorite porphyroblast after biotite, ser after pl

Pronounced S_2 (mu, bi). Subidioblastic poikiloblastic bi with qtz and mu inclusions. Some grains show basal slip. Foliation wraps around bi and some have associated strain-shadows. Subidioblastic poikiloblastic gt with S_i (qtz,op,mu,tm). Late idio- to subidio-blastic chl porphyroblasts have ovegrown S_2. Foliation abuts and wraps around gt. Relic subidioblastic st. No well developed S_i in any porphyroblasts.

85-700b mu(22), pl(20), qtz(29), st(20), bi(5), gt(2), chl(1), op amd tm (1), ky(trace), ?sph(trace)
retrograde: minor ser after pl, minor chl after bi, gt, and st.

Pronounced S_2 (mu,bi,ol). Poikiloblastic to skeletal st with qtz,gt,op inclusions has overgrown foliation and strongly retrograded along late microshears. Gt inclusions in st have straight S_i at high angle to S_2. Gt is subidioblastic and poikiloblastic, moderately fractured. S_i in subidioblastic ky continuous with matrix. S_4 incipient crenulation cleavage deforms S_2. Post-S_2 chl porphyroblasts are twinned, subidioblastic, and partially replace biotite.

85-707b mu(34), bi(20), fsp(25),qtz(20), gt(1), st(trace), tm(trace)
retrograde: ser after fsp (extensive)

Moderate foliation(mu, bi). Xeno- to subidio-blastic poikiloblast of gt with qtz, sericitized fsp, and op inclusions. Subidioblastic bi porphyroblasts (qtz, op, and zr inclusions, no S_i) are wrapped around by mu. Mu and bi also intergrown. Bi pristine. Partially recrystallized qtz porphyroclasts present, qtz subpolygonal. Matrix approaching granoblastic-elongate texture.

85-716a qtz(35), fsp(30), bi(10), gt(3), mu(20), op(1)
retrograde: chl after bi, ser after fsp

Moderate foliation (bi, mu). Subidio- to xeno-blastic gt poikiloblasts with qtz, sericitized fsp, op, and minor chl inclusions. No S_i. Subidioblastic bi (post S_2?) porphyroblasts with qtz, op, and zr inclusions. Foliation wraps around bi and gt. Poorly preserved (polygonalized) quartz porphyroclasts. Minor pl twins in fspar but generally untwinned.

85-722 bi(20), mu(10), st(0.5), gt(5), qtz(40), pl(24), tm(0.2), op (0.2), ap (0.1)
retrograde: chl after bi, minor chl after gt, iron oxide along fractures in gt, ser after pl

Moderate foliation (micas, elongated qtz, and fsp). Granoblastic-elongate texture. Subidio- to xeno-blastic, poikiloblastic to skeletal st with qtz inclusions. Subidio- to xeno-blastic garnet has nucleated on quartz porphyroclasts and has qtz, op, chl, and bi inclusions. No S_i. Foliation wraps around porphyroblasts. Quartz-fsp matrix is polygonalized.

85-723b st(40, gt(8), bi(15), mu(40), ky(4), qtz(22), pl(5), tm(0.5), op(1), chl(0.5)
retrograde: chl after ky and st, minor ser after pl, minor chl after gt

Pronounced foliation (mu,bi). Subidioblastic garnet contains stage 1 S_i (qtz, op, chl) which varys in orientation w.r.t. S_2 throughout thin section. Subidio- to idio-blastic poikiloblastic st with S_i (qtz,op) at stage 2 to 3 or has overgrown S_2 (S_i continuous with matrix). Ky has commonly overgrown S_2 mimetically along mu-rich S_2 cleavage domains. Optically continuous ky grows mimetically over S_2 which has wrapped around st. Gt commonly included in st. Rare, relict asymmetric to symmetric crenulations in matrix.

FISHING COVE RIVER SCHIST

85-732 bi(11), gt(3), st(5), mu(23), qtz(42), p(115), tm(0.5), op(0.5)
retrograde: minor ser after pl, minor chl after bi, submicroscopic phyllosilicate/?clay mineral intergrowth after st in matrix

Pronounced foliation (bi, mu). Xenoblastic, poikiloblastic garnets with inclusions of st, qtz, acicular op, and rare tm. Gt approaching skeletal and S_i not well developed but are sigmoidal. Subidio- to xeno-blastic st in matrix and included in garnet and has inclusions of op, qtz, and tm. Bi and mu intergrown and contain op, zr, and rare tm inclusions.

85-441 ky(3), gt(3), bi(32), mu(1), pl(41), qtz(18.5), ap(0.5), op (0.5), zr(0.5)
retrograde; minor chl and iron oxide intergrowth after gt, ser after pl

Moderate anastomosed foliation (bi, mu) wraps around fsp and qtz grains, ky subidioblastic, poikiloblastic with bi, qtz, and gt inclusions. Some ky is twinned. S_2 gently wraps around ky and garnet. S_i in ky and gt poorly developed but where present are at a high angle to S_2. Possible st inclusion in ky. Gts have no S_i but cores are inclusion-rich. Weak S_i in ky at angle to foliation. Ky generally fresh.

85-445 qtz(22), p(140), bi(30), ky(1), mu(5), gt(1), op(1), ap (trace)
retrograde: ser after pl, mu after ky, and minor chl after kyanite

Moderate anastomosed foliation (bi, mu). Ky partially pseudomorphed by mu. Gt subidio- to xeno-blastic with straight S_i in the core defined by ilm, qtz, and submicroscopic dusty material. S_i is approximately normal to S_2. Core mantled by relatively inclusion-free rim. S_2 wraps around ky, gt, and fsp. Qtz-pl-ap segregation trends parallel to S_2. Pl porphyroblast show weak zonation, contain inclusions of bi,op, and qtz but no S_i. Pl twins common.

85-446 qtz(16), pl(42), bi(33), mu(5), gt(2), op(1), ap(0.5), zr(0.5), tm(trace)
retrograde: minor chl after bi, chl and mu after ky, ser after pl (extensive)

Prounounced foliation (mu,bi). Xenoblastic garnet has inclusions of sericitized fsp, qtz, op but no S_i. Foliation bends around garnet. Mu intergrowth with bi. Mu pseudomorph after ky. Relict ky in core. Fsp strongly sericitized.

85-535 pl(38), qtz(35), bi(21), mu (2.5), gt(2), op(1), ap(0.5), ep(trace)
retrograde: moderately to strongly ser pl

Pronounced fol(bi, mu, qtz). Subidio- to xeno-blastic gt with ser pl and qtz inclusions. One gt with c. gr. bi, qtz, pl aggregate in core (?atoll gt). Subidioblastic bi intergrown with mu and rare zr inclusions. Op common between bi grains. Albite twins and zoning in pl. Possible relict qtz porphyroclasts - elliptical, polygonal qtz concentration elongated parallel to the foliation

85-565 hb(2), bi(15), qtz(35), pl(45), ksp(2), ap+op(0.5), sph(0.5), relict st (trace), gt(trace)
retrograde: ser after pl

Moderate foliation (bi,hb,qtz). Subgranoblastic, polygonal-elongate texture. Subidio- to xeno-blastic, moderately fractured hb contains minor qtz inclusions and is intergrown with bi and qtz. Subidioblastic bi has rare qtz inclusions. Qtz subgrains, minor microcline. Albite twins in plagioclase are well developed. ?st relict in matrix. Subidioblastic sph as individual grains or rimming op.

GEORGE BROOK AMPHIBOLITE

85-621d hb(37), bi(10.5),chl(36),qtz and pl(15), op(1), sph(0.5), zr(trace)
retrograde: ser after pl, chl after bi

Moderate foliation (chl±hb±bi). Hb and bi overprint chlorite-defined foliation. Interstitial to chl masses are polygonal qtz, rare pl with pinned chl. Acicular randomly oriented op (?ilm) disseminated throughout.

85-631g hb(45), chl(37), pl(15), op(2), sph(1), zr(trace)
retrograde: ser and chl after pl

Moderate foliation (hb, pl). Subidio- to xeno-blastic prismatic and fibrous hb with interstitial chl and pl. Pl also as subidio- to xeno-blastic porphyroclasts. Subidioblastic sph and zr included in chl. Some op rimmed by sph. Late fractures are oxidized. Rare twinning in hb.

85-706b hb(60), pl(24), op(10), qtz(1)
retrograde: minor ser after pl

Moderate S_2 (hb). Hb idio-to subidio-blastic, poikiloblastic, and overprints polygonal fsp-qtz matrix. Some iron oxide staining on hb cleavage.

85-708b hb(50), pl(42), qtz(5), op(2), bi(0.5),chl (0.5), sph(trace)
retrograde: ser after pl, minor chl after hb and ?bi

Moderate foliation. Hb xeno- to subidio-blastic, partially recrystallized (weak undulose extinction), cores contain qtz and minor op inclusions, rims generally inclusion free. Fsp and qtz in matrix are polygonal.

85-245 hb(45), pl(43), qtz(10), ep(1.5), ap(0.5), op(trace)
retrograde: ser after fsp

Moderate foliation. Hb subidioblastic and fresh, minor undulose extinction, contains rounded gt and op inclusions. Gt xenoblastic, intergrown with hb. Fsp sericitized, some albite twins.

85-280 hb(45), pl(40), qtz(16), gt(1), op(1), ep(2)
retrograde: ser/mu after fsp

Moderate foliation (hb). Idio- to subidio-blastic hb, completely recrystallized, rounded qtz incl. Subidioblastic gt with minor qtz incl, no S_i. Minor zoning in fspar. Minor perthitic fsp. Quartz partially recrystallized

85-343a hb(35), pl(30), qtz(26), ep(5), gt(2), op(1), ap(0.5), ep(0.5)
retrograde: ser after pl, chl after hb

Moderate foliation (hb). Subidioblastic hb and gt contain minor qtz inclusions. Porphyroblast -matrix relations unclear due to lack of S_i and grain size of matrix. Qtz is partially recrystallized.

85-345 hb(50), pl(38), qtz(11), ep(1), ilm and ap (trace)
retrograde: ser after pl

Well foliated. Subidioblastic, completely recrystallized hb with rare twins, rare ap and qtz inclusions. Polygonal qtz-plag matrix. Pl apparently replaced by hb.

85-643c Vein ep(68), amp(47), qtz(3), prh(14), cc(4), op(1)

Vein consists of essentailly massive ep and prh. Xenoblastic, ragged, patchy blue-green and pale green-yellow amp porphyroblasts are partially ?replaced by prh. Qtz and cc are subgranoblastic and interstitial to ep, prh, and amp. Some qtz and op inclusions in amp.

Host Rock amp(42), qtz and fsp(37), amp(42), chl(7), ep(8), sph(2.5), bi(2), op(1.5)

Xenoblastic amp porphyroblasts are zoned with blue-green rims and pale green-yellow (actinolitic) cores and contains inclusions of qtz, op, and sph but no S_i. Porphyroblast matrix relations are unclear. Foliation defined by chl and bi and truncated by vein. Op rimmed by sph. Sph also as individual subidioblastic grains. Ep as granular masses.

Table A1.1. Summary of petrographic features of the major rock types in the study area. Minerals underlined in the foliation column are the dominant minerals by which the foliation is defined. "fsp" is listed for lithologies in which alkali feldspar and plagioclase are optically indistinguishable. Abbreviations used are as follows:

Minerals

act	= actinolite	ky	= kyanite
amp	= amphibole	mu	= muscovite
ap	= apatite	mt	= magnetite
bi	= biotite	op	= opaque minerals
cb	= carbonate		
cbs	= carbonaceous material	pl	= plagioclase
cd	= cordierite	py	= pyrite
chl	= chlorite	qtz	= quartz
chtd	= chloritoid	rt	= rutile
diop	= diopside	ser	= sericite
ep	= epidote	sill	= sillimanite
fb	= fibrolite	st	= staurolite
fsp	= feldspar	tm	= tourmaline
gt	= garnet	wh. m.	= white mica
hb	= hornblende	woll	= wollastonite
ilm	= ilmenite	zr	= zircon
ksp	= K-feldspar		

Textures and Porphyroblasts/clasts

v.f. gr.	= very fine-grained
f.gr.	= fine-grained
med. gr.	= medium-grained
c. gr.	= coarse-grained
idio	= idioblastic
sub	= subidioblastic
xeno	= xenoblastic

Other

acc = accessories
comp = compositional

Table A1.1 (Continued)

ROCK TYPE	MINERALOGY	TEXTURE	PORPHYRO-		FOLIATION	S_i	RETROGRADE ALTERATION	COMMENTS
			CLASTS	BLASTS				
DAUPHINEE BROOK SCHIST								
MAFIC METAVOL-CANICS	pl, ch, ep, qtz, ±cb act acc:ilm, py, rt	f.gr.,fol locally porphyro-clasts	sub to idio pl, xeno qtz	xeno act or act& hb	chl, qtz act. Spaced discrete, smooth cleavage locally anasta-mosing	absent	see text	syn-to post-tectonic cb veinlets
FELSIC METAVOL-CANICS	qtz, pl, wm.m, chl ±cb acc:gt,py	f.gr. fol locally porphyro-clasts	sub to xeno pl& qtz	xeno to skeletal gt	mu, qtz. Spaced, to continuous planar cleavage locally anasto-mosing	absent	ser after pl	tight to iso-clinally folded & transposed qtz veinlets
LOW-GRADE PELITES	wh.m, chl, qtz fsp,cbs ±gt ± chtd acc:tm,lm	f.gr.,fol locally porphyro-blasts	rare xeno qtz	idio to sub gt, chtd, or bio, mu xeno chl	mu, chl. Planar continuous nondomainal	mod to well developed	ser after pl	foliation parallel qtz veinlets show pinch & swell
LOW-GRADE SEMIPELITES	wh.m, chl, qtz fsp, ±cc acc: op, ap	f.gr.,fol locally porphyro-blasts or clasts	sub to xeno pl & qtz	idio to sub gt, bi	mu, chl. Planar to anasto-mosing	mod to absent	ser after pl	
LOW-GRADE PSAMMITES	qtz, mu, chl, fsp ±cb acc: op,ap	med. gr., fol, porphyro-clasts, grano-blastic-elongate	sub-to xeno pl & qtz	xeno chl	mu, chl. Planar to anasto-mosing	mod to absent	ser after pl	

Table A1.1. (Continued)

ROCK TYPE	MINERALOGY	TEXTURE	PORPHYRO- CLASTS	PORPHYRO- BLASTS	FOLIATION	S_i	RETROGRADE ALTERATION	COMMENTS
DAUPHINEE BROOK SCHIST (continued)								
MEDIUM-GRADE PELITIC TO SEMIPELITIC MICA(-GT) SCHISTS	mu, qtz, bi, fsp, op ±gt ± cb acc: tm, ap zr, ilm, op rt	f. to med. gr. foliated, elongated polygonal porphyro-blasts		sub, poik bi, gt	mu, bi, qtr fsp. Planar schistosity locally anasto-mosing	mod to well developed	ser after pl chl and ksp after bi	
MEDIUM-GRADE PSAMMITIC SCHISTS	qtz, mu, bi, pl (ksp) ±gt ±hb±cc acc: tm, ap, op	med.gr. grano-blastic-elongate		sub to xeno bi gt hb	mu, bi, elongate qtz± fsp. Planar to anasto-mosing schistosity	poor to absent	ser after pl	
QUARTZITES	qtz, pl, mu, bi, (ksp) ±hb acc: op, gt	v.f.gr., grano-blastic, minor porphyro-clasts	pl, qtz	mu, bi, skeletal gt	elongate qtz polygon Weak planar to absent	absent	ser after pl chl after bi	mu & gt nucleating on pl
MARBLES	cb, gt, qtz, diop (?woll)	f.to med. gr, gran-oblastic-elongate, porphyro-blasts		gt, diop (?woll)	elongate cc polygons. Weak, planar	absent		
FELDSPAR SCHISTS	pl, ksp, qtz bi	med. gr., schist-ose, porphyro-blasts		pl, ksp	bi. Well developed anasto-mosing	well developed	chl after bi	ksp is microline

Table A1.1. (Continued)

ROCK TYPE	MINERALOGY	TEXTURE	PORPHYRO- CLASTS	PORPHYRO- BLASTS	FOLIATION	S_i	RETROGRADE ALTERATION	COMMENTS
CORNEY BROOK SCHIST (continued)								
STAUROLITE-GARNET SCHISTS	mu, bi, pl, st gt, ky acc:op, tm, ap (rt)	med.gr., schistose porphyroblasts		sub to idio st. ky, gt, bi, pl	mu, bi well developed, planar to anastomosing	well developed	chl after bi st and ky, ser after pl	
SEMIPELITIC TO PSAMMITIC SCHISTS	mu, bi, pl, gt ±st ±ksp± hb acc: op,tm,ap	med.gr, schistose	fsp qtz	sub to xeno gt		well developed to absent	chl after bi ser after pl rare chl after st gt	
HB-RICH AMPHIBOLITES AND HORNBLENDITES	hb, op, (?act) (ep),(fsp), (qtz)	f.gr., schistose		sub to idio hb	hb. Mod to well developed, planar	absent		hb oriented randomly on the foliation surface
FISHING COVE RIVER SCHIST								
BIOTITE SCHISTS AND PARA-GNEISSES	PELITIC: bi, mu, qtz, pl, (ky), gt, ap ky ±st ±fb acc: zr, ap, tm, ilm, rt	med.gr., schistose, porphyroblasts		xeno to sub ky, gt, st, bi	mu, bi. Well developed, planar to anastomosing	poor to moderate	ser after pl chl & ksp after bi, mu after ky	
	SEMIPELITIC:bi mu, qtz, pl gt ± hb ±ksp acc:zr ±?rt ±op	med. gr., schistose, porphyroblasts	locally pl	sub to xeno bi ± gt±hb	mu, bi.Well developed, planar to anastomosing	absent	ser after pl chl & ksp after bi, mu after pl	rare ksp veinlets

Table A1.1. (Continued)

ROCK TYPE	MINERALOGY	TEXTURE	PORPHYRO-CLASTS	PORPHYRO-BLASTS	FOLIATION	S_i	RETROGRADE ALTERATION	COMMENTS
MUSCOVITE - GARNET ORTHOGNEISS								
	ksp, pl, mu, qtz, gt, bi acc: ap, ?rt, op	med. to c. gr., granoblastic elongate			bi, mu, qtz Planar to anastomosing	absent	ser after pl	albite twins in pl and cleavage in mu bent; gt fractured
GEORGE BROOK AMPHIBOLITE								
RELICT IGNEOUS TEXTURE	hb, pl, qtz, ±py acc:ksp,cb,rt	med.gr., schistose locally porphyroblasts of hb and bi relict dioritic texture		sub hb	hb, plag	absent	ser after pl chl after bi & hb	
AMPHIBOLITES	hb, pl,(qtz), (ksp) mt±sph± bio±gt acc:ap,rt	no relict dioritic texture		sub to xeno hb, gt, bi		absent	ser after pl chl after bi &hb	sph rims op some samples
CHETICAMP PLUTON (GRANODIORITE)								
	pl, qtz, bi, ksp, acc: ap	med.to c. gr, hypoidiomorphic equigranular			absent		chl after bi ser after pl	cataclastic deformation near faults; ksp is microcline
BIOTITE GRANODIORITE								
	pl, qtz, bi, ksp, mu acc: ep, sph, ap	med.to c. gr,hypidiomorphic equigranular			absent to very weak		chl after bi ser after pl	ksp is microcline; pl is zoned; minor myrmekite

Table A1.2. Modal analyses (volume %) of stained slabs of the biotite granodiorite and related intrusive rocks. Percentages based on counting of at least 1000 points on a 1 mm grid. Tn=tonalite, Mg=monzogranite, Gd=granodiorite.

SAMPLE NUMBER	85-215		85-233		85-296		85-307	
	points	%	points	%	points	%	points	%
Quartz	204	21	272	30	228	22	231	23
Plagioclase	749	77	406	44	695	68	727	72
K-feldspar	22	2	233	26	100	10	52	5
Biotite	53		96		78		86	
Muscovite	14		3		tr		tr	
TOTAL	1042		1010		1102		1096	
	Tn		Mg		Gd		Tn	

SAMPLE NUMBER	85-317		85-339		85-354		85-360c	
	points	%	points	%	points	%	points	%
Quartz	243	22	273	25	231	24	281	28
Plagioclase	739	66	635	59	665	68	639	65
K-feldspar	132	12	177	16	75	8	68	7
Biotite	5		97		31		61	
Muscovite	3		tr		18		7	
TOTAL	1122		1183		1020		1056	
	Gd		Gd		Gd		Tn	

Table A1.2. (Continued)

SAMPLE NUMBER	85-447		85-478		85-494c		85-507	
	points	%	points	%	points	%	points	%
Quartz	263	27	304	31	227	22	342	34
Plagioclase	528	20	547	55	676	66	484	49
K-feldspar	194	53	136	14	122	12	166	17
Biotite	37		38		48		49	
Muscovite	32		16		1		5	
TOTAL	1054		1041		1074		1046	
	Gd		Gd		Gd		Gd	

SAMPLE NUMBER	85-374		85-378b		85-390c		85-392c	
	points	%	points	%	points	%	points	%
Quartz	372	32	342	36	347	37	323	34
Plagioclase	658	56	488	51	575	2	479	50
K-feldspar	144	12	129	13	20	61	153	16
Biotite	74		129		32		61	
Muscovite	10		tr		98		7	
TOTAL	1258		1088		1072		1023	
	Gd		Gd		Tn		Tn	

Table A1.3. Modal analyses (volume %) of two fine-grained hornblende-rich amphibolites (85-724f, 742a) and one fine-grained hornblendite (85-727b).

MINERAL	85-724f	85-727b	85-742a
Hornblende	85.6	97.0	65.4
Plagioclase	2.0	trace	16.9
Quartz	9.0	trace	2.0
Biotite	0.0	0.0	9.3
Opaque minerals	2.9	1.4	0.4
Sphene	0.5	1.3	6.0
Rutile	0.0	0.3	0.0
TOTAL	100.0	100.0	100.0

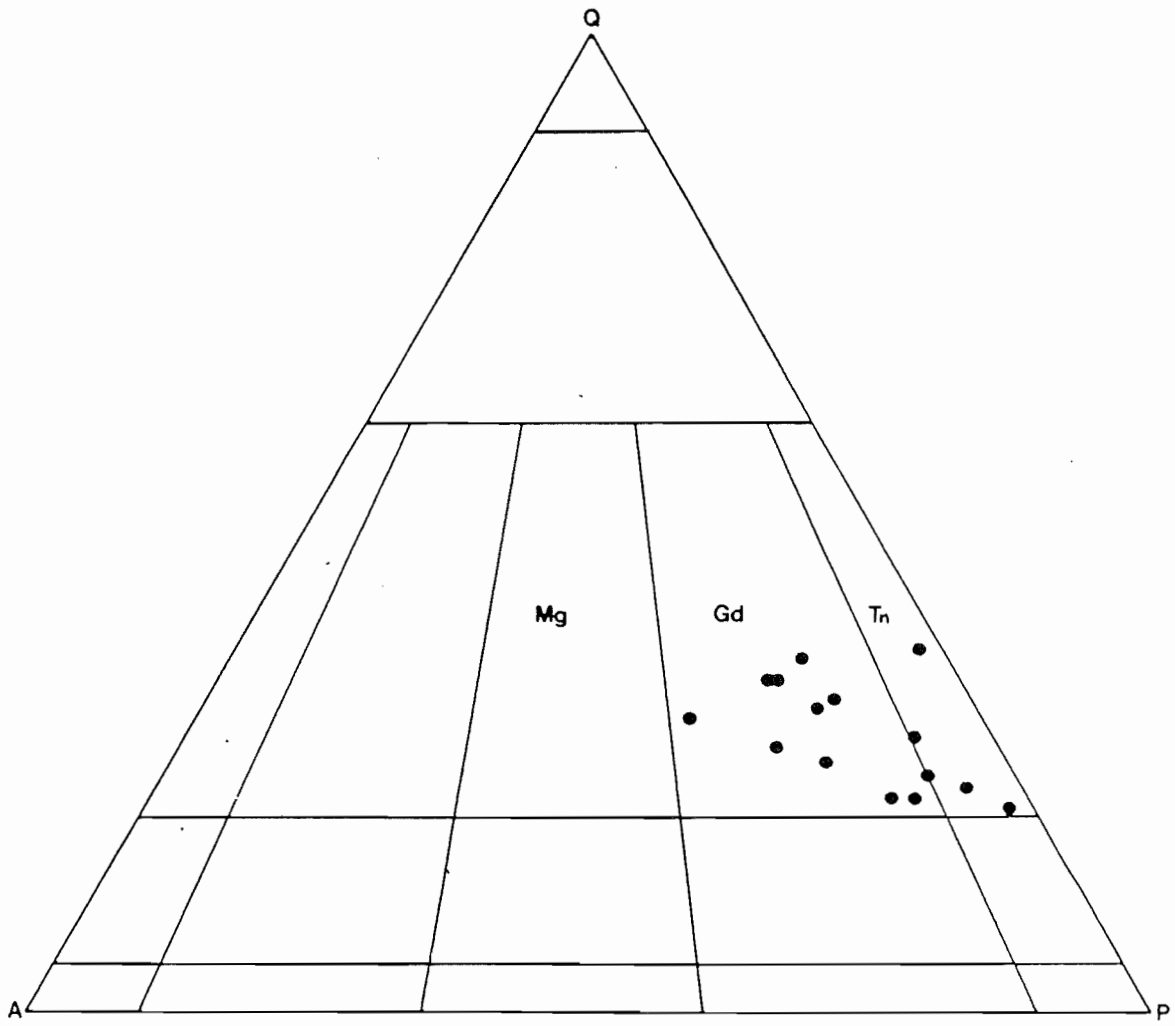

Figure A1.1. Modal quartz (Q) - alkali feldspar (A) - plagioclase (P) ternary diagram for the biotite granodiorite and ?related intrusive rocks which cross cut the Fishing Cove River schist and Pleasant Bay Gneiss Complex. Mg=monzogranite, Gd=granodiorite, Tn=tonalite. Data obtained from point counting of slabs stained for K-feldpar under a binocular microscope on a 1 mm grid of at least 1000 points.

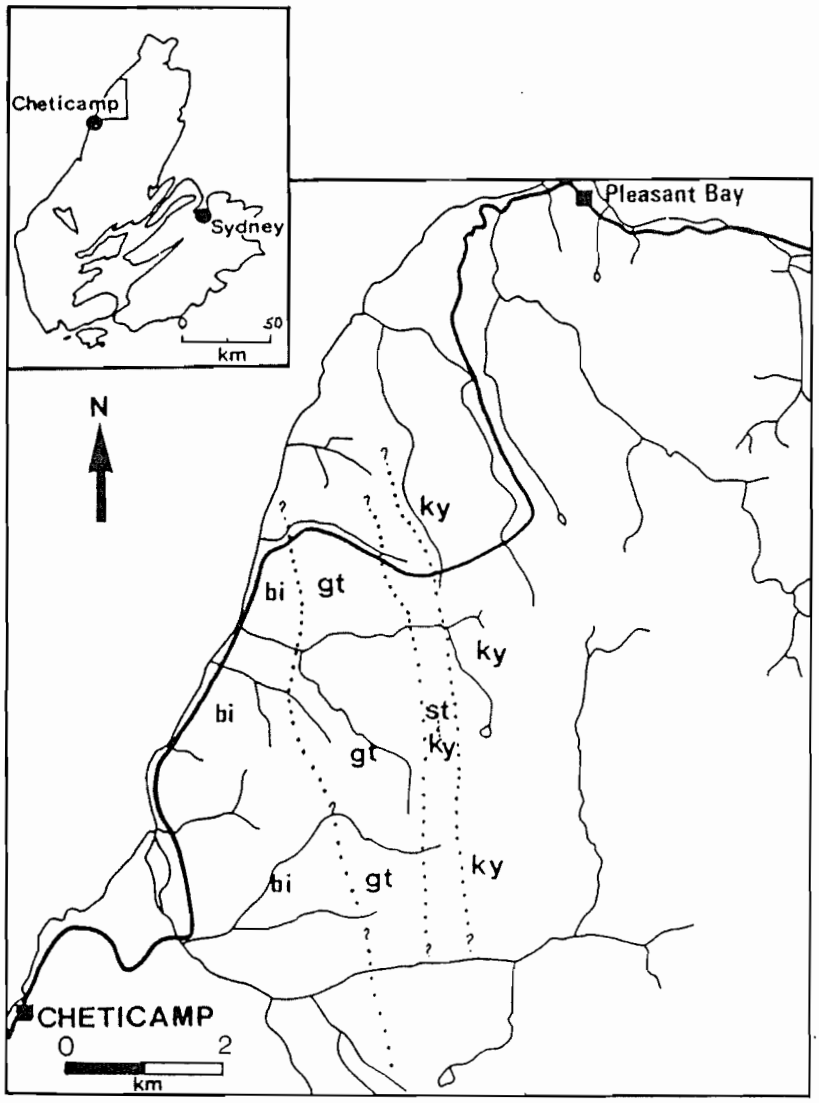

Figure A1.2. Metamorphic mineral zones in the Jumping Brook metamorphic suite as referred to in the text. Dotted lines represent the approximate boundaries of the mineral zones.

APPENDIX 2

ANALYTICIAL METHODS

(1) X-RAY FLUORESENCE

The samples were analysed for 10 major and minor element oxides and 14 trace elements on a Philips PW1400 sequential x-ray fluoresence spectrometer using a Rh-anode x-ray tube at St. Mary's University, Halifax, Nova Scotia. Major oxide determinations were carried out on fused glass discs whereas trace elements were done on pressed powder pellets. International standards with recommended values from Abbey (1983) as well as inhouse standards were used for calibration. Analytical precision, as determined on replicate analyses is generally better the 5% for the major oxides and between 5-10% for trace elements. Loss on ignition (LOI) was determined by heating the sample for 1 and 1/2 hours at 1050^{o}C in an electric furnace. (K. Cameron, written commun., 1986).

(2) ELECTRON MICROPROBE

Major and trace element analyses for chlorite, muscovite, biotite, garnet, plagioclase, staurolite, and amphibole were obtained using an automated Jeol 733 Electron Microprobe at Dalhousie University, Halifax, Nova Scotia. The system uses a wavelength dispersive spectrometer (W.D.S.) and operates at a voltage of 15 Kv and 5 nA. Matrix effects were corrected on-line using a Tracor Northern ZAF matrix correction procedure. Analytical uncertainty is 1 to 1.5 wt % for major elements.

Raw data was recalculated to cations using a Basic computer program (Richard, 1986, unpublished) on the basis assumed OH values for hydrous minerals and number of oxygens suggested by Deer et al. (1978).

(3) ^{40}Ar-^{39}Ar AGE SPECTRUM DATING

The following derivation and notation is taken from Dallmeyer (1979). The ^{40}Ar-^{39}Ar stepwise-heating technique is based on the formation of ^{39}Ar by the

irradiation of K-bearing samples in a fast neutron flux. The amount of ^{39}Ar produced is given by:

$$(1) \qquad {}^{39}Ar = {}^{39}K \, \Delta T \int \varphi(\epsilon)\sigma(\epsilon)\delta t$$

where ΔT = length of irradiation
$\varphi(\epsilon)$ = neutron flux density at energy E
$\sigma(\epsilon)$ = capture cross section of ^{39}Ar neutrons having energy E
τ = half-life

Radiogenic argon ^{40}Ar ($^{40}Ar^*$) formed by the spontaneous decay of ^{40}K is also present in the sample and is given by the standard K-Ar dating equation

$$(2) \qquad {}^{40}Ar^* = {}^{40}K \, (e^{t/\tau} - 1) \left(\frac{\lambda}{\lambda_e + \lambda_\beta}\right)$$

where λ_e = decay constant for ^{40}Ar by electron capture
λ_β = decay constant for ^{40}Ar by beta decay

Combining (1) and (2), the ($^{40}Ar^*/^{39}Ar$)measured for an irradiated sample of age t is:

$$(3) \quad \frac{{}^{40}Ar^*}{{}^{39}Ar} = \frac{{}^{40}Ar}{{}^{39}Ar} \, \frac{\lambda_e}{\lambda_e+\lambda_\beta} \, \frac{1}{\Delta T} \, \frac{e^{t/\tau}-1}{\int \varphi(\epsilon)\sigma(\epsilon)\delta_e}$$

The quantity,

$$\frac{{}^{39}Ar}{{}^{40}Ar} = \frac{\lambda_e+\lambda_\beta}{\lambda_e} \, \Delta T \int \varphi(\epsilon)\sigma(\epsilon)\delta_e$$

is referred to as the J-value or J. Therefore, from equation (3):

$$J = \frac{e^{t/\tau}-1}{{}^{40}Ar^*/{}^{39}Ar}$$

and therefore,

$$t = \tau \ln\left(1 + J\left({}^{40}Ar^*/{}^{39}Ar\right)\right)$$

J is difficult to determine because the energy spectrum of the neutron flux and the cross-section of ^{39}Ar for capture of neutrons of varying energies is

experienced by a sample depends on its position in the sample holder, several standards are placed in the sample holder at known positions between the samples. The ages of the standards are known and thus their J-value can easily be obtained from equation (4). The J-values for the standards are plotted versus the position in the can and the required J-value for the unknown sample is extrapolated from the points of known J (see Ellias, 1986).

Corrections were made for the presence of interferring argon isotopes and atmospheric argon. The significant interferring isotopes are Ca-derived ^{36}Ar and ^{39}Ar and K-derived ^{40}Ar and corrections for them are discussed by Ellias (1986).

In the absence of interference only the atmospheric correction is made. The equation by which $^{40*}Ar/^{39}Ar$ is derived is

$$40^*/39 = (40/39)\text{measured} - 295.5(36/39)\text{measured}$$

assuming all contaminating argon has the atmospheric ratio (40/36) = 295.5. Following the analysis, an air-calibration is conducted in which atmospheric $^{40}Ar/^{36}Ar$ is measured. The difference between this value and the assumed value of 295.5 is used to derive a correction factor used in the calculation of the apparent age (see Table 7.1).

Procedures

Samples were selected in which hornblende and biotite were apparently pristine in thin section. Weathered surfaces were removed and sample broken down using a steel cut-rock and ceramic jaw crusher and finally pulverized using a tungsten carbide shatter box. Samples were then sieved to 50 and 80 mesh.

A Franz magnetic separator was used to separate the felsic minerals from mafic minerals. The final separation was completed by hand picking the separates to >99% purity. All magnetic separation and hand-picking was done by A. Grist at Dalhousie University.

Following irradiation at the McMaster reactor, Hamilton, Ontario, and a cooling-off period, a given sample was placed in a quartz boat, and placed in a quartz extraction tube attached to a glass vaccum line, and outgassed in a stepwise fashion in a conventional argon extraction-purification system (see Parrott, 1976

and Ellias, 1986 for specific details regarding purification).

After purification, the gas fraction released at each step was analysed in an AEI MS 10 mass spectrometer. Following sequential scanning for masses 36, 37, 39, and 40 a peak hoping procedure was begun automatically and the signal sent to an on-line micrcomputer. These masses were measured 15 times and peak locations re-located before the first, sixth, and eleventh measurement (Ellias, 1986).

The mass ratios: 36/39, 37/39, 40/39 were measured for each step of the 15 determinations on a given gas fraction which commonly vary over the time of the analyses. Thus a linear extrapolation back to zero time (time when the gas was first let into the mass spectrometer) was done for each ratio. Corrections were made for the interferring isotopes and for tailing of the ^{40}Ar peak at the ^{39}Ar peak position (Ellias, 1986). Ages for each gas step were calculated by equation (4). Plateau ages were calculated by taking the weighted mean of the ages (with respect to millivolts of ^{39}Ar released) of the steps defining the plateau.

APPENDIX 3
MICROPROBE DATABASE

Table A3-1: Microprobe database, raw data.

CHLORITE

SAMPLE	85-107				85-659b	
LOCATION	Pblast	Pblast	Pblast	Pblast	Pblast	Pblast
SiO_2	22.93	22.86	22.41	22.93	22.95	24.86
TiO_2	0.14	0.13	0.09	0.01	0.45	0.10
Al_2O_3	22.75	22.43	22.50	22.52	22.79	22.97
FeO	31.54	31.44	31.34	31.45	31.79	22.40
MnO	0.47	0.42	0.39	0.45	0.39	0.07
MgO	8.26	8.15	8.20	8.45	8.24	15.91
CaO	0.00	0.00	0.00	0.00	0.00	0.00
Na_2O	0.00	0.03	0.00	0.00	0.00	0.05
K_2O	0.00	0.00	0.00	0.00	0.00	0.00
H_2O	10.73	10.65	10.57	10.70	10.79	11.39
TOTAL	96.82	96.11	95.50	96.51	97.40	97.75

SAMPLE	85-659b	85-723b			85-446
LOCATION	Pblast	Inc(gt)	Inc(gt)	Incl(gt)	Incl(gt)
SiO_2	24.81	23.94	23.71	23.69	26.55
TiO_2	0.00	0.06	0.01	0.08	0.07
Al_2O_3	23.08	22.65	22.52	22.07	18.31
FeO	22.43	28.75	27.55	29.08	29.98
MnO	0.07	0.12	0.16	0.17	1.15
MgO	15.75	11.61	12.11	11.81	10.40
CaO	0.00	0.00	0.00	0.06	0.01
Na_2O	0.00	0.02	0.00	0.00	0.03
K_2O	0.00	0.00	0.00	0.00	0.17
H_2O	11.36	11.08	11.00	11.01	10.89
TOTAL	97.50	98.23	97.06	97.97	97.56

MUSCOVITE

SAMPLE	85-107					
LOCATION	Matrix	Matrix	Matrix	Veinlt	Veinlt	Veinlt
SiO_2	46.49	46.00	46.03	46.99	47.38	47.22
TiO_2	0.16	0.13	0.19	0.10	0.16	0.09
Al_2O_3	35.70	35.33	36.14	36.52	36.28	38.34
FeO	1.42	1.23	1.12	0.91	1.14	0.79
MnO	0.08	0.11	0.06	0.06	0.09	0.07
MgO	0.41	0.39	0.29	0.21	0.33	0.19
CaO	0.00	0.01	0.00	0.00	0.00	0.21
Na_2O	1.60	1.65	1.73	2.08	1.68	4.49
K_2O	8.33	8.73	8.33	9.17	9.01	3.52
H_2O	4.50	4.45	4.48	4.57	4.58	4.63
TOTAL	98.69	98.03	98.37	100.61	100.65	99.55

SAMPLE	85-K45			85-659b		
LOCATION	Matrix	Matrix	Matrix	Rim	Rim	Core
SiO_2	46.51	47.09	44.31	46.52	46.58	45.86
TiO_2	0.22	0.13	0.12	0.48	0.61	0.51
Al_2O_3	36.21	35.97	34.88	35.72	35.93	36.03
FeO	22.43	28.75	27.55	0.81	0.96	0.99
MnO	1.31	1.35	1.20	0.11	0.09	0.06
MgO	0.43	0.47	0.41	0.54	0.55	0.48
CaO	0.01	0.00	0.00	0.00	0.03	0.00
Na_2O	1.55	1.52	1.45	1.47	1.45	1.45
K_2O	8.41	8.53	8.77	9.74	8.91	8.60
H_2O	4.52	4.54	4.33	4.52	4.53	4.48
TOTAL	99.27	99.61	95.55	99.91	99.64	98.46

MUSCOVITE (continued)

SAMPLE	85-659b					85-732
LOCATION	Core	Core	Core	Core	Core	
SiO_2	46.19	45.72	45.74	46.97	46.65	46.77
TiO_2	0.54	0.46	0.41	0.46	0.38	0.54
Al_2O_3	35.95	35.43	35.61	36.69	36.67	35.54
FeO	1.04	1.20	1.09	0.85	0.89	1.46
MnO	0.06	0.00	0.04	0.12	0.01	0.06
MgO	0.49	0.57	0.54	0.62	0.60	0.64
CaO	0.00	0.00	0.00	0.00	0.00	0.01
Na_2O	1.41	1.46	1.48	1.37	1.45	1.39
K_2O	8.93	8.88	8.85	8.77	8.84	9.28
H_2O	4.51	4.46	4.46	4.58	4.68	4.54
TOTAL	99.12	98.18	98.22	100.43	100.05	100.23

SAMPLE	85-732					
LOCATION						
SiO_2	46.37	46.11	46.91	46.45	46.56	47.09
TiO_2	0.54	0.77	0.71	0.58	0.53	0.70
Al_2O_3	35.11	34.50	34.85	34.97	35.37	34.53
FeO	1.53	1.57	1.52	1.35	1.50	1.46
MnO	0.08	0.11	0.04	0.11	0.06	0.08
MgO	0.70	0.76	0.79	0.75	0.71	0.72
CaO	0.05	0.00	0.00	0.00	0.00	0.01
Na_2O	1.46	1.27	1.33	1.27	1.31	1.26
K_2O	8.96	9.02	8.94	8.71	8.76	9.16
H_2O	4.50	4.46	4.52	4.49	4.51	4.51
TOTAL	99.30	98.57	99.61	98.68	99.31	99.52

SAMPLE	85-441					85-446
LOCATION						Rim
SiO_2	46.75	47.15	46.25	46.22	46.30	47.77
TiO_2	0.93	0.48	0.87	0.95	0.67	0.70
Al_2O_3	35.55	35.01	35.53	34.60	35.22	35.09
FeO	1.14	1.22	1.02	0.92	0.94	0.85
MnO	0.03	0.06	0.10	0.10	0.05	0.00
MgO	0.62	0.82	0.58	0.58	0.66	0.69
CaO	0.00	0.03	0.04	0.04	0.00	0.00
Na_2O	1.35	0.91	1.31	1.31	1.34	0.91
K_2O	9.30	7.49	9.49	9.49	9.01	10.32
H_2O	4.55	4.49	4.52	4.52	4.49	4.57
TOTAL	100.22	97.66	99.71	99.71	98.68	100.90

SAMPLE	85-446				85-535	
LOCATION	Rim	Core	Rim	Core	Core	Rim
SiO_2	45.82	46.33	47.28	46.78	46.66	46.54
TiO_2	0.49	0.46	0.53	0.79	0.73	0.80
Al_2O_3	35.64	33.67	35.12	34.40	35.42	35.19
FeO	0.79	0.83	0.91	0.89	0.89	1.15
MnO	0.00	0.06	0.07	0.08	0.12	0.11
MgO	0.58	0.77	0.81	0.83	0.70	0.97
CaO	0.00	0.00	0.00	0.00	0.00	0.03
Na_2O	0.98	1.07	1.03	1.02	1.23	1.22
K_2O	9.66	10.32	10.50	10.12	9.40	9.30
H_2O	4.47	4.42	4.55	4.50	4.52	4.52
TOTAL	98.43	97.93	100.80	99.41	99.67	99.83

MUSCOVITE (continued)

SAMPLE	85-535			85-700b		
LOCATION	Core	Rim	Rim			
SiO_2	46.46	47.36	47.15	47.28	46.02	46.93
TiO_2	0.64	0.86	0.71	0.43	0.42	0.20
Al_2O_3	34.99	35.46	34.68	35.47	35.30	36.64
FeO	1.10	0.94	1.14	0.81	0.82	0.85
MnO	0.09	0.07	0.07	0.09	0.09	0.00
MgO	0.81	0.76	1.00	0.54	0.57	0.40
CaO	0.00	0.02	0.00	0.01	0.08	0.02
Na_2O	1.18	1.21	1.14	1.57	1.49	1.92
K_2O	9.45	9.31	9.91	8.62	8.79	8.47
H_2O	4.50	4.57	4.54	4.53	4.46	4.56
TOTAL	99.22	100.56	100.34	99.35	98.04	99.99

SAMPLE	85-700b					85-722
LOCATION				Inc(gt)	Inc(gt)	
SiO_2	47.55	46.85	46.76	46.60	46.99	46.86
TiO_2	0.34	0.49	0.42	0.44	0.46	0.57
Al_2O_3	36.22	35.95	36.25	36.10	35.65	35.99
FeO	0.80	0.80	0.94	0.88	0.97	1.01
MnO	0.00	0.09	0.07	0.06	0.04	0.06
MgO	0.56	0.59	0.58	0.53	0.59	0.57
CaO	0.00	0.01	0.00	0.01	0.01	0.00
Na_2O	1.59	1.52	1.53	1.66	1.61	1.58
K_2O	8.75	8.54	8.57	8.95	9.04	9.10
H_2O	4.58	4.54	4.55	4.54	4.54	4.56
TOTAL	100.39	99.38	99.67	99.77	99.90	100.30

SAMPLE	85-722					85-723b
LOCATION						
SiO_2	45.99	46.74	45.98	46.60	46.80	47.06
TiO_2	0.45	0.45	0.51	0.50	0.54	0.59
Al_2O_3	34.44	36.16	35.93	35.81	35.80	35.48
FeO	1.58	1.20	1.21	1.10	0.88	0.91
MnO	0.11	0.00	0.04	0.06	0.04	0.02
MgO	0.64	0.54	0.63	0.68	0.63	0.75
CaO	0.13	0.00	0.00	0.00	0.03	0.00
Na_2O	1.49	1.47	1.52	1.55	1.59	1.12
K_2O	8.29	8.91	8.73	8.72	8.79	8.80
H_2O	4.43	4.55	4.50	4.53	4.54	4.53
TOTAL	97.55	100.02	99.05	99.55	99.64	99.26

SAMPLE	85-723b	
LOCATION		
SiO_2	47.06	47.05
TiO_2	0.51	0.66
Al_2O_3	36.38	35.53
FeO	0.76	0.90
MnO	0.05	0.07
MgO	0.56	0.76
CaO	0.04	0.00
Na_2O	1.19	1.30
K_2O	8.50	8.86
H_2O	4.56	4.54
TOTAL	99.61	99.63

GARNET MAP DATA

SAMPLE	85-445					
LOCATION	1	2	3	4	5	6
SiO_2	37.03	37.45	37.33	37.20	36.99	37.37
TiO_2	0.00	0.00	0.00	0.00	0.12	0.00
Al_2O_3	20.63	21.02	21.33	20.93	20.98	20.94
Cr_2O_3	0.00	0.00	0.00	0.00	0.00	0.00
FeO	31.26	31.55	31.33	30.46	30.36	31.79
MnO	2.95	1.90	1.38	2.58	2.98	2.23
MgO	4.70	5.74	5.92	5.00	4.44	5.26
CaO	1.79	2.10	2.09	2.79	3.45	1.73
TOTAL	98.36	99.76	99.38	98.96	99.32	99.32

SAMPLE	85-445					
LOCATION	7	8	9	10	11	12
SiO_2	37.40	37.28	37.44	37.42	37.83	37.86
TiO_2	0.00	0.06	0.00	0.00	0.00	0.03
Al_2O_3	21.05	20.98	20.91	21.10	20.93	20.86
Cr_2O_3	0.04	0.00	0.00	0.00	0.00	0.00
FeO	31.66	30.52	30.17	30.93	31.50	30.98
MnO	1.74	2.02	3.85	2.74	2.02	1.98
MgO	5.60	5.44	3.98	4.89	5.46	5.62
CaO	2.29	2.52	3.34	2.74	2.47	2.55
TOTAL	99.78	98.82	99.69	99.82	100.21	99.88

SAMPLE	85-445					
LOCATION	13	14	15	16	17	18
SiO_2	37.80	37.61	37.75	37.75	37.28	37.05
TiO_2	0.00	0.00	0.01	0.00	0.03	0.00
Al_2O_3	20.83	20.89	20.65	21.18	20.80	20.03
Cr_2O_3	0.00	0.00	0.00	0.00	0.00	0.00
FeO	31.34	31.49	31.63	31.61	28.95	30.17
MnO	1.57	1.47	3.11	1.65	5.71	4.48
MgO	5.63	5.85	4.87	5.61	3.20	3.48
CaO	2.37	2.01	1.78	2.10	3.87	3.53
TOTAL	99.54	99.32	99.80	99.90	99.84	98.74

SAMPLE	85-445					
LOCATION	19	20	21	22	23	24
SiO_2	37.75	37.49	37.46	37.50	37.35	37.80
TiO_2	0.01	0.00	0.00	0.00	0.00	0.12
Al_2O_3	21.06	20.44	20.82	20.82	20.93	20.68
Cr_2O_3	0.00	0.00	0.00	0.00	0.00	0.00
FeO	29.74	29.84	30.49	30.35	30.77	30.11
MnO	3.32	4.44	3.51	3.22	2.93	3.92
MgO	4.49	3.87	4.32	4.44	4.58	4.20
CaO	3.35	3.19	3.18	3.29	3.03	3.28
TOTAL	99.72	99.27	99.78	99.62	99.59	100.11

SAMPLE	85-445					
LOCATION	25	26	27	28	29	30
SiO_2	37.73	37.49	36.90	36.93	36.67	36.46
TiO_2	0.00	0.00	0.08	0.00	0.08	0.00
Al_2O_3	20.89	20.79	21.06	20.70	21.01	20.52
Cr_2O_3	0.00	0.00	0.00	0.00	0.03	0.00
FeO	30.70	31.07	31.27	30.14	31.20	29.72
MnO	3.48	3.48	2.25	3.99	2.35	4.37
MgO	4.17	4.26	5.41	4.02	5.27	3.86
CaO	3.31	3.22	2.57	3.36	2.67	3.34
TOTAL	100.28	100.31	99.54	99.14	99.28	98.27

GARNET

SAMPLE	85-107					
LOCATION	core	core	core	core	core	core
SiO_2	35.75	35.87	35.81	35.56	35.56	35.98
TiO_2	0.00	0.03	0.06	0.04	0.06	0.00
Al_2O_3	20.61	20.84	20.40	20.79	20.50	20.28
Cr_2O_3	0.19	0.16	0.02	0.15	0.15	0.02
FeO	29.57	30.28	29.70	29.59	29.20	30.51
MnO	9.31	8.77	8.43	8.75	9.28	8.95
MgO	0.79	0.80	0.81	0.82	0.80	0.89
CaO	2.25	2.01	2.03	2.32	2.29	1.84
TOTAL	98.47	98.76	97.26	98.02	98.26	98.71

SAMPLE	85-107	85-K45				85-698c
LOCATION	core	rim	rim	rim	core	core
SiO_2	36.17	36.47	36.08	36.43	36.24	37.06
TiO_2	0.06	0.03	0.03	0.01	0.00	0.03
Al_2O_3	20.19	20.64	20.17	19.88	20.70	21.08
Cr_2O_3	0.12	0.17	0.01	0.02	0.15	0.00
FeO	29.40	31.16	30.38	30.33	28.01	30.61
MnO	9.14	6.10	6.96	6.59	9.57	1.01
MgO	0.86	0.91	0.84	0.86	0.72	3.47
CaO	2.20	3.09	3.40	3.67	3.55	5.41
TOTAL	98.14	98.57	97.87	97.79	98.94	98.67

SAMPLE	85-698c				85-659b	
LOCATION	core	rim	rim	xrim	core	core
SiO_2	37.47	37.23	37.58	37.32	36.32	36.09
TiO_2	0.14	0.00	0.03	0.18	0.11	0.12
Al_2O_3	21.32	20.22	21.34	21.54	20.78	20.65
Cr_2O_3	0.08	0.02	0.00	0.00	0.09	0.13
FeO	29.68	31.21	31.37	31.85	32.37	31.15
MnO	2.82	0.93	0.85	0.89	2.64	4.46
MgO	2.70	3.36	3.42	3.42	1.85	1.63
CaO	6.46	5.67	5.52	5.63	5.37	5.10
TOTAL	100.67	98.64	100.11	100.83	99.53	99.33

SAMPLE	85-659b					
LOCATION	core	core	middle	middle	middle	middle
SiO_2	36.59	36.86	36.56	36.55	36.83	36.56
TiO_2	0.17	0.07	0.16	0.05	0.06	0.04
Al_2O_3	20.87	21.02	20.82	20.79	21.09	20.88
Cr_2O_3	0.18	0.16	0.17	0.20	0.14	0.04
FeO	31.27	34.34	31.29	32.94	34.13	34.04
MnO	4.68	1.05	4.57	2.21	0.43	0.32
MgO	1.60	2.18	1.64	1.90	2.32	2.54
CaO	5.40	5.09	5.18	5.36	5.15	4.54
TOTAL	100.76	100.77	100.39	100.00	100.15	98.96

SAMPLE	85-659b					
LOCATION	middle	middle	middle	middle	rim-1	rim-1
SiO_2	36.65	36.50	36.65	36.29	36.79	36.49
TiO_2	0.04	0.04	0.09	0.08	0.01	0.09
Al_2O_3	21.31	21.16	20.82	20.88	21.01	21.24
Cr_2O_3	0.14	0.11	0.15	0.16	0.08	0.15
FeO	34.40	34.31	34.58	33.66	34.46	35.64
MnO	0.26	0.98	0.89	0.50	0.23	0.17
MgO	2.77	2.22	2.19	2.45	3.45	3.61
CaO	4.68	4.66	5.11	5.26	3.34	2.98
TOTAL	100.25	99.98	100.48	99.28	99.37	100.37

GARNET (continued)

SAMPLE	85-659b					85-700b
LOCATION	rim-2	rim-2	xrim	xrim	xrim	core
SiO_2	36.59	36.97	37.15	36.58	36.81	36.14
TiO_2	0.03	0.08	0.03	0.02	0.00	0.05
Al_2O_3	21.31	20.97	21.02	21.25	21.37	20.72
Cr_2O_3	0.15	0.16	0.13	0.14	0.16	0.12
FeO	35.01	33.34	34.02	33.89	34.35	29.69
MnO	0.25	0.05	0.17	0.27	0.06	5.17
MgO	3.25	3.42	3.65	3.40	3.63	1.47
CaO	3.33	4.32	3.71	4.32	4.01	5.44
TOTAL	99.92	99.31	99.88	99.87	100.39	98.80

SAMPLE	85-700b					
LOCATION	core	middle	middle	rim	xrim	xrim
SiO_2	36.51	36.67	36.74	36.83	37.27	36.83
TiO_2	0.10	0.12	0.02	0.12	0.05	0.07
Al_2O_3	20.36	21.08	20.95	21.00	21.23	21.07
Cr_2O_3	0.16	0.15	0.17	0.14	0.14	0.18
FeO	30.10	30.44	33.08	31.34	32.21	33.06
MnO	4.19	3.93	1.21	3.36	0.26	0.21
MgO	1.56	1.56	1.94	1.98	3.54	3.04
CaO	6.27	5.77	4.96	5.33	4.12	4.14
TOTAL	99.25	99.72	99.06	100.10	98.82	98.60

SAMPLE	85-700b	85-716a				
LOCATION	xrim	core	middle	middle	rim	rim
SiO_2	37.02	36.39	37.15	36.43	37.35	36.93
TiO_2	0.13	0.09	0.17	0.03	0.00	0.07
Al_2O_3	20.70	20.57	20.72	20.49	20.71	21.12
Cr_2O_3	0.16	0.14	0.18	0.19	0.17	0.20
FeO	30.92	28.37	29.73	28.00	30.55	31.28
MnO	3.57	5.55	4.44	6.38	1.00	0.99
MgO	1.71	1.52	1.54	1.35	2.83	2.95
CaO	6.02	6.14	5.92	6.12	5.57	5.83
TOTAL	100.23	98.77	99.85	98.99	98.18	99.37

SAMPLE	85-716a	85-722				
LOCATION	xrim	core	core	core	core	core
SiO_2	37.19	36.77	37.19	36.89	36.73	37.04
TiO_2	0.07	0.02	0.00	0.02	0.04	0.00
Al_2O_3	21.01	20.53	20.08	20.86	20.40	20.52
Cr_2O_3	0.18	0.00	0.07	0.04	0.00	0.00
FeO	33.20	33.60	34.42	33.87	33.81	33.20
MnO	0.65	1.10	1.37	1.10	1.18	1.19
MgO	2.24	3.70	3.07	3.78	3.70	3.70
CaO	5.32	3.08	2.83	3.02	2.54	2.80
TOTAL	99.86	98.80	99.03	99.58	98.40	98.45

SAMPLE	85-722					
LOCATION	core	middle	middle	middle	middle	middle
SiO_2	37.12	36.78	36.53	36.89	36.87	37.01
TiO_2	0.03	0.00	0.02	0.02	0.03	0.01
Al_2O_3	20.60	20.42	20.45	20.46	20.38	20.36
Cr_2O_3	0.07	0.01	0.03	0.04	0.02	0.00
FeO	33.22	33.25	33.47	33.79	33.47	33.81
MnO	1.08	1.18	1.17	1.21	1.25	1.23
MgO	3.93	3.65	3.71	3.75	3.68	3.84
CaO	2.93	3.26	2.73	2.64	2.74	2.23
TOTAL	98.98	98.55	98.11	98.80	98.44	98.49

GARNET (continued)

SAMPLE	85-722					
LOCATION	middle	middle	middle	middle	middle	middle
SiO_2	36.73	37.06	36.66	37.14	36.71	36.03
TiO_2	0.00	0.03	0.00	0.01	0.02	0.00
Al_2O_3	20.44	20.33	20.18	20.65	20.80	20.13
Cr_2O_3	0.00	0.02	0.00	0.02	0.04	0.02
FeO	33.26	33.47	33.38	33.61	33.73	33.76
MnO	1.24	1.17	1.33	1.18	1.19	1.38
MgO	3.51	3.79	3.73	3.74	3.69	3.28
CaO	2.70	2.89	2.55	2.73	2.74	2.59
TOTAL	97.88	98.76	97.83	99.08	98.92	97.19

SAMPLE	85-722					
LOCATION	rim	rim	rim	xrim	xrim	xrim
SiO_2	36.61	37.22	37.05	36.75	36.63	36.52
TiO_2	0.13	0.08	0.14	0.00	0.01	0.03
Al_2O_3	20.18	20.20	20.31	20.03	20.57	20.29
Cr_2O_3	0.05	0.02	0.00	0.10	0.00	0.04
FeO	35.26	34.06	33.48	33.80	33.27	33.65
MnO	1.96	1.36	1.60	1.29	1.32	1.22
MgO	2.24	3.10	2.56	3.15	3.34	3.58
CaO	2.31	2.97	3.15	2.72	2.95	3.25
TOTAL	98.74	99.01	98.29	97.84	98.09	98.58

SAMPLE	85-722					
LOCATION	xrim	xrim	xrim	xrim	xrim	xrim
SiO_2	36.90	36.68	37.02	36.41	36.64	36.98
TiO_2	0.03	0.08	0.03	0.01	0.00	0.04
Al_2O_3	20.66	20.54	20.27	20.29	20.33	20.40
Cr_2O_3	0.00	0.05	0.00	0.00	0.00	0.06
FeO	33.11	33.61	32.36	33.46	32.80	33.21
MnO	1.18	1.25	0.80	1.31	1.17	1.24
MgO	3.59	3.74	3.98	3.44	3.69	3.67
CaO	3.35	2.64	3.63	2.61	3.06	2.66
TOTAL	98.82	98.59	98.09	99.58	97.69	98.26

SAMPLE	85-722	85-723b				
LOCATION	xrim	core	core	middle	middle	rim
SiO_2	36.80	36.47	36.82	37.00	36.89	36.80
TiO_2	0.02	0.01	0.00	0.01	0.07	0.07
Al_2O_3	20.30	20.93	20.88	21.24	20.97	21.01
Cr_2O_3	0.03	0.18	0.18	0.14	0.21	0.21
FeO	33.68	33.33	33.68	33.75	32.87	33.39
MnO	1.40	1.66	1.70	1.61	1.55	1.46
MgO	3.42	3.64	3.19	3.61	3.43	3.53
CaO	2.75	3.47	3.16	2.97	3.32	3.34
TOTAL	98.40	99.69	99.61	100.33	99.31	99.81

SAMPLE	85-723b			85-441	
LOCATION	xrim	xrim	xrim	core (ky)	core(ky)
SiO_2	36.69	36.98	37.08	37.13	37.17
TiO_2	0.06	0.06	0.05	0.06	0.01
Al_2O_3	21.10	20.97	20.35	21.18	21.22
Cr_2O_3	0.16	0.19	0.15	0.17	0.17
FeO	32.62	33.36	32.83	31.40	31.59
MnO	1.54	1.64	1.62	1.36	1.28
MgO	3.48	3.48	3.61	5.50	5.61
CaO	3.66	3.32	3.28	1.94	1.92
TOTAL	99.31	100.00	98.97	98.74	98.97

GARNET (continued)

SAMPLE	85-441				
LOCATION	rim(ky)	rim(ky)	xrim(ky)	xrim(ky)	core(m)
SiO_2	36.78	37.24	36.90	37.17	37.07
TiO_2	0.00	0.03	0.05	0.01	0.05
Al_2O_3	20.95	20.92	21.01	21.06	21.32
Cr_2O_3	0.00	0.18	0.16	0.17	0.18
FeO	33.40	31.38	31.75	32.27	31.69
MnO	3.13	2.22	2.59	2.29	1.27
MgO	4.12	4.72	4.59	4.61	5.57
CaO	1.60	1.92	1.66	1.91	1.95
TOTAL	99.98	98.61	98.71	99.49	99.10

SAMPLE	85-441				
LOCATION	middle(m)	middle(m)	rim(m)	rim(m)	rim(m)
SiO_2	37.59	37.07	36.77	36.73	36.72
TiO_2	0.00	0.05	0.05	0.03	0.01
Al_2O_3	21.19	21.32	21.08	20.99	20.96
Cr_2O_3	0.18	0.18	0.21	0.14	0.00
FeO	31.98	31.69	32.58	32.36	33.35
MnO	1.23	1.27	3.45	3.78	2.75
MgO	5.51	5.57	3.73	3.36	4.16
CaO	2.02	1.95	1.86	1.83	1.68
TOTAL	99.70	99.10	99.73	99.22	99.63

SAMPLE	85-441		85-446			
LOCATION	xrim(m)	xrim(m)	core	core	rim	rim
SiO_2	37.58	36.72	37.30	37.43	37.18	37.01
TiO_2	0.00	0.01	0.00	0.00	0.04	0.00
Al_2O_3	21.20	20.90	21.18	21.73	21.00	21.14
Cr_2O_3	0.20	0.20	0.12	0.15	0.07	0.05
FeO	31.71	32.07	32.34	32.31	31.57	30.86
MnO	1.37	1.89	1.73	1.77	4.39	4.37
MgO	5.37	5.01	5.41	5.70	4.26	4.06
CaO	1.93	1.95	1.84	1.71	1.62	1.87
TOTAL	99.36	98.75	99.92	100.80	100.13	99.36

SAMPLE	85-446	85-245				85-280
LOCATION	xrim	core	rim	rim	rim	core
SiO_2	37.16	37.09	36.96	36.59	37.41	37.26
TiO_2	0.07	0.15	0.08	0.02	0.13	0.00
Al_2O_3	21.16	19.75	20.15	19.41	20.22	21.01
Cr_2O_3	0.18	0.00	0.02	0.00	0.00	0.17
FeO	30.32	27.40	26.46	27.59	26.69	27.71
MnO	5.47	3.18	5.44	2.33	2.55	3.06
MgO	3.88	2.95	2.61	3.58	3.48	3.07
CaO	1.39	8.89	7.23	7.58	8.40	7.76
TOTAL	99.63	99.41	98.95	97.10	98.88	100.04

SAMPLE	85-280					85-343a
LOCATION	core	rim	rim	rim	rim	core
SiO_2	37.36	37.35	37.28	37.59	37.72	37.34
TiO_2	0.12	0.07	0.12	0.10	0.04	0.00
Al_2O_3	20.93	20.94	20.65	20.81	21.19	20.73
Cr_2O_3	0.19	0.18	0.18	0.14	0.16	0.16
FeO	27.68	26.85	27.76	28.55	28.08	26.88
MnO	2.32	2.30	2.83	1.72	1.95	2.92
MgO	3.54	3.60	3.05	3.61	3.54	2.82
CaO	8.20	8.06	7.79	7.92	8.13	8.21
TOTAL	100.34	99.35	99.66	100.44	100.81	99.06

SAMPLE	85-343a

GARNET (continued)

SAMPLE	85-343a			
LOCATION	core	rim	rim	rim
SiO_2	37.77	37.80	37.35	37.79
TiO_2	0.05	0.13	0.07	0.06
Al_2O_3	21.04	21.20	21.13	21.06
Cr_2O_3	0.15	0.19	0.19	0.18
FeO	27.84	26.54	27.91	27.93
MnO	1.86	2.60	3.76	2.07
MgO	3.44	2.84	2.81	3.41
CaO	8.37	8.11	6.83	8.13
TOTAL	100.52	99.41	100.05	100.63

BIOTITE

SAMPLE	85-698c				85-659b	
LOCATION	core	core	core	xrim	core	core
SiO_2	37.52	37.19	36.54	36.95	35.80	36.54
TiO_2	1.68	1.33	1.39	1.31	1.15	1.22
Al_2O_3	18.20	17.82	17.64	17.24	19.74	19.84
FeO	16.63	17.04	17.58	17.65	18.10	17.51
MnO	0.17	0.00	0.00	0.06	0.08	0.00
MgO	11.72	12.26	11.89	12.00	10.64	10.69
CaO	0.10	0.02	0.07	0.06	0.04	0.04
Na_2O	0.49	0.21	0.26	0.26	0.40	0.34
K_2O	8.53	9.03	9.19	8.78	8.82	8.80
H_2O	4.01	3.99	3.95	3.95	3.96	3.99
TOTAL	99.05	98.89	98.51	98.26	98.09	98.97

SAMPLE	85-659b					
LOCATION	rim-1	rim-1	rim-2	rim-2	xrim	xrim
SiO_2	36.61	36.07	36.43	36.71	36.38	36.03
TiO_2	1.54	1.47	1.44	1.45	1.21	1.38
Al_2O_3	19.81	19.44	19.47	19.82	19.64	19.80
FeO	17.50	17.60	18.11	17.59	17.37	18.21
MnO	0.08	0.00	0.05	0.00	0.05	0.00
MgO	11.11	11.01	11.30	11.31	10.90	10.63
CaO	0.00	0.00	0.00	0.00	0.02	0.04
Na_2O	8.38	0.26	0.24	0.24	0.35	0.37
K_2O	0.00	8.27	8.24	8.13	8.75	8.78
H_2O	4.01	3.96	4.00	4.02	3.98	3.98
TOTAL	99.14	98.08	99.28	99.27	98.65	99.22

SAMPLE	85-659b		85-700b			
LOCATION	xrim	xrim	core	core	core	core
SiO_2	37.09	36.97	36.90	36.97	37.33	37.20
TiO_2	1.61	1.57	1.69	1.63	1.66	1.65
Al_2O_3	19.61	19.48	19.63	19.65	19.59	19.57
FeO	18.50	17.83	16.59	16.72	17.17	17.23
MnO	0.03	0.01	0.00	0.01	0.03	0.06
MgO	11.11	11.24	11.54	11.90	11.84	11.45
CaO	0.00	0.00	0.00	0.00	0.00	0.00
Na_2O	0.26	0.27	0.26	0.23	0.26	0.30
K_2O	9.07	9.05	8.76	8.61	8.75	9.24
H_2O	4.07	4.04	4.03	4.05	4.08	4.06
TOTAL	101.35	98.08	99.40	99.77	100.71	100.76

BIOTITE (continued)

SAMPLE	85-700b					
LOCATION	core	core	xrim	xrim	xrim	xrim
SiO_2	35.15	37.07	36.76	37.22	36.91	37.06
TiO_2	1.55	1.68	1.66	1.78	1.56	1.65
Al_2O_3	19.13	19.62	19.63	19.56	19.50	19.92
FeO	17.10	16.59	16.91	16.71	17.28	16.71
MnO	0.13	0.06	0.01	0.00	0.06	0.13
MgO	11.66	11.67	11.29	11.55	11.54	11.52
CaO	0.03	0.00	0.00	0.00	0.00	0.00
Na_2O	0.23	0.25	0.28	0.18	0.22	0.18
K_2O	8.53	9.11	8.17	9.21	8.96	9.08
H_2O	3.92	4.05	4.01	4.06	4.04	4.06
TOTAL	97.43	100.10	98.72	100.27	100.07	100.31

SAMPLE	85-700b	85-707b				
LOCATION	rim	core	core	core	core	xrim
SiO_2	37.11	35.89	35.53	36.00	35.96	35.44
TiO_2	1.72	1.64	1.95	1.79	1.89	1.99
Al_2O_3	19.98	19.14	19.21	19.67	19.28	19.08
FeO	16.17	19.27	19.56	18.48	19.46	19.12
MnO	0.13	0.05	0.19	0.03	0.03	0.12
MgO	11.49	9.49	9.22	9.44	9.38	9.38
CaO	0.00	0.04	0.08	0.02	0.02	0.04
Na_2O	0.26	0.23	0.24	0.24	0.23	0.26
K_2O	9.27	9.59	9.09	9.62	9.61	9.09
H_2O	4.06	3.94	3.93	3.96	3.96	3.92
TOTAL	100.19	99.28	99.00	99.25	99.82	98.44

SAMPLE	85-707b	85-722				
LOCATION	xrim	core	core	core	core	core
SiO_2	36.11	37.18	35.99	36.46	36.09	36.04
TiO_2	1.97	1.85	1.74	1.77	1.73	1.66
Al_2O_3	19.56	20.20	19.57	19.64	19.72	19.38
FeO	19.54	17.37	17.23	17.21	16.89	17.60
MnO	0.01	0.15	0.11	0.07	0.08	0.03
MgO	9.43	10.73	10.77	10.74	11.04	10.70
CaO	0.04	0.00	0.00	0.04	0.07	0.01
Na_2O	0.34	0.40	0.32	0.40	0.30	0.31
K_2O	9.57	7.77	9.09	9.13	9.39	9.63
H_2O	3.99	4.05	3.97	4.00	3.99	3.98
TOTAL	100.56	99.70	98.79	99.46	99.30	99.34

SAMPLE	85-722					85-723b
LOCATION	core	xrim	xrim	rim	inc(gt)	core
SiO_2	35.70	36.20	35.93	36.34	35.06	36.34
TiO_2	1.57	1.64	1.60	1.35	1.09	1.73
Al_2O_3	19.24	19.16	18.79	19.72	18.71	19.91
FeO	16.68	16.74	17.56	17.89	20.01	16.39
MnO	0.15	0.00	0.00	0.11	0.01	0.08
MgO	10.60	10.80	10.40	11.23	10.51	10.77
CaO	0.00	0.00	0.04	0.00	0.03	0.00
Na_2O	0.32	0.47	0.45	0.03	0.14	0.35
K_2O	9.87	9.00	9.43	8.56	8.68	9.42
H_2O	3.93	3.95	3.93	4.00	3.89	3.99
TOTAL	98.06	97.96	98.13	99.23	98.13	98.98

BIOTITE (continued)

SAMPLE	85-723b					
LOCATION	core	xrim	xrim	xrim	xrim	xrim
SiO_2	36.84	36.53	36.66	36.49	36.57	36.70
TiO_2	1.19	1.23	1.34	1.31	1.32	1.35
Al_2O_3	19.88	19.29	19.45	19.99	19.13	19.80
FeO	16.65	16.68	16.85	15.94	17.30	16.53
MnO	0.00	0.08	0.05	0.01	0.08	0.11
MgO	10.96	11.16	10.86	10.79	11.13	10.92
CaO	0.01	0.05	0.01	0.04	0.04	0.04
Na_2O	0.39	0.36	0.36	0.34	0.38	0.35
K_2O	9.26	9.03	8.75	8.94	9.06	9.04
H_2O	4.01	3.97	3.98	3.97	3.98	4.00
TOTAL	99.19	98.38	98.31	97.82	98.99	98.84

SAMPLE	85-723b	85-732				
LOCATION	rim	core	core	core	core	core
SiO_2	35.48	35.91	36.43	36.04	36.22	36.05
TiO_2	1.45	1.41	1.26	1.51	1.43	1.97
Al_2O_3	20.32	19.08	19.44	19.17	18.91	18.79
FeO	17.20	19.35	18.01	17.78	18.61	19.08
MnO	0.03	0.00	0.03	0.06	0.00	0.28
MgO	11.18	10.31	10.42	10.29	10.12	10.56
CaO	0.00	0.08	0.00	0.00	0.05	0.00
Na_2O	0.12	0.39	0.35	0.40	0.38	0.26
K_2O	7.54	8.77	9.22	9.20	9.02	9.12
H_2O	3.95	3.96	3.98	3.94	3.94	3.98
TOTAL	97.27	99.26	99.14	98.39	98.68	100.09

SAMPLE	85-441					
LOCATION	rim(m)	rim(m)	inc(ky)	inc(ky)	inc(ky)	inc(ky)
SiO_2	36.75	36.53	37.30	36.91	36.99	36.99
TiO_2	1.98	2.03	2.40	2.49	2.50	2.40
Al_2O_3	19.77	19.41	19.37	19.00	19.17	19.44
FeO	17.22	17.42	17.70	17.59	17.41	17.65
MnO	0.24	0.24	0.22	0.22	0.19	0.25
MgO	10.68	10.85	10.21	10.41	10.44	10.41
CaO	0.00	0.00	0.00	0.00	0.00	0.00
Na_2O	0.15	0.26	0.26	0.30	0.29	0.27
K_2O	9.56	9.28	8.85	8.85	8.92	9.30
H_2O	4.04	4.02	4.05	4.02	4.03	4.05
TOTAL	100.39	100.04	100.36	99.79	99.94	100.76

SAMPLE	85-446					
LOCATION	core	xrim	xrim	rim-1	rim-1	rim-2
SiO_2	35.65	35.77	35.89	35.65	35.93	36.21
TiO_2	2.10	2.14	2.13	2.10	2.32	1.91
Al_2O_3	18.75	18.65	18.82	18.96	18.77	19.13
FeO	16.95	16.89	17.02	16.98	16.78	17.19
MnO	0.24	0.21	0.11	0.24	0.32	0.32
MgO	11.22	10.74	11.05	11.07	10.80	11.05
CaO	0.00	0.00	0.00	0.00	0.00	0.01
Na_2O	0.24	0.22	0.23	0.03	0.14	0.07
K_2O	9.91	9.55	9.61	9.77	9.71	9.57
H_2O	3.96	3.93	3.96	3.95	3.96	3.99
TOTAL	99.02	98.10	98.82	98.75	98.73	99.45

BIOTITE (continued)

SAMPLE	85-535					
LOCATION	core	core	core	xrim	xrim	rim
SiO_2	36.21	36.16	36.62	36.07	36.51	36.45
TiO_2	2.38	2.59	2.03	1.86	2.24	2.06
Al_2O_3	18.54	19.00	19.50	19.24	19.27	19.55
FeO	16.22	16.61	16.69	17.36	17.01	16.62
MnO	0.10	0.15	0.10	0.09	0.14	0.16
MgO	10.96	10.63	11.11	10.75	10.77	11.09
CaO	0.00	0.00	0.01	0.03	0.04	0.02
Na_2O	0.29	0.36	0.36	0.11	0.36	0.34
K_2O	10.06	9.97	9.44	9.56	9.27	9.19
H_2O	3.96	3.99	4.02	3.97	4.01	4.01
TOTAL	98.72	99.46	99.88	99.04	99.62	99.49

SAMPLE	85-535					
LOCATION	rim	rim	rim	inc(gt)	inc(gt)	inc(gt)
SiO_2	36.49	36.88	36.45	35.96	36.57	36.52
TiO_2	2.02	1.91	1.86	2.25	1.98	2.07
Al_2O_3	19.12	19.74	19.93	19.28	19.39	19.69
FeO	17.28	16.54	16.58	16.52	17.17	17.39
MnO	0.16	0.14	0.19	0.22	0.05	0.25
MgO	11.03	11.22	11.28	10.68	11.06	11.14
CaO	0.07	0.03	0.04	0.02	0.08	0.00
Na_2O	0.32	0.36	0.36	0.31	0.43	0.46
K_2O	9.26	9.39	9.08	9.38	8.93	9.08
H_2O	4.01	4.05	4.03	3.97	4.02	4.05
TOTAL	99.76	100.26	99.80	98.59	99.68	100.65

SAMPLE	85-535		85-565			
LOCATION	inc(gt)	inc(gt)	core	core	core	xrim
SiO_2	36.61	36.12	37.20	37.48	36.87	37.05
TiO_2	0.70	1.56	2.02	1.68	1.78	1.88
Al_2O_3	19.94	19.41	16.90	16.18	16.24	16.95
FeO	16.51	16.80	18.28	18.41	19.02	18.92
MnO	0.08	0.21	0.35	0.47	0.35	0.45
MgO	11.57	11.41	10.17	10.62	10.33	10.13
CaO	0.06	0.01	0.06	0.00	0.05	0.03
Na_2O	0.29	0.31	0.01	0.01	0.10	0.09
K_2O	9.42	9.02	10.30	9.77	10.00	9.69
H_2O	4.00	3.98	3.94	3.92	3.90	3.94
TOTAL	99.18	98.83	99.23	98.54	98.64	99.13

SAMPLE	85-565					
LOCATION	xrim	xrim	xrim	xrim	xrim	rim
SiO_2	36.97	36.75	36.61	36.72	36.88	36.80
TiO_2	1.88	2.02	2.16	1.85	1.44	1.65
Al_2O_3	16.84	16.49	16.36	16.49	17.10	16.53
FeO	18.93	18.79	18.59	18.59	18.92	18.83
MnO	0.47	0.72	0.14	0.42	0.37	0.39
MgO	10.32	10.11	10.16	10.24	10.53	10.45
CaO	0.03	0.03	0.02	0.04	0.06	0.07
Na_2O	0.03	0.07	0.03	0.01	0.09	0.01
K_2O	10.11	9.92	9.96	10.21	10.46	10.29
H_2O	3.94	3.91	3.88	3.90	3.94	3.91
TOTAL	99.52	98.81	97.91	98.47	99.79	98.93

SAMPLE	85-565
LOCATION	rim
SiO_2	37.20
TiO_2	1.82
Al_2O_3	16.98
FeO	19.17
MnO	0.39
MgO	10.40
CaO	0.05
Na_2O	0.10
K_2O	10.05
H_2O	3.96
TOTAL	100.12

STAUROLITE

SAMPLE	85-700b					
LOCATION	core	core	core	core	rim	rim
SiO_2	27.27	27.48	27.42	27.85	27.41	27.34
TiO_2	0.70	0.70	0.66	0.67	0.63	0.75
Al_2O_3	54.74	54.04	54.40	54.18	54.24	53.83
FeO	13.42	13.10	13.74	13.38	12.71	13.68
MnO	0.11	0.14	0.15	0.13	0.11	0.11
MgO	1.53	1.49	1.58	1.77	1.91	1.90
CaO	0.05	0.01	0.00	0.00	0.05	0.02
ZnO	0.18	0.24	0.00	0.24	0.00	0.00
H_2O	1.06	1.05	1.06	1.06	1.05	1.05
TOTAL	99.24	98.49	99.01	99.52	98.11	98.68

SAMPLE	85-722					
LOCATION	core	core	core	rim	rim	rim
SiO_2	27.92	27.71	27.00	26.49	27.58	27.59
TiO_2	0.65	0.74	0.73	0.76	0.73	0.73
Al_2O_3	53.82	53.26	53.23	54.04	53.55	53.29
FeO	12.69	12.84	13.78	13.82	12.81	12.83
MnO	0.15	0.14	0.10	0.06	0.09	0.11
MgO	1.35	1.55	1.86	1.66	1.45	1.53
CaO	0.08	0.03	0.06	0.00	0.03	0.01
ZnO	0.16	0.16	0.08	0.25	0.16	0.37
H_2O	1.05	1.05	1.04	1.04	1.05	1.04
TOTAL	98.03	97.64	97.96	98.37	97.61	97.87

SAMPLE	85-722			85-723b		
LOCATION	rim	rim	rim	core	core	core
SiO_2	27.70	27.47	27.53	27.44	27.06	27.48
TiO_2	0.60	0.67	0.68	0.67	0.72	0.62
Al_2O_3	53.96	53.81	53.72	54.01	54.18	53.42
FeO	12.41	12.76	12.81	13.49	13.44	13.53
MnO	0.11	0.07	0.03	0.15	0.11	0.11
MgO	1.33	1.39	1.54	1.77	1.94	1.82
CaO	0.02	0.01	0.00	0.07	0.00	0.00
ZnO	0.00	0.45	0.37	0.04	0.19	0.25
H_2O	1.05	1.05	1.05	1.06	1.05	1.05
TOTAL	97.32	98.13	98.10	98.74	98.88	98.53

SAMPLE	85-723b					
LOCATION	core	core	core	core	core	core
SiO_2	27.40	27.31	27.39	27.35	27.29	27.30
TiO_2	0.70	0.63	0.71	0.71	0.72	0.67
Al_2O_3	54.15	53.97	53.93	53.90	53.96	54.16
FeO	13.41	13.22	13.36	12.80	13.61	13.23
MnO	0.08	0.14	0.15	0.14	0.13	0.04
MgO	1.84	2.08	1.89	2.00	2.03	1.98
CaO	0.00	0.01	0.00	0.00	0.01	0.02
ZnO	0.44	0.24	0.38	0.05	0.02	0.02
H_2O	1.06	1.05	1.06	1.05	1.06	1.05
TOTAL	99.52	98.40	99.25	98.05	98.85	98.49

SAMPLE	85-723b					
LOCATION	core	core	core	core	core	core
SiO_2	27.57	27.26	27.36	27.08	27.44	27.51
TiO_2	0.69	0.72	0.67	0.66	0.66	0.76
Al_2O_3	53.63	53.02	54.20	53.55	53.96	53.84
FeO	13.21	13.02	13.08	13.02	13.13	12.83
MnO	0.02	0.15	0.07	0.14	0.11	0.00
MgO	2.05	2.01	1.89	2.02	2.04	1.95
CaO	0.02	0.00	0.05	0.02	0.00	0.00
ZnO	0.00	0.00	0.04	0.07	0.07	0.00
H_2O	1.05	1.04	1.05	1.04	1.05	1.05
TOTAL	98.24	97.22	98.45	97.67	98.53	97.94

STAUROLITE (continued)

SAMPLE	85-723b					
LOCATION	core	rim	rim	rim	rim	rim
SiO_2	27.56	27.18	27.47	27.52	27.18	27.28
TiO_2	0.66	0.83	0.69	0.69	0.70	0.72
Al_2O_3	53.59	54.14	54.01	54.20	53.31	53.80
FeO	13.29	13.39	13.20	13.75	13.01	13.29
MnO	0.00	0.16	0.10	0.14	0.14	0.17
MgO	1.79	1.96	1.87	1.97	1.84	1.84
CaO	0.03	0.02	0.07	0.04	0.09	0.00
ZnO	0.13	0.16	0.10	0.25	0.10	0.20
H_2O	1.05	1.06	1.06	1.06	1.04	1.05
TOTAL	98.23	99.06	98.67	99.87	97.51	98.55

SAMPLE	85-723b				85-732	
LOCATION	rim	rim	rim	rim	core	core
SiO_2	27.59	27.19	27.17	27.52	26.72	27.10
TiO_2	0.60	0.75	0.81	0.74	0.65	0.73
Al_2O_3	54.00	54.19	53.57	54.27	54.35	52.60
FeO	13.35	13.29	12.98	12.66	13.78	13.49
MnO	0.12	0.13	0.04	0.04	0.00	0.03
MgO	2.00	1.92	2.10	1.92	1.78	1.72
CaO	0.00	0.00	0.00	0.02	0.03	0.00
ZnO	0.08	0.00	0.09	0.13	0.22	0.14
H_2O	1.06	1.05	1.05	1.06	1.05	1.03
TOTAL	98.88	98.52	97.90	98.49	98.80	96.98

SAMPLE	85-732					
LOCATION	core	core	rim	rim	rim	rim
SiO_2	27.14	26.95	27.70	27.04	27.31	27.05
TiO_2	0.68	0.73	0.70	0.72	0.72	0.64
Al_2O_3	53.08	53.07	53.89	53.85	53.05	53.85
FeO	13.65	13.86	13.77	13.64	13.40	13.62
MnO	0.08	0.12	0.06	0.06	0.08	0.08
MgO	1.72	1.80	1.74	1.81	1.89	1.79
CaO	0.04	0.02	0.00	0.00	0.04	0.00
ZnO	0.02	0.00	0.14	0.23	0.05	0.13
H_2O	1.04	1.04	1.05	1.05	1.04	1.05
TOTAL	97.47	97.59	98.19	98.63	97.63	98.34

SAMPLE	85-732	85-659b
LOCATION	rim	relict
SiO_2	27.09	27.35
TiO_2	0.66	0.53
Al_2O_3	53.31	53.38
FeO	13.55	12.15
MnO	0.11	0.00
MgO	1.76	1.64
CaO	0.00	0.00
ZnO	0.04	1.99
H_2O	1.04	1.05
TOTAL	97.60	100.08

PLAGIOCLASE

SAMPLE	85-659b		85-700b			
LOCATION	core	rim	core	core	core	rim
SiO_2	62.02	62.38	61.00	60.31	60.27	61.26
Al_2O_3	24.38	23.46	24.22	25.44	25.24	24.75
FeO	0.09	0.08	0.10	0.15	0.06	0.13
MgO	0.00	0.01	0.03	0.00	0.00	0.02
CaO	5.26	4.91	5.57	6.41	6.70	5.97
Na_2O	8.47	8.83	8.39	7.71	7.64	7.89
K_2O	0.06	0.04	0.04	0.01	0.05	0.01
TOTAL	100.28	97.59	99.35	98.63	99.96	100.03

SAMPLE	85-700b	85-708b		85-722		
LOCATION	inc(st)	rim	rim	core		
SiO_2	61.59	62.25	60.70	62.30	63.09	66.22
Al_2O_3	24.39	24.99	25.38	23.99	24.32	23.44
FeO	0.43	0.17	0.22	0.06	0.13	0.06
MgO	0.03	0.00	0.01	0.00	0.00	0.00
CaO	5.85	6.21	6.36	5.29	5.29	4.86
Na_2O	7.94	7.53	7.03	8.41	7.83	8.95
K_2O	0.07	0.09	0.02	0.06	0.10	0.03
TOTAL	100.30	100.24	99.72	100.11	100.76	99.56

SAMPLE	85-722					85-723b
LOCATION	middle	rim	rim	rim	rim	core
SiO_2	62.47	62.11	62.36	62.01	61.30	61.71
Al_2O_3	23.15	23.34	23.68	24.03	23.97	24.11
FeO	0.13	0.13	0.06	0.08	0.13	0.07
MgO	0.00	0.02	0.00	0.02	0.02	0.00
CaO	4.63	5.08	5.21	5.10	5.37	5.28
Na_2O	8.52	8.25	8.24	8.00	8.40	8.42
K_2O	0.08	0.06	0.04	0.09	0.09	0.12
TOTAL	98.98	98.99	99.59	99.33	99.28	99.71

SAMPLE	85-723b					
LOCATION	core	rim	rim	rim	rim	rim
SiO_2	62.34	61.34	60.92	59.45	60.51	61.27
Al_2O_3	24.12	24.74	24.79	25.34	24.63	24.13
FeO	0.00	0.00	0.05	0.07	0.11	0.00
MgO	0.03	0.00	0.01	0.00	0.00	0.00
CaO	5.53	5.60	6.41	6.92	6.40	5.95
Na_2O	8.10	8.39	7.88	7.99	7.94	8.47
K_2O	0.12	0.06	0.09	0.11	0.10	0.11
TOTAL	100.24	100.13	100.15	99.88	99.69	99.93

SAMPLE	85-732					
LOCATION	core	core	core	core	rim	rim
SiO_2	62.29	57.52	62.19	62.58	62.07	62.07
Al_2O_3	23.49	22.45	23.38	23.66	23.69	23.88
FeO	0.03	0.08	0.01	0.03	0.12	0.06
MgO	0.00	0.03	0.04	0.01	0.01	0.00
CaO	4.96	4.80	5.07	4.74	5.25	5.13
Na_2O	8.18	8.56	8.20	8.64	8.21	8.03
K_2O	0.04	0.01	0.05	0.04	0.06	0.03
TOTAL	98.99	93.45	98.94	99.70	99.41	99.20

SAMPLE	85-732	85-441				
LOCATION	rim	core	core	rim	rim	rim
SiO_2	62.34	63.05	62.56	62.77	61.98	63.18
Al_2O_3	23.97	23.36	23.65	22.89	24.04	24.01
FeO	0.22	0.00	0.09	0.18	0.09	0.07
MgO	0.03	0.00	0.00	0.00	0.00	0.02
CaO	5.19	4.50	4.63	4.72	5.17	4.93
Na_2O	8.36	8.51	8.38	8.60	8.44	8.60
K_2O	0.07	0.17	0.13	0.10	0.09	0.06
TOTAL	100.18	99.59	99.44	99.26	99.81	100.87

PLAGIOCLASE (continued)

SAMPLE	85-441			85-446		
LOCATION	rim	rim	middle	core	core	core
SiO_2	62.58	62.62	62.45	62.42	62.64	63.33
Al_2O_3	23.85	23.97	23.54	23.44	23.35	23.33
FeO	0.18	0.16	0.02	0.16	0.15	0.07
MgO	0.02	0.04	0.00	0.01	0.00	0.00
CaO	4.71	4.84	4.67	4.78	4.40	4.30
Na_2O	8.73	8.92	8.83	8.50	9.02	8.67
K_2O	0.05	0.05	0.12	0.14	0.05	0.17
TOTAL	100.12	100.60	99.63	99.45	99.61	99.87

SAMPLE	85-446			85-535		
LOCATION	rim	rim	inc(gt)	core	core	middle
SiO_2	63.16	63.15	60.18	62.05	62.28	62.39
Al_2O_3	23.23	23.41	19.80	23.84	23.54	23.50
FeO	0.07	0.05	0.34	0.06	0.00	0.11
MgO	0.03	0.01	0.00	0.00	0.00	0.00
CaO	4.90	4.08	0.02	4.91	4.95	4.72
Na_2O	8.38	8.65	10.92	8.63	8.85	8.81
K_2O	0.05	0.15	0.09	0.21	0.14	0.16
TOTAL	99.82	99.50	100.15	99.70	99.77	99.69

SAMPLE	85-535				85-565	
LOCATION	rim	rim	rim	rim	core	rim
SiO_2	62.34	62.18	62.18	62.99	60.40	59.99
Al_2O_3	23.72	23.89	23.88	23.36	24.03	24.63
FeO	0.15	0.09	0.20	0.05	0.10	0.14
MgO	0.00	0.00	0.02	0.00	0.05	0.00
CaO	4.67	4.86	4.54	4.37	6.56	6.96
Na_2O	8.93	9.04	9.10	9.09	7.45	7.47
K_2O	0.06	0.14	0.11	0.13	0.44	0.35
TOTAL	99.87	100.20	100.03	99.99	99.03	99.57

SAMPLE	85-565					85-245
LOCATION	rim	rim	rim	rim	rim	core
SiO_2	60.49	58.76	59.24	59.87	60.67	57.69
Al_2O_3	25.16	25.77	25.10	24.45	24.28	26.80
FeO	0.14	0.03	0.10	0.15	0.10	0.10
MgO	0.00	0.00	0.02	0.00	0.03	0.03
CaO	6.93	7.73	7.47	6.53	6.24	8.84
Na_2O	7.19	7.09	6.74	7.44	7.28	6.59
K_2O	0.25	0.21	0.32	0.39	0.37	0.11
TOTAL	100.16	99.59	98.99	98.83	98.97	100.16

SAMPLE	85-245					85-280
LOCATION	core	core	middle	middle	rim	core
SiO_2	58.14	56.70	58.49	56.81	59.64	58.67
Al_2O_3	26.76	27.70	26.68	27.48	25.84	26.09
FeO	0.14	0.13	0.13	0.13	0.25	0.14
MgO	0.01	0.02	0.02	0.00	0.00	0.00
CaO	8.90	10.21	8.69	9.64	7.61	7.76
Na_2O	6.70	5.64	6.45	5.69	7.08	6.95
K_2O	0.10	0.10	0.09	0.08	0.12	0.15
TOTAL	100.75	100.50	100.55	99.83	100.54	99.76

SAMPLE	85-280					
LOCATION	core	core	rim	rim	rim	rim
SiO_2	58.51	58.62	57.29	57.93	57.17	56.49
Al_2O_3	26.08	26.17	27.19	26.62	27.44	27.06
FeO	0.03	0.09	0.11	0.07	0.12	0.14
MgO	0.00	0.04	0.03	0.00	0.03	0.01
CaO	7.57	8.08	9.36	8.53	9.06	9.12
Na_2O	7.38	6.98	6.34	7.09	6.65	6.63
K_2O	0.17	0.13	0.10	0.10	0.10	0.08
TOTAL	99.74	100.11	100.42	100.34	100.57	99.53

PLAGIOCLASE (continued)

SAMPLE	85-343a			
LOCATION	core	core	rim	rim
SiO_2	56.75	56.85	54.57	58.15
Al_2O_3	27.60	27.77	28.93	26.98
FeO	0.17	0.08	0.20	0.13
MgO	0.00	0.01	0.03	0.04
CaO	9.41	9.76	11.15	8.45
Na_2O	6.44	6.27	5.35	7.10
K_2O	0.15	0.10	0.11	0.01
TOTAL	100.52	100.84	100.34	100.86

AMPHIBOLE

SAMPLE	85-706b					
LOCATION	core	rim	rim	rim	rim	rim
SiO_2	44.14	43.98	44.46	45.96	44.10	43.91
TiO_2	0.39	0.37	0.39	0.41	0.30	0.53
Al_2O_3	16.19	16.18	16.19	13.91	15.93	16.66
FeO	13.46	13.64	13.46	13.08	13.52	13.65
MnO	0.22	0.25	0.22	0.28	0.28	0.29
MgO	10.82	10.33	10.82	11.72	10.83	10.31
CaO	11.41	11.09	11.41	11.15	10.97	10.91
Na_2O	1.12	1.27	1.12	1.10	1.38	1.44
K_2O	0.10	0.07	0.00	0.05	0.14	0.09
TOTAL	97.84	97.18	98.07	97.66	97.50	97.79
SAMPLE	85-245			85-280		
LOCATION	core	core	rim	rim	rim	rim
SiO_2	40.08	40.33	40.90	40.55	40.49	40.78
TiO_2	0.63	0.86	0.92	0.50	0.42	0.42
Al_2O_3	17.44	17.55	17.44	16.01	16.13	15.90
FeO	18.99	18.73	18.82	20.49	20.74	20.19
MnO	0.21	0.17	0.19	0.38	0.42	0.42
MgO	7.25	7.43	7.37	6.68	6.30	6.71
CaO	11.90	11.47	11.37	11.52	11.49	11.86
Na_2O	1.37	1.51	1.50	1.51	1.27	1.28
K_2O	0.60	0.73	0.78	0.59	0.65	0.53
TOTAL	98.47	98.78	98.99	98.23	97.91	98.09
SAMPLE	85-280			85-343a		
LOCATION	rim	rim	core	core	rim	rim
SiO_2	40.15	40.45	40.30	40.69	40.50	40.68
TiO_2	0.34	0.60	0.64	0.60	0.61	0.57
Al_2O_3	16.31	15.82	15.83	15.84	15.63	15.53
FeO	20.42	19.83	19.86	20.26	20.53	20.25
MnO	0.17	0.30	0.36	0.29	0.34	0.34
MgO	6.34	6.94	7.05	6.83	6.56	6.58
CaO	12.15	11.39	11.62	11.86	11.74	11.93
Na_2O	1.35	1.39	1.33	1.50	1.55	1.44
K_2O	0.55	0.67	0.56	0.51	0.47	0.51
TOTAL	97.78	97.89	97.55	98.38	97.93	97.83

AMPHIBOLE (continued)

SAMPLE	85-343a		85-345			
LOCATION	rim	rim	core	core	core	core
SiO_2	40.73	40.32	43.16	43.63	43.73	43.83
TiO_2	0.53	0.46	0.70	0.53	0.77	0.73
Al_2O_3	15.40	15.70	14.95	13.65	14.61	13.61
FeO	20.67	20.92	14.92	14.78	14.81	15.07
MnO	0.37	0.30	0.19	0.18	0.33	0.26
MgO	6.51	6.37	10.43	10.87	10.75	10.99
CaO	11.57	11.91	11.70	11.66	12.24	12.22
Na_2O	1.42	1.48	1.31	1.25	1.46	1.07
K_2O	0.52	0.45	0.00	0.00	0.11	0.20
TOTAL	97.72	97.91	97.12	96.55	98.88	97.98

SAMPLE	85-345					
LOCATION	rim	rim	rim	rim	rim	rim
SiO_2	43.49	43.49	43.98	44.49	43.95	43.67
TiO_2	0.61	0.56	0.70	0.85	0.79	0.73
Al_2O_3	14.40	13.92	13.68	12.84	13.66	13.92
FeO	14.93	14.73	15.15	14.81	15.09	14.67
MnO	0.33	0.19	0.26	0.23	0.29	0.28
MgO	10.62	10.80	11.11	11.62	11.26	10.85
CaO	12.15	11.88	11.99	12.20	12.19	12.14
Na_2O	1.18	0.94	1.29	1.14	1.15	1.20
K_2O	0.00	0.13	0.05	0.38	0.30	0.33
TOTAL	97.71	96.64	98.21	98.56	98.68	97.79

SAMPLE	85-345	85-643c				
LOCATION	rim	core	core	rim	rim	rim
SiO_2	43.53	52.38	53.64	52.45	50.63	51.67
TiO_2	0.74	0.54	0.09	0.40	0.19	0.14
Al_2O_3	14.21	3.62	3.38	3.99	5.19	4.25
FeO	14.77	12.10	11.94	12.49	12.73	12.61
MnO	0.26	0.37	0.26	0.34	0.18	0.20
MgO	10.96	15.60	15.91	15.42	14.37	15.27
CaO	12.02	12.46	12.96	12.43	12.99	12.76
Na_2O	1.47	0.49	0.42	0.51	0.68	0.62
K_2O	0.08	0.09	0.01	0.14	0.04	0.00
TOTAL	98.04	97.65	98.61	98.17	97.00	97.52

SAMPLE	85-643c
LOCATION	intergrowth
SiO_2	43.83
TiO_2	0.35
Al_2O_3	14.18
FeO	16.04
MnO	0.35
MgO	9.67
CaO	12.12
Na_2O	1.54
K_2O	0.35
TOTAL	98.43

REFERENCES

Abbey, S. (1983). Studies in "standard samples" of silicate rocks and minerals, 1969-1982. Geological Survey of Canada Paper 83-15, 114p.

Althaus, E. (1967). The triple point andalusite -sillimanite-kyanite: An experimental and petrologic study. Contributions to Mineralogy and Petrology, 16, 29-44.

Apted, M.J. and Liou, J.G. (1983). Phase relations among greenschist, epidote-amphibolite, and amphibolite in a basaltic system. American Journal of Science, 283-A, 328-354.

Atherton, M.P. (1968). The variation in garnet, biotite, and chlorite composition in medium grade pelitic rocks from the Dalradian of Scotland, with particular reference to the zonation in garnet. Contributions to Mineralogy and Petrology, 18, 347-371.

Atherton, M.P. (1977). The metamorphism of the Dalradian rocks of Scotland. Scottish Journal of Geology, 13, 331-370.

Atherton, M.P. and Smith, R.A. (1979). Chloritoid -staurolite assemblages from Barrow's Zones in Central Perthshire, Scotland. Geological Magazine, 116, 469-476.

Baltatzis, E. (1979). Staurolite-forming reactions in the eastern Dalradian rocks of Scotland. Contributions to Mineralogy and Petrology, 69, 193-200.

Barber, J.P. and Yardley, B.W.D. (1985). Conditions of high grade metamorphism in the Dalradian of Connemara, Ireland. Geological Society of London Journal, 142, 77-86.

Barr, S.M. (1985). Granitoid rocks of the Cape Breton Highlands, Nova Scotia; in GAC-MAC, Program with Abstracts, 10, p. A3.

Barr, S.M., Jamieson, R.A., and Raeside, R.P. (1985). Igneous and metamorphic geology of the Cape Breton Highlands: GAC-MAC Field Guide, Excursion 10, 48p.

Barr, S.M., MacDonald, A.S., and Blenkinsop, J. (1987b). The Cheticamp pluton, a Cambrian granodioritic intrusion in the western Cape Breton Highlands, Nova Scotia. Canadian Journal of Earth Sciences, 23, 1686-1699.

Barr, S.M. and Raeside, R.P. (1986). Pre-Carboniferous tectonostratigraphic subdivisions of Cape Breton Island, Nova Scotia. Maritime Sediments and Atlantic Geology, 22, 252-263.

Barr, S.M., Raeside, R.P, and Jamieson, R.A. (1987a). Geological map of igneous and metamorphic rocks of the northern Cape Breton Island, Nova Scotia, Geological Survey of Canada Open File Report, in press.

Bell, T.H. (1981). Foliation development: The contribution, geometry and significance of progressive, bulk, inhomogeneous shortening. Tectonophysics, 75, 273-296.

Bell, T.H. (1985). Deformation partitioning and porphyroblast rotation in metamorphic rocks: a radical reinterpretation. Journal of Metamorphic Geology, 3, 109-118.

Bell, T.H. (1986). Foliation development and refraction in metamorphic rocks: reactivation of earlier foliations and decrenulation due to shifting patterns of deformation partitioning. Journal of Metamorphic Geology, 4, 421-444.

Bell, T.H. and Brothers, R.N. (1985). Development of P-T prograde and P-retrograde/T-prograde isogradic surfaces during blueschist to eclogite regional metamorphism in New Caledonia as indicated by progressively developed porphyroblast microstructures. Journal of Metamorphic Geology, 3, 59-78.

Bell, T.H. and Rubenach, M.J. (1980). Crenulation cleavage development - evidence for progressive bulk inhomogeneous shortening from "millipede" microstructures in the Robertson River Metamorphics. Tectonophysics, 68, T9-T15.

Bell, T.H. and Rubenach, M.J. (1983). Sequential porphyroblast growth and crenulation cleavage development during progressive deformation. Tectonophysics, 92, 171-194.

Bell, T.H., Rubenach, M.J., and Fleming, P.D. (1986). Porphyroblast nucleation, growth and disolution in regional metamorphic rocks as a function of deformation partitioning during foliation development. Journal of Metamorphic Geology, 4, 37-67.

Berger, G.W. and York, D. (1981). Geothermometry from ^{40}Ar-^{39}Ar dating experiments. Geochimica et Cosmochimica Acta, 45, 795-811.

Best, M.G. (1982). Igneous and Metamorphic Petrology. W.H. Freeman and Company, New York, 630p.

Bickle, M.J. and Archibald, N.J. (1984). Chloritoid and staurolite stability: implications for metamorphism in the Archean Yilgarn Block, Western Australia. Journal of Metamorphic Geology, 2, 179-203.

Binns, R.A. (1969). Hydrothermal investigations of the amphibolite-granulite facies boundary. Geological Society of Australia Special Publication, 2, 341-344.

Bird, G.W. and Fawcett, J.J. (1973). Stability relations of Mg-chlorite-muscovite and quartz between 5 and 10 kb water pressure. Journal of Petrology, 14, 415-428.

Blanchard, M.C. (1982). Geochemistry and petrogenesis of the Fisset Brook Formation, western Cape Breton Island, Nova Scotia. Unpublished M.Sc. thesis, Dalhousie University, 225p.

Blanchard, M.C., Jamieson, R.A., and Moore, E.B. (1984). Late Devonian-Early Carboniferous volcanism in western Cape Breton Island, Nova Scotia. Canadian Journal of Earth Sciences, 21, 762-774.

Bradley, D.C. (1982). Subsidence in late Paleozoic basins in the northern Appalachians. Tectonics, 1, 107-123.

Brady, J.B. (1974). Coexisting actinolite and hornblende from west central New Hampshire. American Mineralogist, 58, 529-535.

Carmichael, D.M. (1969). On the mechanism of prograde metamorphic reactions in quartz-bearing pelitic rocks. Contributions to Mineralogy and Petrology, 20, 244-267.

Chatterjee, A.K. (1980). Mineralization and associated wall rock alteration in the George River Group, Cape Breton Island, Nova Scotia. Unpublished Ph.D. thesis, Dalhousie University, 197p.

Chayes, F. (1955). Potash feldspar as a by-product of the biotite-chlorite transformation. Journal of Geology, 63, 75-82.

Chinner, G.A. (1967). Chloritoid and the isochemical nature of Barrow's Zones. Journal of Petrology, 8, 268-282.

Chorolton, L.B. and Dallmeyer, R.D. (1986). Geochronology of early to middle Paleozoic tectonic development in the southwest Newfoundland Gander Zone. Journal of Geology, 94, 67-89.

Cliff, R.A. (1985). Isotopic dating in metamorphic rocks. Geological Society of London Journal, 142, 97-110.

Cliff, R.A., Droop, G.T.R., Rex, D.C. (1985). Alpine metamorphism in the south-east Tauern Window, Austria: 2. Rates of heating, cooling, and uplift. Journal of Metamorphic Geology, 3, 403-415.

Coleman-Sadd, S.P. (1980). Geology of south-central Newfoundland and evolution of the eastern margin of Iapetus. American Journal of Science, 280, 991-1017.

Collerson, K.D. (1974). Descriptive microstructural terminology for high grade metamorphic tectonites. Geological Magazine, 111, 313-318.

Connors, K.A. (1986). Relationships between sulphide minerals, metamorphism, and deformation in the Faribault Brook area of the Cape Breton Highlands, Nova Scotia. Unpublished B.Sc. thesis, Dalhousie University, 105p.

Conrod, D.M. (1984). The relationship between low and high grade metamorphic rocks in the French Mountain area, Cape Breton Highlands, Nova Scotia. Unpublished B.Sc. thesis, Dalhousie University, 214p.

Cooper, A.F. (1972). Progressive metamorphism of metabasic rocks from the Haast Schist Group of southern New Zealand. Journal of Petrology, 13, 457-492.

Cormier, R.F. (1972). Radiometric ages of granitic rocks, Cape Breton Island, Nova Scotia. Canadian Journal of Earth Sciences, 9, 1074-1086.

Cosgrove, J.W. (1976). The formation of crenulation cleavage. Geological Society of London Journal, 132, 155-178.

Craw, D. (1984). Tectonic stacking of metamorphic zones in the Cheticamp River area, Cape Breton Highlands, Nova Scotia. Canadian Journal of Earth Sciences, 21, 1229-1244.

Currie, K.L. (1975). Studies of granitoid rocks in the Canadian Appalachians. Geological Survey of Canada, Paper 75-1, 265-270.

Currie, K.L. (1977). A note on post-Mississippian thrust faulting in northern Cape Breton Island. Canadian Journal of Earth Sciences, 14, 2937-2941.

Currie, K.L. (1982). Paleozoic supracrustal rocks near Cheticamp, Nova Scotia. Maritime Sediments and Atlantic Geology, 18, 94-103.

Currie, K.L., Loveridge, W.D. and Sullivan, R.W. (1982). A U-Pb age on zircon from dykes feeding basal rhyolitic flows of the Jumping Brook Complex, north-western Cape Breton Island, Nova Scotia; in Current Research, Part C, Geological Survey Canada, Paper 82-1C, 125-128.

Currie, K.L. (1987). Relations betwen metamorphism and magmatism near Cheticamp, Cape Breton Island. Geological Survey of Canada Bulletin, 87-23, in press.

Dallmeyer, R.D. (1974). The role of crystal structure in controlling the partitioning of Mg and Fe^{2+} between coexisting garnet and biotite. American Mineralogist, 59, 201-203.

Dallmeyer, R.D. (1979). $^{40}Ar/^{39}Ar$ Dating: Principles, Techniques, and Applications in Orogenic Terranes; in Lectures in Isotope Geology, Pergamon Press, 77-104.

Davis, G.H. (1984). Structural Geology of Rocks and Regions. John Wiley and Sons, New York, 492p.

Deer, W.A., Howie, R.A., and Zussman, J. (1982). Rock-forming Minerals, Volume 1A - Orthosilicates. Second edition, Longman Group Limited, England, 918p.

Delahay, S.C. (1979). Metamorphism of the George River Group; Gold Brook, Victoria County Cape Breton Island, Nova Scotia. Unpublished, B.Sc. thesis, Dalhousie University, 84p.

Dempster, T.J. (1985). Garnet zoning and metamorphism of the Barrovian type area, Scotland. Contributions to Mineralogy and Petrology, 89, 30-38.

Doucet, P. (1983). The petrology and geochemistry of the Middle River area, Cape Breton Island, Nova Scotia. Unpublished M.Sc. thesis, Dalhousie University, 339p.

Droop, G.T.R. (1985). Alpine metamorphism in the south-east Tauern Window, Austria: 1. P-T variations in space and time. Journal of Metamorphic Geology, 3, 371-402.

Elhers, E.G. and Blatt, H. (1982). Petrology: Igneous, Sedimentary and Metamorphic. W.H. Freeman and Company, San Francisco, 732p.

Ellias, P. (1986). Thermal history of the Meguma Terrane: A study based on $^{40}Ar-^{39}Ar$ and fission track dating. Unpublished Phd thesis, 306p.

Ellis, D.J. and Green, D.H. (1979). An experimental study of the effect of Ca upon garnet-clinopyroxene Fe-Mg exchange equilibrium. Contributions to Mineralogy and Petrology, 71, 13-22.

England, A.B. (1978). Some thermal considerations of the Alpine metamorphism, past, present and future. Tectonophysics, 46, 21-40.

England, A.B. and Thompson, P.C. (1984). Pressure -temperature-time paths of regional metamorphism II. Their inference and interpretation using mineral assemblages in metamorphic rocks. Journal of Petrology, 25, 824-928.

Eskola, P. (1915). As referenced in Elhers, E.G. and Blatt, H. (1982). Petrology: Igneous, Sedimentary and Metamorphic. W.H. Freeman and Company, San Francisco, 732p.

Essene, E.J. (1982). Geologic thermometry and barometry; in Ferry, J.M. (editor). Characterization of metamorphism through mineral equilibria. Reviews in Mineralogy, 10, Mineralogical Society of America, 153-206.

Evirgen, M.M. and Ashworth, J.R. (1984). Andalusitic and kyanitic facies series in the central Menderes Massif, Turkey. Neues Jahrbuch fur Mineralogie Monatschefte, 5, 219-227.

Faribairn, H.W., Hurley, P.M., Pinson, W.H., and Cormier, R.F. (1960). Age of the granitic rocks of Nova Scotia. Geological Survey of America Bulletin, 71, 399-414.

Faure, G. (1977). Principles in Isotope Geology, John Wiley and Sons, New York, 165-177.

Ferry, J.M. and Spear, F.S. (1978). Experimental calibration of partitioning of Fe and Mg between garnet and biotite. Contributions to Mineralogy and Petrology, 66, 113-117.

Fleck, R.D., Sutter, J.F., and Elliot, E. (1977). Interpretation of discordant $^{40}Ar/^{39}Ar$ age spectra of Mesozoic tholeiites from Antarctica. Geochimica et Cosmochimica Acta, 41, 15-32.

Foster, T. Jr. (1986). Thermodynamic models of reactions involving garnet in a sillimanite/staurolite schist. Mineralogical Magazine, 50, 427-439.

Frank, E. (1983). Alpine metamorphism of calcareous rocks along a cross-section in the Central Alps: Occurrence and breakdown of muscovite, margarite, and paragonite. Schewizerische Mineralogische und Petrographische Mitteilungen, 63, 37-93.

Freer, R. (1981. Diffusion in silicate minerals and glasses: A data digest and guide to the literature. Contributions to Mineralogy and Petrology, 76, 440 -454.

Ghent, E.D. (1985). Plagioclase-garnet-Al_2SiO_5-quartz: a potential geobarometer-geothermometer. American Mineralogist, 61, 710-714.

Ghent, E.D., Robbins, D.B., and Stout, M.Z. (1979). Geothermometry, geobarometry, and fluid compositions of metamorphosed calc-silicates and pelites, Mica Creek, British Columbia. American Mineralogist, 64, 874-885.

Ghent, E.D. and Stout, M.Z. (1981). Geobarometry and geothermometry of plagioclase-biotite-garnet-muscovite assemblages. Contributions to Mineralogy and Petrology, 76, 92-97.

Graham, C.M. (1974). Metabasite amphiboles of the Scottish Dalradian. Contributions to Mineralogy and Petrology, 47, 165-185.

Graham, C.M. and Powell, R. (1984). A garnet-hornblende geothermometer: calibration, testing, and application to the Pelona Schist, Southern California. Journal of Metamorphic Geology, 2, 13-31.

Gray, D.R. (1979a). Microstructure of crenulation cleavages: An indicator of cleavage origin. American Journal of Science, 279, 97-128.

Gray, D.R. (1979b). Geometry of crenulation-folds and their relationship to crenulation cleavage. Journal of Structural Geology, 1, 187-205.

Guidotti, C.V. (1968) Prograde muscovite pseudomorphs after staurolite in the Rangeley-Oquossoc area, Maine. American Mineralogist, 53, 1368-1376.

Guidotti, C.V. (1973). Compositional variation of muscovite as a function of metamorphic grade and assemblage in metapelites from Northwestern Maine. Contributions to Mineralogy and Petrology, 42, 33-42.

Guidotti, C.V. (1984). Micas in metamorphic rocks; in Bailey, S.W. (editor). Micas. Reviews in Mineralogy, 13, Mineralogical Society of America, 357-468.

Guidotti, C.V. and Sassi, F.P. (1976). Muscovite as a petrogenetic indicator mineral in pelitic schists. Neues Jahrbuch fur Mineralogie Abhandlungen, 127, 97-142.

Hawthorne, F.C. (1981). Crystal chemistry of the amphiboles; in Veblen, D.R. (editor). Amphiboles and other hydrous pyriboles - Mineralogy. Reviews in Mineralogy, 9A, Mineralogical Society of America, 1-95.

Hey, M.H. (1954). A new review of the chlorites. Mineralogical Magazine, 30, 277-292.

Hobbs, B.E., Means, W.D., and Williams, P.F. (1976). An Outline of Structural Geology. John Wiley and Sons, New York, 571p.

Hodges, K.V. and Spear, F.S. (1982). Geothermometry, geobarometry, and the Al_2SiO_5 triple point at Mt. Moosilauke, New Hampshire. American Mineralogist, 67, 1118-1134.

Hoinkes, G. (1986). Effect of grossular-content in garnet on the partitioning of Fe and Mg between garnet and biotite. Contributions to Mineralogy and Petrology, 92, 393-399.

Holdaway, M.J. (1971). Stability of andalusite and the aluminum silicate phase diagram. American Journal of Science, 271, 97-131.

Holland, T.J.B. and Richardson, S.W. (1979). Amphibole zonation in metabasites as a guide to the evolution of metamorphic conditions. Contributions to Mineralogy and Petrology, 70, 143-148.

Hollister, L.S. (1966). Garnet zoning: an interpretation based on the Rayleigh fractionation model. Science, 154, 1647-1651.

Hoschek, G. (1969). The stability of staurolite and chloritoid and their significance in metamorphism of pelitic rocks. Contributions to Mineralogy and Petrology, 14, 123-162.

Hoschek, G. (1976). Melting relations of biotite + plagioclase + quartz. Neues Jahrbuch Fur Mineralogie Monatshefte, 1976, 79-83.

Hsu, L.C. (1968). Selected phase relationships in the system Al-Mn-Fe-Si-O; a model for garnet equilibria. Journal of Petrology, 9, 40-83.

Hynes, A. (1982). A comparison of amphiboles from medium- and low-pressure metabasites. Contributions to Mineralogy and Petrology, 81, 119-125.

Indares, A. and Martignole, J. (1984). Evolution of P-T conditions during a high-grade metamorphic event in the Maniwaki area (Grenville Province). Canadian Journal of Earth Sciences, 21, 853-863.

Indares, A. and Martignole, J. (1985). Biotite-garnet geothermometry in granulite-facies rocks: evaluation of equilibrium criteria. Canadian Mineralogist, 23, 187-193.

Jamieson, R.A. (1981). Metamorphism during ophiolite emplacement. The petrology of St. Anthony Complex. Journal of Petrology, 22, 397-449.

Jamieson, R.A. and Craw, D. (1983). Reconaissance mapping of the southern Cape Breton Highlands - a preliminary report; in Current Research, Part A, Geological Survey of Canada, Paper 83-1A, 263-268.

Jamieson, R.A., Tallman, P., Marcotte, J.A., and Plint, H.E. (1987). Geology of the west-central Cape Breton Highlands, Nova Scotia, in Current Research, Part B, Geological Society of Canada, Paper 87-1B, in press.

Jamieson, R.A., van Breeman, O., Sullivan, R.W., and Currie, K.L. (1986). The age of igneous and metamorphic events in the western Cape Breton Highlands, Nova Scotia. Canadian Journal of Earth Sciences, 23, 1891-1901.

Jamieson, R.A. and Vernon, R.H. (1987). Timing of poprhyroblast growth in the Fleur de Lys Supergroup, Newfoundland. Journal of Metamorphic Geology, in press.

Karabinos, P. (1985). Garnet and staurolite producing reactions in a chlorite-chloritoid schist. Contributions to Mineralogy and Petrology, 90, 262-275.

Keen, C.E. and Lewis, T. (1982). Measured radiogenic heat production in sediments from continental margin of eastern North America: Implications for Petroleum Generation. American Association of Petroleum Geologist Bulletin, 66, 1402-1407.

Keppie, J.D. (1979). Geological map of the province of Nova Scotia. Nova Scotia Department of Mines and Energy.

Keppie, J.D. and Smith, P.K. (1978). Compilation of isotopic age data of Nova Scotia. Nova Scotia Department of Mines, Report 78-4.

Kwak, T.A.P. (1974) Natural staurolite breakdown reactions at moderate to high pressures. Contributions to Mineralogy and Petrology, 44, 57-80.

Lasaga, A.C. (1983). Geospeedometry: an extension of geothermometry; in Saxena, S.K. (editor). Kinetics and equilibrium in mineral reactions, 81-114.

Laird, J. (1980). Phase equilibria in mafic schist from Vermont. Journal of Petrology, 21, 1-30.

Laird, J. and Albee, J.L. (1981). Pressure, temperature, and time indicators in mafic schists: their application to reconstructing the polymetamorphic history of Vermont. American Journal of Science, 281, 127-175.

Leake, B.E. (1965). The relationship between compositions of calciferous amphiboles and grade of metamorphism. American Mineralogist, 50, 843-851.

Liou, J.G. (1973). Synthesis and stability relations of epidote, $Ca_2Al_2FeSi_3O_{12}(OH)$. Journal of Petrology, 14, 381-413.

Liou, J.G., Kunyioshi, K. amd Ito, K. (1974). Experimental studies of the phase relations between greenschist and amphibolite in a basaltic system. Ameriacn Journal of Science, 274, 613-632.

Liou, J.G., Maruyama, S., and Cho, M. (1985). Phase equilibria and mineral parageneses of metabasites in low-grade metamorphism. Mineralogical Magazine, 49, 321-33.

Lister, G.S. and Williams, P.F. (1983). The partitioning of deformation in flowing rock masses. Tectonophysics, 92, 1-34.

Macdonald, A.S., and Smith, P.K. (1980). Geology of Cape North area, northern Cape Breton Island, Nova Scotia. Nova Scotia Department of Mines and Energy, Paper 80-1, 60p.

Marlow, P.C. and Etheridge, M.A. (1977). Development of a layered crenulation cleavage in mica schists of the Kanmantoo Group near Macclesfield, South Australia. Geological Society of America Bulletin, 88, 873-882.

McLaren, A.S. (1955). Cheticamp River, Inverness and Victoria Counties, Cape Breton Island, Nove Scotia. Geological Survey of Canada, Preliminary Map 55-36.

Milligan, G.C. (1970). Geology of the George River Series, Cape Breton. Nova Scotia Department of Mines, Memoir 7, 111p.

Miyashiro, A. (1964). Oxidation and reduction in the earth's crust with special reference to the role of graphite. Geochimica et Cosmochimica Acta, 28, 717-729.

Miyashiro, A. (1975). Metamorphism and Metamorphic Belts. George Allen and Unwin Ltd, London, 492p.

Miyashiro, A. and Shido, F. (1973). Progressive compositional change of garnet in metapelite. Lithos, 6, 13-20.

Moles, N.R. (1979). Metamorphic conditions and uplift history in central Perthshire: evidence from mineral equilibria in the Foss celesian-barite-sulphide deposit, Aberfeldy. Geological Society of London Journal, 142, 39-52.

Neale, E.R.W. (1963). Geology of Pleasant Bay, Cape Breton Island, Nova Scotia. Geological Survey of Canada, Map 119A.

North American Commission on Stratigraphic Nomenclature (1983). The North American Stratigraphic Code. The American Association of Petroleum Geologists Bulletin, 67, 841-875.

Oxburgh, E.R. and Turcotte, D.L. (1974. Thermal gradients and regional metamorphism in overthrust terrains with special reference to the eastern Alps. Schweizerische Mineralogische und Petrographische Mitteilungen, 54, 641-662.

Orville, P.M. (1972). Plagioclase cation exchange equilibria with aqueous chloride solution at 700°C and 2000 bars in the presence of quartz. American Journal of Science, 272, 234-272.

Plint, H.E., Connors, K.A., and Jamieson, R.A. (1986). Geology and mineral occurrences of the Jumping Brook Complex, Cheticamp-Pleasant Bay area, Cape Breton Island, Nova Scotia; in Current Research, Part B, Geological Survey of Canada, Paper 86-1B, 557-566.

Powell, R. (1985). Geothermometry and geobarometry: a discussion. Geological Society of London Journal, 142, 29-38.

Raase, P. (1974). Al and Ti contents of hornblende, indicators of pressure and temperature of regional metamorphism. Contributions to Mineralogy and Petrology, 45, 231-236.

Rast, N. and Sturt, B.A. (1957). Crystallographic and geological factors in the growth of garnets from Central Perthshire. Nature London, 179, 215.

Rao. P.B.B. and Johannes, W.H. (1979). Further data on the stability of staurolite and quartz and related assemblages. Neues Jahrbuch fur Mineralogie Monatsheft, 1979, 437-477.

Richardson, S.W. (1968). Staurolite stability in part of the system Fe-Al-Si-O-H. Journal of Petrology, 9, 467-488.

Richardson, S.W., Gilbert, M.C., and Bell, P.M. (1969). Experimental determination of the kyanite-andalusite and andalusite-sillimanite equilibria; the aluminum silicate triple point. American Journal of Science, 267, 259-272.

Rosenfeld, J.L. (1968). Garnet rotations due to the major Paleozoic deformations in southeastern Vermont. in White, W.S., Zen, E., Hadley, J.B., and Thompson, J.B. (editors). Studies of Appalachian Geology: Northern and Maritime. Wiley Interscience, New York, 185-202.

Roydon, L.H. and Hodges, K.V. (1984). A technique for analyzing the thermal and uplift histories of eroding orogenic belts: a Scandinavian example. Journal of Geophysical Research, 89, 7091-7106.

Salje, E. (1986). Heat capacities and entropies and andalusite and sillimanite: The influence of fibrolitization on the phase diagram of the Al_2SiO_5 polymorphs. American Mineralogist, 71, 1366-1371.

Schoneveld, C. (1977). A study of some typical inclusion patterns in strongly paracrystalline rotated garnets. Tectonophysics, 39, 453-471.

Sclater, J.G., Jaupart, C., and Galson, D. (1980). The heat flow through oceanic and continental crust and the heat loss of the earth. Reviews of Geophysics and Space Physics, 18, 269-311.

Self, S. (1982). Terminology and classifications for pyroclastic deposits; in Pyroclastic volcanism and deposits of Cenozoic intermediate to felsic volcanic islands with implications for Precambrian greenstone -belt volcanoes, Geological Association of Canada, Short Course Notes, 2, Winnipeg.

Selverstone, J. (1985). Petrologic constraints on imbrication, metamorphism, and uplift in the SW Tauern window, eastern Alps. Tectonics, 4, 687-704.

Spear, F.S. (1976). Ca-amphibole composition as a function of temperature, fluid pressure, and oxygen fugacity in a basaltic system. Carnegie Institution of Washington, 75, 775-779.

Spear, F.S. and Selverstone, J. (1983). Quantitative P-T paths from zoned minerals: theory and tectonic applications. Contributions to Mineralogy and Petrology, 83, 348-357.

Spear, F.S., Selverstone, J., Hickmott, D., Growley, P., and Hodges, K.V. (1984). P-T paths from garnet zoning: a new technique for deciphering tectonic processes in crystalline terranes. Geology, 12, 87-90.

Spear, F.S., Selverstone, J., Hickmott, D., Growley, P., and Hodges, K.V. (1984). P-T paths from garnet zoning: a new technique for deciphering tectonic processes in crystalline terranes - a reply. Geology, 13, 80-81.

Spry, A. (1969). Metamorphic textures. Pergamon Press, New York, 350p.

Stephenson, N.C.N. (1979). Coexisting garnets and biotites from Precambrian gneisses of the south coast of Western Australia. Lithos, 12, 73-87.

Streckeisen, A. (1976). To each plutonic rock its proper name. Earth Science Reviews, 12, 1-13.

Thompson, A.B. (1976). Mineral reactions in pelitic rocks: II. Calculation of some P-T-X (Fe-Mg) phase relations. American Journal of Science, 276, 425-454.

Thompson, A.B. (1982). Dehydration melting of pelitic rocks and the generation of H_2O-undersaturated granitic liquids. American Journal of Science, 282, 1567-1595.

Thompson, J.B. (1957). The graphical analyses of mineral assemblages in pelitic schists. American Mineralogist, 42, 842-858.

Thompson, J.B., Tracy, R.J., Lyttle, P.T., and Thompson, J.B., Jr. (1977). Prograde reaction histories deduced from compositional zonations and mineral inclusions in garnet from the Gassetts schist, Vermont. American Journal of Science, 227, 1152-1167.

Thompson, J.B. and Norton, S.A. (1968). Paleozoic regional metamorphism in New England and adjacent areas; in E. Zen, White, W.S., Hadley, J.B., and Thompson, J.B. (editors). Studies of Appalachian Geology, Northern and Maritime. Wiley Interscience, New York, 319-327.

Tracy, R.J. (1982). Compositional zoning and inclusions in metamorphic minerals in: Ferry J.M. (editor). Characterization of metamorphism through mineral equilibria. Reviews in Mineralogy, 10. Mineralogical Society of America, 355-397.

Treloar, P.J. (1985). Metamorphic conditions in central Connemara, Ireland. Geological Society of London Journal, 142, 87-96.

Triboulet, C. and Audren, C. (1985). Continuous reactions between biotite, garnet, staurolite, kyanite-sillimanite and P-T-time deformation path in mica schists from the estuary of the river Vilaine, South Brittany, France. Journal of Metamorphic Geology, 3, 91-105.

Turner, F.G. (1981). Metamorphic Petrology - Mineralogical, Field, and Tectonic Aspects. 2nd edition, McGraw-Hill Book Company, New York, 524p.

Vernon, R.H. (1976). Metamorphic Processes, Reactions and microstructure development. George Allen and Unwin, London, 247p.

Vernon, R.H. (1978). Porphyroblast-matrix microstructural relationships in deformed metamorphic rocks. Geologischen Rundschau, 67, 288-305.

Weeks, L.J. (1954). Southeast Cape Breton Island, Nova Scotia. Geological Survey of Canada, Memoir 277, 112p.

Williams, P.F. (1976). Relationships between axial-plane foliations and strain. Tectonophysics, 30, 181-196.

Williams, H. (1979). Appalachian orogen in Canada. Canadian Journal of Earth Sciences, 16, 792-807.

Winkler, H.G.F. (1974). Petrogenesis of Metamorphic Rocks. Third edition, Springer-Verlag, New York, 310p.

Woodsworth, G.J. (1977). Homogenization of zoned garnets from pelitic schists. Canadian Mineralogist, 15, 230-242.

Wright, J.A., Jessop, A.M., Judge, A.S., and Lewis, T.J. (1980). Geothermal measurements in Newfoundland. Canadian Journal of Earth Sciences, 17, 1370-1376.

Yardley, B.W.D. (1977). Am empirical study of diffusion in garnet. American Mineralogist, 62, 793-800.

Yardley, B.W.D., Leake, B.E., and Farrow, C.M. (1980). The metamorphism of Fe-rich pelites from Connemara, Ireland. Journal of Petrology, 21, 365-399.

Yoder, H.S. and Tiley, C.E. (1962). Origin of basaltic magmas: An experimental study of natural and synthetic rock systems. Journal of Petrology, 3, 345-532.

Zwart, H.J. (1962). On the determination of polymetamorphic mineral associations, and its application to the Bosost area (central Pyrenees). Geologischen Rundschau, 52, 38-65.

STRUCTURAL CROSS-SECTION

SYMBOLS

- inferred geological contact
- fault
- shear
- foliation, S_1, S_2

unit numbers as for MAP 1

LINE XY - MAP 1

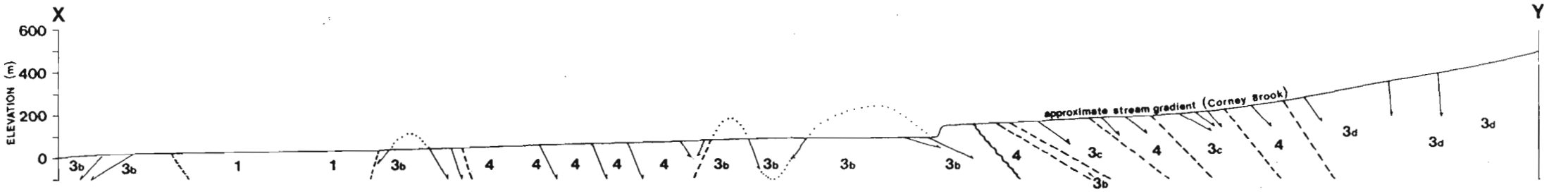

LITHOLOGIES

UNKNOWN AGE

10 Foliated muscovite granitoid

CARBONIFEROUS

9 Undifferentiated sedimentary rocks including Horton and Windsor Groups

DEVONIAN – CARBONIFEROUS

8 Fisset Brook Formation
v = volcanic, s = sedimentary rocks

7 Salmon Pool pluton, syenogranite

6 Margaree pluton, granodiorite

5 Dominately biotite granodiorite, minor tonalite, monzogranite

SILURIAN OR OLDER

4 George Brook amphibolite

3 Jumping Brook metamorphic suite

- d Fishing Cove River schist
- c Corney Brook schist
- b Dauphinee Brook schist
  m = marble
- a Faribault Brook metavolcanics

2 Pleasant Bay Gneiss Complex

- b Dominantly MacKenzies Mountain megacrystic orthogneiss
- a Dominantly MacIntosh Brook quartzo-feldspathic schist

CAMBRIAN

1 Cheticamp pluton

UNKNOWN AFFINITY

BG brecciated granitoid

- R rhyolite
- D diabase

SYMBOLS

- compositional layering
- schistosity – generation unknown, S_1, S_2
- gneissosity – generation unknown, S_2
- foliation – dip unknown
- extensional lineation, kink fold axis
- crenulation lineations, D_4, D_5
- mineral lineation, L_1 and L_2
- mesoscopic fold axial trace
- regional fold axial trace
- geological contact: inferred, arbitrary, approximate, observed
- outcrop
- shear zone, observed
- shear zone, inferred
- fault

ISOGRADS

- almandine – in
- staurolite – in
- staurolite – out

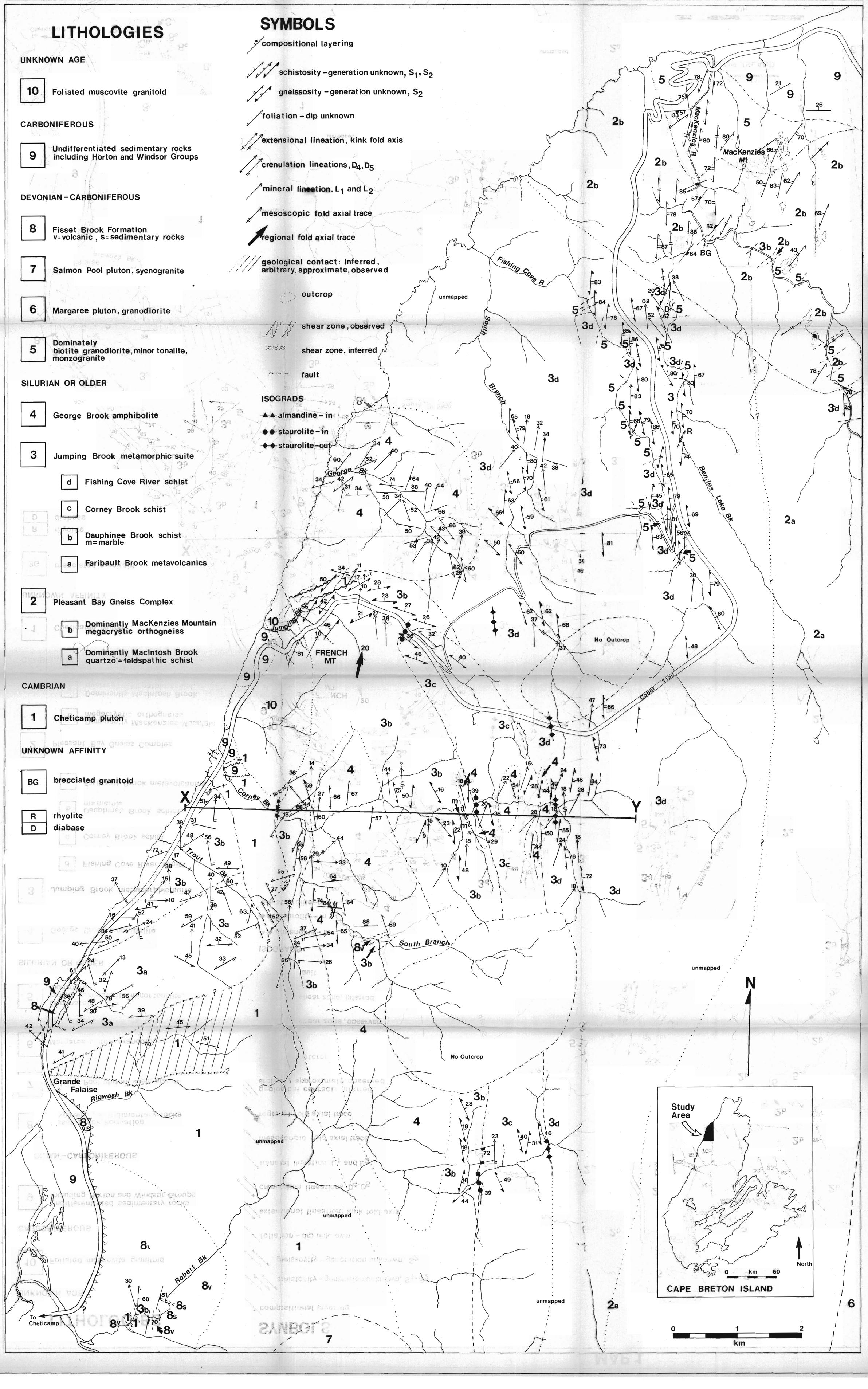

SAMPLE LOCALITIES

outcrop

532 sample number

unmapped

No Outcrop

Cabot Trail

To Cheticamp

Study Area

North

0 km 50

CAPE BRETON ISLAND

0 1 2 km

N